University of Alberta

An Electrochemical Impedance Spectroscopic Diagnostic Device for Characterization of Liquid-Liquid Systems and Phase Separation Detection in Emulsions

by

Seyedehsan Shahidi

A thesis submitted to the Faculty of Graduate Studies and Research in partial fulfillment of the requirements for the degree of

Master of Science

Department of Mechanical Engineering

Fall 2013
Edmonton, Alberta

I would like to share the moment of accomplishing my MSc years with my mom and dad, who have always been such great supports for me, and with my dear wife, Azin, my source of inspiration.

Abstract

Rapid characterization of complex fluids, especially sensing emulsion stability, is crucial for many industrial applications, ranging from pharmaceutical industry to petroleum production. Electrochemical impedance spectroscopy (EIS) is a powerful tool for electrical characterization of such systems. In this study, a "milli-fluidic" EIS test fixture which is inexpensive, easily fabricated, yet robust, is designed and fabricated using 3D printing technology, which allows reliable experiments, and can then be disposed of after each test. The developed cell is tested using solutions, liquid-liquid mixtures, and oil-water emulsions. Frequency response analysis and equivalent circuit modeling have been performed to find the effective electrical properties of the liquids, and relate them to their physical properties, such as stability. EIS is applied to reveal the electrical behavior of emulsions during phase separation. It is found that creaming can be sensed based on permittivity decay, and capacitance-based measurements can be utilized to detect phase separation in emulsions.

Acknowledgements

Special thanks to Professor Subir Bhattacharjee, whose relationship with me has been the optimum between mentorship and student-teacher relationship. His knowledge, experience, and industrial point of view has been an invaluable help in my MSc thesis project, as well as in developing my independent thinking and problem solving skills. I would also like to express my gratitude to Professor Bob Koch, whose unique way of looking at engineering challenges provided me with a broader point of view, helped me to think outside the box and define engineering problems in a way that has never been seen by others. Subir and Bob have been more than supervisors for me, it was an honor to work with them and it is a pleasure to be friends with them.

I would like to express my thanks to Josie and Ni for kindly helping me with all the logistics I needed during my project. I wish to thank the Technical Advisory Committee members of the NSERC Industrial Research Chair Program in Water Quality Management for Oil Sands Extraction, especially Amir and David, for providing helpful feedbacks from an industrial application point of view. I also thank Dr. Zhenghe Xu for providing the size distribution measurement apparatus for my experiments, and the Mechanical Engineering Machine Shop team, especially Roger and Michael, for helping me with fabrication of my test fixture.

I thank my friends, members and alumni of the CCFLab, Mohtada, Arnab, Abhijit, Hadi, Behnam K., Soundarajan, Jannat, Micah, Tathagata, Mamun, Shahab, Behnam S., Ahsan, Soubhayan, and Samia who maintain a friendly and dynamic environment of hard work in our group. Last but not least, big thank you to my wife for standing beside me throughout the busy days of my MSc years and writing this thesis.

CONTENTS

List of Tables

List of Figures

Nomenclature

Abbreviations

EIS	Electrochemical (Electrical) Impedance Spectroscopy
DS	Dielectric Spectroscopy
IS	Impedance Spectroscopy
EC	Equivalent Circuit
O/W	Oil-in-Water
W/O	Water-in-Oil
P.F	Packing Factor
CNLS	Complex Non-linear Least Squares
CPE	Constant-Phase Element
FRA	Frequency Response Analyzer (Analysis)
CMC	Critical Micelle Concentration

Symbols

C	Electric capacitance
R	Electric resistance
Z	Electric impedance
ω	Angular frequency
A	Surface area

d and D	Distance
t	Thickness
ϵ	Permittivity
ϕ	Volume fraction, Electric potential
X	Volume fraction
ρ	Density
V	Volume, Voltage
g	Gravitational acceleration
R	Radius
γ	Surface tension
Bo	Bond number
ρ_f	Free charge density
Q	Electric charge
W	Electric energy (work)
I	Electric current
σ	Electric conductivity
i and j	Imaginary unit number
$R\|C$	Parallel RC configuration
$R-C$	Serial RC configuration
Ω	Ohm
F	Farad
μ	Micro

M	Molar

Subscripts

eff	Effective
r	Relative
o	Pertaining to vacuum
0	Initial
W	Pertaining to water
W/O	Pertaining to water-in-oil phase
O/W	Pertaining to oil-in-water phase

CHAPTER 1

INTRODUCTION

1.1 BACKGROUND AND OVERVIEW

Electrochemical methods play a central role in characterization of materials, and sensing and diagnostics in a wide variety of industries including petroleum, cosmetics, pharmaceutical industry, biosensing, and electronics [1–3]. Electrochemical fluid sensing uses two electrodes immersed in a test fluid. The electrodes can be actuated using a direct current (DC), or alternating current (AC). The potential difference results in a flow of current through the system, which is measured, either using the same driving electrodes, or through another set of measuring electrodes. The correlation between the voltage and current provides a measure of electrical characteristics of the system, which is referred to as the system impedance. For a purely DC potential, the impedance only consists of resistance. For AC potentials, the system impedance may consist of capacitance, inductance, and resistance. AC impedance measurements, therefore, provide considerable insight regarding the electromagnetic properties of a system, such as dielectric permittivity and susceptibility, along with its electrical resistivity [2, 3]. AC measurements also avoid the commonly encountered problem of strong system polarization during DC measurements [2]. Since different electrochemical phenomena occur in different frequencies, AC measurements are done over a frequency spectrum, hence, the technique is called electrical (electrochemical) impedance spectroscopy (EIS or only IS), or dielectric spectroscopy

(DS).

In the scientific fields and industrial applications named previously, multiphase and multicomponent complex liquids, such as mixtures, dispersions, and emulsions, are encountered, and characterization of these systems in terms of volume fraction of different components, dispersed phase properties, stability, etc. is crucial and has been studied for decades [1]. For determining the volume fraction of different components of emulsions, chemical and titration techniques, as well as physical separation via centrifugation and membrane filtering have been developed [1]. In terms of properties of the dispersed elements, chromatographic and light-scattering techniques have been applied [4]. For characterizing the shape of the dispersed elements and their interactions with other elements and the host medium, optical and electron microscopy have been used [4]. Finally, for stability characterization, microscopy, as well as rudimentary techniques of bottle test and centrifugation, have been used [1]. In addition to the techniques mentioned above, electrical measurement techniques have also been utilized to measure properties of complex fluids in terms of dispersed phase volume fraction, dispersed particle size and shape, flocculation of dispersed elements, and stability. It is a convenient approach to detect physical, chemical, or biological processes that have an effect on the electrical properties of the systems [1, 2, 4]. Compared to many other techniques, electrical methods, especially EIS, are fast and highly sensitive, and usually do not require extensive chemical pre-treatment of samples [2]. EIS-based techniques also allow fast, yet accurate, detection of small-scale properties such as dispersed particle shape with relatively larger-lengthscale (in the order of a millimeter) bulk measurements. However, the high sensitivity of EIS necessitates extreme care in sample loading, electrode surface properties, etc. to avoid experimental measurement errors [3]. While electrical techniques can reveal properties which are not observable with other methods, they often need extensive sample calibration to be applicable to industrially relevant processes [1].

Dielectric spectroscopy is based on measuring polarization of materials at different

frequencies. It is used to relate the permittivity and resistivity at different frequencies, to physical phenomena in the system [5]. Extremely high-frequency measurements are sensitive to properties related to "electronic" physical phenomena due to the small length scale and wavelength of such processes [5,6]. Atomic and molecular-level polarizability, as well as ionic movements are captured by relatively high frequencies. However, larger ("meso-scale" [5]) physical phenomena, such as phase differentiation processes including droplet flocculation and coalescence, can be captured at lower frequencies. Since complex liquid systems (e.g. emulsions), have interfaces where different phases meet, the characteristic dielectric phenomenon in such systems is interfacial polarization [7]. The heterogeneous structure, and the arrangement of the interfaces of a multi-component liquid system are affected by the phase dynamics of the system. Hence, information about different properties of emulsions, such as particle shape, structure of the dispersed elements, and phase behavior, can be obtained by EIS for these complex liquid systems.

EIS of emulsions has been extensively studied, and different analytical studies, as well as experiments, have been reported that investigate the effect of droplet shape and size, and flocculation on dielectric behavior of emulsions. Comprehensive reviews of these studies are provided by Sjoblom [8] and Asami [5]. Different phenomena in the interaction of the dispersed drops with one another and with the host medium that can affect the dielectric response of the systems have been studied. These studies only consider homogeneous distribution of the dispersed phase in the continuous medium. Current models do not investigate dielectric behavior of emulsions when phase separation occurs, and do not provide details of dielectric changes during phase separation processes such as creaming and sedimentation. The effect of phase separation on permittivity of two-phase oil-water emulsions is addressed in this thesis.

Based on different targeted applications, EIS has been applied in different length scales from micro-scale experimental setups to larger bulk EIS commercial test cells. Micro-scale EIS is needed for applications such as biosensing where the variations in electrical

properties are so small that minuscule volumes of test liquids are studied to enable the experiment to detect impedance changes [9]. Micro-scale EIS has also been applied to oil-water emulsions [10–13]. However, no systematic work has been reported investigating the appropriate length scale for EIS of emulsion samples. In this work, it is shown that microfluidic approach may be flawed when the characteristic length scale of the sample, for instance, the mean droplet diameter of an emulsion, is in the same order of magnitude as the electrodes separation in a microfluidic test cell. In addition to that, microfluidic test setups are expensive to fabricate, tend to have large electrode polarization errors, and are prone to fouling when used with industrially relevant liquids. On the other hand, larger-scale (bulk) EIS of industrial samples, especially the ones related to petroleum industry, are associated with lack of sensitivity, and difficulty with respect to cleaning the test cell for conducting multiple experiments. In this work, an inexpensive, easily fabricated "milli-fluidic" test cell is introduced that allows reproducible multiple experiments and disposing of the test cell after each test.

1.2 OBJECTIVES AND SCOPE OF THE THESIS

The main objectives of this thesis that define the scope of the work are:

- Development of an inexpensive, easily fabricated, disposable, yet robust experimental platform for applying EIS to multicomponent and multiphase complex fluids.
- Investigation of the appropriate length scale for applying EIS to different oil-water emulsions.
- Theoretical and experimental investigation of the dielectric behavior of oil-water emulsions during phase separation, and investigating the application of dielectric measurement as a sensing tool for detecting creaming and sedimentation.

1.3 SUMMARY OF THE METHODOLOGY

In this work, the experimental impedance measurement cell is computer-aided-designed and fabricated using 3D printing technology after a few steps of optimization. Different characteristics of the setup that may affect the EIS measurements have been studied experimentally. Also, finite-element modeling has been employed to investigate the effect of experimental length scale, and phase separation process on permittivity behavior of oil-water emulsions. The developed experimental setup is tested using solutions, liquid-liquid mixtures, and oil-water emulsions. Dielectric behavior of oil-water emulsions during phase separation has been studied analytically, numerically, and experimentally using the developed experimental platform. The sensitivity of permittivity-based, as well as conductivity-based, measurements for detecting phase separation dynamics of emulsions has been investigated.

1.4 THESIS ORGANIZATION

In chapter 1 (Introduction), a brief background of the application of EIS in characterization of emulsions is detailed, and an overview of the scope of the contributions of this thesis is given.

In chapter 2 (Literature Review), a detailed literature review of EIS is provided with a focus on the application of this technique to oil-water emulsions. The current status of the analytical models as well as numerical and experimental works is outlined. Based on the literature review, the significance of the objectives of this thesis is justified and the novelty of this work is related to the applications of EIS and the previous works done in this area.

Chapter 3 (Analytical and Numerical Modeling) discusses the theoretical basis of this work. First, different multiphase dielectric theories are discussed and their relations with the systems studied in this thesis are explained. Then, a simple analytical explanation for permittivity variation as a result of phase separation is provided followed by expressions

derived for giving creamed layer thickness as a function of capacitance, and permittivity as a function of degree of phase separation. Following that, a finite-element simulation for modeling permittivity of complex media and investigating the effect of droplet length scale, as well as phase separation, on permittivity is developed and the results are discussed in terms of physics of emulsions. Finally, the computational data analysis scheme (equivalent circuit modeling) for interpreting the EIS data is explained.

In chapter 4 (Experimental Methodology), the computer design, optimization steps, and fabrication of the experimental setup are explained. Different issues that can affect the EIS measurements, such as electrode material, signal amplitude, etc. are addressed. Following that, calibration of the test cell in terms of lead impedance and dry capacitance is explained. Finally, the sample preparation method (liquid mixture and emulsion preparation) of this thesis is described.

In chapter 5 (Experimental Results and Discussion), the results of the different experiments conducted in this study, including liquid mixtures, emulsions, phase separation experiments, etc. are presented and discussed in detail.

Finally, in chapter 6 (Conclusions and Future Work), the main concluding remarks of the experimental, numerical, and analytical studies are explained and the main contributions of this work are highlighted. Following that, an overview of possible future steps that can be taken in this field, and future directions that can be pursued beyond this research are listed.

CHAPTER 2

LITERATURE REVIEW

2.1 INTRODUCTION

Electrochemical impedance spectroscopy (EIS) has been applied to many problems in different fields ranging from solid electronics to membrane characterization, soft material characterization, and emulsion physics [3, 5, 8, 14]. Many physical processes and phenomena applied to systems result in changes in electric behavior such as dielectric relaxation properties, which may be captured with impedance spectroscopic techniques in different frequency ranges. As a result, EIS, and it's closely related parallels, dielectric spectroscopy (DS) and dielectric relaxation/dispersion analysis (often used interchangeably with EIS), have been used in developing new understanding of little known phenomena based on reverse analysis of impedance spectroscopy data [15]. For understood physical systems and phenomena, EIS can be used as a rapid and sensitive non-invasive diagnostic tool for sensing physical properties and tracking physical changes [3, 16]. Thus, implemented with enough experimental care, EIS is a powerful sensing tool for characterizing physicochemical systems and processes. EIS is an AC electrical method which uses AC impedance measurements as opposed to DC measurements. AC measurements are preferred in many electrochemical sensing systems for two main reasons. Firstly, many physical properties result in different dielectric relaxation behaviors which can only be sensed in high frequencies. Secondly, many systems contain aqueous salt solutions and

the salt present in the system results in large electrode polarization (EP) for DC and low-frequency inputs which can mask the other dielectric properties of the system, making sensing them difficult [3, 5, 8, 14].

Materials are polarized at different frequencies. Specifically, heterogeneous systems show frequency-dependent variation of permittivity [3, 5, 8]. Heterogeneous media have interfaces where different components meet. These interfaces are prone to charge build-up which can affect the dielectric behavior of the systems [5]. In heterogeneous media, characteristic polarization at certain frequencies is strongly dependent on interfacial polarization. This can be used to study different structural, topological, and physicochemical properties of heterogeneous systems that are related to interfacial polarization. Hence, EIS can be utilized to characterize multi-component systems based on the heterogeneous structure to characterize different properties of these systems such as particle shape and nonuniformity.

Multi-component systems are encountered in a variety of industries such as cosmetics, pharmaceutics, food processing, biomedics, and petroleum production. In many of these industrial applications, the multi-component systems are actually complex liquids such as liquid-liquid mixtures, colloidal dispersions, and emulsions. Therefore, the impedance properties of complex liquid systems has been extensively studied. The impedance spectroscopic (dielectric) behavior of multi-phase media has been studied analytically as well as numerically and experimentally.

One main goal of this thesis is to investigate different aspects of developing an inexpensive practical device for rapid characterization of the phase behavior and phase separation process of industrially relevant two-phase liquids. To do this, a thorough theoretical understanding of the dielectric properties of two-phase media validated by experimental characterization is detailed in subsequent chapters. Dielectric properties consist of both dielectric loss (resistivity or conductivity) and dielectric constant (permittivity). As shown in chapters 3 and 5, dielectric constant is typically a more sensitive parameter to phase be-

havior for the systems investigated here, therefore, the main focus of the literature review is on permittivity of complex media.

2.2 BASICS OF IMPEDANCE SPECTROSCOPY

The fundamental electric phenomenon behind impedance spectroscopy and dielectric dispersion analysis is the phase lag/lead of a system's response when subjected to an AC electric field. Impedance of a system, Z, defined as the ratio of electric potential (assumed to be the input, V) to electric current (assumed to be the output, I), is defined as a complex number that can present the phase shift, as well as the magnitude of the $\frac{V}{I}$ transfer function. Therefore, Z has a complex form of

$$Z = Re(Z) + jIm(Z) \tag{2.1}$$

where j is the unit imaginary number. Complex permittivity is similarly defined as [5]

$$\epsilon^* = \epsilon' - j\epsilon'' = \epsilon + \frac{\kappa}{j\epsilon_o\omega} \tag{2.2}$$

where ϵ' or ϵ, the real part of permittivity, is known as the dielectric constant (or just permittivity), and ϵ'' is known as the dielectric loss. As shown in equation 2.2, the dielectric loss (loss factor) is related to conductivity (κ). In equation 2.2, ω is angular frequency and ϵ_o is vacuum permittivity.

The typical way of presenting dielectric spectroscopy data is to plot imaginary part of impedance versus real part (Nyquist plot [3]), and both parameters versus frequency (Bode plots [3]). Alternatively, loss factor and permittivity can be plotted. The typical single-relaxation behavior of dielectric dispersion is a semi-circular plot known as Debye type relaxation [17] which is associated with a simple parallel $R|C$ circuit and can represent a "leaky" dielectric. If the system contains more physical complexity that can be captured in

distinguishable frequency ranges (different relaxation characteristic times), the EIS behavior can deviate from Debye [5] relaxation. The deviation has been formulated by different relations by many researchers including Cole and Cole [18, 19], Davidson and Cole [20], Williams and Watt [21], and many others. Asami [5] provides a comprehensive review and summary of the formulated dielectric relaxation modes. In practice, however, systems studied with EIS may not show a behavior already described by a model. Therefore, equivalent circuit modeling and inverse analysis, by choosing appropriate circuit elements that correspond to the physical behavior of the systems, are applied to interpret EIS data [3] and the equivalent circuit elements are parameterized using the data.

2.3 THEORY OF DIELECTRIC PROPERTIES OF COMPLEX MEDIA

2.3.1 Overview: dielectric relaxation phenomena - application to emulsion stability sensing

The dielectric response of a system is frequency-dependent and also depends on the physical phenomena in the system. The frequency range of response depends on the characteristic time of the process which, in turn, depends on the length scale of the physical phenomenon [6, 8]. Typically, the smaller the length scale of a physical process, the larger the characteristic relaxation frequency. Generally, processes related to electronic phenomena are associated with the smallest length scales and the highest frequencies. Next come atomic, dipolar, and ionic processes, respectively, which are associated with larger length scales and lower frequencies [6, 8]. The typical frequency range of effect for different physical phenomena is summarized and displayed schematically in figure 2.1. Processes related to large scale structural changes are associated with lower frequencies. It is therefore reasonable to conclude that sensing changes in static permittivity can be used for detecting phase changes in emulsions. However, in oil-in-water (O/W, water-continuous) emulsions, static measurements are associated with large electrode polarization (EP) er-

rors [8, 22, 23]. Therefore, instead of DC measurement, EIS and equivalent circuit (EC) modeling in a frequency range where the permittivity of each component can be assumed constant, (below 10^{-3}), can be applied for detecting phase changes in O/W emulsions using permittivity variation.

2.3.2 General mixture models

One of the first attempts to describe dielectric properties of two-phase mixtures was made by Maxwell in 1873 [24] and slightly modified later by Garnett [25] and Wagner [26]. The Maxwell-Garnett model reads

$$\epsilon_{eff} = \epsilon_{medium}\left(1 + \phi\frac{3(\epsilon_{dispersed} - \epsilon_{medium})}{\epsilon_{effective}(1-\phi) + \epsilon_{medium}(2+\phi)}\right) \tag{2.3}$$

where ϕ is the dispersed phase volume fraction in the mixture. Maxwell-Garnett equation is based on approximation of electric field between two parallel plates in presence of spherical droplets and assumes homogeneous distribution of a low volume fraction (below 2%) of spherical particles dispersed in the host medium. It is also applicable for liquid-liquid homogeneous mixtures [25]. Later, Bruggeman [27], Hanai [28], and Boyle [29] proposed models for dielectric properties of homogenous composite systems with higher concentrations of the disperse phase. Boyle's model is specifically of interest in this work because it is a simple model that takes into account deviation from spherical shape to spheroids. During phase separation, as spherical droplets cream and hit the top electrode, they are likely to deform to spheroids (see chapter 3). Boyle's model is defined as:

$$1 - \phi = \frac{\epsilon_{eff} - \epsilon_{disperse}}{\epsilon_{medium} - \epsilon_{disperse}}\left(\frac{\epsilon_{medium}}{\epsilon_{eff}}\right)^{A_a} \tag{2.4}$$

where ϕ is the dispersed phase volume fraction, and the exponent A_a is the depolarization factor of spheroidal flocs (a cluster of small droplets that form larger, usually spheroidal, bodies, and surface tension prevents them from coalescence) which is considered 0.1 for a

typical spheroid with axial ratio between 0.2 and 0.5 [30].

Different models were later developed by many researchers (especially Sillars [31], Asami [32], Skodvin [33], and Sjoblom [15]) who take into account shape and orientation of dispersed particles as well as other cases such as core-shell dispersed particles [5,34,35] and nonuniformity [14]. Based on the properties of the system tested in this thesis, the experimental results are compared to Maxwell and Boyle models.

2.4 EIS OF OIL-WATER EMULSIONS

2.4.1 Effect of particle size, shape, and flocculation

Unlike solid dielectrics, emulsions are likely to undergo topological changes, heterogeneity, and droplet shape change that can affect the structure of the interfaces between the components and phases, which changes the dielectric behavior of the systems [3, 5, 8, 14]. Analytical investigation and numerical modeling has been performed to understand the dielectric dispersion in emulsions. Some of the previous analytical work was outlined in the previous section.

In a series of publications about analysis of dielectric spectroscopy of emulsions, Hanai et. al. [28, 36–38] investigated dielectric properties of emulsions. They extended the Maxwell-Wagner theory to involve higher concentrations and heterogeneities. Hanai found little dependence of high-frequency permittivity on frequency in O/W emulsions. He also observed that increasing shear rate results in a decrease in the static permittivity which was attributed to the shear-driven disintegration of droplet flocs and larger drops. Skodvin et. al. [30] and Genz et. al. [39] also applied shear to their system as a means of disintegrating droplet flocs and larg drops and observed the effect of degree of flocculation on EIS response.

The effect of colloidal particle geometry on the EIS response has also been investigated. Sun et. al. [40] developed an equivalent-circuit-based analysis of single colloidal

particles in form of microcapsules, a core-shell configuration faced in biomedical suspensions, and found a resistive-capacitive behavior affected by the hollowness of the microcapsules, inner permittivity, and conductivity of the shells. The effect of particle shape has also been numerically investigated. Asami [7] studied a single micron-sized living cell with a special geometry using a 3D finite-element model (FEM). Tuncer et. al. [41, 42] applied FEM modeling to investigate the effect of particles' arrangement on EIS response. Effect of different particle shapes including varying core-shell structures has been studied using numerical simulations [43, 44]. Recently, simple permittivity modeling of homogenous dispersions in micro-channels and the effect of movement of dispersed water droplets in oil in the vicinity of the electrodes has been reported. Zhang et. al. [45] modeled charged aqueous droplets dispersed in oil under electrophoretic forces in micro-channels as serial capacitors affecting the total electric field. Then they determined the appropriate dielectric thickness associated with the capacitors, and experimentally verified their capacitive model for linear particle line-up. In emulsions, one of the main mechanisms that determine the shape of the dispersed elements, is flocculation of droplets which results in formation of flocs with a variety of shapes and sizes [8,30], making theoretical and experimental EIS investigation of flocculated emulsions important.

To investigate the effect of flocculation on dielectric properties of emulsions, Boned and Peyrelasse [46] assumed linear flocs of droplets. Later, Sjoblom et. al. [15] extended the Boned-Peyrelasse equation to involve flocculated emulsions with randomly flocculated drops. They studied drops forming spherical and spheroidal flocs forming bigger spheroidal flocs and investigated the effect of different structural parameters such as volume fraction of the flocs, packing factor of smaller flocs inside bigger ones, and the spheroid shape factor on the EIS response of W/O emulsions. Chapman [47] looked into the effect of emulsifying agents on the EIS of W/O emulsions and found that emulsions stabilized with magnesium stearate-based surfactant are well described by the Maxwell-Wagner model for spheres even with high volume fractions while the emulsions stabilized

with Span80 (non-ionic surfactant, partly soluble in water) had systematically higher static permittivities. This was attributed to linear flocculation caused by Span80. In a separate work by Sjoblom et. al. [15], it was shown for a different emulsion, that a flocculation-based correction to the sphere-based equations results in a more accurate prediction of the behavior of many flocculated systems. The structure of the flocs and the degree of coalescence, as opposed to flocculation, can vary based on the physical and chemical properties of emulsions which affects the dielectric behavior.

Genz et. al. [39] and Skodvin et. al. [48] each experimentally investigated the dielectric behavior of W/O emulsions under flow conditions. Both report lower static permittivity in the flowing emulsions compared to the stationary ones. However, the flocculation models are reported not accurate due to the complex dynamics of flocculation/disintegration processes as well as droplet-electrode contact. Midttun et. al. [49] studied the flocculated drop line-up under high external electric fields in W/O emulsions and found a decrease in the static dielectric loss and an increase in the static dielectric permittivity compared to the homogeneous floc models.

Current analytical models are based on homogeneous distribution of flocs and droplets (see also [8]). So these models fail when phase separation occurs. Phase separation in form of sedimentation or creaming can cause emulsion systems to behave differently and deviate from the behavior predicted by the analytical models describing homogenously distributed flocs. In this thesis, permittivity and resistance during transition from a well-emulsified to a separated system is theoretically and experimentally studied.

2.4.2 Percolation behavior and EIS

Percolation is a sudden morphological change in emulsions and microemulsions that changes the single-droplet structure to a fractal semi-continuous one [50]. This structural change can cause emulsion systems to behave in different ways. Since the effect of morphological structure on dielectric behavior is within the scope of this thesis (specifically, phase

separation is studied in this thesis), percolation is also of interest and is introduced here.

Lagues and Sauterey [50] observed an abrupt increase in conductivity of W/O emulsions during percolation transition by increasing dispersed phase volume ratio. Same behavior was reported by Zhang et. al. [51], Mehta et. al. [52], Baptista and Tran [53], and Mathew et. al. [54]. Feldman et. al. [55] observed a decrease in the low-frequency relaxation time (a relaxation shift towards higher frequencies) at the percolation onset that was initiated by temperature rise. Fordedal and Sjoblom [56] applied a DC field when measuring the dielectric response of a W/O emulsion sample. They observed an increase in the static permittivity of the sample up to a certain point when an abrupt decrease was observed, after which the increase re-appeared. This was attributed to percolation which caused a sudden geometric change in the emulsion. In summary, one of the main outcomes of percolation in W/O emulsions is a sudden change (increase) in conductivity which has not been reported for O/W emulsions. However, percolation can also affect the topological structure and therefore permittivity of emulsions, but this behavior, and even occurrence of percolation itself, highly depends on sample thickness and EIS electrode configuration [57].

2.4.3 EIS of O/W emulsions versus W/O emulsions

EIS is typically more appliecable to oil-continuous emulsions rather than water-continuous ones. The reason is that in low-frequency dielectric spectroscopy of electrolytes, the ions accumulate on the electrode surface [8, 22, 23, 58, 59]. The impedance and capacitance caused by this type of polarization can easily become dominant in low frequencies and outweigh other properties of the system and the corresponding relaxation behaviors [8,22,23]. The consequence of this is that low-frequency EIS of O/W emulsions is very difficult while high-frequency measurements can still be performed. Even in oil-continuous emulsions stabilized with ionic surface active agents, a low frequency dispersion (LFD) due to electrode polarization (EP) was reported at below 1Hz [60].

In many applications of EIS including biological applications (for instance see [9]), the sample is conductive, so different approaches have been taken to extract bulk sample properties from the EIS data. One approach is to consider the accumulated ion layer caused by EP as a serial R-C [8]. It is likely to observe deviation from pure capacitor behavior and get a constant-phase-element (CPE) behavior instead [9, 61, 62]. These method are most effective when the frequency range of interest is generally larger than the frequencies where EP is observed. If low-frequency behavior of a system is of interest, it is likely to have considerable errors in distinguishing between EP effects and actual sample properties. In those cases, four-electrode EIS is applied as first suggested by Schwan and Ferris [63]. Unlike 2-electrode EIS, in four-electrode measurements, the electric current carrier electrodes (which are prone to EP) are not used for potential measurements. Instead, two other electrodes, known as reference electrodes, are used [63, 64]. However, 4-electrode measurements do not resolve all concerns about EIS of conductive media [5]. Even with 4-electrode measurements applied, the conductivity gradient in the system may still affect the EIS response. Also, if the measurement terminals are needle-shaped electrodes, they will only measure the potential in specific points in the sample while the blocking surface or mesh electrodes measure a surface average potential. If the electrodes are chosen to be blocking surfaces or meshes, they can distort the electric field considerably and disturb the experiments. Depending on the physicochemical and geometrical properties of samples, different configuration of test cells may be used. For instance, Asami [7] developed a test cell for EIS of biological cell suspensions by using membranes that are freely permeable to ions but not to biological cells.

In this thesis, since the high frequency behavior shows a classic semi-circle $R|C$ behavior, it is possible to distinguish the sample properties from EP effect (which shows a CPE behavior) with apropriate equivalent circuit modeling. However, 4-electrode measurements are also carried out in special cases to show the validity of the measurements (see chapter 4).

2.4.4 EIS as a process monitoring tool

Since EIS is sensitive to complex medium phase changes, it can be used as a tool for monitoring processes. Araujo and Oliviera [65] were able to detect a temperature-driven phase inversion in O/W/O emulsions where the system was shown to reversibly shift from oil-continuous to water-continuous by measuring a reversible decrease in the real part of impedance. Barbosa et. al. [66] detected the process of micro-emulsion formation by observing multiple relaxation frequencies. Beer et. al. [67] looked into the process of making O/W/O double emulsions using EIS and showed that permittivity measurement can be a potential tool for determining when to stop stirring or to adjust stirring speed to prepare stable O/W/O emulsions. Perini et. al. [68] reported changes in the equivalent circuit element values as a result of treating petroleum with strong static electric fields. The experimental measurement platform developed in this thesis, can be used for monitoring processes involving or prone to phase separation. It is also noteworthy that a milli-fluidic device for oil-water separation has been reported [69] giving high separation efficiency. The separation process in such a device may be monitored by integrating the milli-scale EIS fixture (as proposed in this thesis) with the milli-fluidic separation device, which is beyond the scope of this work.

2.4.5 EIS applied to crude oil

EIS is often applied to carefully prepared samples as it is very sensitive to sample properties. However, the dielectric behavior of crude oil emulsions has also been investigated, and interesting results have been obtained. Skodvin et. al. [33] stabilized different volume fractions of water drops in crude oil and compared the dielectric behavior of the emulsion to theoretical relations for spherical droplets and spheroidal flocs. At low water volume fractions, water droplets flocculate to form high aspect ratio spheroids while at higher water volume fractions, they more symmetrical flocs [33].

Lesaint et. al. [70] investigated the relation between conductivity and viscosity in crude oil diluted in toluene and heptane and found an inverse relation between conductivity and viscosity. They also observed different conductivities in systems diluted with toluene and heptane. They concluded that conductivity of crude oil is determined by the aggregation pattern of asphaltene rather than their concentration because asphaltene is known to aggregate more in heptane than in toluene. Lesaint et. al. [71] attempted to relate different crude oil characteristics such as viscosity and aggregation state of different molecules present in crude oil such as asphaltene to dielectric dispersion observed in EIS. However, the complexity and the large number of components in crude oil makes this analysis extremely difficult. EIS of crude oil components separated and studied independently has also been reported [72]. The effect of water in petroleum has been studied by Perini et. al. [68]. They found an increase in the resistance when water was added to dehydrated oil, which seems to contradict what is expected. They attributed this to formation of rigid films on water-oil interfaces and higher stability of W/O emulsions.

In this subsection, previous literature was highlighted to show that EIS investigation of either bulk or interfacial properties of industrially relevant liquids is possible. However, due to complexity of these samples, analysis of the EIS results and relating them to physical properties of the systems is extremely difficult. Thus improving these technologies, is an important challenge requiring detailed analysis and a comprehensive experimental data set. Cleaning experimental setups from industrial samples such as bitumen, in order to carry out multiple experiments, is challenging. As a result, development of an inexpensive disposable test cell (which is one contribution of this thesis) can help enable progress of EIS for industrially relevant samples.

2.5 EXPERIMENTAL PLATFORMS FOR EIS

2.5.1 Commercial test fixtures

Sample holder plays an important role in EIS experiments. Sample holders should ensure reliable and reproducible experiments through repeatable sample loading and should minimize systematic errors such as fringing on the electrode edges. While custom-made fixtures may be needed to be fabricated for different experiments (as in [60, 68]), there are commercial test fixtures available for EIS of solids and liquids. In this section, the most commonly used test fixtures are briefly discussed.

2.5.1.1 Solartron 12962A and 12963A

These two parallel-plate sample holders are designed for EIS of solid materials using a 2-electrode configuration with circular electrodes. The sample holder consists of two parallel electrodes, one of which is fixed in position and the other which can be moved into contact with the sample by adjustment of a micrometer. The sample holder makes use of guard ring and reference techniques in order to reduce fringing effects at the edge of the sample. The electrodes provided are 10mm diameter to 40mm diameter.

2.5.1.2 Solartron 12964A

This sample holder is similar to 12962A and 12963A. It also makes use of guard ring techniques but is shaped as a container in order to be able to measure small samples of liquid or powders. This is also a 2-electrode test cell, however, the reference electrodes can be designed and placed in the sample [65].

2.5.1.3 Novocontrol BDS 1307

This is a co-axial cylindrical cell for liquids with sample thickness of 2.7mm and inner diameter of 20mm and gold-coated electrodes.

2.5.1.4 Novocontrol BDS 1308 and 1309

These two sample holders are parallel-plate 2-electrodes test cells with 0.5mm (BDS 1308) to 5mm (BDS 1309) sample thicknesses. These two sample holders are designed for EIS of volatile liquids and provide good sealing of the sample by pressing the elctrodes by means of small springs. The electrodes are gold plated. In the BDS 1309, the sample space is thicker to enhance bulk properties as opposed to electrode surface effects and reduce the EP impedance. The manufacturer states that different parts of the test cell can be disassembled and cleaned, and the parts can withstand different solvents.

2.5.1.5 IRlab, CL-1 142

This test cell is a co-axial probe with a 2-electrode configuration with 6cm length and 3.3mm separation distance which is immersed in the liquid sample [71].

2.5.1.6 Agilent 16451B

This is a parallel-plate two-electrode test fixture with a 10mm sample thickness and 10mm-50mm electrode diameter suitable for EIS of solid samples by sandwiching the sample between the two electrodes.

2.5.1.7 Agilent 85070E and 85070D Dielectric Probe Kits

Agilent 85070E is a package consisting of a probe as well as a frequency response analyzer suitable for high-temperature dielectric measurements. It provides a co-axial 2-electrode configuration with 2.2mm sample thickness between stainless steel (outer) and nickel-plated tungsten (inner) and is suitable for liquid and semi-solid dielectrics. The working frequency range of the FRA is 200MHz to 50GHz which is suitable for solid electronics applications. 85070D is similar to 85070E with a 7mm sample thickness between Inconel and stainless steel electrodes. 85070D is suitable for wide temperature range from -40 to

+200 degrees Celsius.

2.5.1.8 Commercial test cells cleaning

As described in the instructions of commercial EIS test fixtures, cleaning test setups is an important issue when conducting multiple experiments. Since EIS is very sensitive to cleanness of the electrodes and is affected by contamination of the sample, cleaning the test cells after each experiment is crucial. However, many industrially relevant samples contain solids in them which can foul in the EIS test cells. Samples may be so viscous that cleaning them from the electrodes becomes difficult. For example, bitumen is not easily removed from surfaces, and even if appropriate strong solvents are used, the solvents may affect the electrode surface properties which, in turn, may affect EIS results. Fabrication of inexpensive disposable EIS test cells is reported in this thesis. One of the contributions of this thesis is fast and inexpensive fabrication of EIS text fixture which allows disposing of the sample and the sample holder after testing "dirty" samples.

2.5.2 EIS in micro-scale

Capability of EIS in sensing properties of biological systems has attracted attentions of researchers to apply this technique in biosensors. However, many biological systems are small and require fabrication of micron-sized EIS electrodes or electrode arrays [73]. In fact, processes such as bacterial activity can only be captured if the electrodes closely enclose the medium with bacteria culture. Since the sensitivity of EIS devices drop by increasing sample size [5], it is advantageous to use micro-scale EIS setups. In the literature, EIS has been performed with different electrode separations ranging from micrometers to 10 centimeters and this will be described next.

Iliescu [74] et. al. developed a micro-fluidic test setup for EIS of biological samples especially for detection of dead and living yeast cells. Tan et. al. [75] developed a microfluidic test cell with characteristic length of 60μm for E-Coli detection. Other cell detection

applications of EIS in micro scale has been done mostly to track processes associated with bacterial growth in different tissues [76–79]. Integration of microfluidic EIS sensors on a chip to develop bacterial metabolism sensors has been performed by Gomez-Sjoberg et. al. [80]. Also, since many biological samples are water-based, EP is likely to happen which can disturb experimental measurements. Characterization of EP in microscale has been performed by Pradhan et. al. [23].

EIS of oil-water emulsions has also been studied at a micro scale. Wang et. al. [13] studied the EIS response of lubricants on a 12μm sample with ITO-coated glass electrodes. Lvovich and Smiechowski [12] studied dielectric properties of lubricants on 100μm samples. Mostowfi et. al. [10, 11] characterized oil-water interface in a single droplet with EIS. These studies show that EIS at a microfluidic length is highly sensitive but requires extreme care in fabricating and handling the devices. The microfluidic devices are expensive to fabricate, and foul readily when subjected to industrially relevant fluids.

To my knowledge, there has been no systematic work reported to determine right length scale for EIS of different types of samples. One of the contributions of this thesis is to study the permittivity of different two-phase systems to understand the relation between the characteristic length scale of the dispersed element with the appropriate length scale of the EIS experiments.

2.6 OTHER APPLICATIONS OF EIS

For completeness, some miscellaneous applications of EIS are briefly mentioned in this section.

2.6.1 Biosensors

Use of EIS to sense cell growth or detect living organisms is usually done by confining very thin samples between electrodes (to achieve a reasonable sensitivity) and is thus

considered microfluidic. Cheng et. al. [76] developed a microfluidic device for counting bacteria during binary fission in a low-conductivity medium based on sensing the conductivity increase. Accumulation of bacteria on the electrodes was a problem and can be regarded as the biological counterpart of the electrode polarization phenomenon in O/W emulsions. Zhu et. al. [77] tried to limit the medium under study to very thin layers (in the order of 10 microns) while avoiding extreme microfabrication difficulties. They developed a microfluidic device with a channel width of 100 microns and used KCl solutions to both squeeze the non-ionic non-polar bacterial culture and to act as electrodes. Since the biological applications of EIS are most effective in small scales, improving the surface qualities of electrodes for EIS as a biosensing tool is an ongoing field of research [81].

2.6.2 Food processing

EIS has been investigated as a tool for conductivity-based detection of salt in food technology [82]. Permittivity measurements have also been applied to characterization of quality of edible oil products [83].

2.6.3 Solid electronics

EIS of composite materials has been used is solid electronics to develop dielectrics and capacitors with different functionalities. Dielectric properties of multi-component solids has been studied theoretically and experimentally. The dielectric properties of multiphase solids and liquids are closely related in many cases and both started with the effective medium theories of Maxwell-Wagner. In solid electronics, most analytical effective dielectric models are based on geometrical configuration, while in liquid samples, the models are more based on the interactions of the dispersed elements with one another and with the host medium.

Brosseaus and Beroual [84] numerically investigated electric field and dielectric properties in homogeneous dispersion of inclusions in a solid host medium and studied the

effect of particle shape (for instance spheres, cylinders, and ellipsoids) on permittivity. Their results can be compared to the works of Skodvin et. al. [30] and other researchers who studied dielectric properties of flocculation in emulsions, as mentioned in section 2.4. Other numerical and analytical works have also reported EIS investigation of the homogeneous dispersion patterns in composite dielectrics [85–87] as well as conductor-insulator materials [88]. In some cases, completely different approaches from the ones seen in the field of EIS of emulsions have been taken. For instance, Ono et. al. [14] calculated the effective permittivity of a specific solid dielectric with inclusions, not by using modified effective medium theories or solving the electric field, but by dividing the whole composite domain to small increments (assuming each increment to be a capacitor with uniform dielectric) and integrating the increments to determine the effective permittivity of the composite dielectric.

2.7 SUMMARY OF EXPERIMENTAL CHALLENGES IN EIS OF EMULSIONS

In sections 2.4, 2.5.1, and 2.5.2, main experimental challenges for the application of EIS are described. Those challenges are summarized below:

- Electrode polarization in conductive samples at low frequencies
- Choice of length scale
- Cleaning test setups from viscous samples

2.8 ANALYSIS OF EIS DATA

Two main ways of looking at EIS data are detailed in the literature. One, (for instance [15, 30]) focus on observing relaxations in different frequencies and detect or characterize new physical behaviors based on the relaxations of the samples. Two, (for instance [3, 16, 35, 89]) predominantly use the equivalent circuit (EC) analysis technique to quantify the

EIS behavior and relate the physical behavior of the samples to an equivalent circuit, or measure certain physical properties based on the EC modeling. In this thesis, the second approach is taken to relate the equivalent electrical properties of the sample to physical properties such as stability and phase separation.

Correlating the EIS behavior of a system to electric circuit elements such as capacitors and resistors is the basis of this method [3]. While EIS data might generally be caused by dielectric dispersion and variations of permittivity (especially in wide frequency ranges), the equivalent circuit scheme considers circuit elements with frequency-independent properties (for instance a capacitor with constant permittivity) which produce frequency-dependent impedances. For example, impedance of a capacitor is $\frac{-j}{\omega C}$ and is a function of frequency while C itself is frequency-independent. Different circuit elements with different parameter values can mimic the EIS response in different frequency ranges. For example, in an equivalent circuit with two capacitors, the capacitor with a large value (small $\frac{1}{C}$ magnitude) reflects lower frequencies compared to a capacitor with a small value which highlights higher-frequency data.

In EC modeling, an equivalent circuit model of sufficient complexity to match the physics to the desired accuracy should be chosen. Then the EIS data is used to parameterize the equivalent circuit by minimizing the overall difference between the model and the measurements. The most widely used method for fitting is complex nonlinear least squares [89] that minimizes a weighted summation of the real and imaginary error of the measurements and the model.

To graphically depict EIS data, Nyquist and Bode (magnitude and phase) plots are often used. Three dimensional presentation of Bode plots showing magnitude and phase of the impedance simultaneously as a function of frequency has also been done [3]. For Bode plots, to display impedance changes over a wide frequency range, a logarithmic frequency scale is often used. Distinguishing frequency shifts (caused by capacitance change) may be difficult in Bode plots, hence, EC values is the best way to present the

differences caused by capacitance changes.

2.9 SUMMARY

In this chapter, a literature review of EIS was performed with a focus on topics relevant to this thesis. General composite dielectric models were introduced and analytical formulations modeling dielectric properties of homogeneous emulsion systems with different particle shapes and structures based on flocculation modes were outlined. The current status of the field of EIS analysis of emulsions was detailed based on the literature in different aspects including numerical, analytical, and experimental works. Commercial test fixtures as well as some custom-made test setups were discussed and implementation of EIS in micro-fluidic systems was also detailed. Moreover, applications of EIS of emulsions in different fields from crude oil characterization to biosensors were briefly mentioned. The challenges in EIS of emulsions in different applications were listed.

Based on the literature review of this chapter, the following areas in which more scientific work can be done are identified. These areas are addressed in different chapters of this thesis using a combination of analytical, numerical, and experimental techniques. These areas are:

- The dielectric behavior of oil-water systems during phase separation processes, such as sedimentation and creaming, has not been studied.
- It was explained in the literature review that different length scales have been used in EIS experiments of various systems including micro-scale. While micro-fluidic measurements are highly sensitive, there has been no systematic scientific work to show whether they are applicable to emulsions or not and how droplet size may flaw micro-fluidic EIS experiments for emulsions.
- The idea of making inexpensive, fast-fabricated, and disposable EIS test cells is proposed.

- Sensing stability and phase separation of O/W emulsions based on permittivity measurements (phase separation is detected based on permittivity decay during phase change). Interesting characteristics of the permittivity-based sensing technique are revealed by EIS of O/W emulsions where unlike W/O emulsions, where conductivity variations reflect different physical attributes of the emulsions, their variations are not considerable in O/W emulsions.

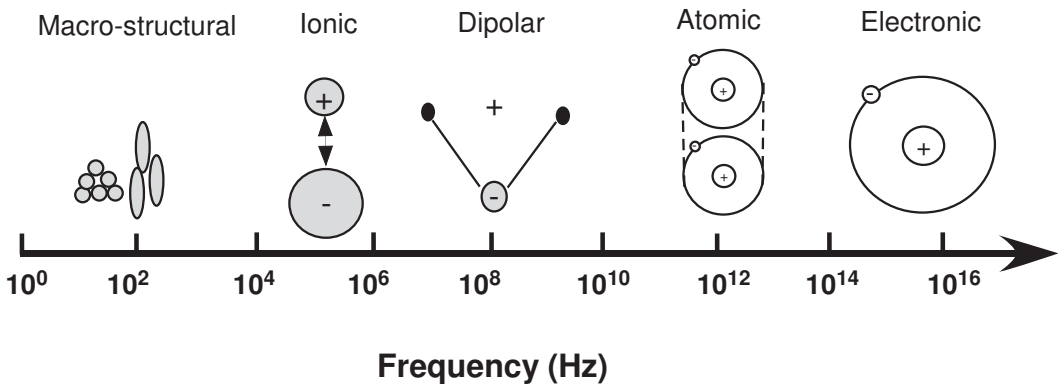

Figure 2.1: Schematic of approximate frequency spectrum of effect for different physical phenomena.

CHAPTER 3

ANALYTICAL AND NUMERICAL MODELING

3.1 INTRODUCTION

Determining different experimental attributes of the developed device and relating the electrochemical impedance spectroscopy (EIS) data to the phase behavior of emulsions are not possible without a thorough theoretical understanding of the electrical characteristics of two-phase liquid systems. In this chapter, the theory behind the effective capacitance (permittivity) and resistance (resistivity) of two-phase media is introduced. A simple analytical explanation is provided for describing the effect of gradual phase separation of an emulsion sample on the emulsion permittivity. Moreover, based on a finite element numerical model of the experimental setup, the effect of droplet coalescence and changes in the structure of the dispersed phase on permittivity is investigated. The theoretical discussions of this chapter are referred to for justifying the decisions made for the design of the experimental setup (chapter 4) and are compared to the experimental results in chapter 5.

3.2 PERMITTIVITY OF TWO-PHASE MEDIA

Electric permittivity and susceptibility are measures of how natural molecular-scale dielectrics of a medium align (polarize) in response to an external electric field. In other

words, permittivity is a measure of the capability of a medium to transmit (permit) electric field. Permittivity is also related to the capability of different materials to store electric energy in response to an external electric field. Permittivity (or dielectric constant) of a single-phase medium is determined by the atomic/molecular properties of the medium. However, dielectric constant of a two-phase medium, either an emulsion or a solid dielectric with inclusions, is affected by different parameters including the permittivity of each component, proportions of different components, and the geometrical (topological) structure of the dispersed phase (or inclusions in solid dielectrics) in the host medium.

In chapter 2, the analytical models for homogeneous two-phase mixtures were discussed based on the literature. Also, parameters such as particle shape and droplet flocculation and their effect on dielectric spectroscopy of emulsions were reviewed. Since one of the attributes of the developed experimental platform in this thesis is the capability of capturing phase separation dynamics with variations in capacitance (permittivity), in this section, different structures of the dispersed phase and how they affect the effective permittivity is investigated.

Figure 3.1 illustrates a schematic of extreme configurations of the dispersed phase in the host medium and their capacitor electrical analogy. As shown in this figure, the dispersed phase may be homogeneously distributed in the host medium or may form different geometries including the extreme cases of columnar, laminar or brick-wall configuration. In figure 3.1, the capacitor model of the aforementioned configurations is also illustrated. The homogeneous distribution (figure 3.1-i) may be modeled as one capacitor with an effective dielectric constant determined from one of the models described in section 2.3 of chapter 2. The columnar configuration (figure 3.1-ii) may be modeled as parallel capacitors. The effective capacitance and dielectric constant of the system can be represented as:

$$C_{eff} = C_1 + C_2 + C_3 + ... \tag{3.1}$$

$$\epsilon_{eff} = X_1\epsilon_1 + (1 - X_1)\epsilon 2 \tag{3.2}$$

where C_{eff} and ϵ_{eff} are the effective capacitance and dielectric constant, C_1 and C_2 are capacitances of each column of the dispersed phase or the host medium, ϵ_1 and ϵ_2 are dielectric constants of each component, and X_1 is the volume fraction of component 1. As implied in equation 3.2, the effective dielectric constant linearly depends on the dielectric constant of each component weighted by the component volume fraction and this is independent of how many columns of the dispersed phase are formed in the host medium.

The laminar configuration (figure 3.1-iii), may be modeled as serial capacitors. The effective capacitance and dielectric constant of the system can be represented as:

$$\frac{1}{C_{eff}} = \frac{1}{C_1} + \frac{1}{C_2} + \frac{1}{C_3} + ... \tag{3.3}$$

$$\frac{1}{\epsilon_{eff}} = \frac{X_1}{\epsilon_1} + \frac{1 - X_1}{\epsilon_2} \tag{3.4}$$

or

$$\epsilon_{eff} = \frac{\epsilon_1\epsilon_2}{(1 - X_1)\epsilon_1 + X_1\epsilon_2} \tag{3.5}$$

with the same nomenclature as equations 3.1 and 3.2. Equations 3.4 and 3.5 hold no matter how many layers of the dispersed components form in the host medium.

The brick-wall configuration (figures 3.1-iv and 3.1-v) illustrate an extreme case where the dispersed phase sediments (creams) but does not form a layer covering the bottom (top) electrode (for example due to viscosity). This configuration may be modeled with capacitors in two ways as shown in figures 3.1-iv and 3.1-v. The effective dielectric constant of the system based on the two models can be calculated using serial and parallel capacitor formula as:

model 1 (figure 3.1-iv):

$$\frac{\epsilon_{eff}}{\epsilon_2} = \frac{1}{1 - X_1^{1/3} + \frac{{X_1}^{1/3}}{1 - X_1^{2/3}\left(1 - \frac{\epsilon_1}{\epsilon_2}\right)}} \tag{3.6}$$

model 2 (figure 3.1-v):

$$\frac{\epsilon_{eff}}{\epsilon_2} = 1 - X_1^{2/3} + \frac{X_1^{2/3}}{1 - X_1^{1/3}\left(1 - \frac{\epsilon_2}{\epsilon_1}\right)} \tag{3.7}$$

Models introduced in figures 3.1-i to 3.1-v and equation 3.1 to 3.7 result in different variation of dielectric constant (capacitance) with dispersed phase volume fraction. In other words, the structure of the dispersed phase and how it is distributed in the host medium affect the effective dielectric constant of the two-phase liquid. Figure 3.2 depicts the effective dielectric constant of oil-water emulsions calculated based on different homogeneous-mixture and multiple-capacitor models as discussed above. The dielectric constant of water is $\epsilon_{r,water}$=80 and the dielectric constant of oil is considered to be $\epsilon_{r,oil}$=2, which is the case for decane with which several experiments were done (the results will be discussed in chapter 5). As shown in figure 3.2, the homogeneous-mixture (Maxwell-Garnett and Boyle, see chapter 2) models which represent systems with homogeneously distributed inclusions, are close to the parallel-capacitor (linear) model, especially in very low or very high volume fractions of oil. However, when the dispersed phase is assumed to sediment or cream, which is best described by the serial-capacitor model, the deviation from homogeneous-mixture and parallel-capacitor models becomes more prominent. Therefore, it can be concluded that phase separation in the form of creaming or sedimentation can be sensed very well with a parallel-plate capacitance test cell. The experimental setup developed in this thesis is shown to be capable of capturing the phase separation dynamics of emulsions as the emulsion becomes unstable and the less dense phase (oil) gradually creams. This feature of the developed system can be used for stability sensing

of emulsions in different applications. On the other hand, as figure 3.2 suggests, if an emulsion system undergoes droplet coalescence , but remains homogeneous with no considerable phase separation (only the droplets become larger), the variations in the effective dielectric constant of the emulsion sample will not be considerable compared to a system undergoing phase separation. Therefore, the main capability of a capacitance-based measurement cell, in terms of emulsion stability sensing and process monitoring, is to capture *phase separation* based on variations of capacitance.

3.3 RESISTANCE OF TWO-PHASE MEDIA

Electric resistance of a system is a measure of capability of the system in resisting passage of electric current through it. Resistance and conductivity measurement in emulsions is extensively used for investigating colloidal structure of oil-continuous emulsions rather than water-continuous ones [50, 51, 90] especially in determining the onset of percolation in water-in-oil microemulsions [52–54, 57, 91]. The percolation threshold is sensed with a sudden increase in conductivity. As shown in figure 3.3-a, before percolation in a W/O emulsion, the main mechanism of current passing through the emulsion is through the highly resistive oil phase or movement of micro-droplets. However, with increasing water (salt-water electrolyte) volume fraction, the system reaches percolation. As a result of this phenomenon, multiple passages of the electrolyte form between the two electrodes for the current and at the onset of percolation, the conductivity abruptly increases. Different parameters, such as temperature and presence of surface-active agents may affect the percolation threshold. However, in water-continuous emulsions (O/W emulsions), since the passage for current is already provided by the continuous phase, percolation cannot be detected using conductivity measurements. In O/W emulsions, the resistance of the system does not change considerably with increasing the oil volume fraction unless either the dispersed phase is miscible with the host medium (causing a change in the medium effective

conductivity, as in glycerol-water mixtures), or oil is added to a level (more than 50%) where phase inversion occurs and the system turns into a W/O emulsion where current passages may be blocked by the continuous oil phase.

Based on the above discussion, while resistance measurements with the developed test cell in this thesis may be used for detecting percolation in oil-continuous emulsions, this type of measurement may not be useful in sensing oil/water ratio or phase separation in water continuous emulsions. In O/W emulsions, even if phase separation occurs, presence of percolated water droplets in the creamed oil-rich phase may delay or inhibit a sudden decrease in conductivity. Therefore, the focus of this thesis is on using capacitance (permittivity) measurements for determining the stability of emulsions.

3.4 PHASE SEPARATION AND EFFECTIVE PERMITTIVITY OF EMULSIONS

3.4.1 Physical process

As discussed in section 3.2, if the geometrical structure of an emulsion film confined between parallel plate electrodes changes, the effective dielectric constant of the emulsion may change. In particular, as shown in figure 3.2, if the dispersed phase forms a creamed or sedimented layer, the changes in the effective permittivity of the emulsion and therefore the capacitance of the test cell will become more considerable. In this section, the forces acting on droplets that may cause them to cream or sediment are discussed.

As shown in figure 3.4, the fresh O/W emulsion (figure 3.4-a) forms a homogeneously distributed two-phase system, which is best described by the Maxwell-Garnett model for homogeneous dispersion of spherical droplets as discussed in chapter 2. However, if the emulsion becomes unstable over time, the droplets coalesce or flocculate to form larger drops or flocs. The larger drops/flocs of oil then move upward under buoyancy force. This process may be explained by introducing a dimensionless parameter for comparing buoyancy and interfacial forces. The Bond (Bo) number is defined as the ratio of gravitational

to interfacial forces [92]. Assuming spherical drops (or spheroids with small aspect ratios), the *Bo* number can be expressed as

$$Bo = \frac{\texttt{net gravitational force}}{\texttt{interfacial forces}} = \frac{\Delta\rho V g}{2\gamma/R} \tag{3.8}$$

where $\Delta\rho$ is the density difference between the dispersed phase and the host medium, V is the drop volume, R is the drop radius and γ is the interfacial tension between the two phases. Equation 3.8 can be further simplified to

$$Bo = \frac{\texttt{buoyancy force per unit area}}{\texttt{interfacial pressure}} = \frac{\Delta\rho g R^2}{\gamma} \tag{3.9}$$

As equation 3.9 suggests, the ratio of buoyancy force per unit area to the pressure caused by interfacial tension is proportional to R^2 and as the droplet size increases due to coalescence of smaller droplets, the buoyancy force becomes more and more dominant, resulting in upward movement of large drops and flocs. This is shown in figure 3.4-b. As the larger drops reach the top electrodes, they will be squished to spheroids under the buoyancy force as shown in figure 3.4-c. Therefore, the oil-rich creamed portion of the emulsion may be best described by Boyle's (see chapter 2) model for a mixture of spheroidal particles in a continuous medium. As time passes, the oil-continuous portion becomes richer in oil and may completely break (as it was the case for the decane-water emulsions tested in this thesis) and form a completely separate layer (figure 3.4-d). As schematically illustrated in figure 3.4, some oil will be left in the water-continuous layer and some droplets form a relatively more stable O/W emulsion with lower fraction of oil in the water-continuous part.

While an emulsion system undergoes the above process, the capacitance (dielectric constant) of the emulsion gradually changes from a homogeneous (or parallel-capacitor) value to a much lower value close to the series-capacitor configuration. Depending on the degree of breaking of the spheroids in the oil-rich part and the continuity of the oil-rich

layer, the capacitance may vary. In other words, if the oil-rich emulsion completely ripens to a pure oil layer, the capacitance will be closer to the serial value and, on the other hand, if more water is present in the oil-rich creamed portion, the deviation from the serial-capacitor value will be higher. This will be numerically investigated in section 3.5. Also, depending on how much oil is present in the water-continuous phase, the capacitance may deviate from the serial-capacitor model.

3.4.2 Thickness of the creamed layer as a function of capacitance

Thickness of the creamed layer is a measure of ripening of an emulsion system and a theoretical formula relating the measured capacitance to the creamed thickness can provide a quantitative measure of how much of the dispersed phase has been separated from the emulsion. It will be discussed in chapter 5 that a decay function can be fitted to experimental values of capacitance, and provide capacitance of the emulsion as a function of time while the emulsion undergoes phase separation. With this fitted function, industrially relevant emulsions can be calibrated based on how fast their capacitance decays, and with a formula relating capacitance to the separated thickness, real-time capacitance measurement of calibrated systems can instantly provide the separated layer thickness and the degree of phase separation. In this section, the formula relating capacitance to the thickness of the separated phase is derived.

As shown in figure 3.5, it is assumed that the oil-rich layer completely breaks and no water is trapped in it. The permittivity of the water-continuous phase which is an O/W emulsion is shown by $\epsilon_{O/W}$, which will change as more oil creams. The permittivity of the oil layer is denoted by ϵ_O, and the permittivity of pure water is denoted by ϵ_W. The thickness of the oil layer is denoted by d_{oil}, the maximum (final) oil thickness with 100% of oil content creamed is denoted by d_{oil}^{max}, and the total film thickness is denoted by D. The water-continuous phase can be considered a homogeneous mixture and its permittivity can be approximated with a parallel-capacitor model described by equation 3.2. However, the

oil ratio of the O/W layer is not constant and decreases as more oil creams. Presenting volume ratio in terms of thickness, the permittivity of the water-continuous phase will be

$$\epsilon_{O/W} = \frac{d_{oil}^{max} - d_{oil}}{D - d_{oil}}\epsilon_O + \left(1 - \frac{d_{oil}^{max} - d_{oil}}{D - d_{oil}}\right)\epsilon_W \tag{3.10}$$

The O/W film and the oil film can be considered as two capacitors in series and the permittivity of the whole sample film can be calculated based on serial-capacitor model (equation 3.5):

$$\epsilon_{eff} = \frac{\epsilon_O \epsilon_{O/W}}{\left((1 - \frac{d_{oil}}{D})\epsilon_O + \frac{d_{oil}}{D}\epsilon_{O/W}\right)} \tag{3.11}$$

where ϵ_{eff} is the total effective permittivity of the cell. Knowing that $C = \epsilon\frac{A}{D}$, the capacitance of the cell will be

$$C_{eff} = \frac{\epsilon_O \epsilon_{O/W}}{\left((1 - \frac{d_{oil}}{D})\epsilon_O + \frac{d_{oil}}{D}\epsilon_{O/W}\right)}\frac{A}{D} \tag{3.12}$$

where C_{eff} is the effective capacitance of the cell and A is the surface area of the electrodes. Substituting $\epsilon_{O/W}$ from equation 3.10 into equation 3.12, the effective capacitance becomes

$$C_{eff} = \frac{A\epsilon_O(D\epsilon_W - d_{oil}\epsilon_O + d_{oil}^{max}\epsilon_O - d_{oil}^{max}\epsilon_W}{D^2\epsilon_O + d_{oil}d_{oil}^{max}\epsilon_O - d_{oil}d_{oil}^{max}\epsilon_W - 2Dd_{oil}\epsilon_O + Dd_{oil}\epsilon_W} \tag{3.13}$$

Solving equation 3.13 explicitly for d_{oil} gives the oil thickness as a function of the measured capacitance (C_{eff}):

$$d_{oil} = \frac{D\epsilon_W + d_{oil}^{max}\epsilon_O - d_{oil}^{max}\epsilon_W - \frac{C_{eff}D^2}{A}}{\epsilon_O + \frac{C_{eff}(D\epsilon_W - 2D\epsilon_O + d_{oil}^{max}\epsilon_O - d_{oil}^{max}\epsilon_W)}{A\epsilon_O}} \tag{3.14}$$

The calculations were done using the symbolic math software MathCad. Equation 3.14 provides the oil layer thickness (degree of emulsion breaking) explicitly as a function of the measured capacitance. Therefore, the test cell may be used to determine the degree of

emulsion breaking based on capacitance measurements.

3.4.3 Effective permittivity as a function of degree of phase separation

Recalling equations 3.10 and 3.11, permittivity of the water-rich phase ($\epsilon_{O/W}$) from equation 3.10 can be substituted into equation 3.11 to give the effective permittivity of the system as a function of oil layer thickness, d_{oil}. Defining η as $\eta = \frac{d_{oil}}{d_{oil}^{max}} \times 100$ and knowing that this parameter can be regarded as the degree of phase separation, and also recalling $\frac{d_{oil}^{max}}{D} = \phi_{oil}$, where ϕ_{oil} is the total oil volume fraction in the emulsion, the effective dielectric constant of the system can be presented as a function of the degree of phase separation (η) during the phase separation process for different oil volume fractions (ϕ_{oil}). Figure 3.6 illustrates the decay in the effective permittivity as a function of degree of phase separation ($\eta = \frac{d_{oil}}{d_{oil}^{max}}$) for different oil volume fractions as the systems undergo phase separation. Figure 3.6 shows that the ϵ_{eff} curves start at the parallel-capacitor value and decay to the serial-capacitor value as more oil creams. It is also evident that as the oil ratio is increased, the difference between ϵ_{eff} of a well-emulsified system and a completely separated system becomes smaller and less detectible. This is due to the fact that ϵ_{eff} of oil is much smaller than water and as more oil is added to the system, even the well-emulsified (parallel-plate) permittivity becomes smaller. Therefore, the decay to the serial-capacitor value becomes less visible. In other words, capacitance-based measurements give best results for O/W emulsions rather than W/O emulsions.

3.5 NUMERICAL INVESTIGATION OF EMULSION PERMITTIVITY: EFFECT OF PHASE SEPARATION AND TOPOLOGICAL STRUCTURE

3.5.1 Overview of the model

The dispersed phase of an emulsion may take numerous geometrical structures in the host medium. The topology of the dispersed phase can be affected by parameters such as in-

terfacial tension, presence of surface active agents, degree of emulsification and size distribution, phase separation, etc. Developing a comprehensive analytical model describing permittivity of all possible colloidal structures is not possible. Therefore, numerical modeling should be employed for shedding more light on how electric permittivity is affected by the geometrical structure of the dispersed phase in the host medium. The results and conclusions of this numerical study are later used in chapter 5 to relate the results of the developed experimental platform to emulsion properties.

In this thesis, a finite-element model is developed in COMSOL MultiPhysics to determine the static permittivity of emulsions based on different dispersion patterns of the dispersed phase. In this 2D numerical model, two parallel plates are drawn in COMSOL which resemble the two electrodes of the experimental setup. The dispersed phase (oil with ϵ_r=2 or 4) is placed in the continuous phase (water with ϵ_r=80) between the two electrodes in form of droplets or separate phases. The upper electrode is given an electric potential (V) and the lower electrode is grounded.

The governing equation of the system is the Poission's equation:

$$\nabla^2\phi = -\frac{\rho_f}{\epsilon} \tag{3.15}$$

where ϕ, ρ_f, and ϵ are electric potential, free charge density, and permittivity, respectively. Since salt concentration, without charge gradients, does not affect permittivity of water [93, 94], the volumetric free charge density of water (ρ_f) is considered to be zero. Therefore, Laplace's equation holds in the system:

$$\nabla^2\phi = 0 \tag{3.16}$$

It is noteworthy that salt concentration may affect droplet coalescence and dispersed phase structure, but it (with concentration below 0.01M) does not change the permittivity

of the water phase [95–97].

The boundary conditions of the governing Laplace's equation (equation 3.16) are $\phi = V$ on the top electrode (a numerical value of 1V was set for V), ϕ=0 at the bottom, symmetry on the left and right boundaries, and continuity on oil-water interfaces. An unstructured mesh was used for discretizing the solution domain and grid independence was tested for each solution. Figure 3.7 illustrates a portion of the solution domain, boundary conditions and meshing for a sample case of oil droplets in water. The convergence criterion of the numerical solution was set to 10^{-6}. The permittivity of the samples are determined in the post-processing phase of the solution by integrating surface charge on the charged (1V) electrode and using the following relations for calculating the permittivity (dielectric constant) of the emulsions:

$$C = \frac{Q}{V} \tag{3.17}$$

$$C = \epsilon_o \epsilon_{r,eff} \frac{A}{d} \tag{3.18}$$

or

$$\epsilon_{r,eff} = \frac{1}{C} \frac{1}{\epsilon_o} \frac{d}{A} \tag{3.19}$$

where C is the capacitance of the film, Q is the surface charge of the capacitor, V is the potential across the two electrodes, ϵ_o is vacuum permittivity, $\epsilon_{r,eff}$ is the effective dielectric constant of the emulsion, A is the surface area of the electrode, and d is the thickness of the dielectric (emulsion). The dielectric constant may also be calculated by integrating the energy stored in the capacitor over the film volume and using the following relation:

$$W = \frac{1}{2} C V^2 \tag{3.20}$$

where W is the energy stored in the capacitor. Dielectric constant can be then calculated

from equation 3.19.

Since the governing equation of the system is Laplace's equation (the dimensionless form is identical to the dimensional form), there is no need to run the numerical solution based on dimensionless parameters. However, when the dielectric constant is determined, the calculated value is dimensionless and independent of the dimensions (thickness and surface area) of the test cell and is only a function of the permittivity of the two phases, volume fractions, and geometrical structure of the dispersed phase.

3.5.2 Effect of droplet size

In order to study the effect of droplet size on permittivity of a two-phase system, a constant 10% volume fraction of oil (ϵ_r=4) is placed in water (ϵ_r=80) with different uniform sizes. Figure 3.8 shows the solution of the Laplace's equation for spherical droplets with 320μm-diameters. In this figure, the surface colors and contours represent the electric potential and the vectors (perpendicular to the potential contours) represent the electric field. As illustrated in figure 3.8, the relatively large diameter of the droplets causes large distortions and changes in the electric potential and field. On the other hand, as illustrated in figure 3.9, the electric potential and field are less distorted and changed if the droplets are smaller. Figure 3.9 shows the electric potential contours for 10% oil in water emulsion with 25 μm-diameter droplets. It is observed that smaller droplets cause less distortion in the electric potential. Field vectors are not shown, however, being perpendicular to the potential field, field vectors show small distortion as well. Since permittivity is physically defined based on the ability of a medium to transmit (permit) electric field, the distortion pattern of the electric field by the dispersed droplets directly affects the permittivity of the medium.

To investigate the effect of droplet size on permittivity in a quantitative fashion, different grids of droplets (m rows × n columns, with m and n changed between 1 to 6 and 6 to 300, respectively) were modeled between the two parallel plates keeping the oil ratio constant. It was found that if the droplets (initially 6×300) coalesce to form fewer number of

rows between the two electrodes (for instance, to form a 3×300 grid), the permittivity decreases. On the other hand, it was found that if the droplets coalesce to form fewer number of columns (for instance, to form a 6×100), permittivity increases. This behavior is illustrated in figure 3.10 that shows the dielectric constant as a function of volume-to-surface ratio of droplets.

In conclusion, although EIS can be applied in micro-scale for sensing micro-scale phenomena such as biological processes or bacterial activity, [13, 74–77, 80], it was shown that for investigating bulk oil-water emulsions, the EIS test cell and sample thickness need to be at least one order of magnitude larger than the droplets dispersed in the system. Therefore, for emulsions with droplet size ranging between 10 μm to 1000μm, micro-scale EIS is flawed. On the other hand, it was shown that bulk properties can be captured by EIS sensors with sample thicknesses 1-10 orders of magnitude larger than droplet size. Therefore, test cells with milli-fluidic scale thickness can be employed for applying EIS to emulsion studies. Larger sample size may necessitate larger signal amplitudes to increase signal-to-noise ratio, which may, in turn, disturb the emulsion system and add errors to the EIS measurement.

3.5.3 Effect of creaming (sedimentation)

In section 3.4.2, an analytical model was developed to relate capacitance of the cell to the thickness of the oil layer as creaming causes the oil layer to grow. However, it was assumed that the creamed layer does not contain any water. In this section, different cases of partial creaming (sedimentation) of the oil phase are studied to investigate permittivity during creaming process considering the fact that some water is also present in the oil-rich phase. In other words, in this section, ripening phenomena and the degree of emulsion breaking in the oil-rich creamed phase and its effect on permittivity are studied.

As schematically shown in figure 3.5, some water may be trapped in the oil-rich creamed phase that can affect the permittivity of the system. A packing factor (P.F.) is de-

fined in the oil-rich film as $P.F. = \frac{\texttt{Oil volume in the oil-rich phase}}{\texttt{Total volume of the oil-rich phase}}$ representing the amount of water or degree of emulsion breaking in the oil-rich layer. Variation of capacitance for different packing factors is studied in a 10% O/W emulsion. The squished droplets are approximated by 4 layers of rectangles and the packing factor is implemented by changing the distance between layers of rectangles (for example distance=0 for P.F.=1). In the water-rich phase, well-emulsified parallel-capacitor model is used to determine ϵ_r. Figure 3.11 shows the geometry and mesh of an example case where 80% of the total oil has creamed with a packing factor of $P.F. = 0.4$, and figure 3.12 shows the electric potential contours of the same case.

The variation of permittivity versus the amount of creamed oil is acquired for different packing factors in the creamed layer during phase separation and is illustrated in figure 3.13. It is noteworthy that for P.F.=1 (the case where no water is trapped in the oil-rich layer), the curve shown in figure 3.13 is the same as the curve for $\phi_{oil} = 0.1$ in figure 3.6. Figure 3.13 shows that as the emulsion undergos phase separation, if some water is trapped in the creamed oil layer, the permittivity of the system does not reach the serial-capacitor value. In other words, the more the oil-rich phase breaks into a layer of pure oil, the closer the system becomes to serial-capacitor model.

In the numerical simulations, by solving the Laplace's equation for different droplet sizes, it was observed that if the thickness of the EIS test cell is of the same order of magnitude as the droplet size of the tested emulsion, the distortions in the field will be so high that the bulk properties of the emulsion may not be detectible. It was also observed that if the amount of water in the oil-rich creamed phase of an emulsion is negligible, the permittivity of the system can be formulated based on the serial-capacitor model. However, if some water gets trapped in the oil-rich layer, the permittivity decays to a larger value than the serial value. The effect of degree of phase separation (the amount of creamed oil) on permittivity was analytically investigated in section 3.4.3 and the effect of presence of water in the oil-rich layer was numerically studied in section 3.5.3.

3.6 ANALYSIS OF THE EXPERIMENTAL DATA WITH EQUIVALENT CIRCUIT MODELING

3.6.1 Overview

The result of electrochemical impedance spectroscopy is a set of data showing the variation of complex impedance with frequency in the frequency range of the measurements. The data provided by EIS can be interpreted in a qualitative fashion based on the physical properties revealed by different curves in Bode or Nyquist plots. However, most thorough and informative interpretation of EIS data is only possible by quantitative modeling. In this thesis, equivalent circuit (EC) modeling has been used to quantify the EIS results in form of electrical element values. In this section, the scheme of fitting an equivalent circuit to the EIS spectrum and the algorithm used for fitting, the equivalent circuits used for modeling the experimental data and the rationale behind the choice of the ECs, and the method for modeling the electrode-sample interface polarization and subtracting that from the bulk properties are explained.

3.6.2 Fitting scheme

One of the most commonly used methods of modeling the EIS data is "equivalent circuit" modeling. In the first step of this method, an electrical circuit which produces a frequency response similar to that of the electrochemical system is selected. The electrical circuit is chosen based on the physical and electrochemical properties of the studied sample. In the second step, the values of the model parameters (circuit elements) are determined by carrying out a fitting algorithm, i.e., minimization of the difference between experimental data and the model values by changing the model parameters (circuit element values).

The most widely used minimization method is the Complex Non-linear Least Squares (CNLS) [89] method. In CNLS, the complex sum of squares defined in equation 3.21:

$$S = \sum_{i=1}^{N} \{w_i'[Z'_{i,experiment} - Z'_{i,model}]^2 + w_i''[Z''_{i,experiment} - Z''_{i,model}]^2\} \tag{3.21}$$

is to be minimized [89, 98]. In equation 3.21, $Z'_{i,experiment}$ and $Z''_{i,experiment}$ are the measured real and imaginary parts of the complex impedance, respectively, while $Z'_{i,model}$ and $Z''_{i,model}$ are the real and imaginary parts of the impedance calculated based on the model. w_i' and w_i'' are statistical weights. Statistical wights can be set inversely proportional to the experimental or calculated values to bring the effect of extremely large or small values to the same order of magnitude. Due to the iterative nature of minimization, the statistical weights can be set as unity without any significant effect on the converged values.

The minimization is often carried out by application of the Levenberg-Marquard [89] algorithm. The LEVM software package developed by MacDonald [99] embedded in SAI ZView software is used to fit the EIS data to the equivalent circuit models in this thesis. Also, a custom equivalent circuit fitting code was developed for this study in MATLAB, which is capable of fitting any equivalent circuit to experimental data. Unlike LEVM, it is possible in the custom program to modify the statistical weights (w_i' and w_i'') of equation 3.21 for fitting. The MATLAB program is attached in Appendix B. Due to the fact that LEVM is embedded in ZPlot and ZView software packages, this program is used for fitting EC models to experimental measurements.

In modeling impedance data with equivalent circuits, it should be noted that the minimization algorithm is dependent on the initial guess values. Therefore, not only should the equivalent circuit be consistent with the physics of the experimental system being studied, but also the model and the residuals should be monitored to verify convergence to the experimental data. Moreover, it should be noted that the eventual objective of equivalent circuit modeling is to model a real electrochemical system with electrical circuits and the corresponding circuit element values based on EIS data. Therefore, in order for the

model to be informative and helpful in terms of describing the electrochemical system, the electrical model should be kept as simple as possible so that interpretation of the circuit element values becomes possible.

3.6.3 Choice of the equivalent circuit

Physically, a film of oil-water emulsion can be viewed as a leaky dielectric, i.e. a medium with limited capability of conducting current, and at the same time, capability of transmitting electric field. Therefore, the first candidate for equivalent circuit of the system is a parallel R|C circuit. The transfer function of such a circuit is

$$Z_{RC} = \frac{-Rj/\omega C}{R - j/\omega C} \tag{3.22}$$

or

$$Z_{RC} = \{\frac{R}{(RC\omega)^2 + 1}\} + \{-\frac{R_2 C\omega}{(RC\omega)^2 + 1}\}j \tag{3.23}$$

where j is the unit imaginary number. The typical Nyquist and Bode plots of a parallel R|C circuit for a frequency spectrum ranging from zero to infinity are schematically shown in figures 3.14 to 3.16.

Unlike a parallel R|C circuit, in the experimental EIS measurements, the semicircle does not start from the origin. This can be attributed to the resistance in the leads and electrodes, R_s in series with the R|C circuit. Also, in the experimental results, an increase in the phase of the impedance in lower frequencies was observed ending at a constant phase at the lowest frequencies. This type of behavior, which is caused by the electrode-electrolyte interface polarization [22,23,58,59], can be best modeled by adding a constant-phase-element (CPE) [8, 9, 61, 62] to the circuit. A CPE is an artificial electric element which does not have a real physical counterpart but is found useful in modeling electrode

surface properties in EIS of electrochemical systems. The impedance of a CPE is

$$Z_{CPE} = \frac{1}{Q\omega^n e^{-\frac{\pi}{2}ni}} \tag{3.24}$$

where Q and n are frequency independent. Q of a CPE is similar to capacitance of a capacitor. If n=1, the CPE becomes identical to a capacitor and if n=0, the CPE becomes a pure resistor.

Based on the above discussion, the equivalent circuit selected for interpreting the experimental data consists of a resistor (R_s) in series with a parallel $R|C$, in series with a constant phase element (CPE), representing the leads resistance, sample permittivity and resistance, and low-frequency electrode surface polarization, respectively. The equivalent circuit and the physical counterpart of each element of it are illustrated in figure 3.17. Sjoblom [8] proposes a similar circuit for EIS of conductive media, with a capacitor (a specific form of a CPE) instead of a CPE for modeling the electrode polarization, but our experiments show that the CPE is a better model than a capacitor. Sjoblom [8] mentions that the element modeling the electrode polarization greatly depends on the electrode, as well as electrode-electrolyte interaction and a general circuit cannot be prescribed. The typical Nyquist and Bode plots of the circuit for a frequency spectrum ranging from zero to infinity are schematically illustrated in figures 3.18 to 3.20 (for a CPE with $Q \backsimeq 10^6 C$) and figures 3.21 to 3.23 (for a CPE with $Q \backsimeq 10^2 C$). After circuit element values are determined by the fitting algorithm, the equivalent circuit chosen (figure 3.17) shows an excellent fit to the experimental data of the systems tested in this thesis.

3.6.4 Modeling the low-frequency electrode-sample interface polarization

As stated in chapter 1, one of the main contributions of this thesis is to investigate the fabrication of an inexpensive experimental platform for applying EIS to characterization of liquid-liquid systems. To achieve this goal, the setup was designed and fabricated as

a two-electrode EIS platform. The main barrier to applying EIS to conductive media is that the polarization effects in the close vicinity of the electrodes may outweigh the sample "bulk" properties [5, 15]. This problem specifically arises in micro-fluidic applications of EIS when the physical thickness and the Debye length of the polarized layer near the electrodes become considerable compared to the total sample length. As mentioned in the previous section, the equivalent circuit shown in figure 3.17 (also see [8]) is capable of simulating both bulk sample properties and electrode polarization. When fitted to the experimental data, the magnitude of the CPE (Q) is found to be at least 2 orders of magnitude larger than the magnitude of the capacitance (C) in the $R|C$ circuit representing the emulsion film. Since Q and C are both in the denominator of the element impedance and are multiplied by ω (see equations 3.23 and 3.24), the CPE effect on the impedance only becomes considerable in low frequencies (two orders of magnitude smaller compared to the $R|C$ frequency range of effect). Therefore, the CPE represents the low-frequency data. As a result, it is reasonable to assume that the CPE is actually the representative of the low-frequency electrode surface polarization and the $R|C$ represents the sample properties. In other words, after fitting the EC shown in figure 3.17 to the measurements and finding the circuit element values, the R and C can be related to the emulsion properties. The Nyquist and Bode plots may be re-generated for an $R|C$ circuit with the found values (not including the CPE and R_s elements) to show the pure behavior of the emulsion in the whole frequency range. However, as discussed above, the result would be identical to the high-frequency portion of the original plots. Therefore, high frequency data can be used for analyzing emulsion properties. In chapter 4, four-electrode measurement has been applied to special cases and it is found that results from two-electrode measurements with the above-discussed correction for low-frequency electrode polarization are in agreement with four-electrode measurements where electrode surface polarization does not affect the system considerably.

3.7 Conclusions

In this chapter, by numerical investigation of the effect of droplet size on permittivity, it was shown that EIS in micro scale, especially permittivity measurement in micro scale, is fundamentally flawed because of the fact that when the droplet diameter is of the same order of magnitude as the sample thickness, the electric field is affected by the droplet to the extent that bulk properties may be outweighed. Therefore, in this thesis, a larger "milli-fluidic" scale (at least one order of magnitude larger than the droplet size) is used. While EIS is traditionally applied to W/O emulsions, it can also be applied to O/W emulsions for characterization of water-rich industrial liquids, for instance for monitoring organic content during water treatment processes. In fact, it was shown that sensing phase separation through permittivity measurement can be more conformably done in O/W emulsions because the phase separation-driven decay of permittivity is more visible in water-rich emulsions than oil-rich ones (see figure 3.6). As mentioned in chapter 2, one of the main barriers of applying EIS to O/W emulsions is the low-frequency electrode polarization, especially in micro scale EIS where the thickness of the polarized layer on the electrodes becomes more considerable. This effect is modeled with a CPE and the high-frequency data is modeled with an $R|C$ circuit to represent the sample emulsion film.

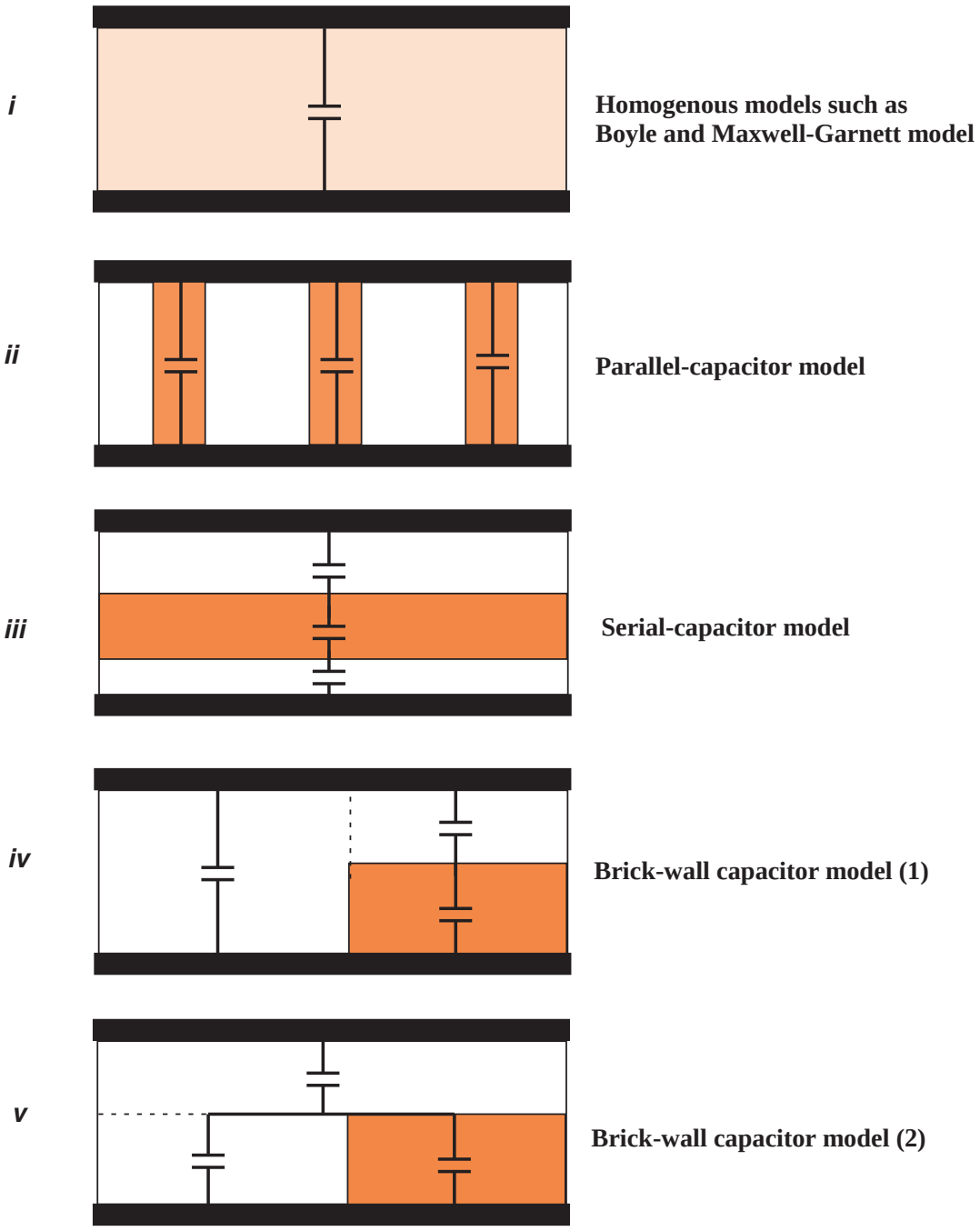

Figure 3.1: Schematic of the extreme cases of dispersed phase distribution in host medium and corresponding capacitor analogy. *i*: Homogeneously distributed, *ii*: Columnar configuration, *iii*: Laminar configuration, *iv*: Brick-wall configuration - model 1, and *v*: Brick-wall configuration - model 2.

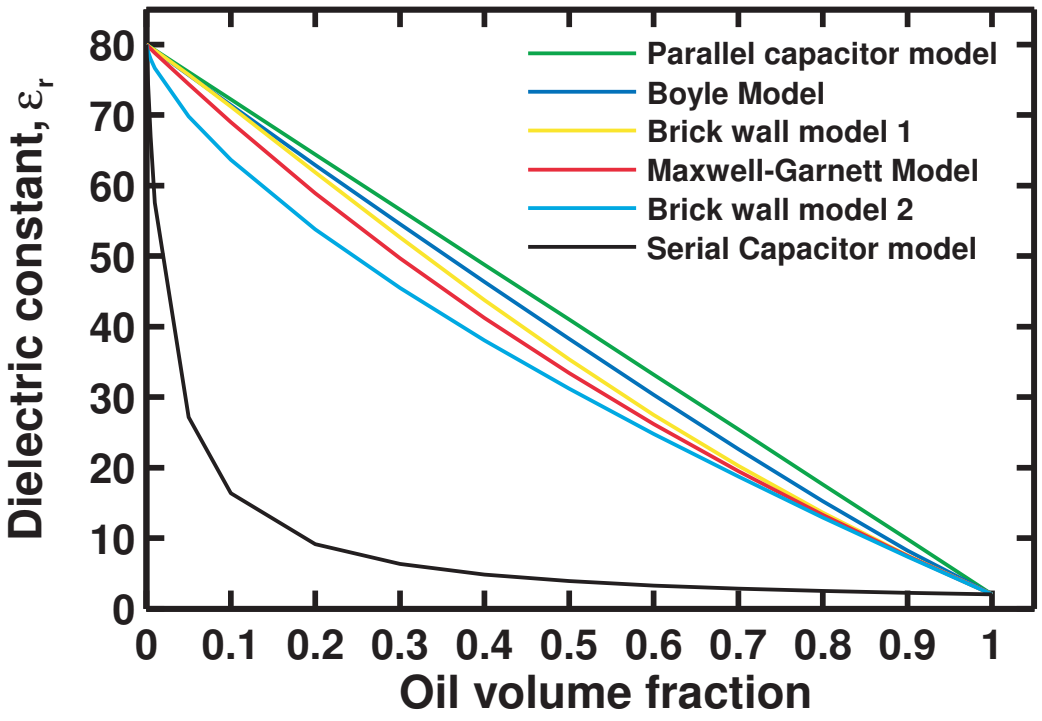

Figure 3.2: Dielectric constant of oil (ϵ_r=2)-water (ϵ_r=80) emulsions with different oil contents based on different homogeneous-mixture and multiple-capacitor models

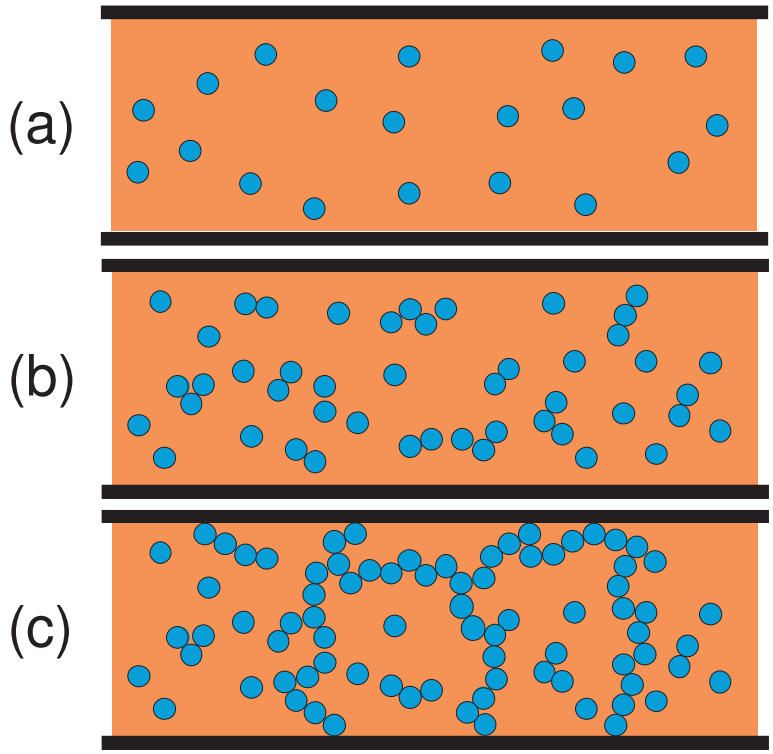

Figure 3.3: Schematic representation of percolation behavior in oil-continuous (W/O) emulsions. An abrupt increase in conductivity is a sign of the onset of percolation. The blue droplets show the water (electrolyte) phase and the orange medium shows the oil phase. (a) Low volume fraction of the dispersed electrolyte. (b) Adding more electrolyte causes more droplets to attach/coalesce. (c) When percolation happens, multiple current passages made of electrolyte form.

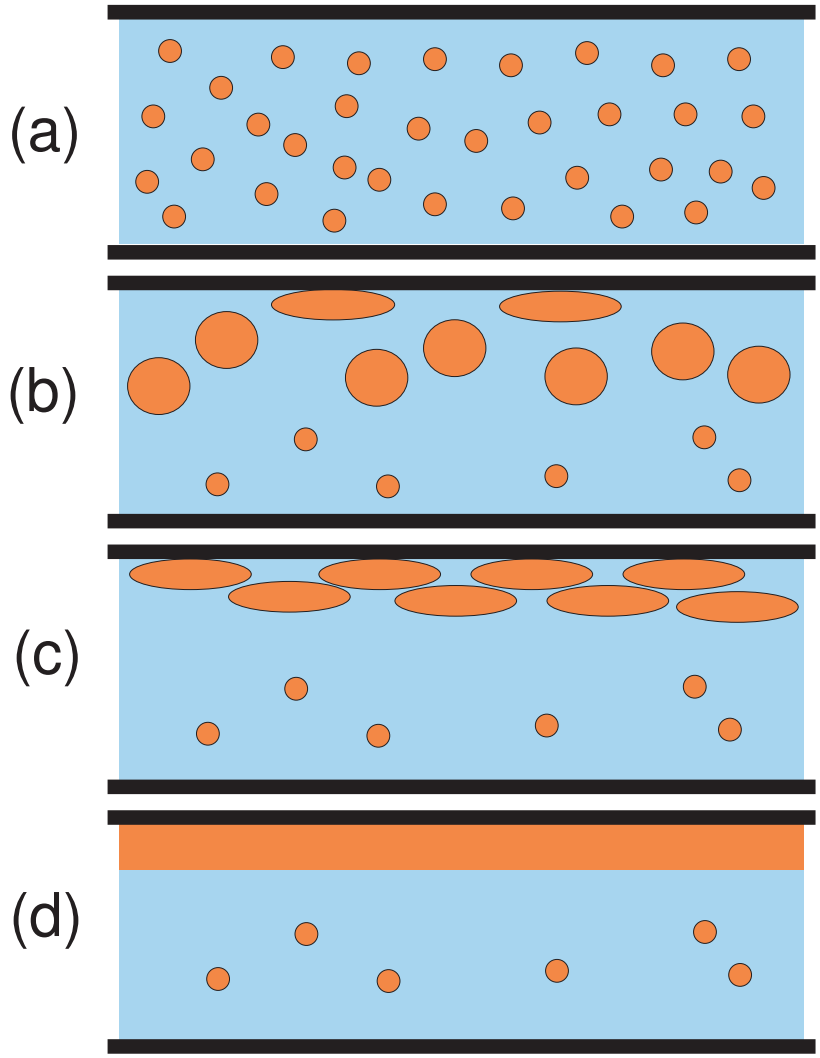

Figure 3.4: Schematic illustration of partial phase separation and creaming of the dispersed phase. The orange droplets show the oil phase and the blue medium shows the water phase. (a) Fresh emulsion, (b) Coalescence of droplets, (c) Large droplets move upwards under buoyancy force and are squished to spheroids when touching the upper electrode, (d) The separated phase creams at the upper electrode and as the oil-rich phase breaks, the system approaches the laminar (serial capacitors) structure.

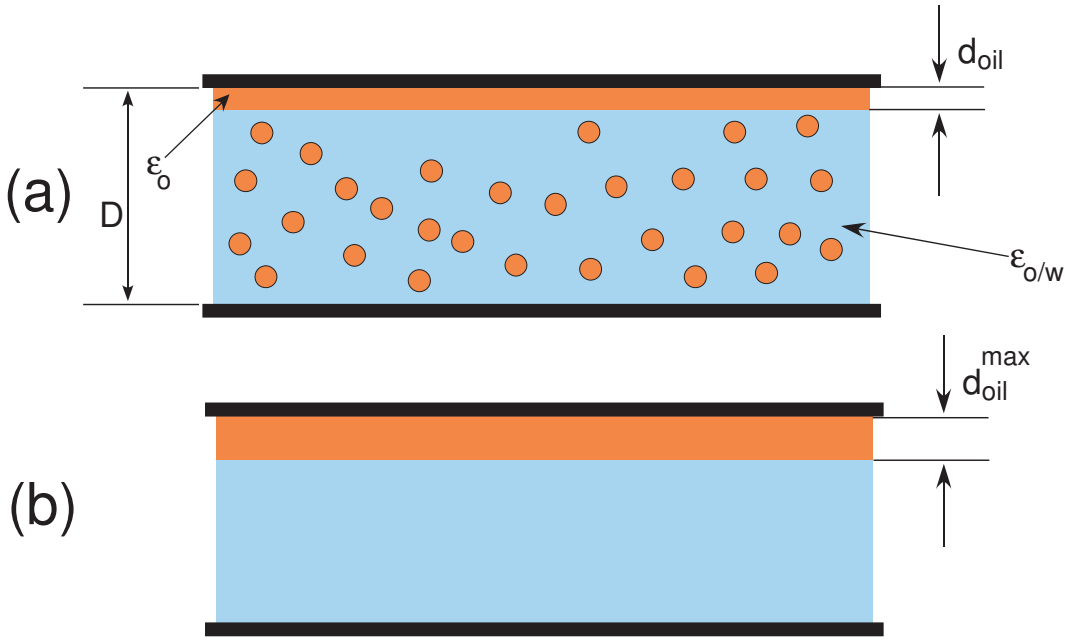

Figure 3.5: Schematic illustration of the growth of the oil layer as the emulsion undergoes phase separation. ϵ_O is oil permittivity, $\epsilon_{O/W}$ is the permittivity of the water-rich phase, D is the total film thickness, d_{oil} is the oil layer thickness, and d_{oil}^{max} is the final thickness of the oil layer. (a) The oil thickness grows gradually. (b) If all the oil creams up, the thickness reaches d_{oil}^{max}

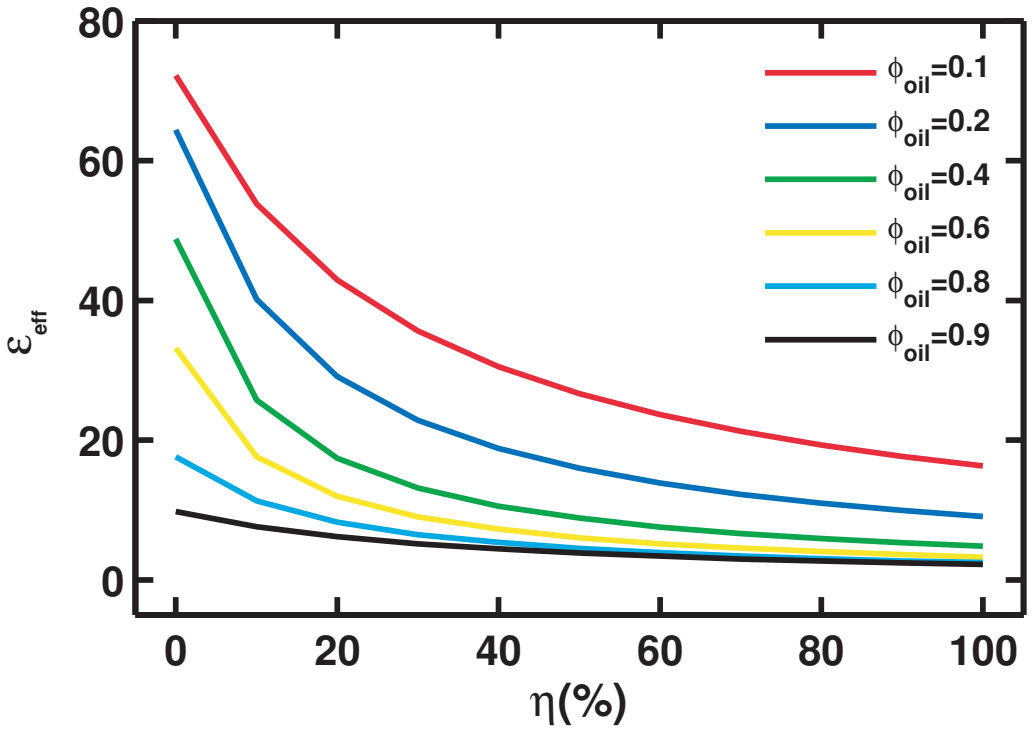

Figure 3.6: Dielectric constant ϵ_{eff} versus degree of phase separation ($\eta = \frac{\text{Volume of separated (creamed) oil}}{\text{Total volume of oil}}$) for different total oil volume fractions.

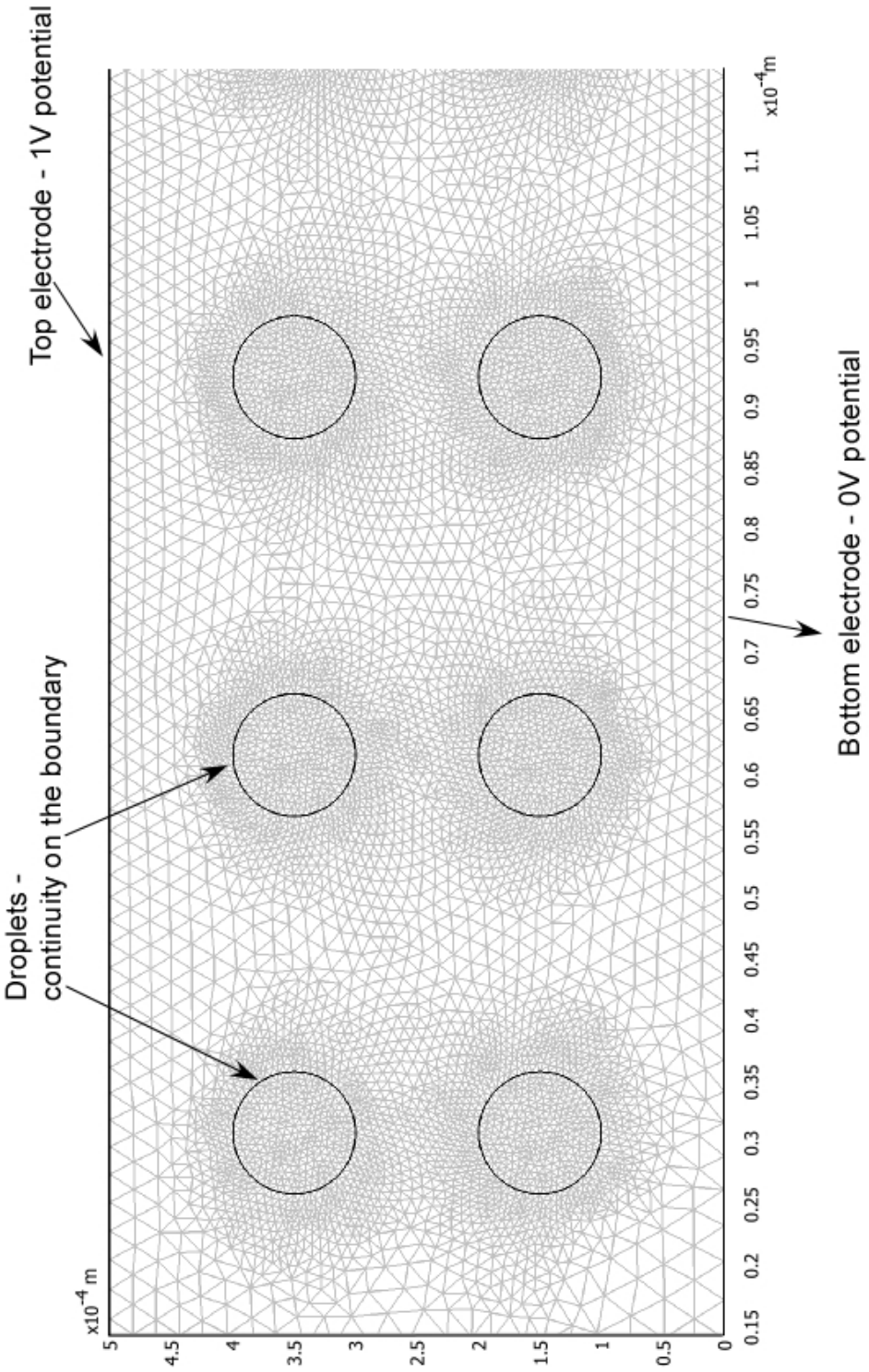

Figure 3.7: Geometry and unstructured mesh of the finite-element model for solving Laplace's equation for electric field in emulsions confined between two parallel plates (similar geometry to the test setup). The figure shows a portion of the solution domain.

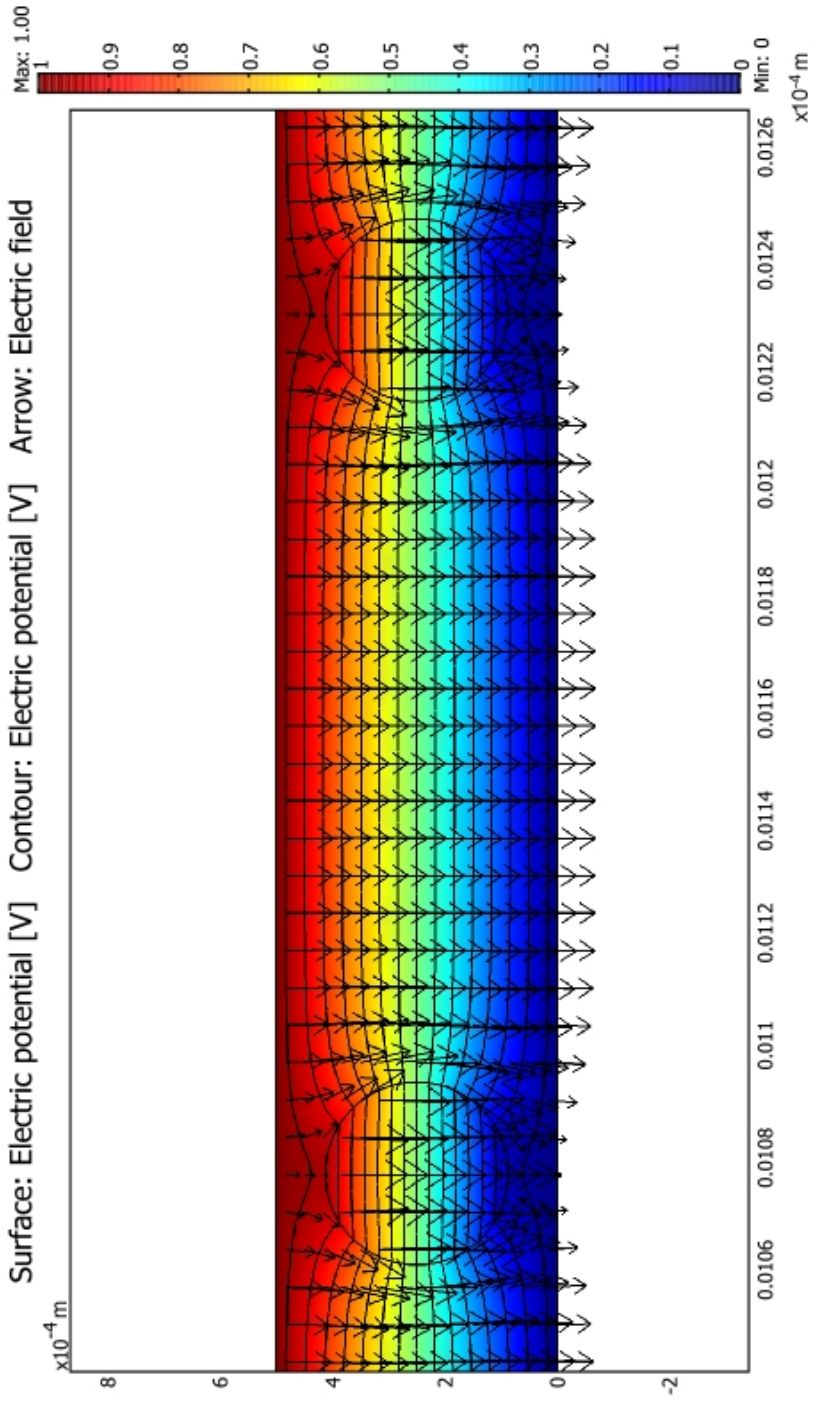

Figure 3.8: Electric potential (contours and surface colors) and electric field (vectors) of an emulsion with droplet size in the same order of magnitude as sample thickness. The diameter of the droplets is 320μm. Droplets are oil with $\epsilon_r = 4$ and the medium is water with $\epsilon_r = 80$

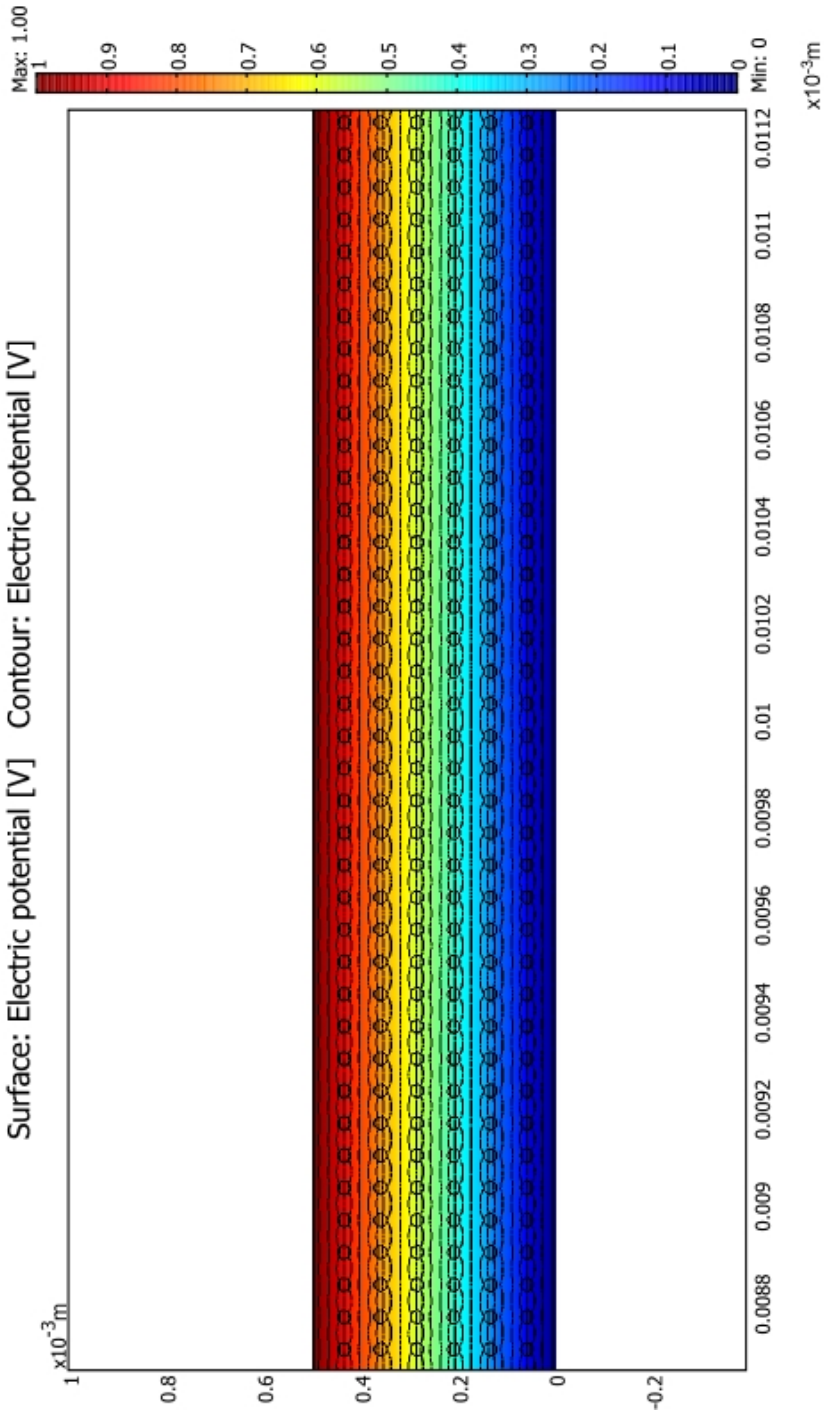

Figure 3.9: Electric potential (contours and surface colors) and electric field (vectors) of an emulsion with droplets much smaller than sample thickness. The diameter of the droplets is 25μm. Droplets are oil with $\epsilon_r = 4$ and the medium is water with $\epsilon_r = 80$

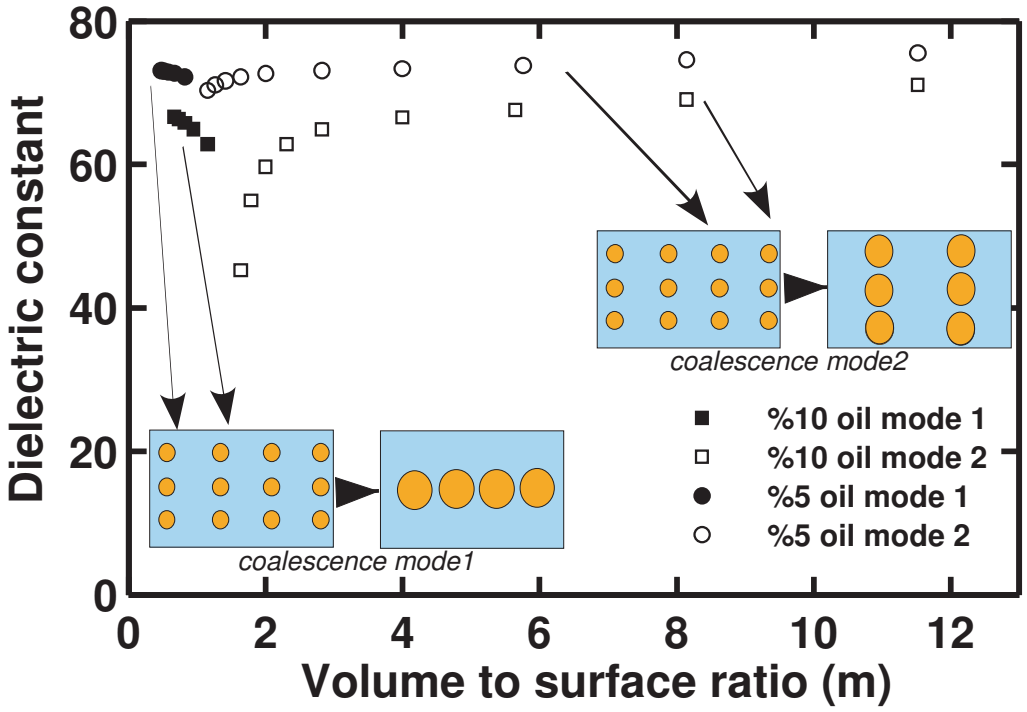

Figure 3.10: Dielectric constant of emulsions as a function of volume-to-surface ratio of droplets for different coalescence modes.

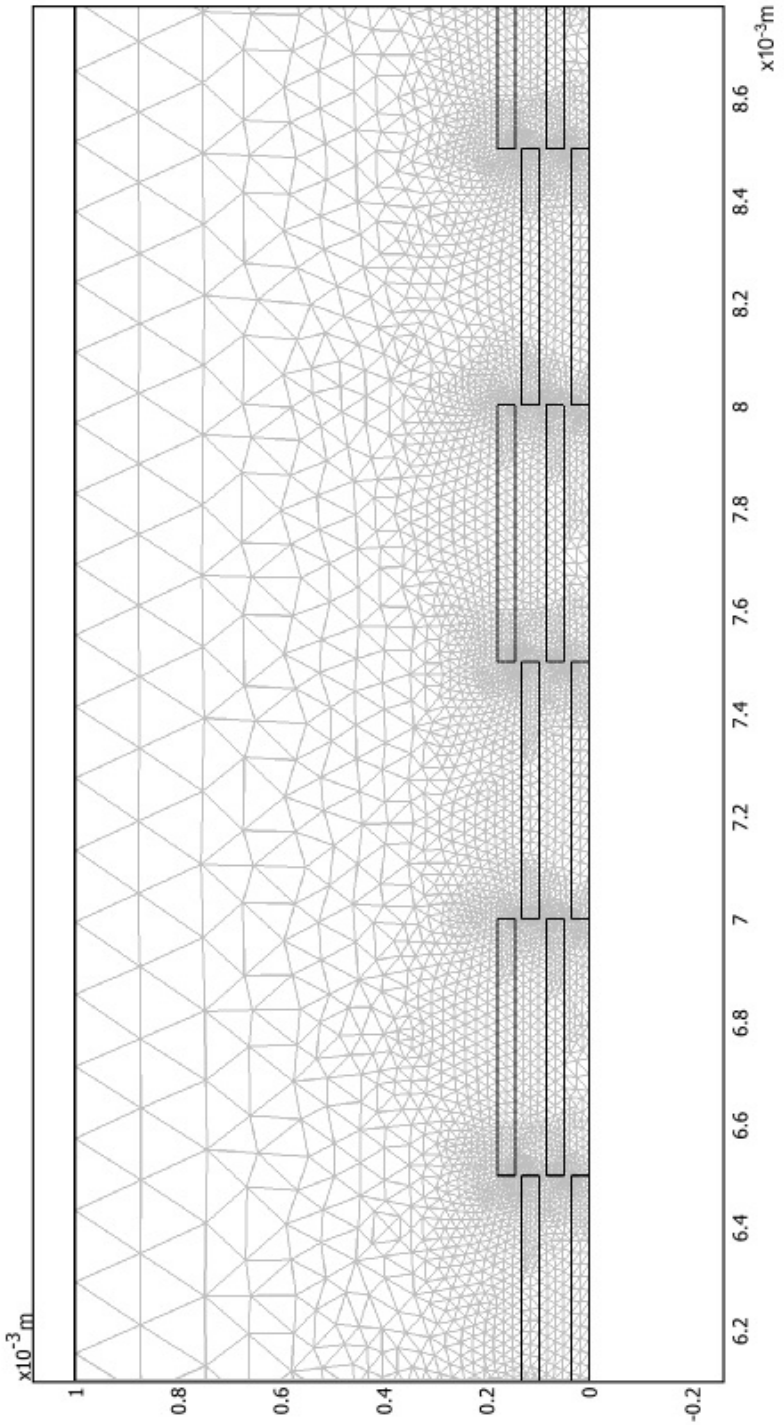

Figure 3.11: Geometry and mesh for simulation of creaming with water present in the oil-rich phase. This figure shows 80% of the oil creamed with a packing factor of $P.F. = \frac{\text{Oil volume in the oil-rich phase}}{\text{Total volume of the oil-rich phase}} = 0.4$ in the creamed layer

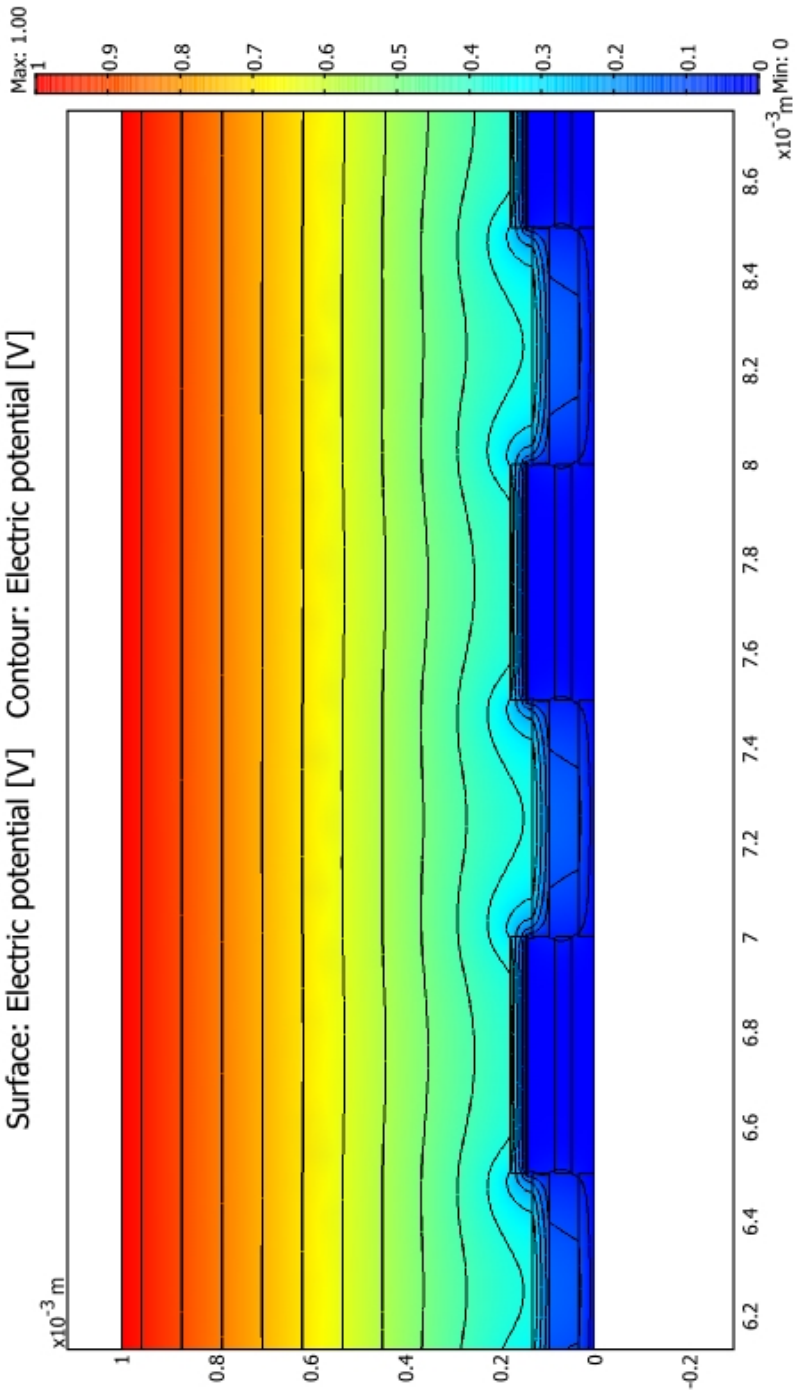

Figure 3.12: Electric potential of the creamed emulsion with 80% of oil creamed and P.F.=0.4.

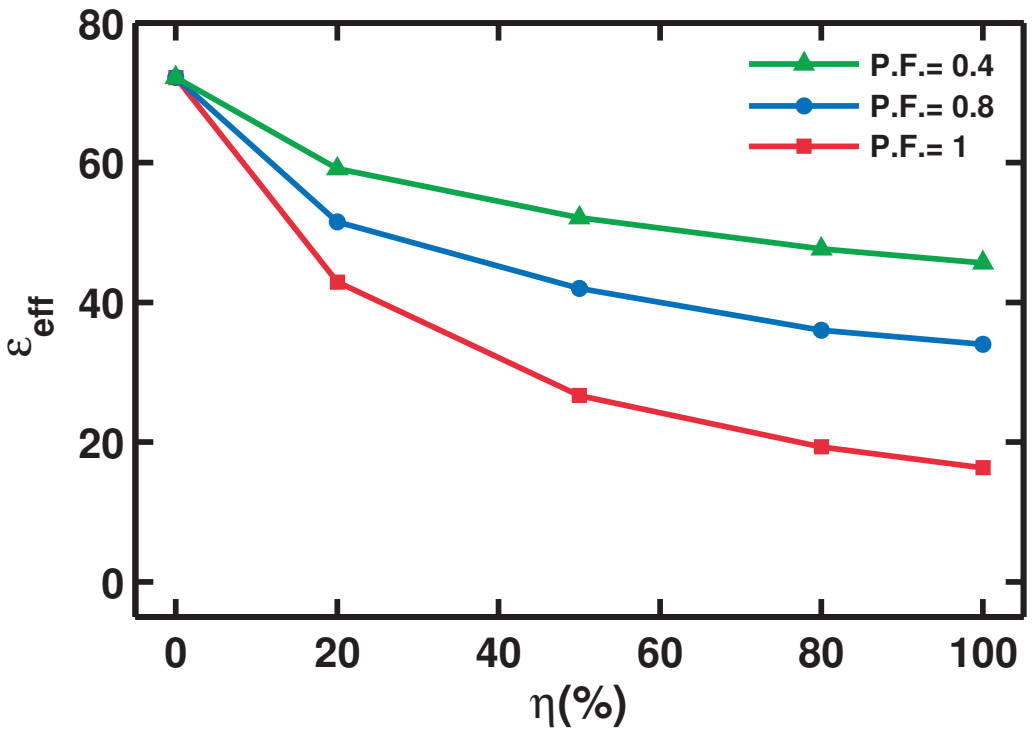

Figure 3.13: Dielectric constant of the emulsion versus the degree of phase separation ($\eta = \frac{\texttt{Volume of separated (creamed) oil}}{\texttt{Total volume of oil}}$) with water present in the oil-rich phase for different packing factors ($P.F. = \frac{\texttt{Oil volume in the oil-rich phase}}{\texttt{Total volume of the oil-rich phase}}$)

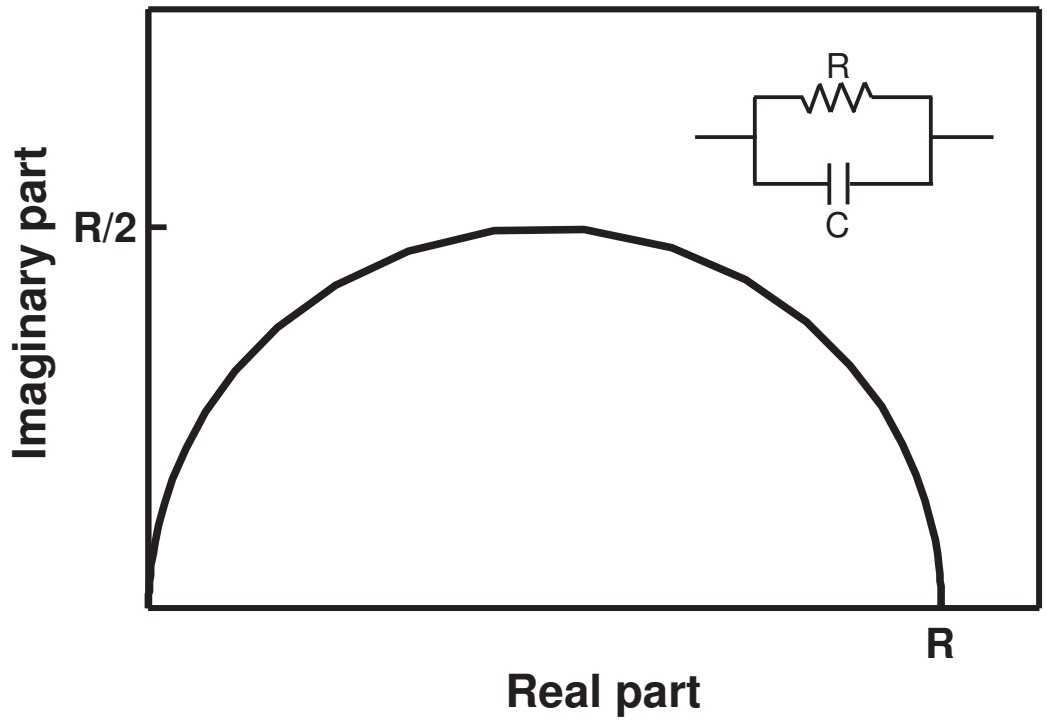

Figure 3.14: Schematic Nyquist plot of an $R|C$ circuit in a frequency spectrum ranging from 0 to infinity.

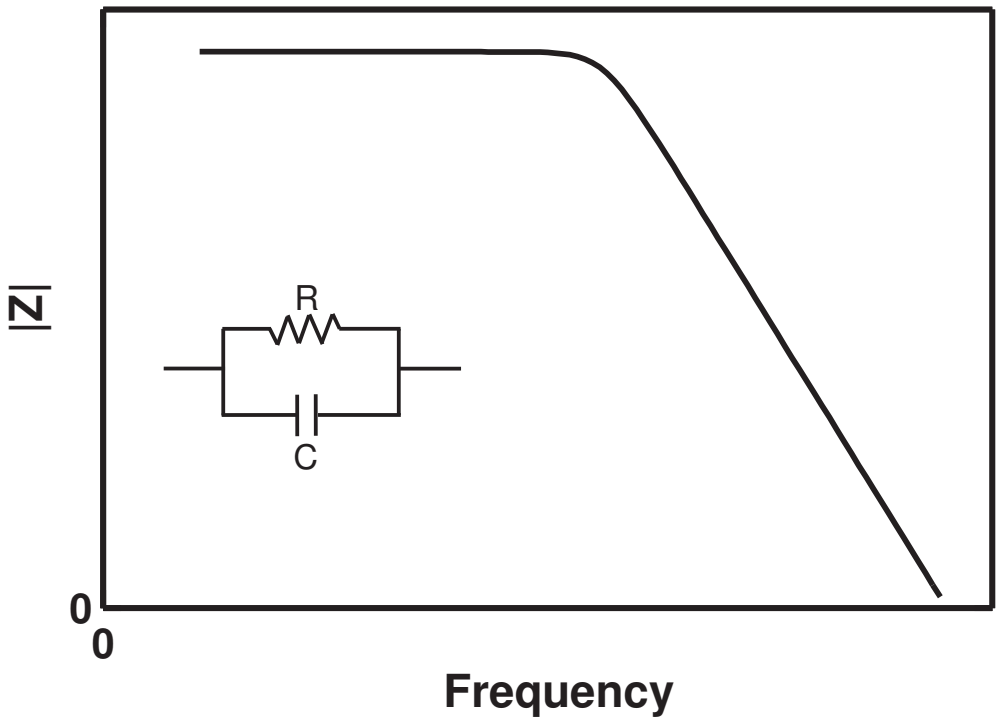

Figure 3.15: Schematic magnitude Bode plot of an $R|C$ circuit in a frequency spectrum ranging from 0 to infinity.

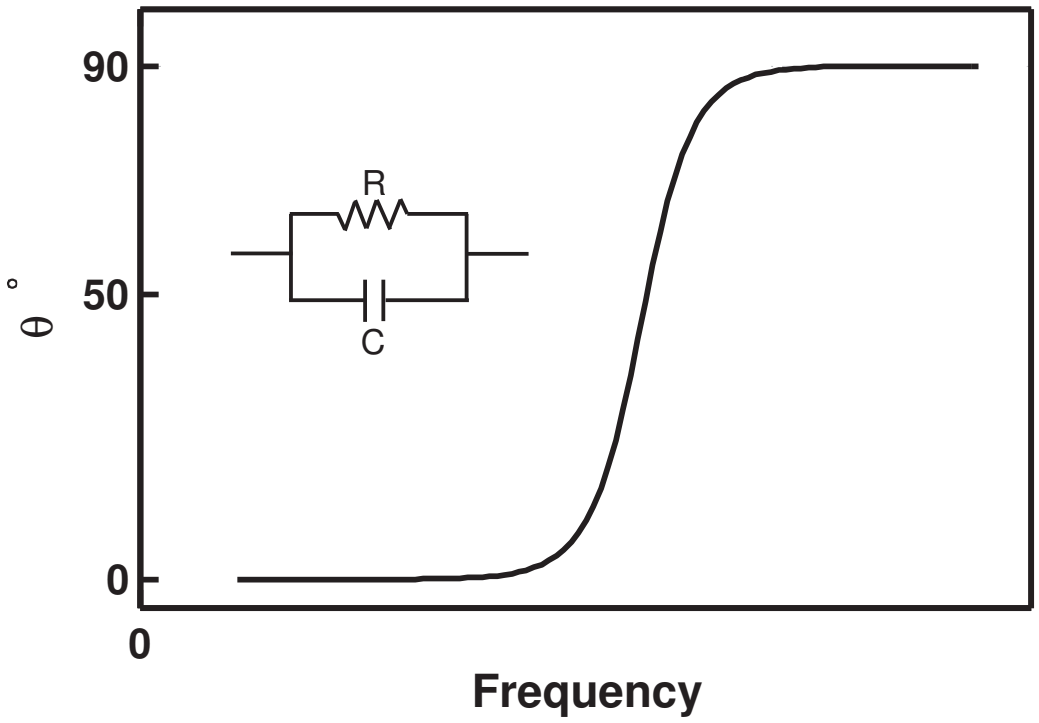

Figure 3.16: Schematic phase Bode plot of an $R|C$ circuit in a frequency spectrum ranging from 0 to infinity.

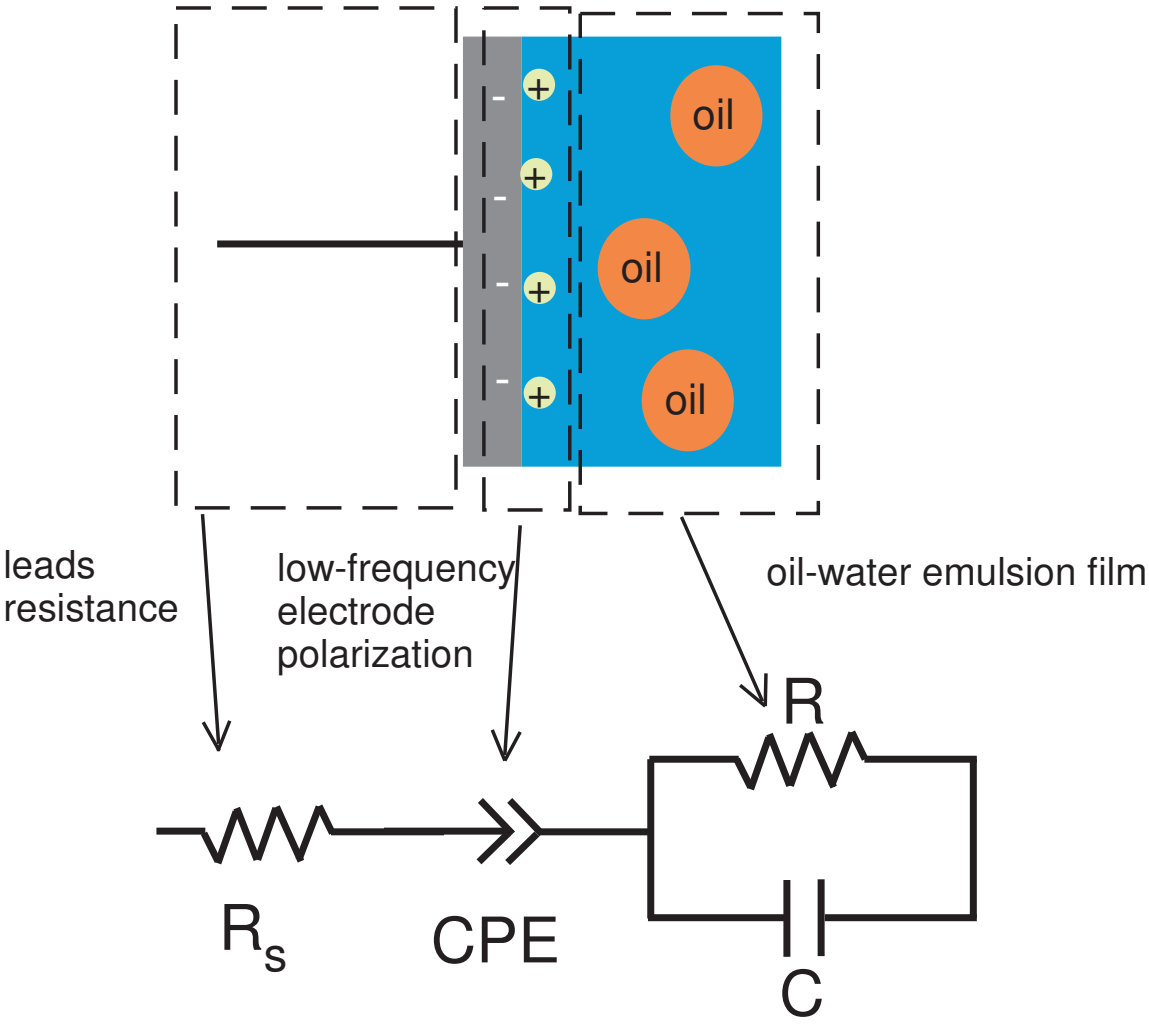

Figure 3.17: The equivalent circuit used for quantitative interpretation of the EIS measurements. The $R|C$ represents the emulsion properties, the CPE represents the electrode surface polarization in low frequencies, and R_s represents the leads and electrodes resistance.

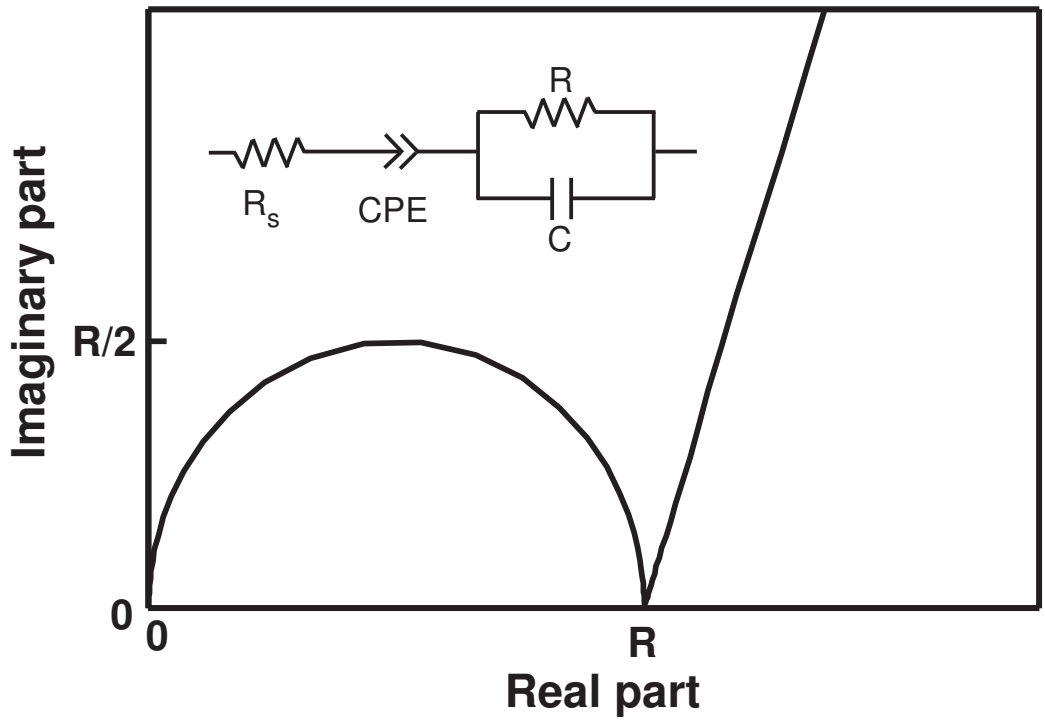

Figure 3.18: Schematic Nyquist plot of the $R-R|C-CPE$ circuit in a frequency spectrum ranging from 0 to infinity for a CPE with $Q \simeq 10^6 C$.

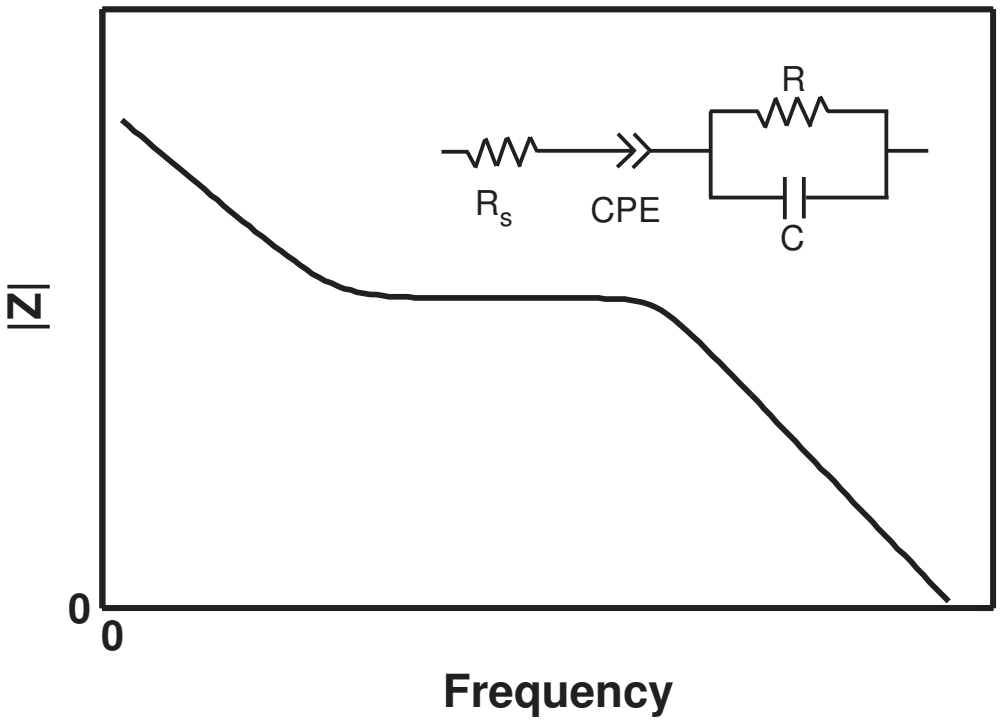

Figure 3.19: Schematic magnitude Bode plot of the $R - R|C - CPE$ circuit in a frequency spectrum ranging from 0 to infinity for a CPE with $Q \backsimeq 10^6 C$.

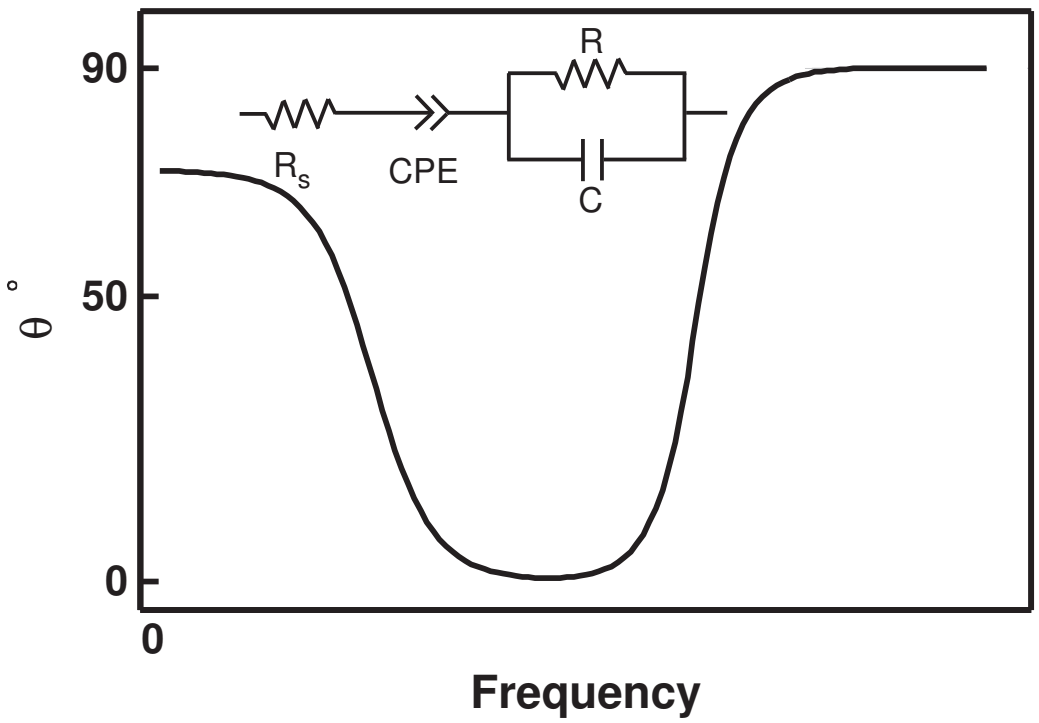

Figure 3.20: Schematic phase Bode plot of the $R - R|C - CPE$ circuit in a frequency spectrum ranging from 0 to infinity for a CPE with $Q \simeq 10^6 C$.

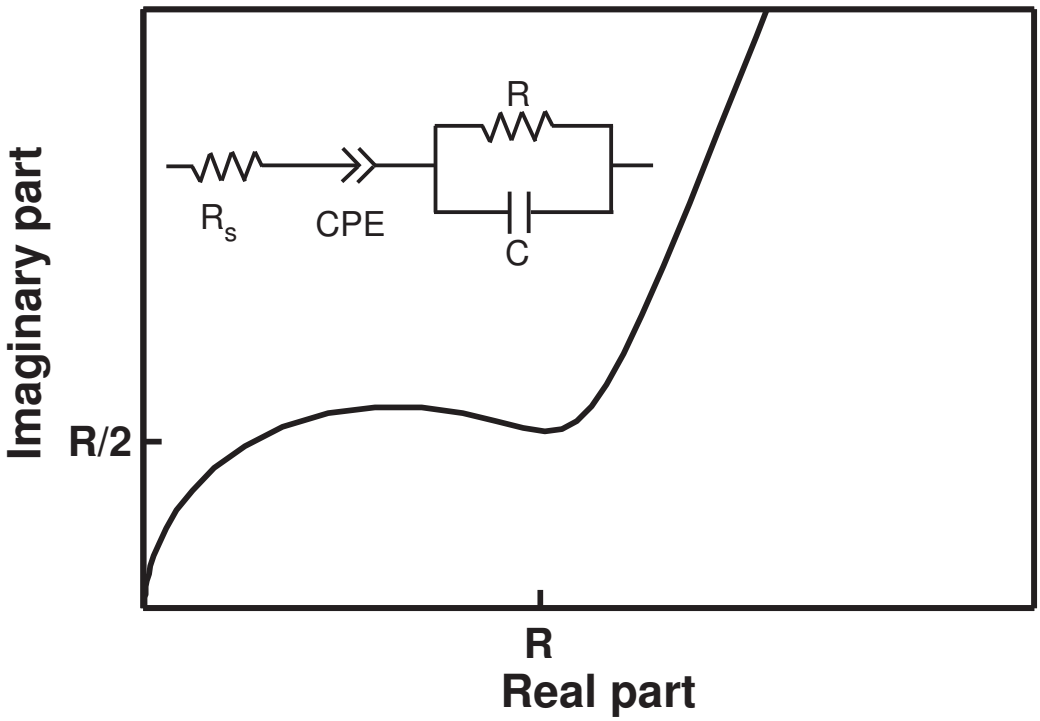

Figure 3.21: Schematic Nyquist plot of the $R-R|C-CPE$ circuit in a frequency spectrum ranging from 0 to infinity for a CPE with $Q \simeq 10^2 C$.

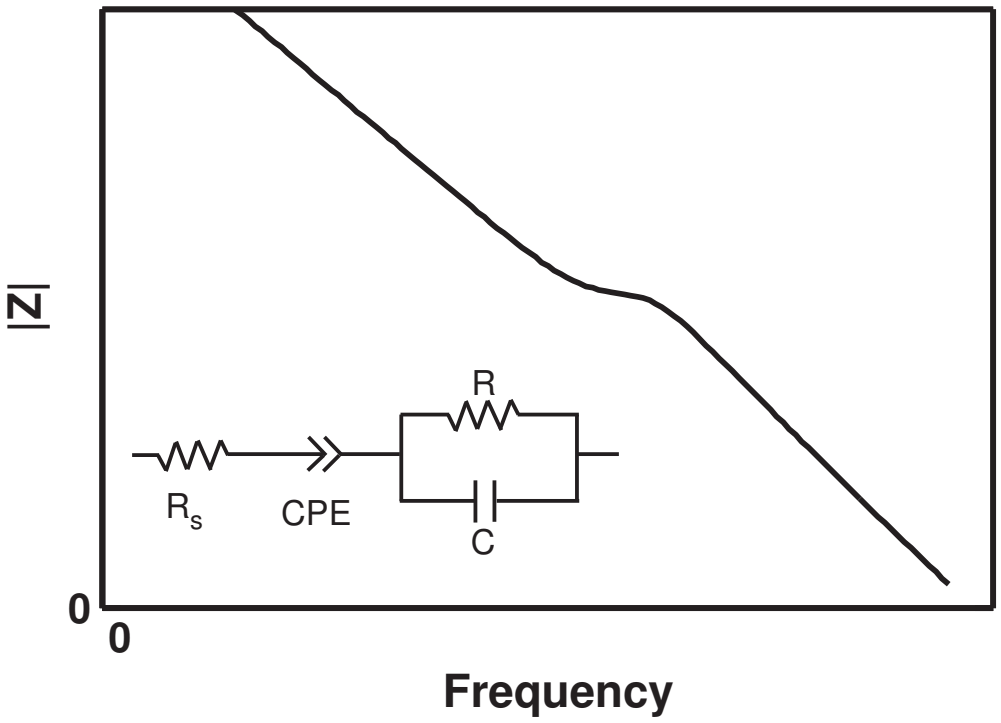

Figure 3.22: Schematic magnitude Bode plot of the $R - R|C - CPE$ circuit in a frequency spectrum ranging from 0 to infinity for a CPE with $Q \backsimeq 10^2 C$.

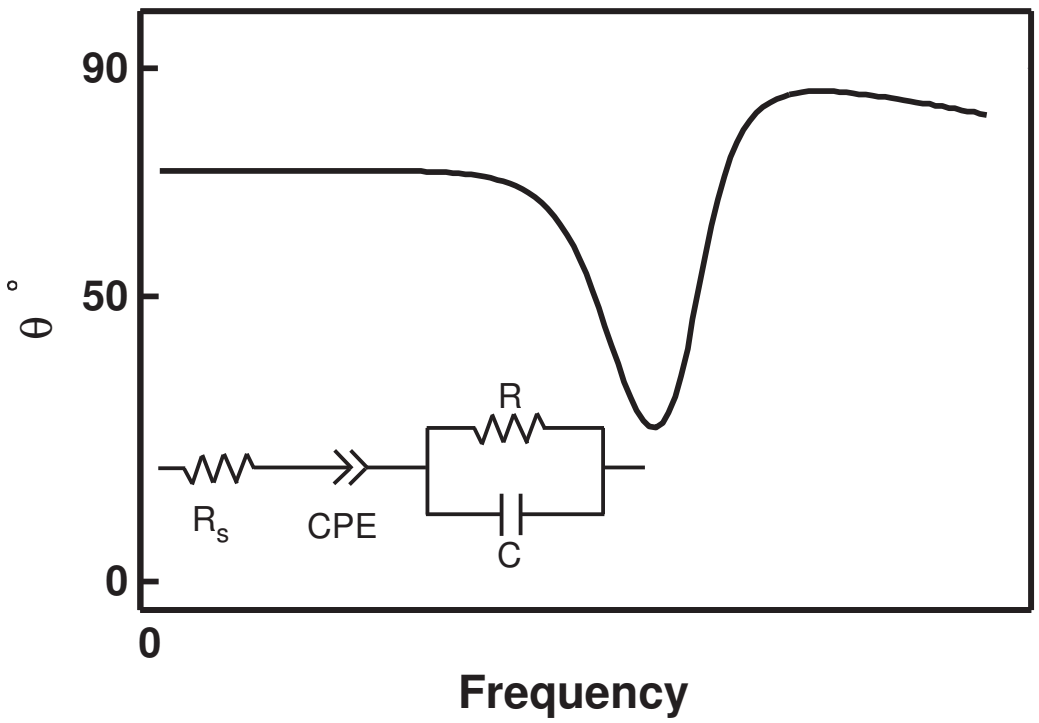

Figure 3.23: Schematic phase Bode plot of the $R - R|C - CPE$ circuit in a frequency spectrum ranging from 0 to infinity for a CPE with $Q \simeq 10^2 C$.

CHAPTER 4

EXPERIMENTAL METHODOLOGY

4.1 INTRODUCTION

As stated in chapter 1, one goal of this thesis is to introduce an inexpensive, easily fabricated, disposable, yet robust, experimental setup that ensures repeatable EIS experiments and reliable measurements. To achieve this goal, a "milli-fluidic" (as opposed to micro-fluidic) parallel-plate design is conceptualized for the test cell and is fabricated using 3D printing technology after a few steps of optimization. Different physical properties of the test fixture that can potentially affect the impedance response of the samples are then tested. In this chapter, the details of the experimental design, the specifications of the experimental procedure, the rationale behind the decisions made for different characteristics of the test setup (including the length scale of the test cell and sample thickness), and calibration of the test cell (the impedance of the leads and the dry capacitance of the cell) are explained. Also, the sample preparation process for investigating emulsions is discussed. Some aspects of the experimental setup design that need to be discussed with detailed results and discussion are introduced in this chapter and discussed in more details in chapter 5.

4.2 DESIGN OF THE EXPERIMENTAL SETUP

4.2.1 Overview

Figure 4.1 shows the schematic representation of the experimental setup that was developed for performing two-electrode electrochemical impedance spectroscopy. The sample, in the form of thin films with thicknesses ranging from 500μm to 5mm (hence, the system is called "milli-fluidic"), is placed between two electrodes as schematically shown in figure 4.1. The surface area of the test cell is 45mm×20mm. The electrodes that were initially used are made of glass with indium tin oxide (ITO) coating (Prazisions Glass & Optik) to allow optical microscopy of the samples. However, electrodes made from other materials were also tested and the effect of the electrode material on the EIS results is investigated and discussed in chapter5. The electrodes are connected to voltage generation and measurement ports of the frequency response analyzer (FRA), Solartron 1260, (Solartron Analytical) via shielded leads. To minimize the stray impedance caused by high frequency current in the test cell and the leads, and also to avoid interference of the electro-magnetic fields surrounding the leads, the shields of the leads are short-circuited together as demonstrated in figure 4.1 in dashed lines coming out of the FRA. The FRA was connected to a computer via a GPIB cable for data acquisition. The FRA is controlled by the ZPlot software for performing frequency sweep. Figure 4.2 shows a photograph of the test setup (the test cell and the measurement apparatus). As illustrated in figure 4.2, the electrodes are connected to the leads with short (below 5cm) copper strips.

4.2.2 Sample Holders Design

To ensure reproducible experiments and reliable results, sample holders must allow easy and invariant loading of samples with desired thicknesses. Also, sample holders must allow avoiding air bubbles in the test cell for air bubbles dramatically change the resistance and capacitance of the test cell. The sample holders were designed using the commercial

solid design software, SolidWorks. Figure 4.3 shows the initial design of the sample holders. The design shown in figure 4.3 was modified to the final design (shown in figure 4.4) which allows seeing through the test chamber. The electrodes are placed in the designed position and the sample is placed between the two electrodes and is confined between them using spacers with desired thicknesses. The holders are then pressed against one another by tightening screws. The modified design of the sample holders (figure 4.4) has two benefits compared to the initial design: first, it allows optical microscopy of the samples, and second, the experimenter can see through the cell and make sure there are no air bubbles trapped in the cell. The modified design was used for performing all experiments. Figure 4.5 demonstrates the drawings of the sample holder parts (top holder is shown) and figure 4.6 shows the photograph of the test cell (sample holders).

4.2.3 Electrode Separation Distance

As discussed in chapters 1 and 3, for characterizing emulsions with the EIS technique, care should be given to choosing the appropriate length scale for the sample dimensions and electrode clearance. Based on numerical simulations, it was shown in chapter3 that if the sample thickness is in the same order of magnitude as the droplet diameter in the emulsion, the electric field gets distorted by the droplets so intensely that the bulk characteristics of the emulsions, that are determined by physical attributes such as droplet size distribution, are not detectable. On the other hand, if the clearance of the electrodes is too large, the signal-to-noise ratio will be too small unless a larger-amplitude input wave is applied, which in turn, adds an important artifact to the experiments by disturbing the sample, for example by causing the droplets to coalesce under strong electric fields and potentials. Based on the above discussion, the length scale for electrode separation distance that can reflect the bulk properties of the emulsions under investigation, is chosen to be 500 μm to 5 mm and therefore, the test cell is referred to as a milli-fluidic rather than a micro-fluidic system. The mean droplet size for the emulsions investigated is around 10 μm (see section

4.7.4). The effect of sample thickness on the EIS response is discussed in chapter 5.

In this work, the electrodes are separated using plastic spacers with the desired thicknesses. The spacers are hollow rectangles which form the test chamber between a 2mm-wide enclosing wall. The width of the spacer allows avoiding fringing effect in the test chamber and ensure a uniform electric field inside the test chamber.

4.2.4 Four-electrode configuration

The setup was designed and fabricated as a two-electrode EIS platform. The main barrier to applying EIS to conductive media is that the polarization effects in the close vicinity of the electrodes may outweigh the sample "bulk" properties [5, 15]. This problem specifically arises in micro-fluidic applications of EIS when the physical thickness and the Debye length of the polarized layer near the electrodes become considerable compared to the total sample length. In this study, the distance between the electrodes, or in other words the milli-fluidic nature of the test cell, reduces some of the electrode polarization effects. However, at low frequencies, the electrode-sample interface polarization may still be considerable. The main technique used in this thesis to avoid the experimental artifact caused by the electrode surface polarization is to correct the low-frequency polarization-affected impedance data by adding a constant phase element (CPE) in series with the R|C circuit (representing the sample) to account for the lower frequencies and model the polarization. In other words, the R|C circuit represents sample properties in higher frequencies and the CPE represents low-frequency electrode polarization. This approach was explained in details in chapter 3. In order to ensure the reliability of the two-electrode measurements, the clean mixture (glycerol-water) experiments were repeated with a four-electrode setup (first suggested by Schwan and Ferris [63]) as well.

In 2-terminal EIS, the measurements of potential is carried out on the same electrodes that are designated to carry the input wave. Therefore, the electrode polarization on the current-carrier electrodes may affect the potential measurements. However, in four-

electrode measurements [63, 64], the potential is measured on separate electrodes. This technique allows using higher potentials in the current-carrier electrodes and using lower frequencies in samples with higher ionic strength without facing the electrode polarization problem on the measurement electrodes. However, as explained in chapter 2, there are two drawbacks in using the 4-terminal technique. The first disadvantage is, if the measurement terminals are needle-shaped electrodes, they will only measure the potential at specific points in the sample while the blocking surface or mesh electrodes measure a surface average potential, and if the electrodes are chosen to be blocking surfaces or meshes, they will distort the electric field considerably and add an artifact to the experiments themselves. The second disadvantage is that the presence of extra electrodes in the system adds to the complexity of manufacturing an industrially applicable test cell. In this project, 4-electrode measurements are carried out for clean mixtures and are later (in chapter 5) compared to the two-electrode results to assess the reliability of the test cell and the measurements. In this section, the design of the 4-terminal configuration is explained.

The same sample holders used for two-electrode measurements were used for 4-terminal experiments as well. Based on the method used by Lvovich et. al. [16] and Padmaraj et. al. [100], mesh electrodes were used as measurement electrodes. The samples were placed between two blocking surface electrodes (current carrier electrodes) while the two mesh electrodes (measurement electrodes) were placed between the two current carrier electrodes as shown schematically in figure 4.7. Both sides of the mesh electrodes were in contact with the samples and the sample was allowed to pass through the mesh electrodes when being placed into the cell. Since the potential measurement electrodes are connected to high-impedance terminals of the FRA, and are not subject to electrical current or polarization, the electrode material and surface properties can be selected with more flexibility. The mesh electrodes used in this project are 35-mesh (500 microns) stainless steel (SAE 1020) woven wires with 500 μm thickness and the same surface area dimensions as the current-carrier electrodes (45mm×20mm). Figure 4.8 shows the photograph of the mesh

electrodes.

4.3 FABRICATION OF THE EXPERIMENTAL SETUP

As stated in chapter 2, studying emulsions has been attempted in micro-scale [13, 101] mainly to investigate the breakdown of the nano-scale film forming between droplets. While micro-fluidic approach may reveal unknown physics of emulsions, fabrication of micro-fluidic test setups is associated with numerous difficulties and expensive time consuming processes. Moreover, micro-fluidic chips are prone to fouling when used with industrially relevant liquids. On the other side of the spectrum, test cells that are used for bulk EIS of emulsions are expensive experimental setups that need to be cleaned after each run, which makes the application difficult for highly viscous and sticky industrial samples. In this work, the milli-fluidic design allows fabrication of the sample holders with 3D printing technology which provides a much simpler, less expensive, and faster fabrication process compared to the fabrication process of micro-fluidic chips. Also, the inexpensive fabrication process allows disposing of the test cell after testing viscous or sticky industrial samples. In other words, the milli-fluidic design does not have the disadvantage of being fouled due to the capability of being fabricated using 3D printing technology. In this thesis project, the design files of the sample holders with a ".STL" extension were exported to the ObJet Eden350/350V 3D printer and up to 10 samples were fabricated in less than 3 hours. The material used for fabrication is Vero Gray™resin. However, any plastic material that is not too soft for tapping screw threads and is compatible with the 3D printing device can be used for the fabrication process.

4.4 CHOICE OF ELECTRODE MATERIAL

As discussed in chapter 3, one of the difficulties of EIS for conductive media is polarization on electrode-sample interface in relatively low frequencies. The polarization can be

affected by the electrode material and/or surface properties. The effect of electrode material on the EIS response of the conductive samples (KCl solutions) is investigated in detail in the results and discussion chapter (5). In order to be able to see through the test cell and ascertain that no air bubble is trapped in the cell, indium tin oxide (ITO) coated glass (Prazisions Glass & Optik) chips were used as electrodes in all experiments (except the experiments studying the effect of electrode material). Being transparent and conductive inside, the ITO-coated glass electrodes allow optical microscopy of the samples while being studied with EIS or being subject to strong electric fields (not the topic of this thesis) to study coalescence of the droplets under electric fields.

4.5 SPECIFICATIONS OF THE ELECTROCHEMICAL IMPEDANCE SPECTROSCOPY

A sinusoidal electric signal with an amplitude of 10mV was applied to the cell using the Solartron 1260 FRA, and frequency was swept between 10 MHz to 0.1 Hz. The typical semi-circular Nyquist plot representing the relaxation behavior of emulsions was observed in this range. The accuracy of the impedance measurement at each single frequency was 0.1% (according to Solartron 1260 gain phase analyzer specifications), and the effect of possible relaxation-related errors in the frequency range of the measurements is reflected in the error bars for the effective values of capacitance or resistance. A comprehensive standard operating procedure (SOP) of the EIS experiments including the appropriate connection of the electrodes to the FRA is provided in Appendix A.

4.6 IMPEDANCE OF THE LEADS AND DRY CAPACITANCE OF THE CELL

4.6.1 Impedance of the leads

In order to calibrate the experimental setup, the impedance of the system with short-circuited electrodes was measured. Figure 4.9 shows the impedance of the leads, elec-

trodes, and copper strips combined. The measurements were performed with fresh copper strips as well as wrinkled and twisted ones with different lengths using both an Ohm meter and the FRA (5 measurements each). As shown in figure 4.9, the resistance of the leads, electrodes and copper strips does not exceed 40Ω while the resistance of the samples placed in the test cell (see chapter 5) are normally at least one order of magnitude larger than that. It is also noteworthy that for electric potential measurement, the reference terminals of the Solartron 1260 provide a high impedance of 100GΩ (Solartron 1260 manual).

4.6.2 Dry capacitance of the test cell

As part of the calibration process of the test cell, the capacitance of the dry cell (with a 500μm spacer) was measured using the FRA. Figures 4.10 to 4.12 illustrate the Nyquist and Bode plots for the frequency response of the dry cell. A parallel $R|C$ circuit was used to model the dry cell data. The capacitance and resistance of the dry cell are as follows:

R (Ω)	C (F)
1.18×10^{16}	5.58×10^{-11}

Assuming a dielectric constant of 3 for the plastic spacer and modeling the air sample as a capacitor in parallel with the spacer, the capacitance of the air sample will be 1.75309×10^{-11} which corresponds to a dielectric constant of 1.081. The relative humidity of air in the lab during the experiments was measured 30%. The measured dielectric constant of air is in agreement with the studies ([102] and [103]) that investigated the effect of RH on permittivity of air.

4.7 SAMPLE PREPARATION AND PROPERTIES

In this project, three types of samples were prepared for different experiments: clean mixtures (glycerol-water), decane-water emulsions, and castor-oil-water emulsions. In this

section, the sample preparation process and the emulsion size distribution for fresh emulsions is presented.

4.7.1 Glycerol-water mixtures

Glycerol with 99% purity (Sigma Aldrich 99% for Molecular Biology) was added to water (with different concentrations of KCl) drop wise in a 250mL beaker while being stirred by a magnetic stirrer at 600rpm for approximately 10 minutes. Glycerol contents of 0% to 100% was used for the experiments. The stirring results in clean homogenous mixtures of glycerol-water.

4.7.2 Decane-water emulsions

In order to prepare decane-water emulsions, first the emulsifying agent, Tween 80 (Polysorbate 80, Fisher Scientific), was added drop wise to water (with different concentrations of KCl) while being stirred at 700rpm until visually dissolved and for 10 minutes thereafter. Different concentrations of Tween (0CMC to 20CMC with CMC of Tween being 13-15 mg/L [104]) was used to achieve different levels of stability in the decane-in-water emulsions to test the ability of the EIS test cell in sensing phase separation. After dissolving Tween 80 in water, decane (99% Fisher Scientific - $CH_3(CH_2)_8CH_3$) was added drop wise to water-salt-Tween solution while being stirred at 700rpm. Then the mixtures were homogenized for 20 minutes using IKA T25 Digital Ultra-Turrax homogenizer at 13000rpm with the tip of the homogenizer 2cm above the bottom of the beakers. For decane contents of more than 50% (water-in-decane emulsions), Tegopren 700 (GoldSchmidt Chemical - Evonik Industries) with concentration of 1 CMC (CMC of Tegopren 700 is 0.05mM [105]) was dissolved in decane and then added to the water-KCl-Tween solution. The rest of the preparation process was unchanged. The surfactant dosages were chosen to make the samples stable enough so that they wouldn't undergo quick phase separation before the experiments, but at the same time not too stable, so that the capability of the developed

device for sensing phase separation would be tested in reasonable time spans. Some unhomogenized samples were tested as well.

4.7.3 Castor oil-water emulsions

As castor oil showed higher stability in water, lower Tween 80 dosages were used to stabilize the emulsions. Tween 80 with concentrations between 0CMC to 2CMC was dissolved in water as described in the previous section. Castor oil (Sigma Aldrich) was added drop wise to the solution and then homogenized as described above. Emulsions with oil contents up to 10% were prepared.

4.7.4 Size distribution of the emulsions

the size distribution of the oil droplets dispersed in water was acquired by light scattering measurements using the Mastersizer 2000 (Malvern Instruments). Since this device utilizes water-based dilution for size distribution, it will not give reliable results for oil-rich emulsions. Therefore, size distribution measurement has only been done for water-rich emulsions.

Figures 4.13 to 4.15 illustrate the measured size distribution for decane-water emulsions with different surfactant dosages. The emulsion with 0 concentration of surfactant showed quick phase separation, however, all size distribution measurements were done right after emulsion preparation and hence, the emulsions were all fresh and no observable phase separation occurred by the time the size distribution measurement was completed. Figures 4.16 to 4.18 illustrate the size distribution of castor oil-water emulsions.

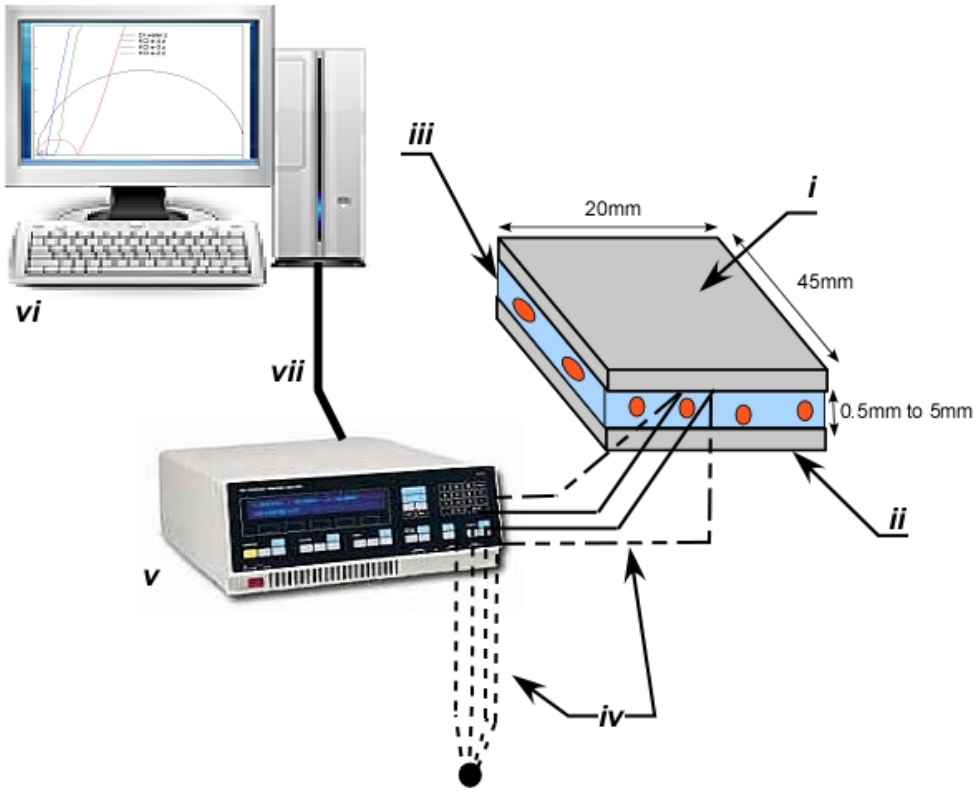

Figure 4.1: Scheme of the experimental platform for performing two-electrode electrochemical impedance spectroscopy. *i*, *ii*: Electrodes, *iii*: Sample, *iv*: Leads and connections (dotted lines coming out of the FRA show the shields of the leads shorted, dashed lines show the measurement leads and solid lines represent current carrier leads), *v*: Frequency Response Analyzer (FRA), Solartron 1260, *vi*: Computer with ZPlot software to control the FRA, *vii*:GPIB.

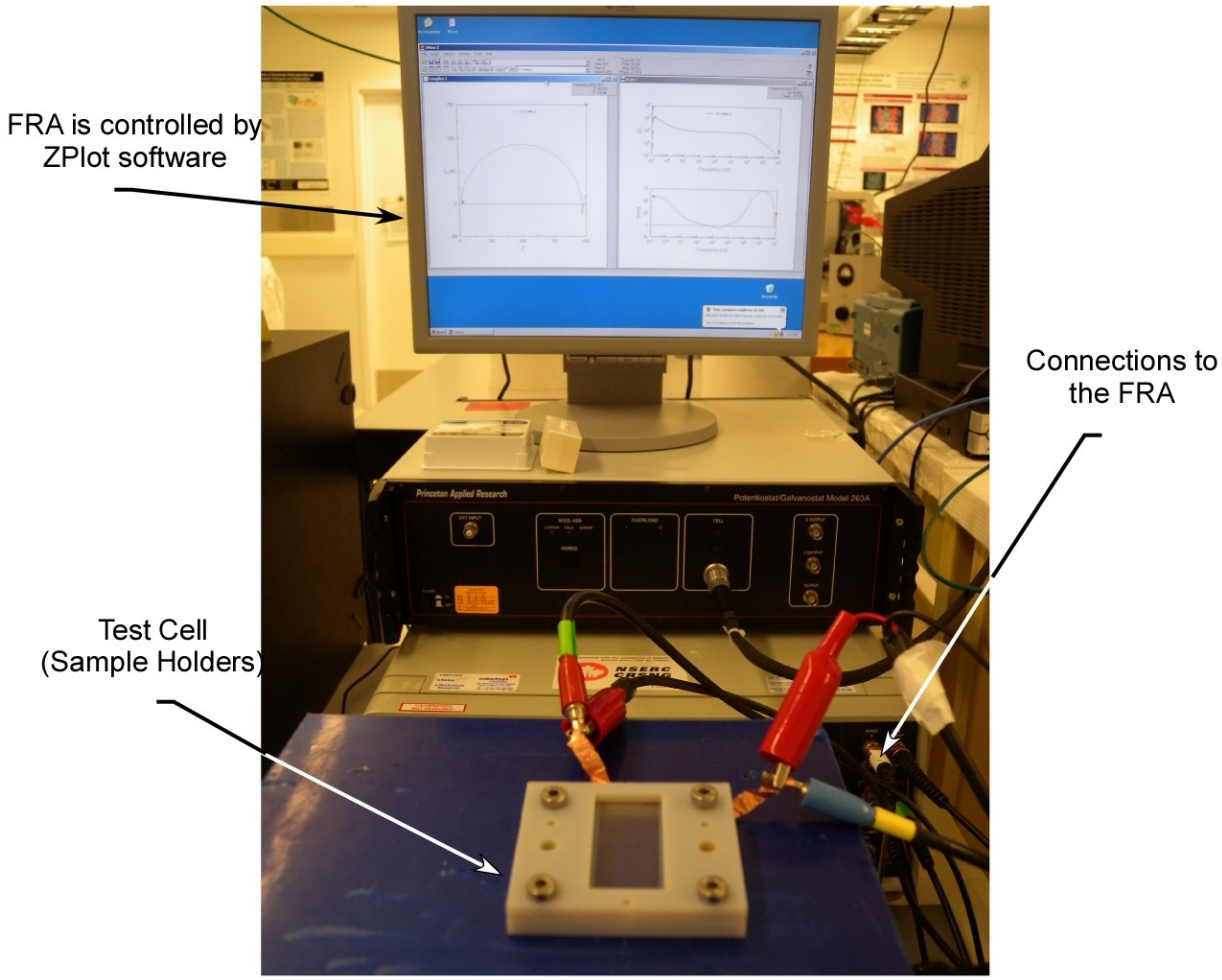

Figure 4.2: Photograph of the experimental setup showing the test cell (sample holders), the FRA, and the PC used for controlling the FRA.

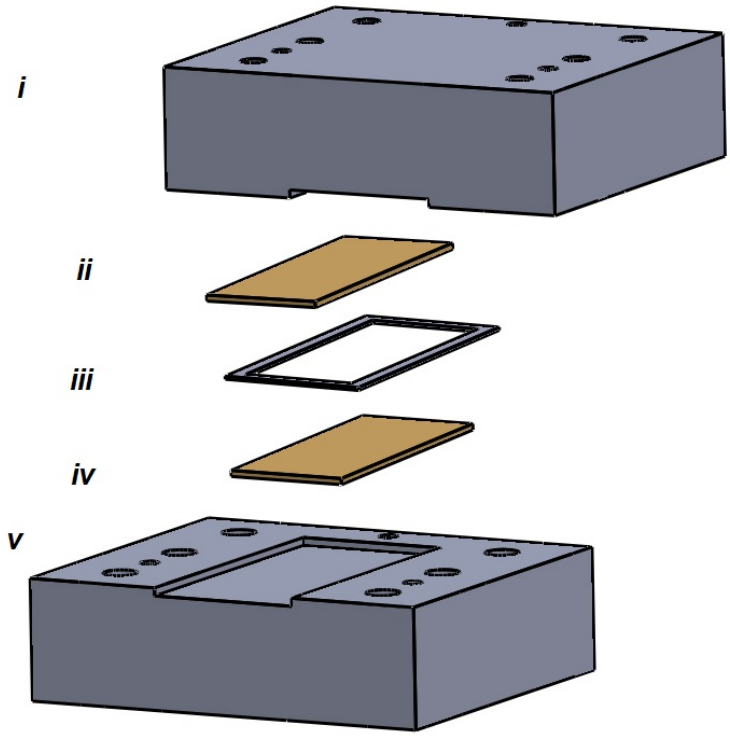

Figure 4.3: Schematic of the initial design for the sample holders. *i*: top holder, *ii*: top electrode, *iii*: spacer (shim), *iv*: bottom electrode, *v*: bottom holder.

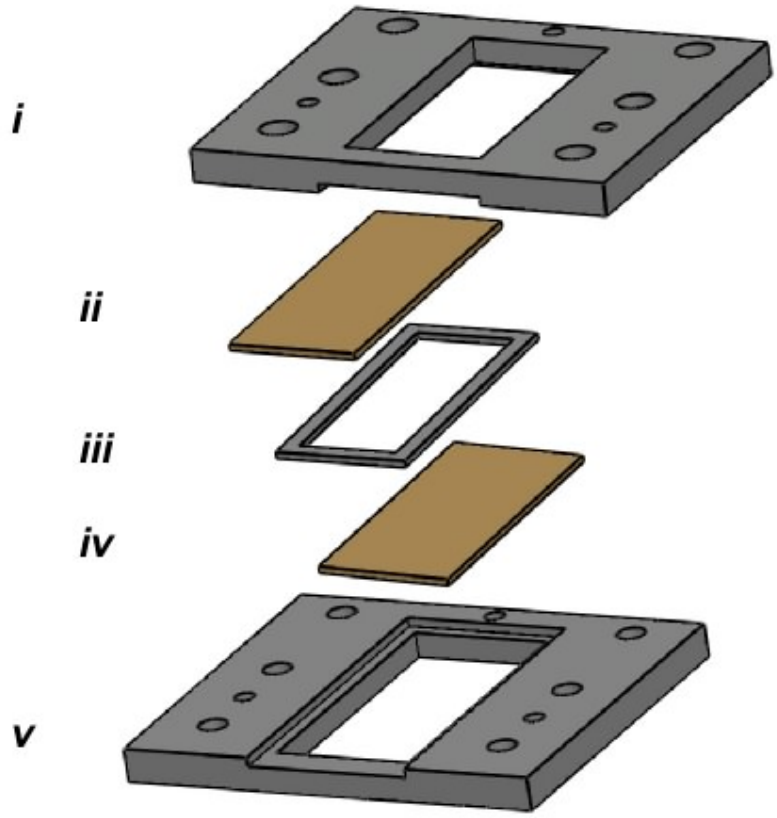

Figure 4.4: Schematic of the sample holders and the test setup allowing optical microscopy. *i*: top holder, *ii*: top electrode, *iii*: spacer (shim), *iv*: bottom electrode, *v*: bottom holder.

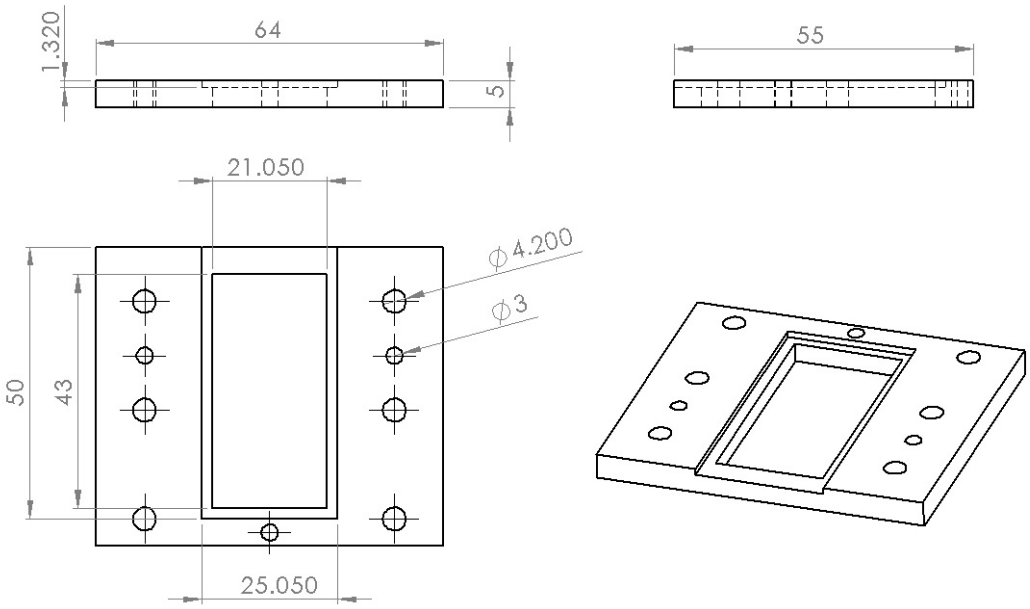

Figure 4.5: Drawings (front-top-right) of the sample holders (dimensions are in millimeter).

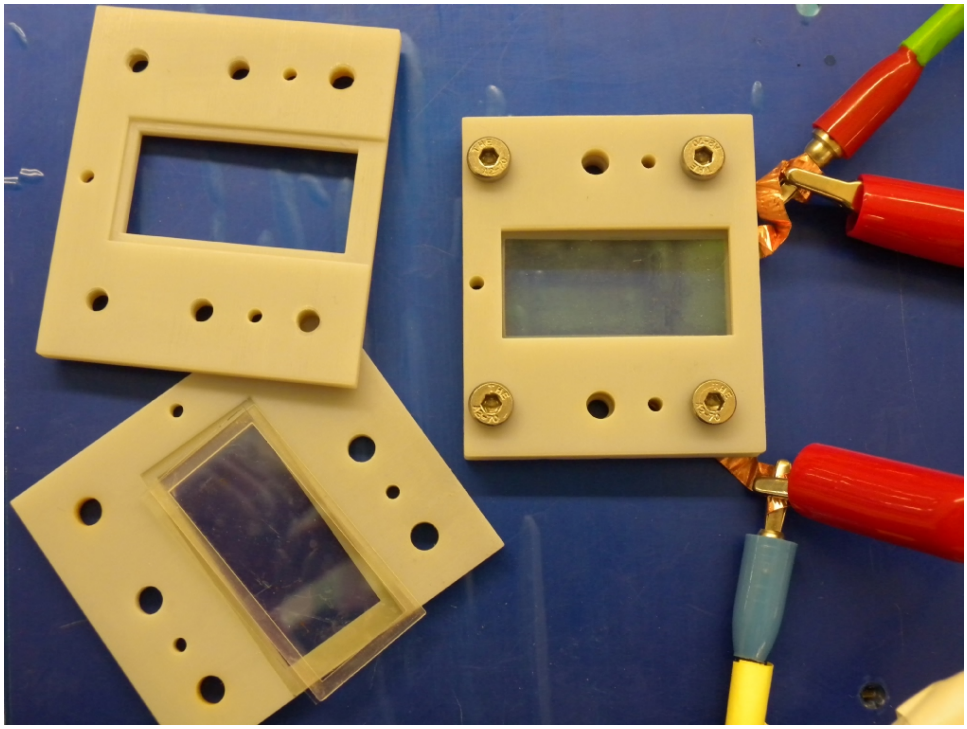

Figure 4.6: Photograph of the the test cell (sample holders).

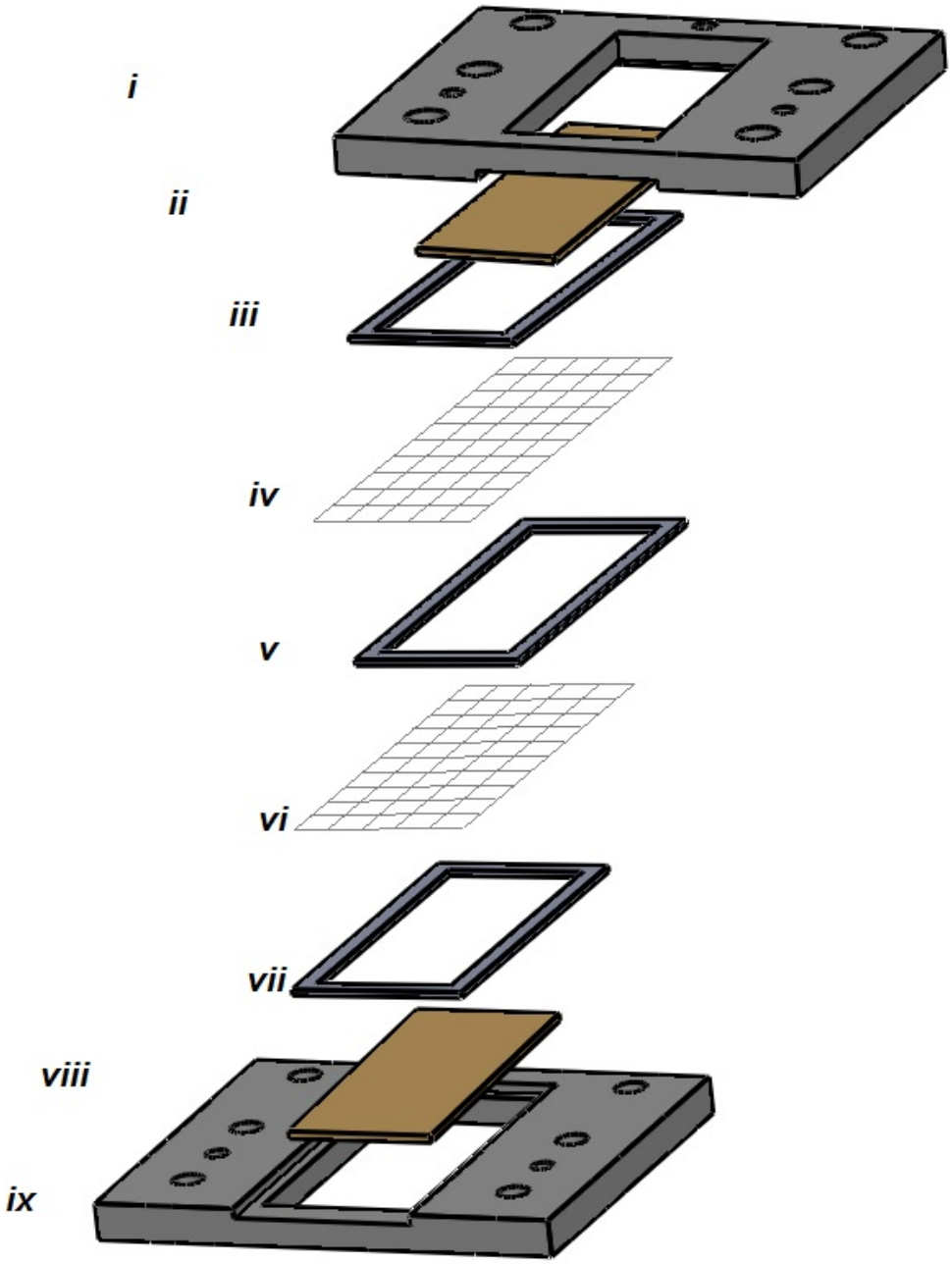

Figure 4.7: Schematic view of the 4-electrode setup used for EIS. *i*:top holder, *ii*: top current carrier electrode, *iii*: spacer, *iv*: top measurement (mesh) electrode, *v*: spacer, *vi*: bottom measurement (mesh) electrode, *vii*: bottom current carrier electrode, ix:bottom holder.

a

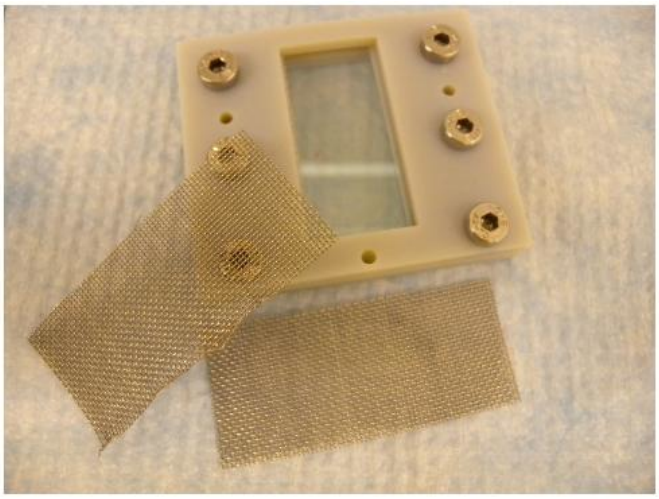

b

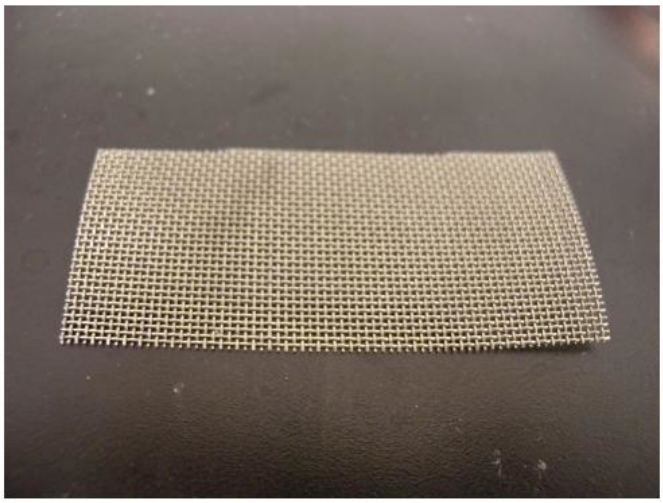

Figure 4.8: Photograph of the the mesh electrodes. *a*- mesh electrodes and the test cell and *b*- a mesh electrode.

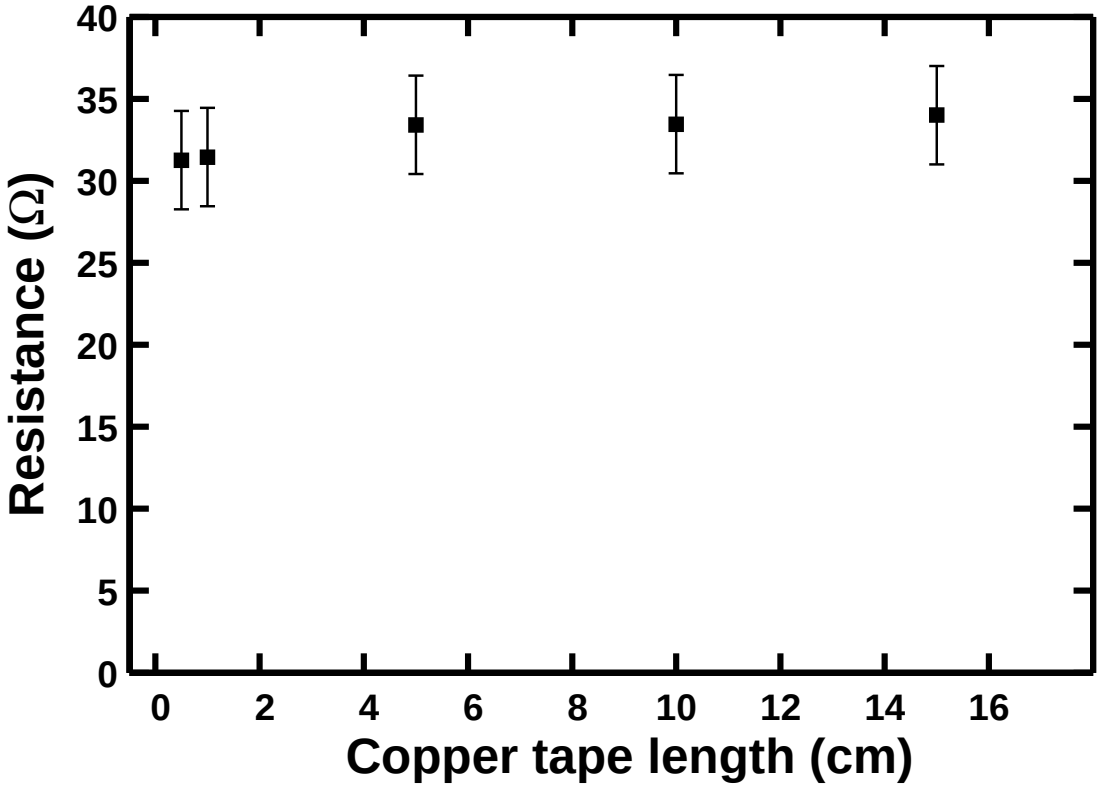

Figure 4.9: Resistance of the leads, electrodes, and copper strips of the test cell.

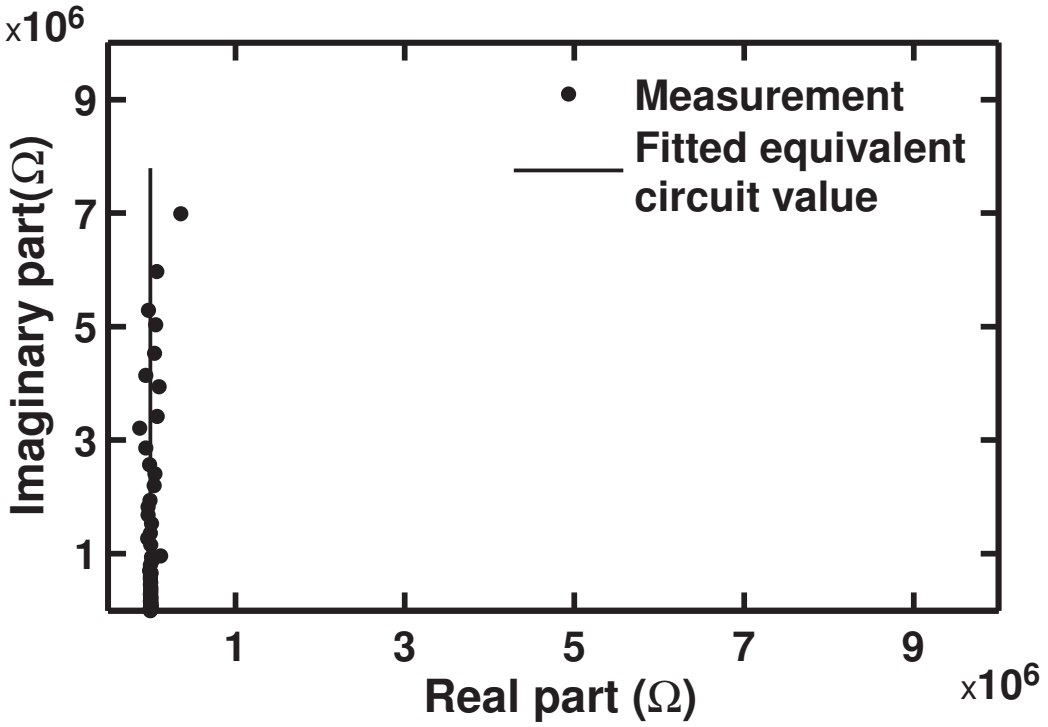

Figure 4.10: Nyquist plot of the dry test cell.

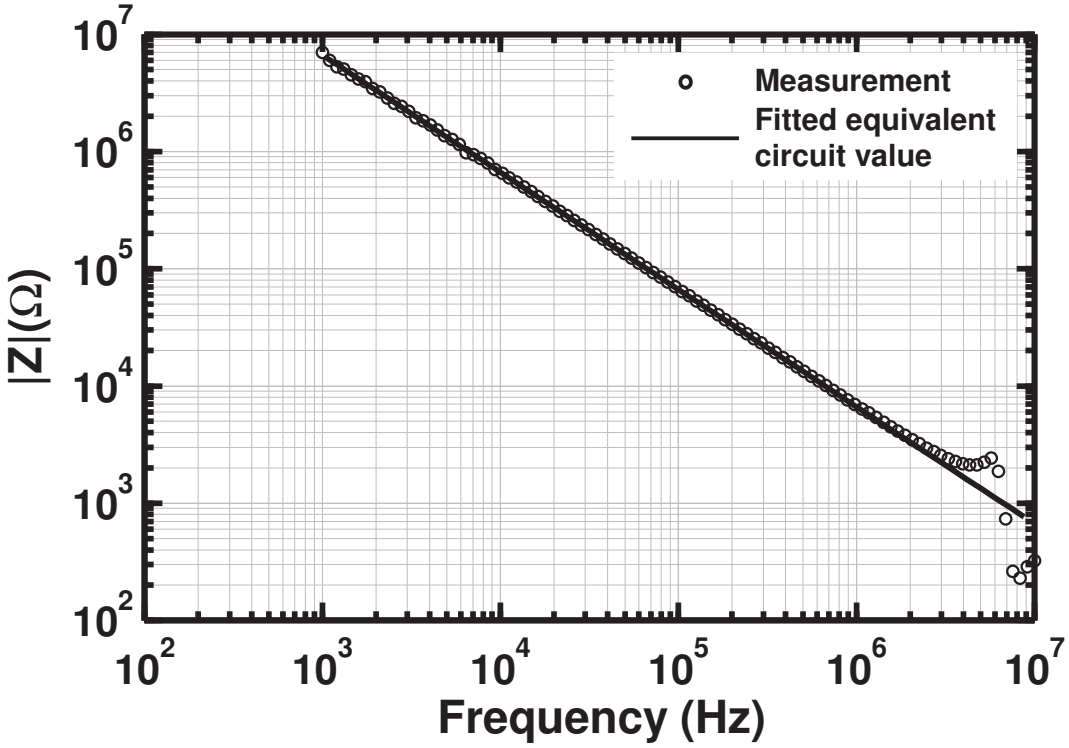

Figure 4.11: Bode plot (magnitude) of the dry test cell.

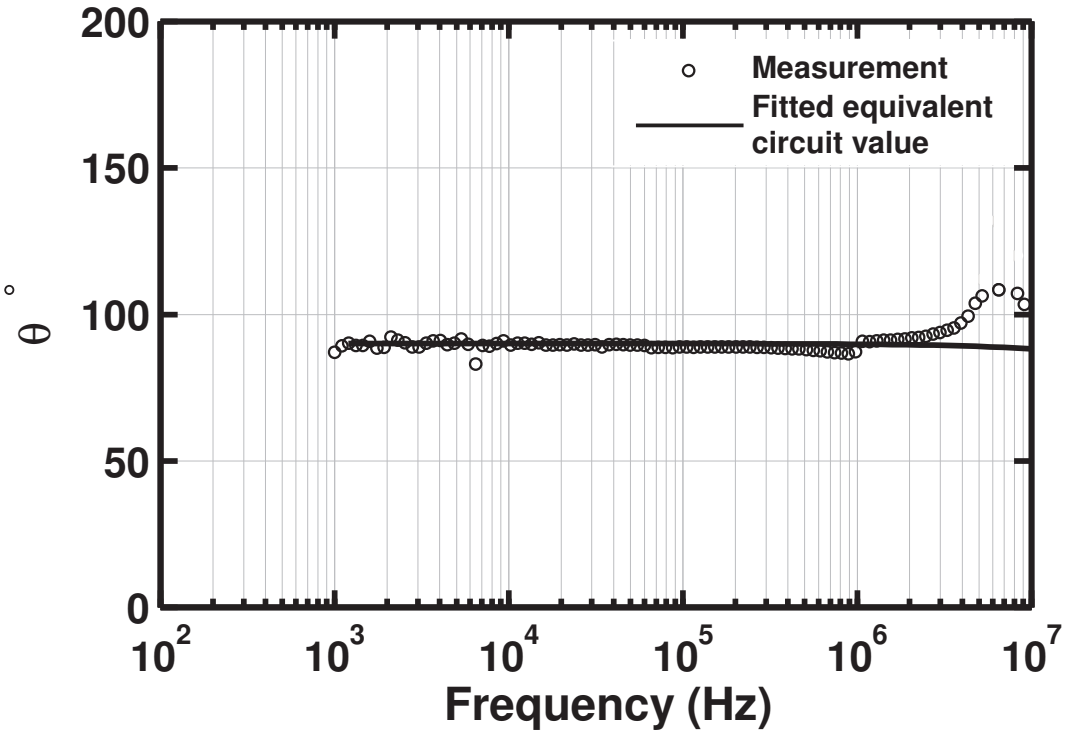

Figure 4.12: Bode plot (phase) of the dry test cell.

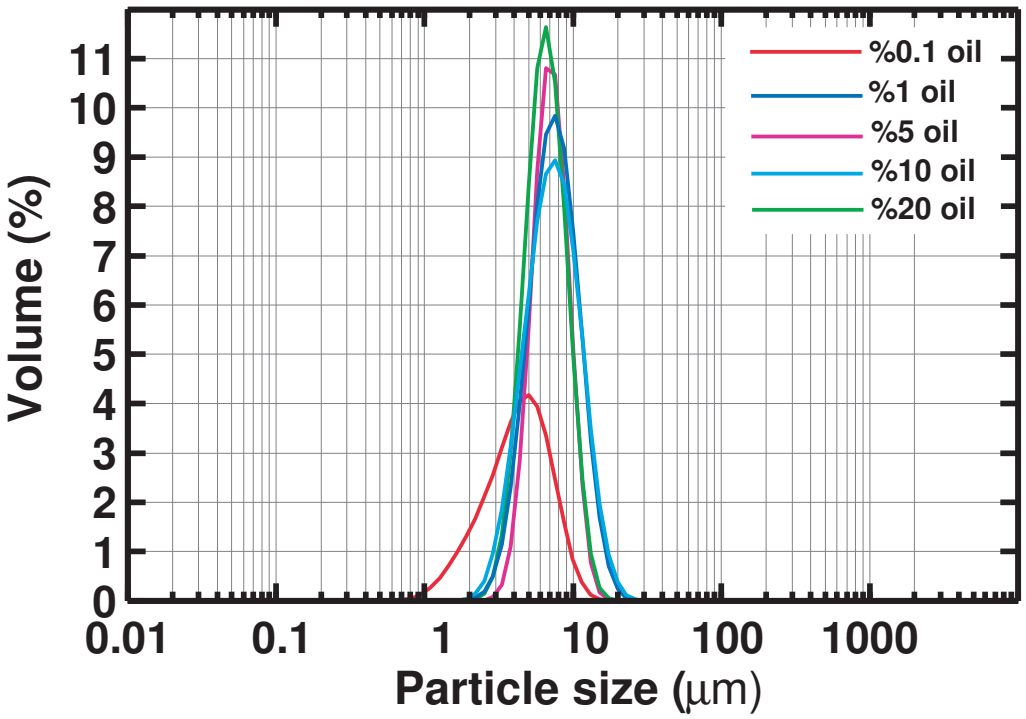

Figure 4.13: Size distribution of fresh decane-water emulsions without surfactants.

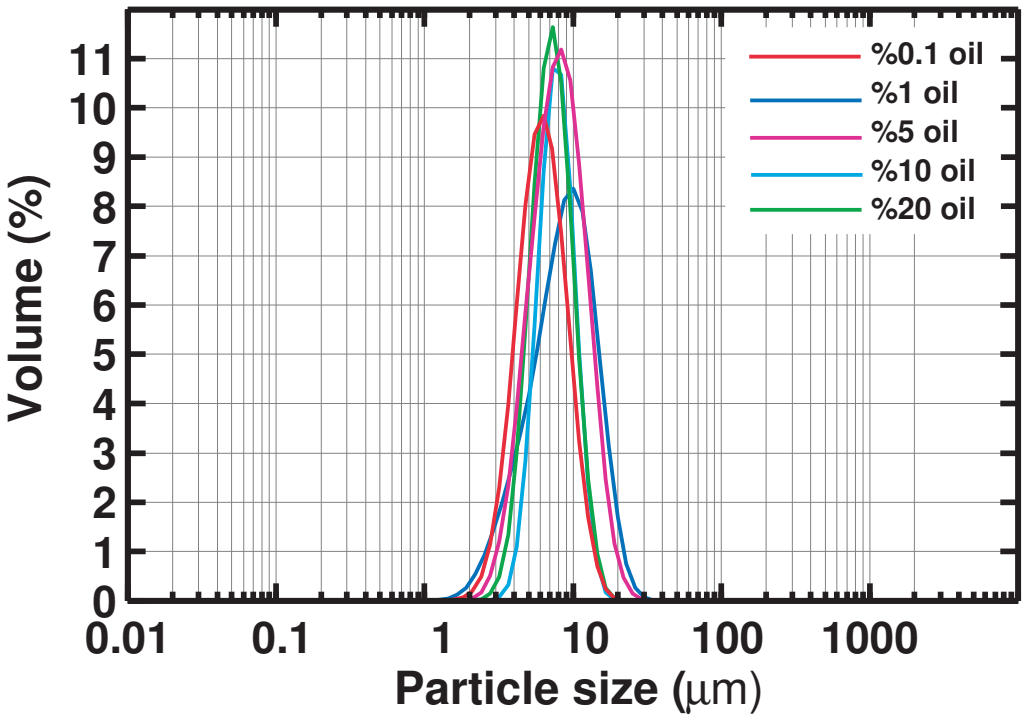

Figure 4.14: Size distribution of fresh decane-water emulsions with 1CMC of Tween80.

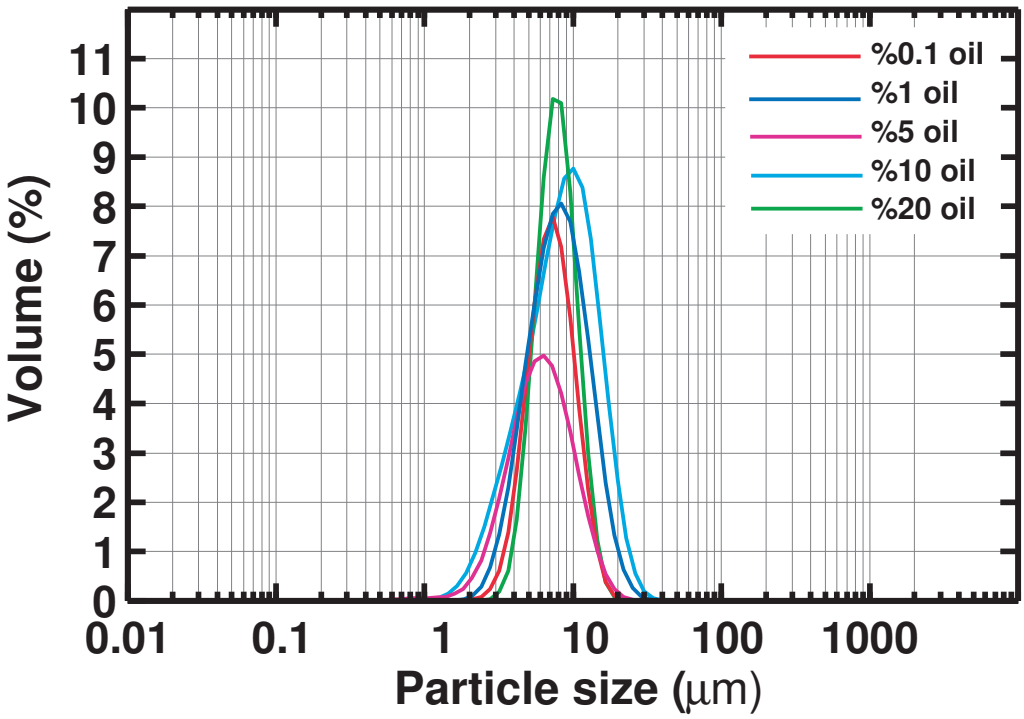

Figure 4.15: Size distribution of fresh decane-water emulsions with 20CMC of Tween80.

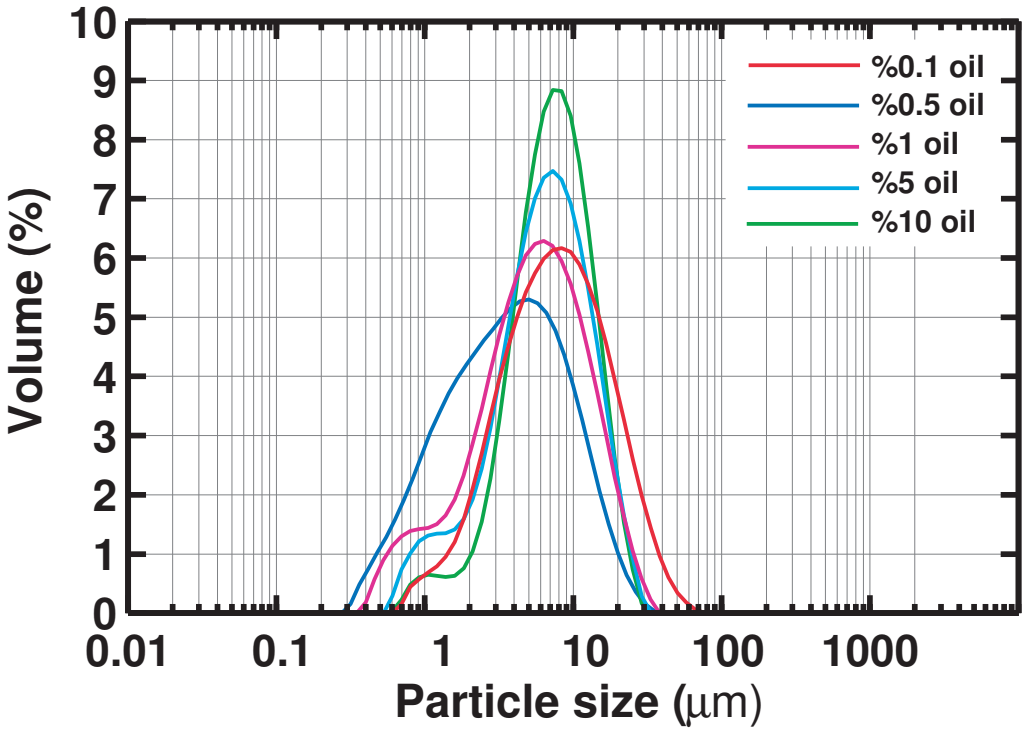

Figure 4.16: Size distribution of fresh castor oil-water emulsions without surfactants.

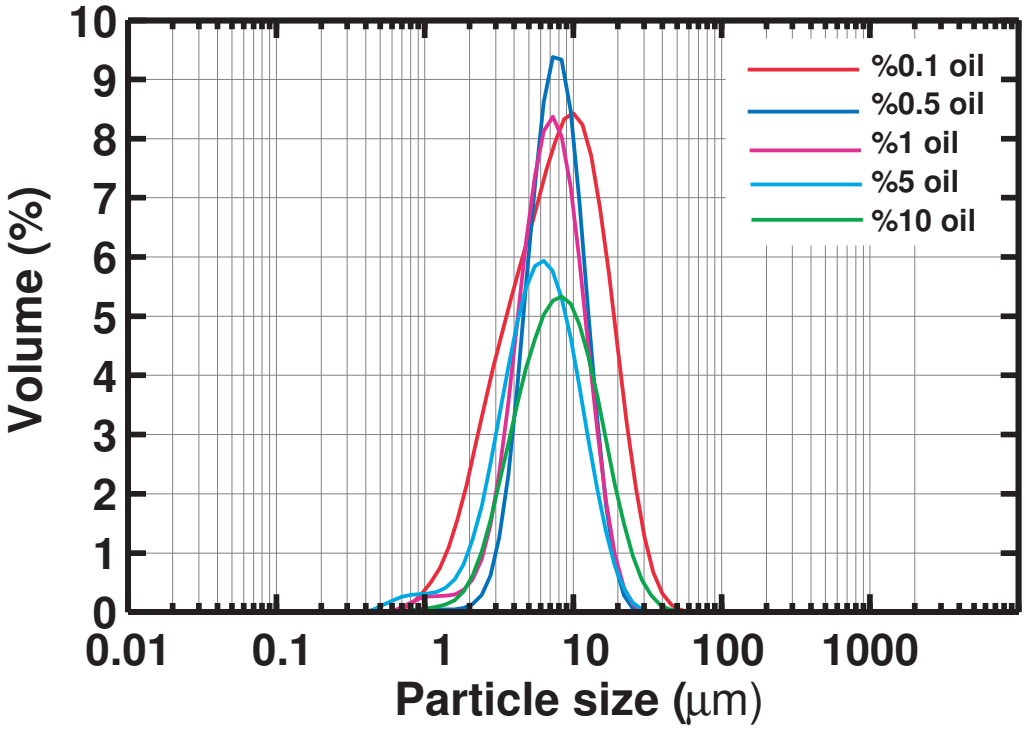

Figure 4.17: Size distribution of fresh castor oil-water emulsions with 0.1CMC of Tween80.

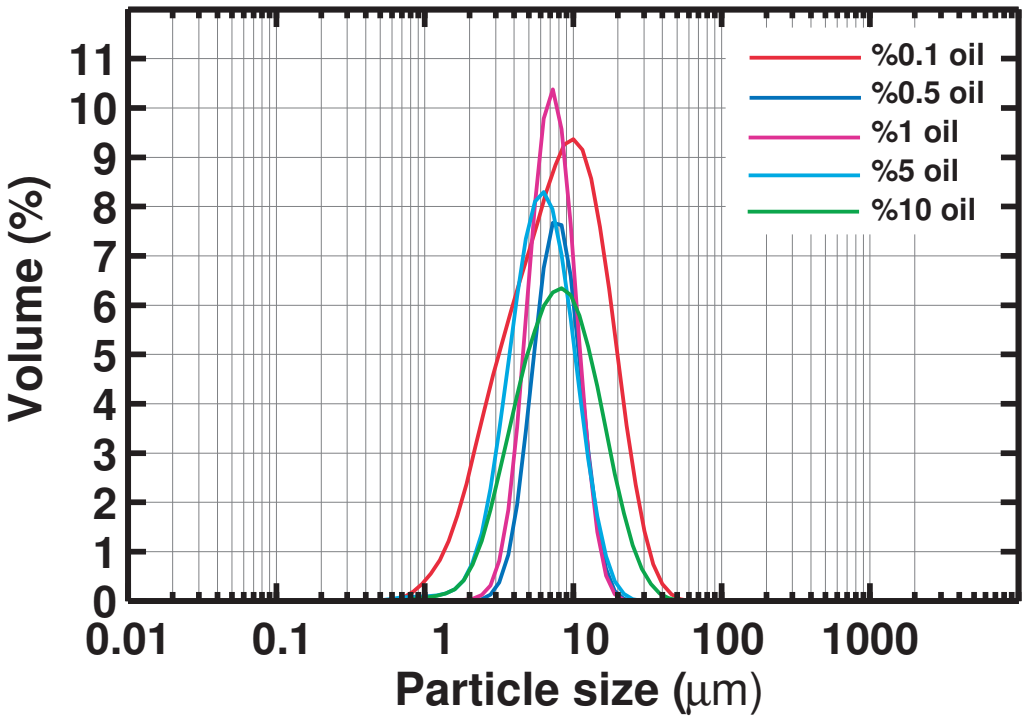

Figure 4.18: Size distribution of fresh castor oil-water emulsions with 2CMC of Tween80.

CHAPTER 5

EXPERIMENTAL RESULTS AND DISCUSSION

5.1 INTRODUCTION

It was shown in chapter 3 that EIS can be applied to O/W emulsions where oil/water ratio as well as phase separation dynamics affect permittivity and therefore can be captured by EIS. It was further shown that in EIS, in order for the bulk properties to be measured, the test cell needs to be at least an order of magnitude larger than droplet size of the emulsion. In chapter 4, a "milli-fluidic" experimental setup for EIS of liquids was introduced and the resistance of the leads and electrodes, as well as the dry capacitance of the test cell was discussed. In this chapter, the capability of the developed device in estimating electrical properties of complex liquids is assessed through extensive experiments. As part of developing this experimental platform, different parameters and design decisions that can affect the EIS measurements are studied. Different samples including salt-water electrolytes, clean liquid-liquid mixtures (glycerol-water), and model oil-water emulsions have been tested. One main focus of this chapter is to study the electrical properties (resistance and capacitance) of oil-water emulsions during phase separation and investigate the application of dielectric measurements in sensing phase separation.

5.2 SALT-WATER ELECTROLYTES

5.2.1 Effect of ionic strength on dielectric constant and conductivity

Different concentrations of KCl in DI water were tested to study the effect of salt concentration on capacitance, and to relate the measured resistance (conductivity) to the theoretical values. Figures 5.1 and 5.2 illustrate the Bode and Nyquist plots of KCl-water electrolytes with KCl concentrations of $0M$, $10^{-5}M$ $10^{-4}M$ and $10^{-3}M$. In these figures, the symbols exhibit the experimental measurements and the lines show the equivalent circuit model fitted to the measurements based on the circuit shown in figure 3.17. As shown in figures 5.1 and 5.2, the equivalent circuit is a good fit for the experimental data and the sample properties can be interpreted as electrical element values based on the discussions of sections 3.6.3 and 3.6.3. The capacitance and resistance of the samples (as illustrated in figure 3.17) are determined based on the EC modeling and the dielectric constant of the samples can be determined based on the following equation:

$$C = \epsilon_o \epsilon_{r,eff} \frac{A}{d} \tag{5.1}$$

where C is the capacitance of the film, ϵ_o is vacuum permittivity, $\epsilon_{r,eff}$ is the effective dielectric constant of the sample, A is the surface area of the electrode, and d is the thickness of the dielectric (sample). The dimensions of the sample are mentioned in section 4.2 (with d=500µm).

The dielectric constant of electrolytes with different KCl concentrations are illustrated in figure 5.3. As discussed in section 3.5, salt concentration can only affect permittivity by producing charge density gradients and otherwise does not affect water permittivity. Since the high-frequency data is being used for determining the sample properties, charges are not given enough time to respond to the electric field and produce charge gradients in the sample. Therefore, the measured dielectric constant is expected to remain unchanged for

different KCl concentrations (in the concentration range used). On the other hand, the frequency range of the measurements does not reach GHz frequencies where molecular relaxation phenomena affect permittivity (see chapter 1). Therefore, the static permittivity of water holds in the experiments. Figure 5.3 shows that the dielectric constant of all salt concentrations are close to the static dielectric constant of water. This behavior is in agreement with the results of the fundamental work by Drake et. al. [95] in measuring dielectric constant of KCl solutions as well as works of [96] and [97].

Based on the discussions of section 3.3, permittivity measurements are more sensitive to phase separation of O/W emulsions. Therefore, the focus of this thesis is on characterization of complex liquids based on their permittivity. However, the developed device can provide resistance (conductivity) measurements as well.

For an electrically neutral electrolyte in the absence of concentration gradients, the Ohm's law can be expressed as [92, 106]

$$i = -\sigma \nabla \psi \tag{5.2}$$

where i is the electrical current per unit area, σ is the electrolyte conductivity and $\nabla\psi = E$ is the electric field.

Comparing equation 5.2 with the conventional expression of Ohm's law

$$V = RI \tag{5.3}$$

electric field can be expressed as

$$E = \frac{V}{d} = \frac{RI}{d} = \frac{RiA}{d} \tag{5.4}$$

where d and A are the sample thickness and surface area. Substituting i from equation 5.2 into the last term in equation 5.4 and solving for R, the resistance of an electrolyte can be derived:

$$R = \frac{d}{A}\frac{1}{\sigma} \tag{5.5}$$

the effective conductivity of the samples can be calculated based on the following equation:

$$\sigma = \frac{d}{A}\frac{1}{R} \tag{5.6}$$

The measured conductivity for different KCl concentrations are illustrated and compared with reference values in figure 5.4. The reference values are calculated based on the molar conductivity data adapted from *CRC Handbook of Chemistry and Physics* [107]. Reference value for conductivity of the DI water is determined based on the deionizer resistivity value ($16M\Omega cm$). Figure 5.4 shows that the measured conductivity is in agreement with reference values.

5.2.2 Effect of electrode material

It was mentioned in chapter 4 that as a step towards introducing the developed experimental platform as a simple, yet robust device for applying EIS to liquids, different characteristics of the device that may affect the EIS experiments are tested. These characteristics include electrode material, sample thickness, and signal amplitude. In this section, the effect of electrode material is investigated.

As discussed in chapter 4, most of the experiments were carried out with ITO-coated glass chips which (a) allow the experimenter to see through the sample and make sure that

no air bubble is trapped in the cell, and (*b*) are suitable for optical microscopy. However, in order to explore the possibility of using other materials, different electrode materials (gold, stainless steel, and copper) have also been tested. The sample was KCl $10^{-4}M$ with 500μm thickness, and signal amplitude of $25mV$. Gold was sprayed on glass chips with nano-fabrication spraying technique with a thickness of 100nm. Steel and copper electrode surfaces were initially ground with an 800 grit size abrasive disk and polishing was performed with metal buffing rouge.

Figures 5.5 and 5.6 illustrate the Nyquist and Bode plots of the EIS response with different electrode materials. As observed in figure 5.6, in gold and ITO experiments, the impedance of the constant phase element has a smaller magnitude compared to copper and steel and therefore affect the total impedance of the test cell in lower frequencies compared to copper and steel. In other words, investigation of the film with ITO and gold is more reliable because a wider frequency range can be attributed to the liquid sample. In copper and steel experiments, the electrode-sample interface impedance outweighs that of the samples when frequency reaches as low as $10^5 Hz$ whereas for gold and ITO, this minimum frequency is $100Hz$ and $1000Hz$ respectively. This can be attributed to the surface polarization on the electrodes. The magnitude of the CPE element ($\frac{1}{Q}$ in equation 3.24) as well as R and C for different electrode materials are listed in table 5.2.2. The difference in the measured capacitances can be attributed to the fact that the frequency range used for characterization of the electrolyte samples with steel and copper electrodes is short and this adds some errors to the capacitance values found through (equivalent circuit) EC fitting.

5.2.3 Effect of sample thickness

As discussed in section 3.5, the sample thickness for EIS of emulsions need to be at least one order of magnitude larger than size of the dispersed droplets. In this section, the

Electrode Material	**R (Ω)**	**C (F)**	$\lvert Z_{CPE}\rvert = \frac{1}{P}$ **(Ω)**
ITO	395	1.26×10^{-9}	1.12×10^{4}
Gold	380	1.29×10^{-9}	2.21×10^{4}
Copper	403	1.54×10^{-9}	1.23×10^{6}
Steel	450	1.66×10^{-9}	1.31×10^{7}

Table 5.1: Electrical element values for EIS experiment of water-KCl 10^{-4}M with different electrode materials.

effect of sample thickness on EIS experiments with salt-water samples is studied. Water with KCl concentration of $10^{-4}M$ was used with signal amplitude of 25mV. The effect of thickness on EIS of emulsions is discussed in section 5.5.3.

Nyquist and Bode plots of the EIS experiment with different sample thicknesses are shown in figures 5.7 and 5.8. It is shown that for the maximum thickness (5mm), the measurements becomes too noisy at low frequencies. This is attributed to the fact that basically, low frequency measurements are associated with more error than high frequencies because of reasons such as dynamics of the sample (even slowest dynamics may happen too fast to be captured with low-frequency measurements) and interference with the working frequency of the lamps at the laboratory (below 50Hz). The hypothesis was that the noise in the low frequency measurements with the thickest sample, is caused by too small signal-to-noise ratio and can be solved with increasing the signal amplitude. This hypothesis is tested in the next section. The capacitances measured with different thicknesses are plotted in figure 5.9 and compared with theoretical values based on equation 5.1 (higher frequencies (minimum 1000Hz) are used for fitting the 5mm experiment). The same behavior was reported by Lvovich and Smiechowski [12].

5.2.4 Effect of signal amplitude

Since the main aim of this thesis is to use EIS as a diagnostic tool, the amplitude of the signals are kept as small as possible. However, the signal should be large enough to ensure a reasonable signal-to-noise ratio. For all experiments, the signal amplitude is

25mV. For oil-water samples, some experiments were repeated with 10mV to make sure same results were acquired. In this section, the effect of signal amplitude is studied on 500μm and 5mm thick KCl 10^{-4}M samples. The applied AC signal amplitudes are 25mV, 100mV, 200mV, and 1V. Figures 5.10 and 5.11 illustrate the Nyquist and Bode plots for different signal amplitudes. It is shown that the system with 5mm thickness is noisy at low frequencies. As figures 5.10 and 5.11 suggest, when signal amplitude is increased in the 5mm sample, the signal-to-noise ratio increases and the system becomes less noisy in low frequencies. In both 500μm and 5mm samples, when amplitude was increased to 1V, a large anomaly was observed at frequencies below 1000Hz. This is attributed to coating degradation on the electrodes at high amplitudes and low frequencies. At this amplitude, light brown patches were observed on the ITO-coated glass chips showing coating degradation on the ITO surface. The increase in the amplitude results in a slight increase in the measured capacitance which is in agreement with the experiments reported by Lvovich and Smiechowski [12] and is exhibited in figure 5.12. No significant change in resistance was observed.

5.3 MODEL CLEAN SYSTEMS: GLYCEROL AND WATER MIXTURES

The performance of the developed experimental platform in estimating liquid sample properties is first tested with clean liquid-liquid mixtures of glycerol ($\epsilon_r \simeq 40$) and water ($\epsilon_r \simeq 80$). Different glycerol contents (from 0% to 100%) were mixed with water with different salt concentrations (DI water, KCl 10^{-4}M, 10^{-3}M, and 10^{-2}M).

5.3.1 Effect of glycerol content and ionic strength

Figures 5.13 to 5.20 show the Nyquist and Bode plots for different glycerol contents with various salt concentrations. It is observed that while salt concentrations affects resistance (dielectric loss), it does not affect permittivity (dielectric constant) considerably. This can

be attributed to the fact that the high frequency portion of the frequency range is used to model the emulsion sysytem as a parallel $R|C$ circuit. Permittivity, on the other hand, is affected by glycerol content. Glycerol volume ratio also affects the effective resistance.

As discussed in sections 3.3 and 3.2, since glycerol mixes very well with water, not only the capacitance (dielectric constant) of the mixtures are affected by the glycerol content, but also the effective conductivity (resistance) depends on the glycerol content. Figures 5.21 and 5.22 show the variations of capacitance and resistance of glycerol-water mixtures with different glycerol contents (figure 5.22 is for glycerol in aqueous solution of 10^{-4}M KCl). Based on the discussions in chapters 2 and 3, the permittivity of glycerol-water mixtures is best described by Maxwell-Garnett model. The permittivity behavior observed in this experiment shows the same trend as the results of Behrends et. al. [108] for the respective frequency range of their dielectric spectroscopy. In figure 5.21, the measured capacitance is compared with the capacitance calculated based on Maxwell-Garnett model for homogeneous mixture permittivity and in figure 5.22, the resistance of the glycerol-water (KCl 10^{-4}M) mixtures is compared with the experimental data provided by [109]. The acquired results with the developed experimental platform show acceptable agreement with theoretical and reference values.

In terms of conductivity of DI water, it is observed that the resistance obtained for DI water in the experiments of section 5.2 (fresh DI water from deionizer) is different from the experiments with glycerol and oil. This difference is not observed in salt-water solutions. The reason is that stirring DI water with glycerol or oil causes the carbon dioxide in the air to dissolve in water and produce carbonic acid which increases the conductivity of DI water considerably. However, the salt dissolved in water causes the conductivity to be already so large that is not affected by the carbon dioxide in the air. In the DI water-glycerol and DI water-oil experiments, the DI water was stirred alone first so that the conductivity became stable. This was not needed in experiments with salt-water electrolytes.

5.3.2 4-electrode experiment

As mentioned in section 4.2.4, in this thesis, the main mechanism of extracting bulk sample properties from EIS experiments, and the main method of avoiding electrode-polarization-induced artifacts in the measurements, is basing the sample properties in form of resistance and capacitance on high-frequency data and relating the electrode polarization to the CPE behavior in low frequencies. However, in order to make sure that the experiments give reliable results, some of the glycerol-water experiments with KCl 10^{-4}M were repeated with 4-electrode configuration as explained in section 4.2.4. Figures 5.23 and 5.24 illustrate the Nyquist and Bode plots for 4-electrode measurements with different glycerol contents. It is observed that the low-frequency constant-phase element that was observed in 2-electrode measurements no longer exists in 4-electrode experiments. All cases show a behavior very close to an $R|C$ circuit similar to the high-frequency portion of the 2-electrode experiments.

5.4 MODEL EMULSION SYSTEMS I: FRESH OIL-WATER EMULSIONS

5.4.1 Decane-water emulsions: effect of oil volume fraction

In this section, the developed experimental platform is tested in estimating oil volume fraction based on capacitance (dielectric constant) measurements. Figures 5.25 to 5.28 illustrate the Nyquist and Bode plots of the EIS experiment with different decane volume fractions as well as two ionic strengths (DI water and KCl $10^{-4}M$). It is observed that the equivalent circuit model is a very good fit to the system behavior in high frequencies (parallel $R|C$ representing the emulsion) as well as low frequencies (CPE representing the electrode-sample interface). Figure 5.29 illustrates the measured capacitance of the decane-DI water as well as decane-KCl $10^{-4}M$ electrolyte versus oil volume fraction. The experimental results are compared with Boyle model for permittivity of homogeneous complex media. As illustrated in figure 5.29, the capacitance of the fresh emulsions are very close to the Boyle model. This demonstrates that stable or fresh emulsions can be

regarded as homogeneous media. It is also observed that while the capacitance of the oil-electrolyte emulsions are slightly higher than the oil-DI water emulsions, both types of emulsions are very close to the Boyle capacitance value.

Figure 5.30 illustrates the resistance of the decane-DI water and decane-KCl $10^{-4}M$ fresh emulsions versus oil volume fraction. It is observed that the resistance (conductivity) of the emulsions show very little variation up to oil volume fraction of 90% where a sudden resistance increase (conductivity decrease) happens. Based on the discussions of section 3.3, it can be concluded that with the sample preparation method of this thesis, the percolation onset of decane-water emulsions can be estimated to be between 10% and 20% electrolyte volume fraction. It should be noted that percolation onset can potentially be a function of droplet size distribution, droplet shape, temperature, surface active agents, etc. [52–54, 57, 91] and a thorough study is needed to investigate the effect of different parameters on percolation onset of decane-water emulsions, which is not in the scope of this thesis.

5.4.2 Castor oil-water emulsions: effect of oil volume fraction

The experiments described in section 5.4.1 were conducted with castor oil-water emulsions as well. In general, castor oil showed a higher stability in water compared to decane. Figures 5.31 to 5.34 illustrate Nyquist and Bode plots for experiments with fresh castor oil-DI water and castor oil-KCl $10^{-4}M$ emulsions. The same trend as decane-water emulsions was observed. In high frequencies, the classic semi-circular Nyquist plot was obtained while in lower frequencies, a constant phase behavior was observed. Figure 5.35 depicts the capacitance of the castor-oil water emulsions. It is observed that the capacitance of oil-electrolyte emulsions are slightly larger than the oil-DI water emulsions but both types of emulsions are well described by Boyle model. As in decane-water emulsions, it can be concluded that fresh castor oil-water emulsions can be treated as homogeneous complex media in terms of their permittivity.

The resistance of the castor oil-water emulsions is depicted in figure 5.36. Similar to decane-water emulsions, a sudden increase is observed when oil content is increased to 90%. However, the maximum resistance of castor oil -water emulsion is smaller than that of decane-water emulsion.

5.5 MODEL EMULSION SYSTEMS II: GRADUAL PHASE SEPARATION IN OIL-WATER EMULSIONS

The goal of this thesis is to explore different aspects of developing a device which can be used for applying EIS for characterization of industrially relevant complex liquids. One of the fundamental issues in multiphase liquids, particularly emulsions, is stability and phase separation. Therefore, in this section, phase separation of different oil-water emulsions is investigated with EIS using the developed experimental system to shed light on the capacitance-based measurements of emulsion stability and phase separation.

It was theoretically (chapter 3) and experimentally (section 5.4) shown that permittivity of fresh emulsions can be best represented by homogeneous mixture models, for instance Boyle model. Moreover, it was theoretically shown in chapter 3, that as a two-phase liquid system undergoes phase separation, the permittivity of the system is expected to deviate from the homogeneous-mixture value and decay to a lower value, and in the extreme case of complete laminar phase separation, the permittivity converges to the lowest possible value which can be described by serial-capacitor model. Based on the literature and the theoretical discussion in chapter 3, it was also proposed that while conductivity measurement may be useful in oil-continuous emulsions to detect percolation or phase separation, it is not the best tool in detecting phase separation of water-continuous emulsions because of the fact that current passages are not blocked unless a 100% phase separation happens. On the other hand, based on analytical and numerical discussions of chapter 3, it was shown that permittivity is sensitive to the geometrical configuration of the dispersed phase

in the host medium rather than electrical current passages, and therefore, permittivity measurements can be utilized to detect phase change in water-continuous emulsions even if a 100% phase separation does not happen and water is present in the creamed oil-rich layer.

In this section, different model oil-water emulsions are tested using EIS with the developed experimental platform over approximately 9 hours to experimentally study the effect of phase separation on electrical properties of the samples.

5.5.1 Effect of emulsification degree and stability

5.5.1.1 Homogenized decane-water emulsions

In order to study the effect of emulsification degree, 5% decane-water (KCl $10^{-4}M$) emulsions were prepared with surfactant (Tween 80) dosages of 0, 1CMC, and 20CMC according to the sample preparation methodology described in section 4.7. The experiments were done on two sets of samples, one set was homogenized at 13000 rpm after stirring at 700 rpm and the other one was only stirred at 700 rpm. The homogenized samples showed higher stability and homogeneity. The results of the homogenized samples are shown in this section and the unhomogenized samples are discussed in the next section.

As examples of the first-level (Nyquist and Bode) plots of this set of experiments, figures 5.37 and 5.38 show the Nyquist and Bode plots of homogenized emulsions with no surfactant, and figures 5.39 and 5.40 show the same plots for homogenized emulsions with surfactant dosage of 20CMC (CMC of Tween in water is 13-15 mg/L [104]). The frequency range shown in the figures have been limited to 10^3Hz-10^7Hz to show the changes in the curves more clearly. However, it should be noted that since we try to show a relatively wide frequency range, logarithmic scale is used for the x-axis of the Bode plots, therefore, small changes and shifts in the curves may actually reflect shifts as large as several hundred Hertz. As a result, the changes in the electrical properties of the samples are best described with equivalent circuit element quantitative values rather than qualitative

discussion about changes in in the Bode curves.

Figures 5.41 and 5.42 show the capacitance and resistance of the homogenized emulsions. In figure 5.41, it is observed that capacitance of all emulsions start at a large capacitance and decay to a smaller value. The capacitance of the emulsion with 20CMC of surfactant starts at a value almost equal to the capacitance obtained based on the Boyle model permittivity for homogeneous media and decays to a smaller value which is still much larger than the serial capacitor value. This behavior indicates that the 20CMC emulsion is so stable that after 9 hours, there is still considerable amount of oil emulsified in the system. On the other hand, the emulsions with 0 and 1CMC surfactant show a capacitance decay to a lower value (the 0 surfactant emulsion goes down close to the serial capacitance) showing that the emulsions undergo considerable phase separation. The equation derived in section 3.4.2 can be used to estimate the thickness of the separated layer as a function of time based on capacitance measurements. An exponential decay function is fitted to the experimental measurements and shown in dashed, dashed-dot and dotted lines. The decay function is

$$C(t) - C_f = (C_0 - C_f)e^{-mt} \tag{5.7}$$

where $C(t)$ is the capacitance of the emulsions as a function of time, C_0 and C_f are the initial and final capacitances, and m is the decay parameter. The decay parameter, m, of the 20CMC, 1CMC and 0CMC emulsions are 0.04, 0.10, and 0.26, respectively. In other words, the permittivity decay or phase separation rate of the 0CMC emulsion is approximately 3 times faster than that of the 1CMC emulsion and the same parameter of the 1CMC emulsion is approximately 3 times larger than that of the 20CMC sample.

Figure 5.42 shows the resistance of the studied emulsions over time. It is observed that only in the emulsion with 0CMC, the resistance shows an increase (after 400 minutes) and in other cases, the resistance does not show any considerable variation. This can be attributed to the fact that in the systems emulsified with surfactant, the water present in

the creamed oil-rich layer maintains current passages while in the 0CMC case, the system separates to a degree where current passages are no more present in the creamed oil layer.

5.5.1.2 Unhomogenized decane-water emulsions

The same set of experiments were carried out on unhomogenized samples (only stirred at 700 rpm). Figure 5.43 shows the capacitance of the unhomogenized samples with different surfactant dosages over time. It is observed that unhomogenized emulsions show a trend similar to the homogenized ones. However, in the case with 0 surfactant, oil and water phases were already separated when the sample was loaded on the test cell and the first measured capacitance was already close to the serial value. The decay parameter, m (as described in equation 5.7), of the 20CMC and 1CMC cases were 0.06 and 0.15, respectively. The decay parameters show that capacitance decay and phase separation in 1CMC emulsion occurs approximately 2.5 times faster than the 20CMC emulsion. The decay function is not fitted to the 0CMC case.

Figure 5.44 shows the resistance of the unhomogenized samples with different surfactant dosages over time. It is observed that the 1CMC and 20CMC samples don't show any considerable change in resistance while the 0CMC emulsion shows an increase in resistance after approximately 200 minutes, 200 minutes earlier than the resistance increase in the homogenized 0CMC emulsion.

5.5.1.3 Castor oil-water emulsions

The permittivity (capacitance) decay due to phase separation was also observed in tests with castor oil-water emulsions. Castor oil showed higher stability in water. 10% castor oil-water (KCl $10^{-4}M$) emulsions were prepared in two ways: one, only with stirring at 700 rpm and two, by homogenizing at 13000 rpm after stirring. Figures 5.45 and 5.46 show the Nyquist and Bode plots of the homogenized emulsions and figures 5.47 and 5.48 show the same plots for unhomogenized emulsions.

The capacitance decay of castor oil-water emulsions is illustrated in figure 5.49. It is observed that both emulsions have a capacitance close to the value obtained from Boyle model for permittivity of complex media and decay to lower values. The homogenized emulsion decayed slowly to a value half way between Boyle and serial capacitance while the unhomogenized emulsion decayed faster to a value closer to the serial capacitance. Castor oil showed higher stability in water compared to decane and due to presence of some emulsified oil in the water phase and/or some water in the oil-rich layer, the permittivity did not reach the serial capacitor.

Figure 5.50 depicts the resistance of the castor oil-water emulsions over time. No considerable change was seen in the resistance over time while the system underwent phase separation. This can be attributed to the fact that some water remains present in the oil-rich phase which maintains the electric current passages in the oil layer. This (and the similar resistance results in decane-water emulsions) show that permittivity measurement is sensitive to topology of the dispersed phase rather than electric current passages in the system and is a better tool than conductivity measurement for monitoring phase behavior of O/W emulsions.

5.5.2 Effect of oil content

The phase separation is sensed based on permittivity decay in the oil-water systems. It was shown in chapter 3 that when the oil content in the system is low, the permittivity of fresh well-emulsified systems (described by homogeneous mixture models) is high and is usually close to permittivity of water. However when oil content is increased to the point that the emulsion can be considered W/O rather than O/W emulsion, even the fresh emulsion permittivity becomes smaller. Therefore, the decay in capacitance due to phase separation becomes less sensible. This behavior is experimentally tested in this section by showing the capacitance decays for emulsions with different oil contents. The water-rich emulsions were prepared with 1CMC of Tween 80 (dissolved in water) and the two oil-rich

emulsions had 1CMC of Tween 80 in the water phase and were stabilized with additional 1CMC of Tegopren 700 dissolved in the oil phase (because without adding the oil-soluble surfactant, the oil-rich emulsions were so unstable that separated almost instantly). All emulsions were homogenized.

Figure 5.51 shows the capacitance decay for emulsions with different oil contents. It is observed that the fresh capacitance of the water-rich emulsions are much higher than the fresh capacitance of the oil-rich emulsions. All systems decay to lower values of capacitance as they undergo phase separation. Based on these results and the discussion in the previous paragraph, it can be concluded that permittivity-based measurement for sensing phase separation can be best applied to O/W emulsions rather than W/O emulsions.

5.5.3 Effect of sample thickness

While capacitance is a function of dielectric thickness, as discussed in chapter 3, the variations of permittivity with different volume fractions of the dispersed phase is not a function of thickness. In other words, if every geometrical attribute is scaled accordingly with the thickness, and the oil/water ratio is kept constant, permittivity must remain constant. However, varying sample thickness may affect the rate at which one phase creams and therefore may potentially affect the electrical properties of the systems. In this section, the effect of sample thickness on the measured electrical properties of the samples is investigated.

Figure 5.52 shows the variation of the measured capacitance (left y-axis) with sample thickness. The samples are all 10% decane-water (KCl $10^{-4}M$) emulsions stabilized with 1CMC Tween 80 with thicknesses from 500μm to 5mm. It can be observed in figure 5.52 that all emulsions face capacitance decay over time. The capacitance of the thinner samples are higher than the thicker ones as expected but the permittivity (dielectric constant, right y-axis) of the the samples are almost equal and show the same trend.

Figure 5.53 shows the resistance of the emulsions with different sample thicknesses. An increase in the resistance of the thickest (5mm) sample can be observed after 200

minutes while the 1mm sample shows a slighter increase at a later time (400 minutes) and the 500μm sample does not show any increase in resistance at all. The reason for this behavior can be understood based on the fact that as sample thickness is increased, while the system undergoes phase separation, the probability of existence of electric current passages in the oil-rich layer becomes lower. In other words, the amount of water present in the oil phase appears to not increase proportionally to the total sample thickness, rather, a maximum amount of water remains stable in the creamed oil-rich layer which appears to be constant even when the total thickness (and the oil layer thickness) is increased. Assuming the same amount of water present in the oil-rich phase, as the total thickness and therefore the creamed oil layer thickness is increased, the water present in the oil-rich layer becomes less likely to form electric current passages in the oil layer. As a result, as the sample thickness is increased, the increase in the resistance of the samples occurs earlier and is more considerable.

5.6 ERRORS AND UNCERTAINTIES IN THE EXPERIMENTAL RESULTS

Ideally, if an experiment can be repeated "many" times, enough independent data points will be collected for statistical interpretation of errors. However, many important engineering and scientific experiments cannot be repeated enough times to provide meaningful statistical information about errors [110]. High-speed digital data acquisition systems provide a good tool for "multiple-sample" experiments, but experimental difficulties, such as costly and time-consuming sample preparation, often limit data collection to a few data points. As a result, in many experiments, error analysis should be based on uncertainty *prediction* rather than *statistics*. These experiments are referred to as "single-sample" experiments [110, 111]. The EIS experiments in this thesis are multiple-sample in one sense, and single sample in another, which is explained next.

The EIS experiment is actually the measurement of the magnitude and phase of an out-

put signal over a frequency range, which also results in determining electrical capacitance and resistance of the sample over the frequency range. Each single measurement at a certain frequency can be regarded as one data point, and statistical error analysis techniques can be applied to them. On the other hand, after measuring the frequency response, the experimental data is modeled by an equivalent circuit, and equivalent electrical elements (capacitance and resistance) are determined for each sample. Each set of equivalent circuit element values can be regarded as one data point. In this latter sense, EIS tests are single-sample experiments because it is almost impossible to carry out a complete EIS test (including sample preparation and loading) enough times (at least 20 [110, 111]) for statistical error analysis. In this section, experimental errors are discussed from both points of view explained above: multiple-sample data acquisition over a frequency range, and single-sample experiments determining equivalent resistance and capacitance.

If each measurement at a certain frequency is regarded as an independent data point, standard deviation can be determined and can be used for drawing error bars as a measure for precision. Therefore the results can be displayed as

$$X = X_{measured} \pm 2\sigma \tag{5.8}$$

where $X_{measured}$ is typically the mean of the measurements which is assumed to be the best estimate for the actual value, and σ is the standard deviation. The uncertainty prediction is expected to be reliable with 95% confidence. However, the equivalent circuit values in EIS experiments are not the mean of capacitance and resistance at each frequency, rather, they are found by minimization of a complex-value non-linear summation (see section 3.6). Therefore, the well-known standard deviation cannot be used to display the precision of the EIS measurements. In this study, $X_{measured}$ is the equivalent value found from the scheme explained in section 3.6, and σ is a deviation defined as

$$\sigma = \sqrt{\frac{1}{N}\sum_{i=1}^{N}(X_i - X_{eq})^2} \tag{5.9}$$

where N is the number of measurements and X_{eq} is the equivalent value obtained according to the method explained in section 3.6. The data points used in the deviation defined in equation 5.9 belong to the frequency range where the sample properties are determined (1kHz to 10MHz, see section 3.6.4). The value of the deviation defined in equation 5.9 is used to draw the error bars in the figures of this thesis.

Precision errors, as discussed above, will reflect frequency-dependent and relaxation-related errors over the measurement frequency range, but do not include experimental errors such as sample loading and instrument reading. In order to understand such errors, since repeating the experiments to the level of *statistical* error analysis is extremely difficult, single-sample uncertainty *prediction* is performed by identifying the sources of random and bias errors, and by repeating the experiments a few times [110, 111]. This is explained next.

The main source of bias error in the experiments is air bubbles in the test cell. Air bubbles decrease the surface area of the electrode in contact with the sample and reduce the capacitance. In all experiments, when air bubbles larger than approximately 5% of the surface area were observed, the experiment was disregarded and was performed again. Calibration of the test cell (leads impedance and dry capacitance measurement) is performed, which minimizes bias errors related to calibration. There is no method to understand the bias errors of an experiment by only looking at the measured data [110, 111], so identifying possible sources of fixed errors and a valid theoretical explanation of the experimental results are the only methods to ensure that bias errors are negligible. The main sources of random error are sample preparation and loading. To ensure reliability of the results, the same method of sample preparation was used in all cases (see chapter 4). Also, for all experiments, sample loading and measurements were performed in three

test cells in parallel, and the whole process of the experiment (from sample preparation to measurements) was carried out twice. The variations in different runs (6 values for each test) are also included in the error bars.

5.7 SUMMARY

In this chapter, several homogeneous and multiphase liquid mixtures were studied by employing EIS in the developed test apparatus. The results indicate the ability of the system to provide reliable estimates of the electrical characteristics of these systems. The test cell is also capable of measuring the time dependent phase separation of oil-in-water emulsions.

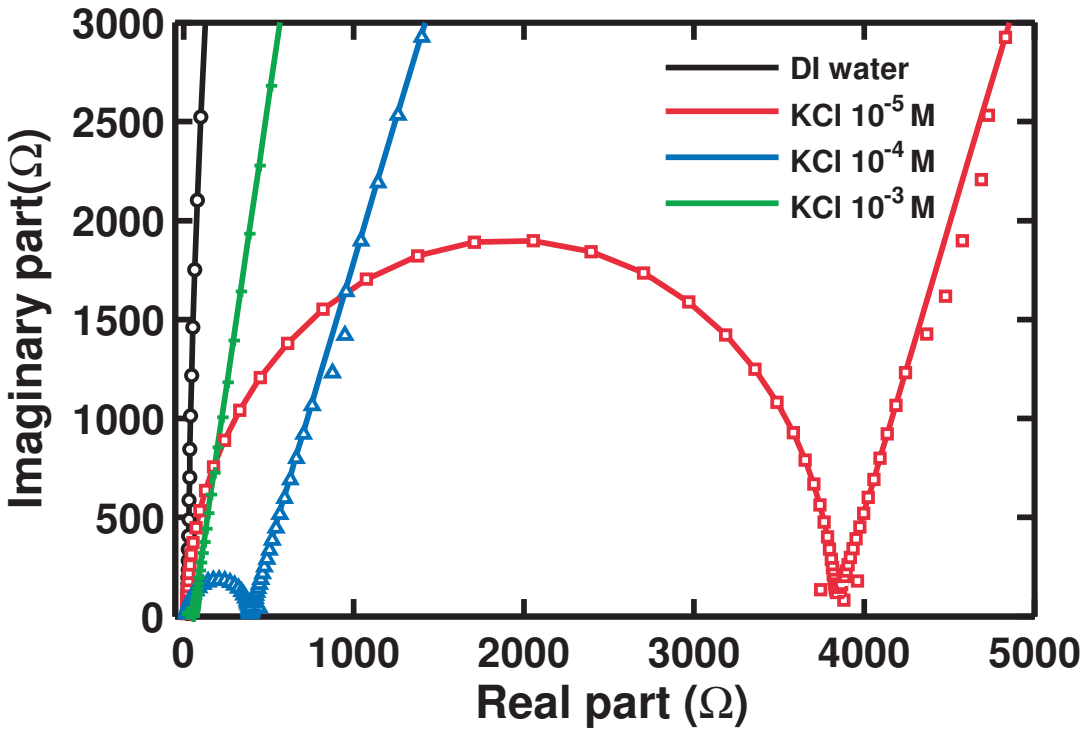

Figure 5.1: Nyquist plot of EIS experiment with salt-water electrolyte with different salt concentrations. Symbols represent measurements and lines represent equivalent circuit model fit to the measurements.

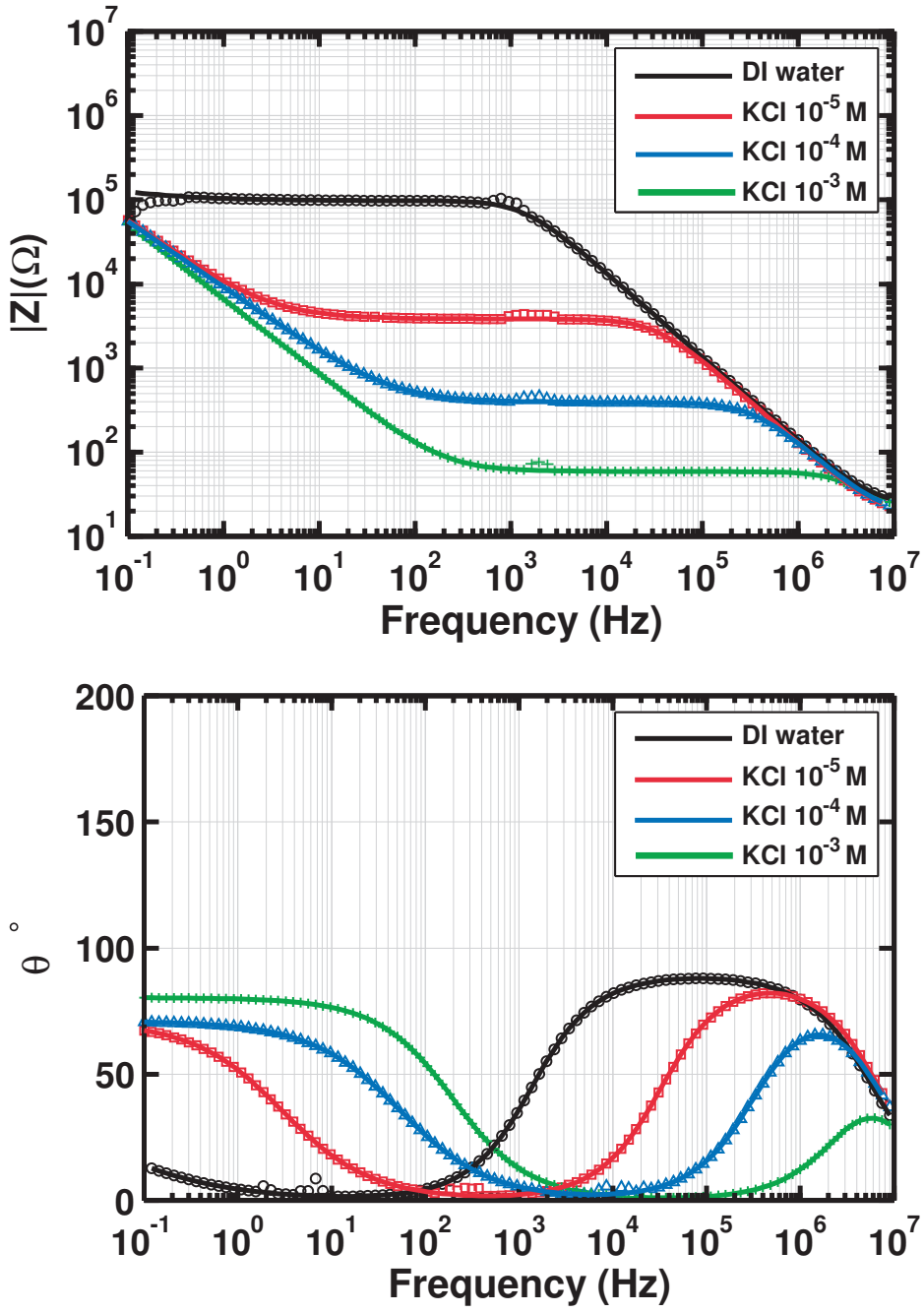

Figure 5.2: Bode plots (magnitude and phase) of EIS experiment with salt-water electrolyte with different salt concentrations. Symbols represent measurements and lines represent equivalent circuit model fit to the measurements.

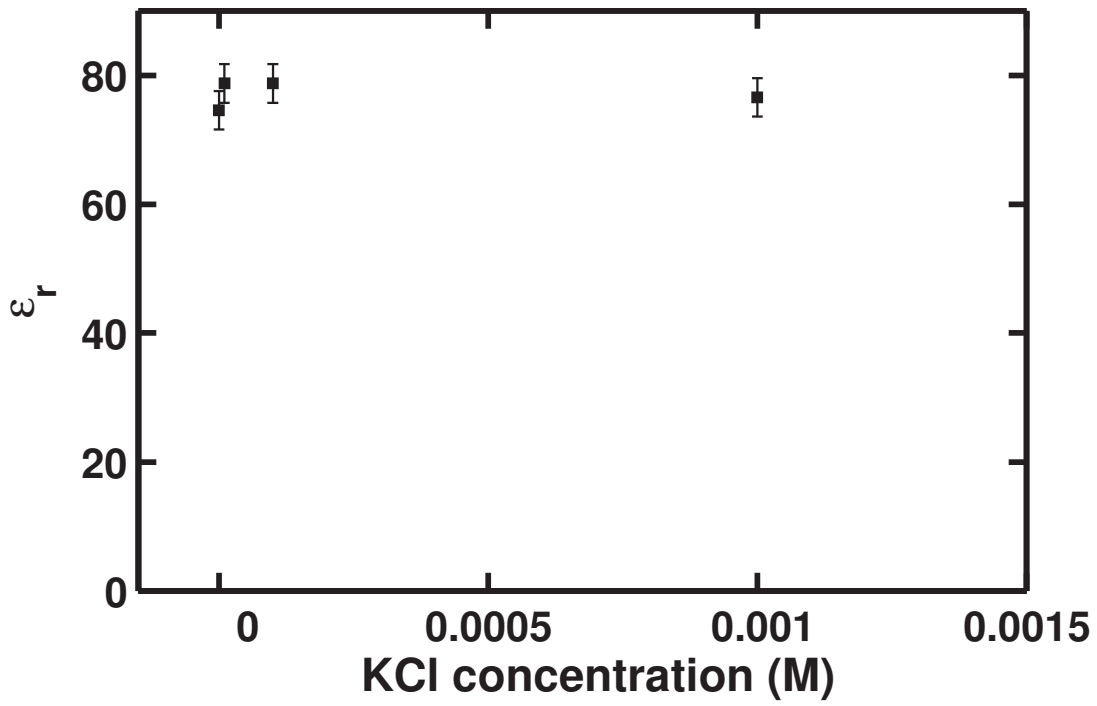

Figure 5.3: Relative permittivity of electrolytes with different salt concentrations based on the capacitance obtained from equivalent circuit modeling.

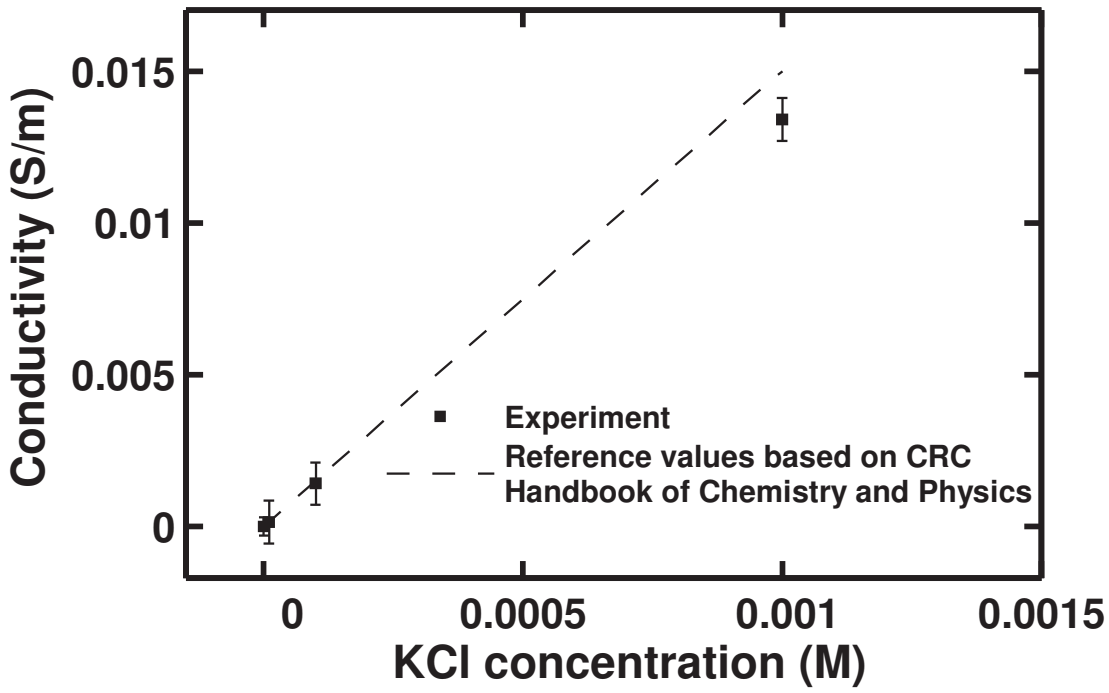

Figure 5.4: Conductivity of electrolytes with different salt concentrations based on the resistance obtained from equivalent circuit modeling.

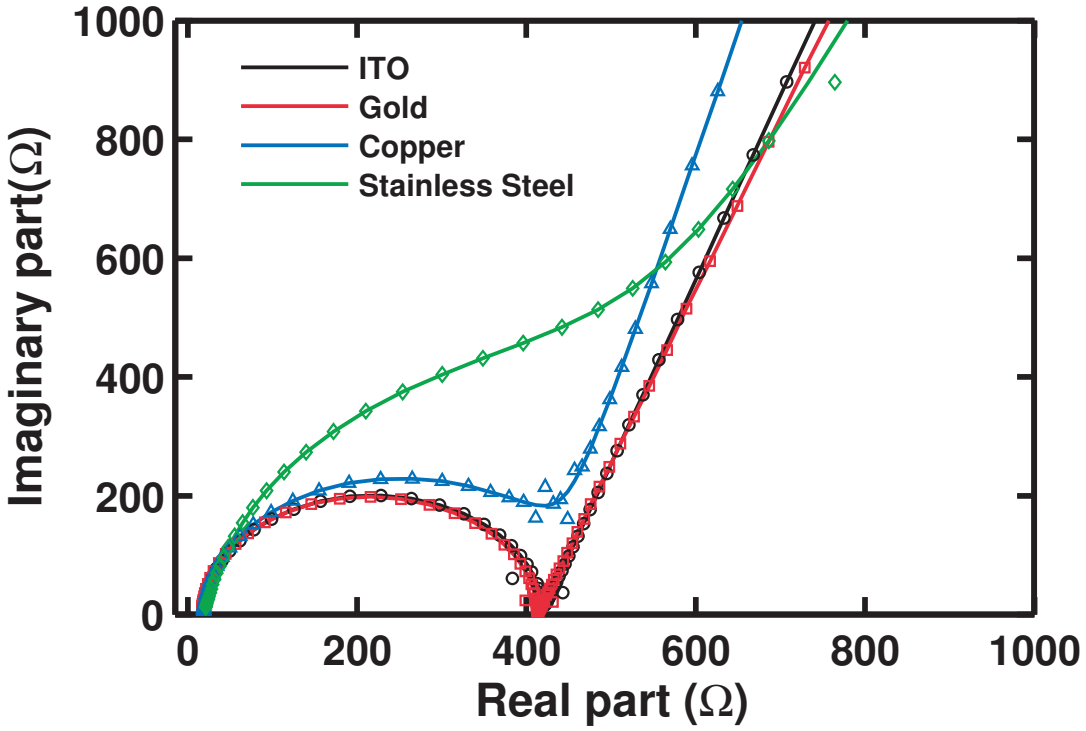

Figure 5.5: Nyquist plot of EIS experiment for different electrode materials with salt-water electrolyte of KCl 10^{-4}M. Symbols represent measurements and lines represent equivalent circuit model fit to the measurements.

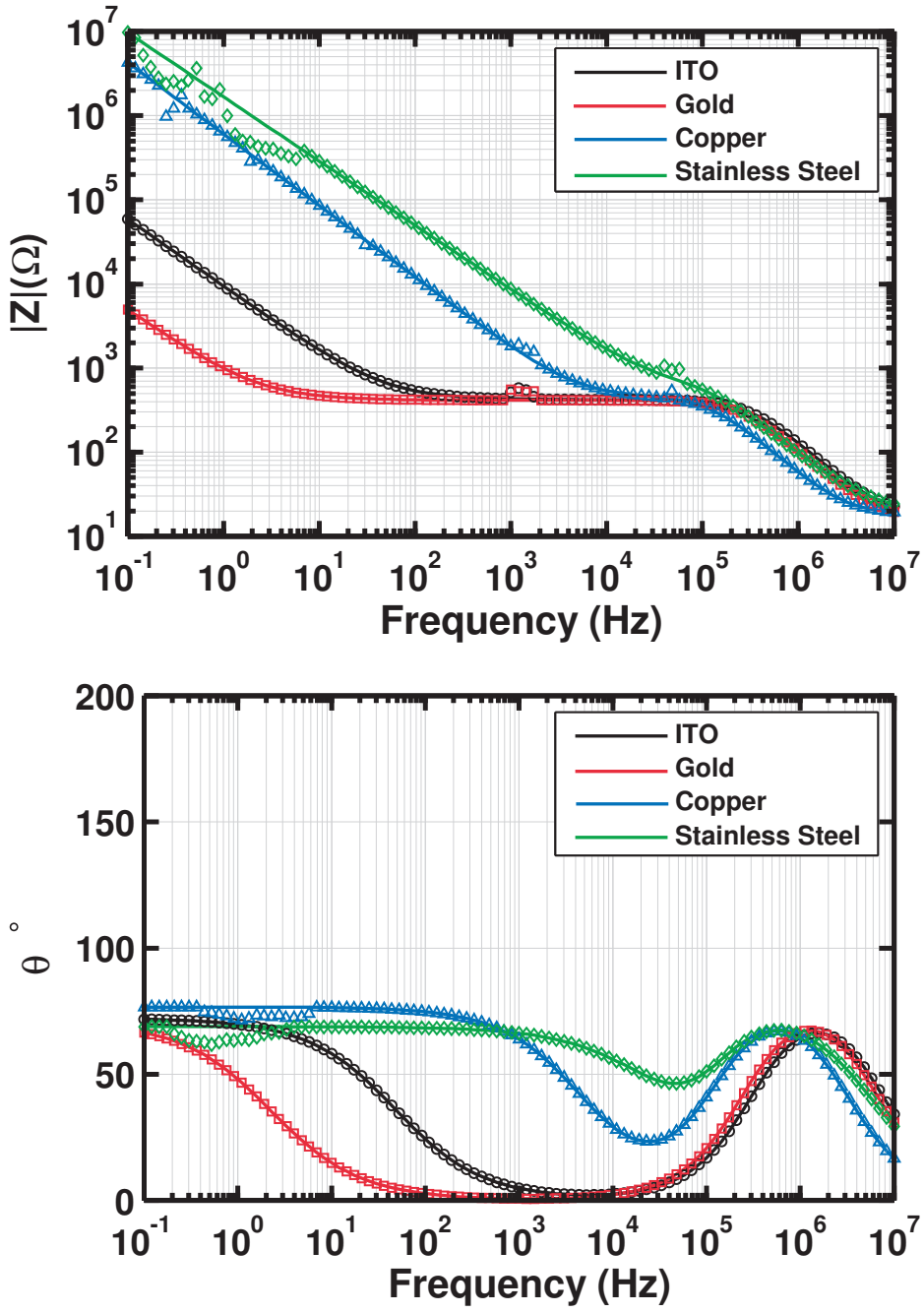

Figure 5.6: Bode plots (magnitude and phase) of EIS experiment for different electrode materials with salt-water electrolyte of KCl 10^{-4}M. Symbols represent measurements and lines represent equivalent circuit model fit to the measurements.

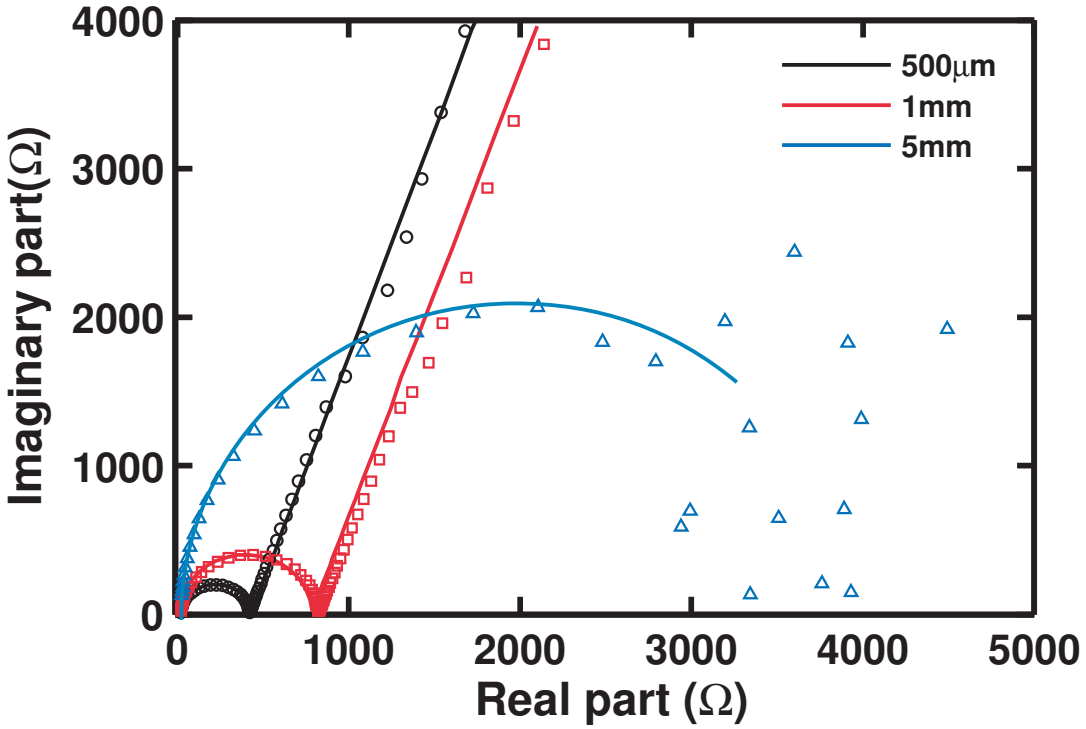

Figure 5.7: Nyquist plot of EIS experiment for different sample thicknesses with salt-water electrolyte of KCl 10^{-4}M. Symbols represent measurements and lines represent equivalent circuit model fit to the measurements.

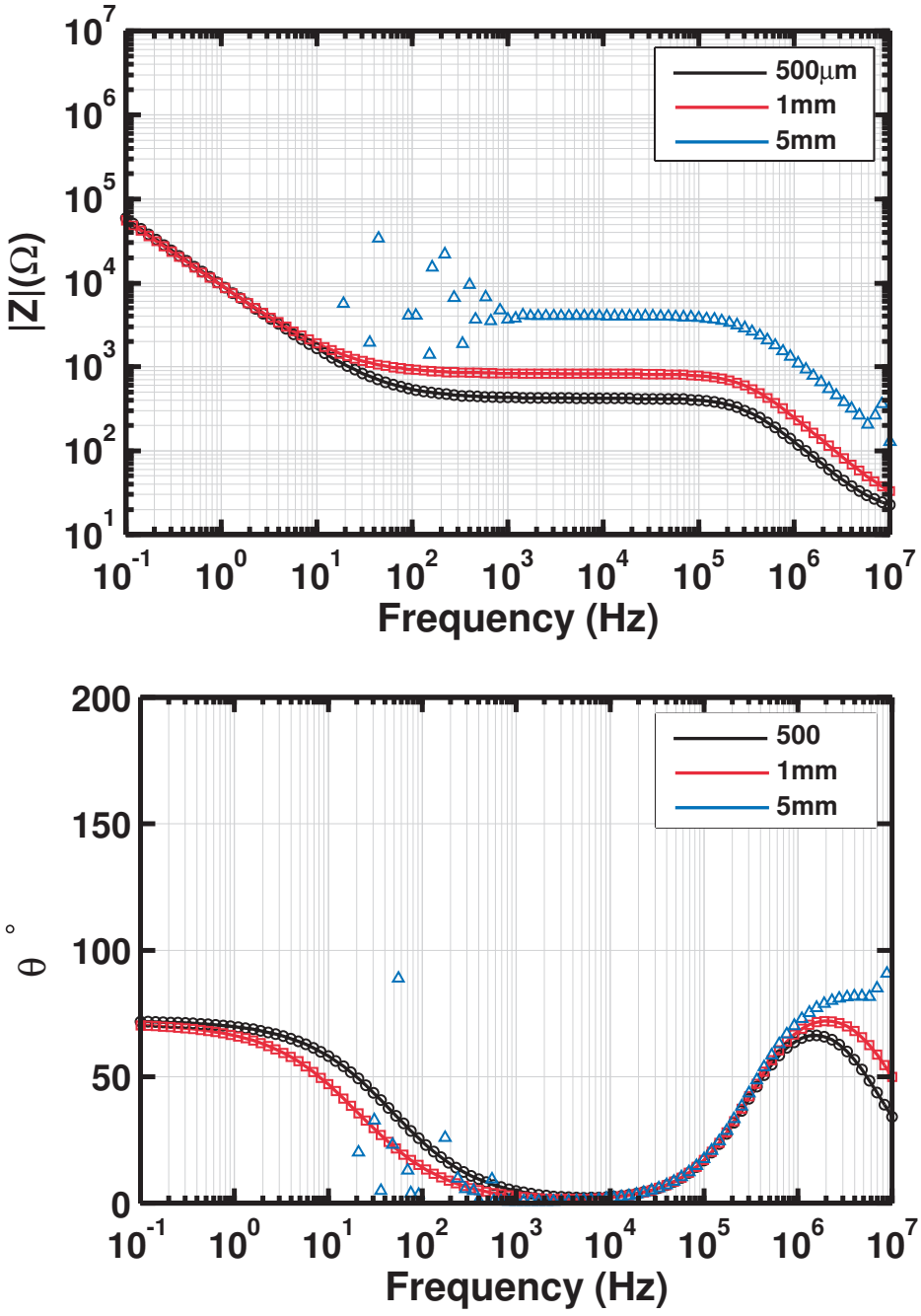

Figure 5.8: Bode plots (magnitude and phase) of EIS experiment for different sample thicknesses with salt-water electrolyte of KCl 10^{-4}M. Symbols represent measurements and lines represent equivalent circuit model fit to the measurements.

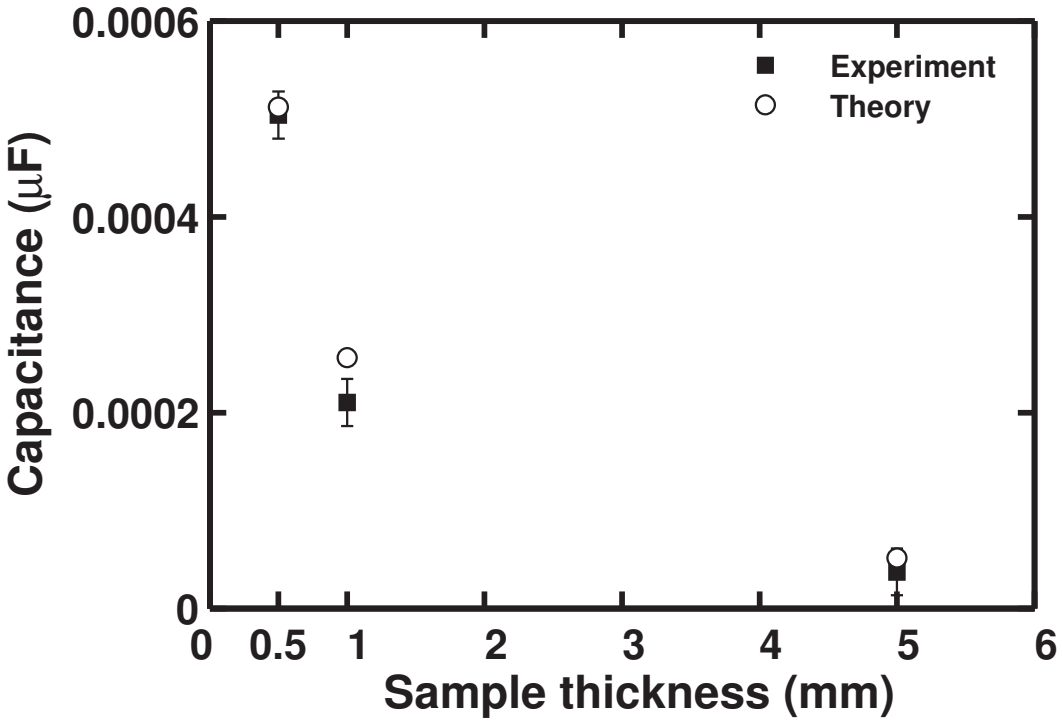

Figure 5.9: Capacitance of the test cell filled with KCl 10^{-4}M electrolyte with different thicknesses. The experimental results are compared with theoretical variation of capacitance with sample thickness.

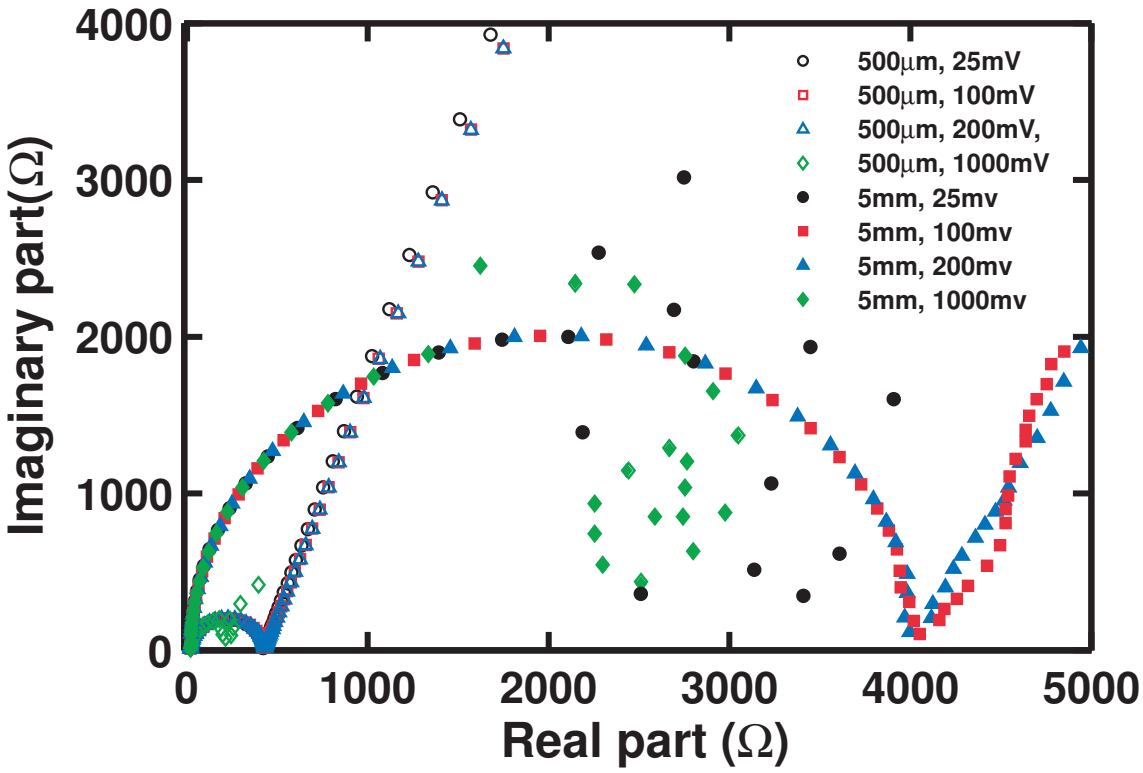

Figure 5.10: Nyquist plot of the EIS experiment with the test cell filled with KCl 10^{-4}M electrolyte with different thicknesses and different input signal amplitudes. It is observed that with thicker samples, increasing the input signal amplitude results in less noisy measurements.

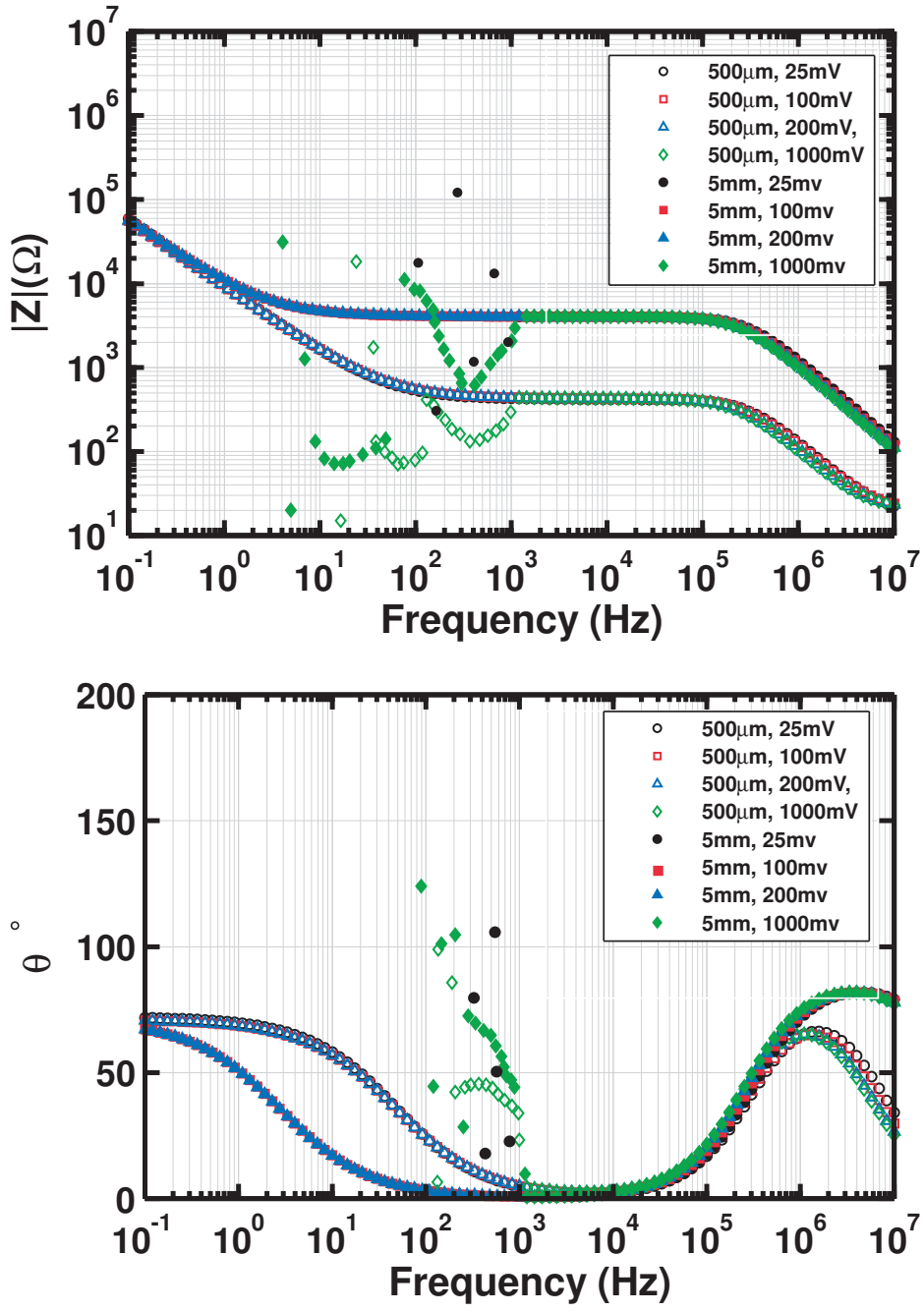

Figure 5.11: Bode plots of the EIS experiment with the test cell filled with KCl 10^{-4}M electrolyte with different thicknesses and different input signal amplitudes. It is observed that with thicker samples, increasing the input signal amplitude results in less noisy measurements.

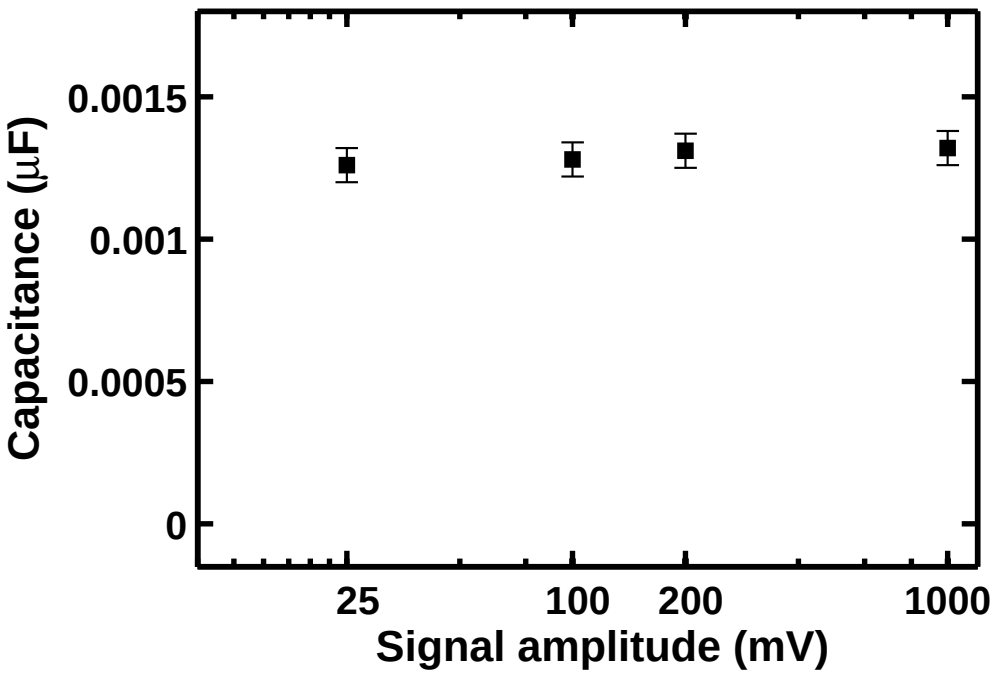

Figure 5.12: Capacitance of the test cell filled with 0.5mm thick KCl 10^{-4}M electrolyte with different signal amplitudes obtained from equivalent circuit modeling of the EIS data.

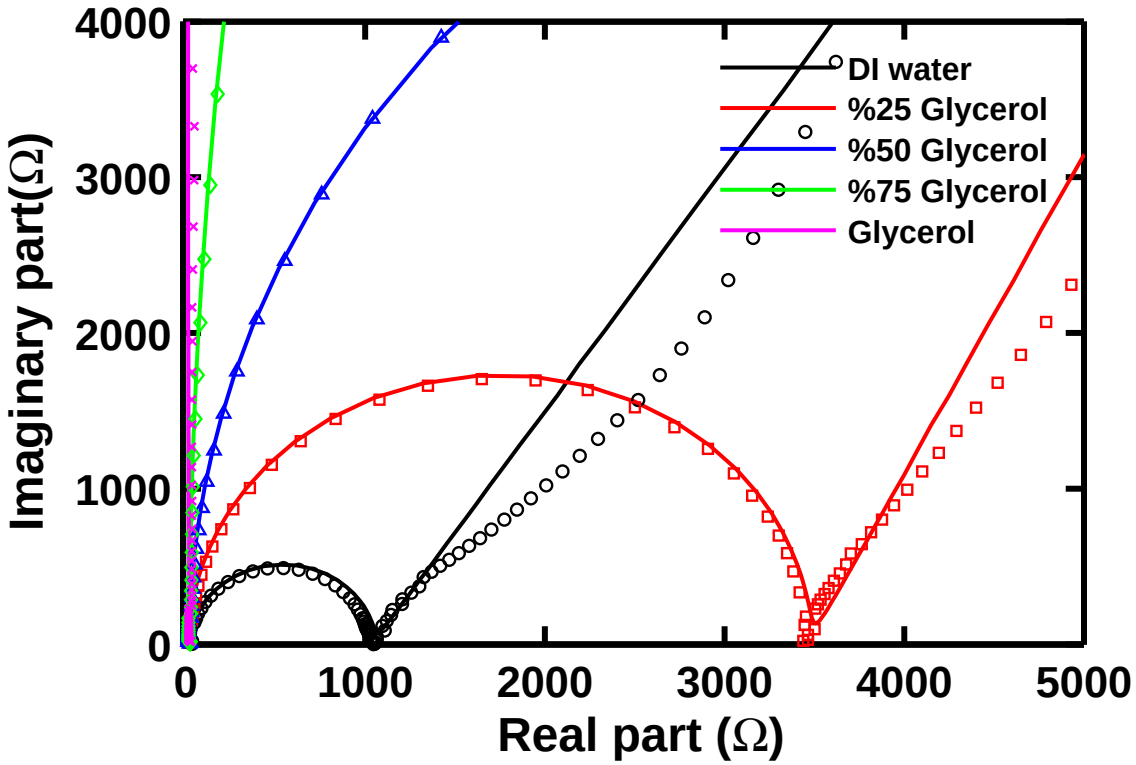

Figure 5.13: Nyquist plot of the EIS experiment with glycerol-DI water mixtures for different glycerol contents. Symbols represent measurements and lines represent equivalent circuit model fit to the measurements.

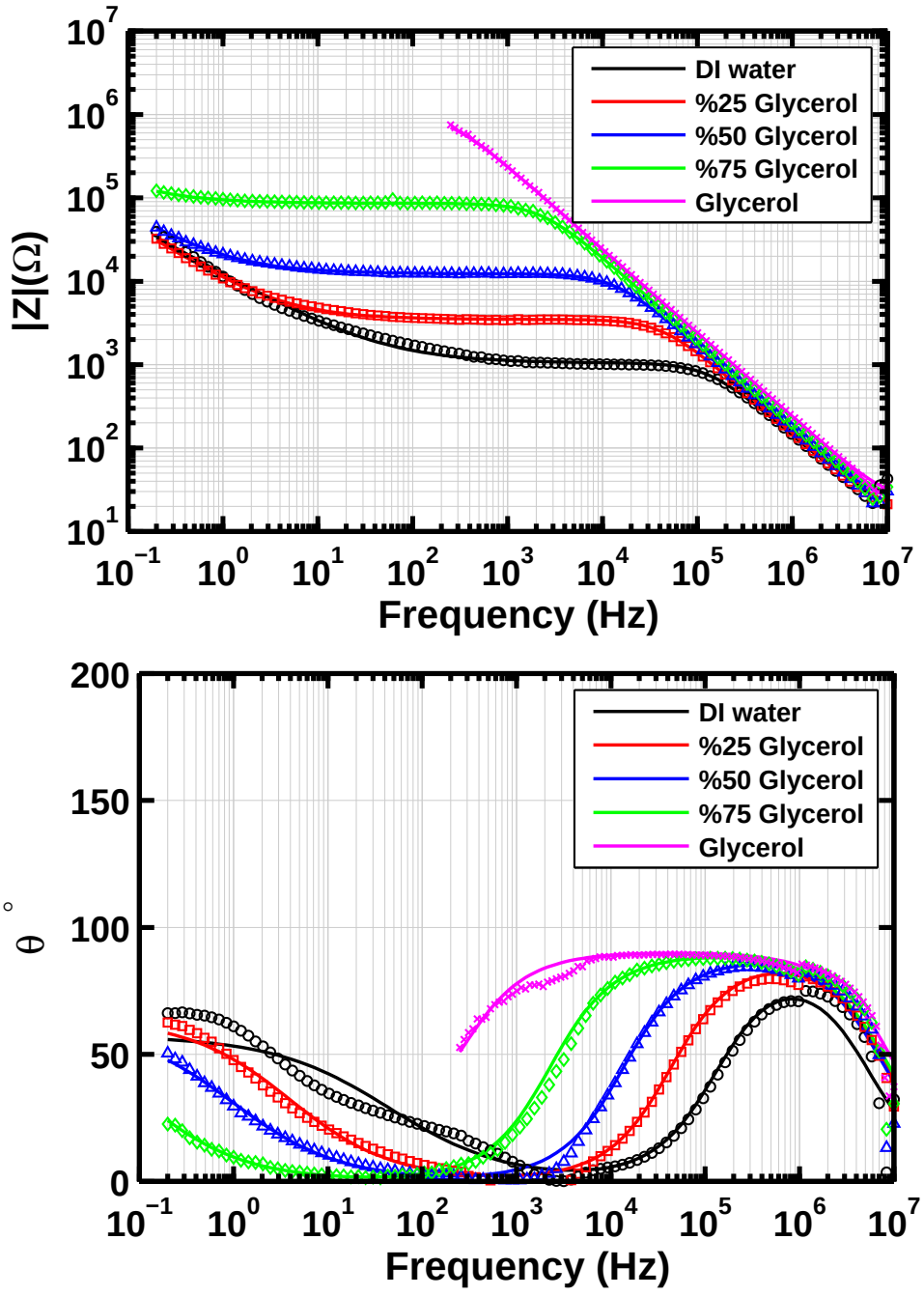

Figure 5.14: Bode plots of the EIS experiment with glycerol-DI water mixtures for different glycerol contents. Symbols represent measurements and lines represent equivalent circuit model fit to the measurements.

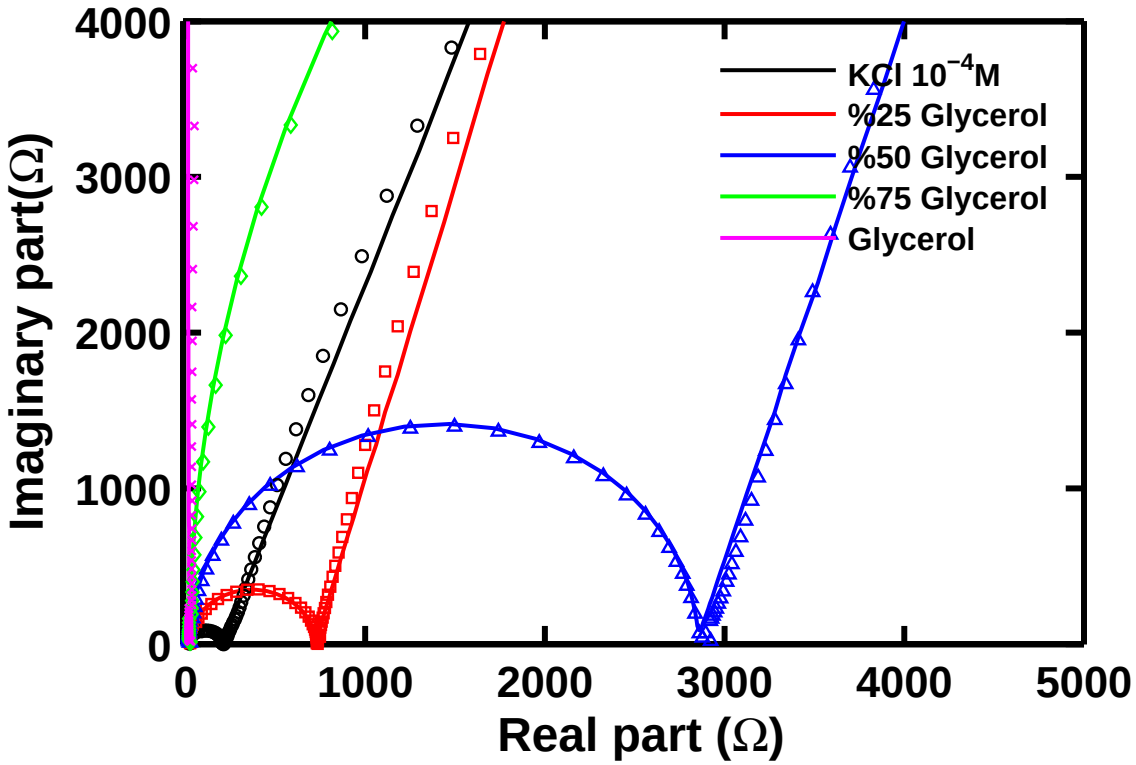

Figure 5.15: Nyquist plot of the EIS experiment with glycerol-salt water (KCl 10^{-4}M) mixtures for different glycerol contents. Symbols represent measurements and lines represent equivalent circuit model fit to the measurements.

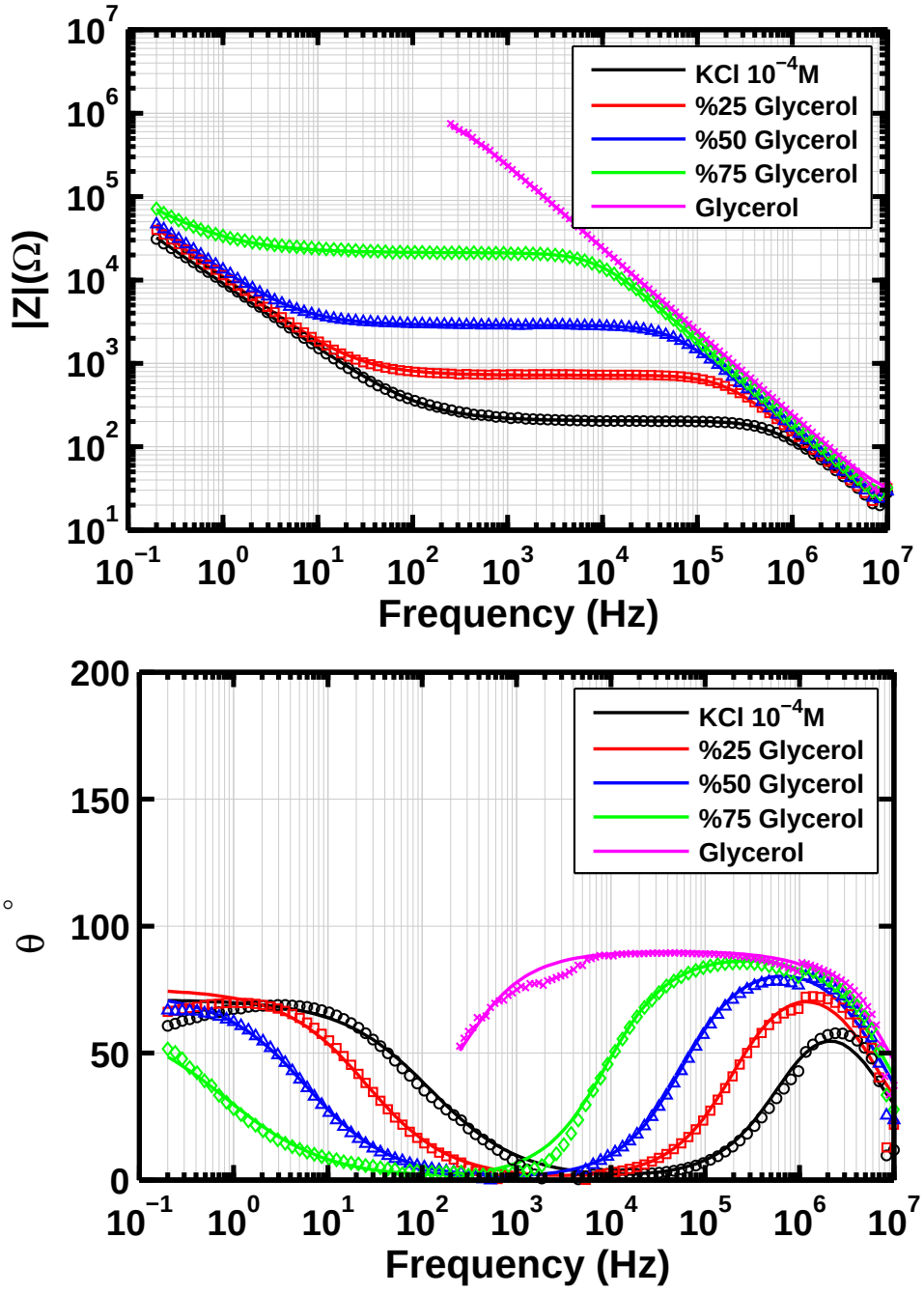

Figure 5.16: Bode plots of the EIS experiment with glycerol-salt water (KCl 10^{-4}M) mixtures for different glycerol contents. Symbols represent measurements and lines represent equivalent circuit model fit to the measurements.

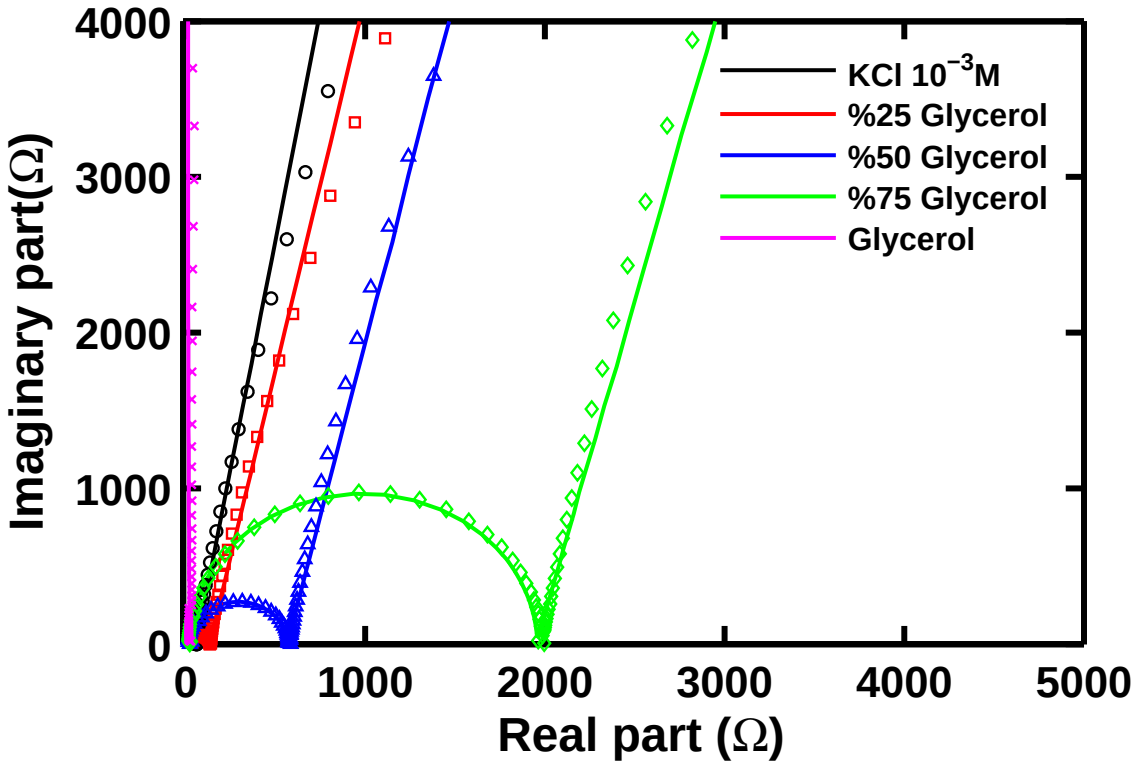

Figure 5.17: Nyquist plot of the EIS experiment with glycerol-salt water (KCl 10^{-3}M) mixtures for different glycerol contents. Symbols represent measurements and lines represent equivalent circuit model fit to the measurements.

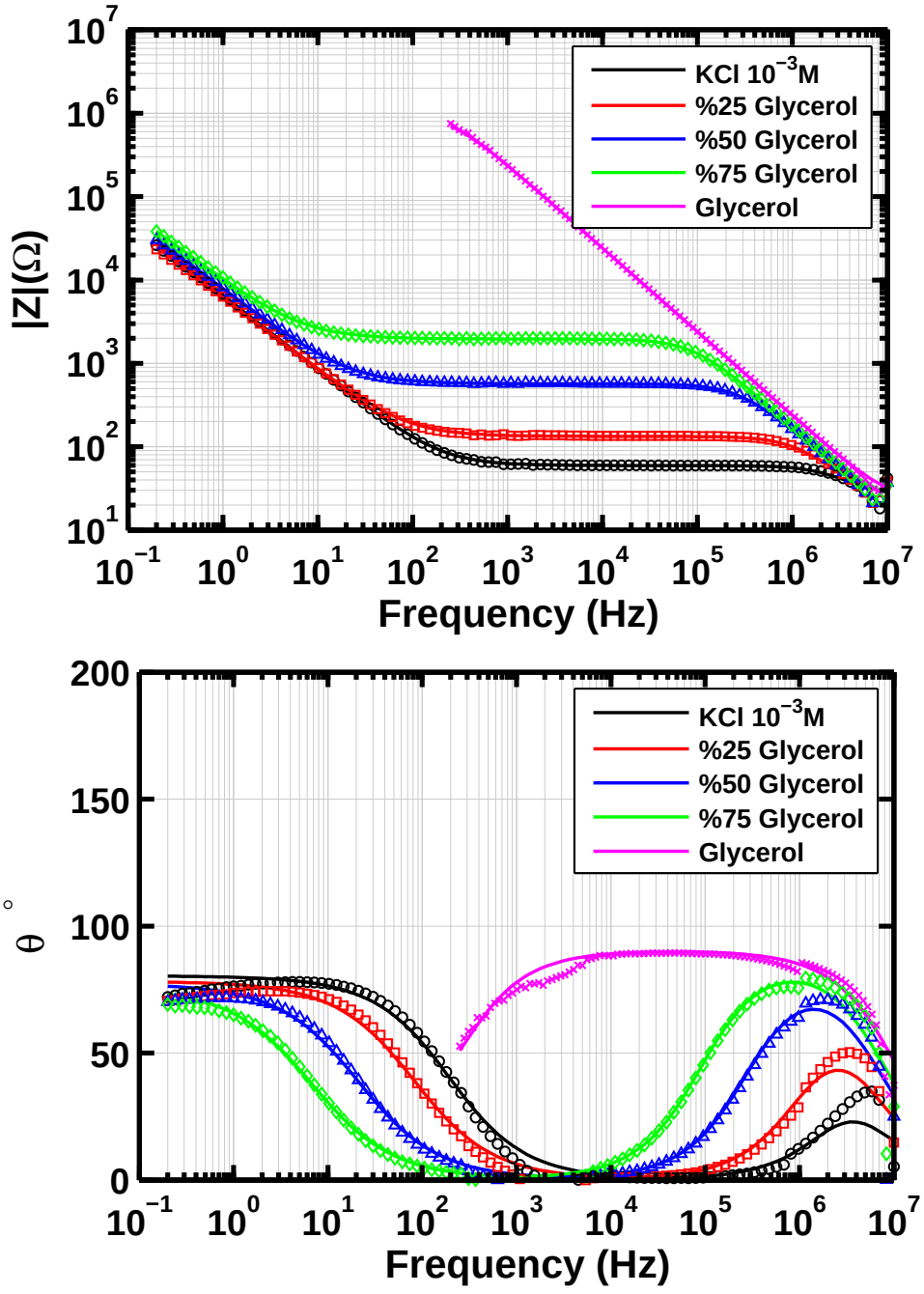

Figure 5.18: Bode plots of the EIS experiment with glycerol-salt water (KCl 10^{-3}M) mixtures for different glycerol contents. Symbols represent measurements and lines represent equivalent circuit model fit to the measurements.

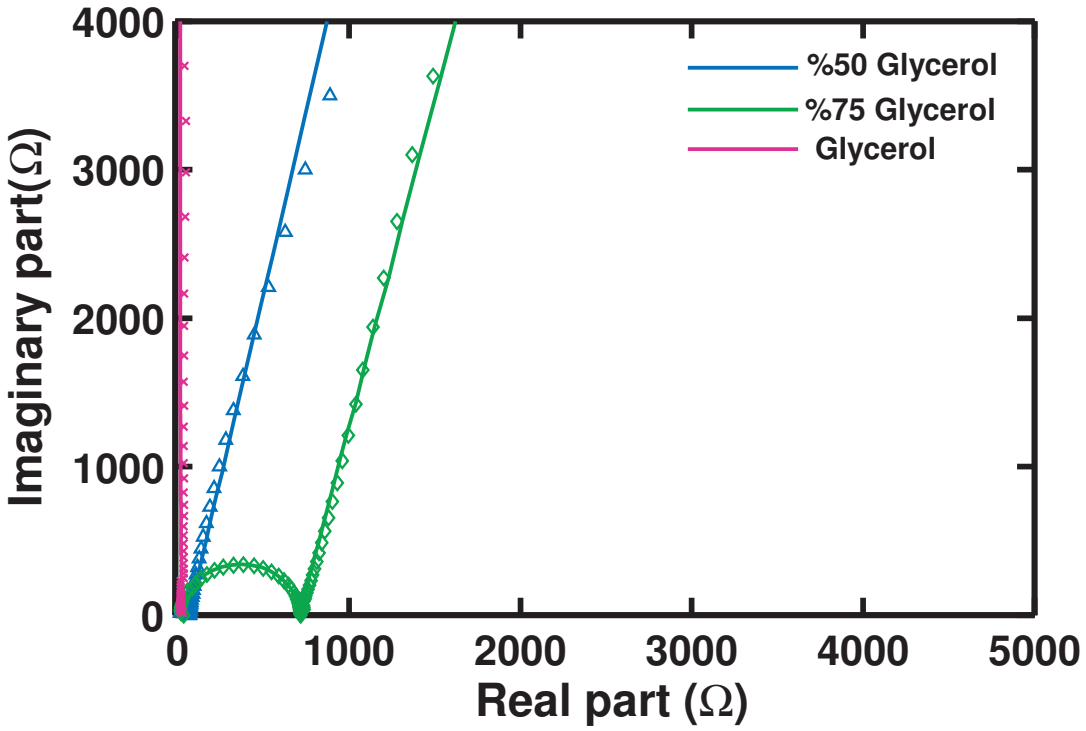

Figure 5.19: Nyquist plot of the EIS experiment with glycerol-salt water (KCl 10^{-2}M) mixtures for different glycerol contents. Symbols represent measurements and lines represent equivalent circuit model fit to the measurements.

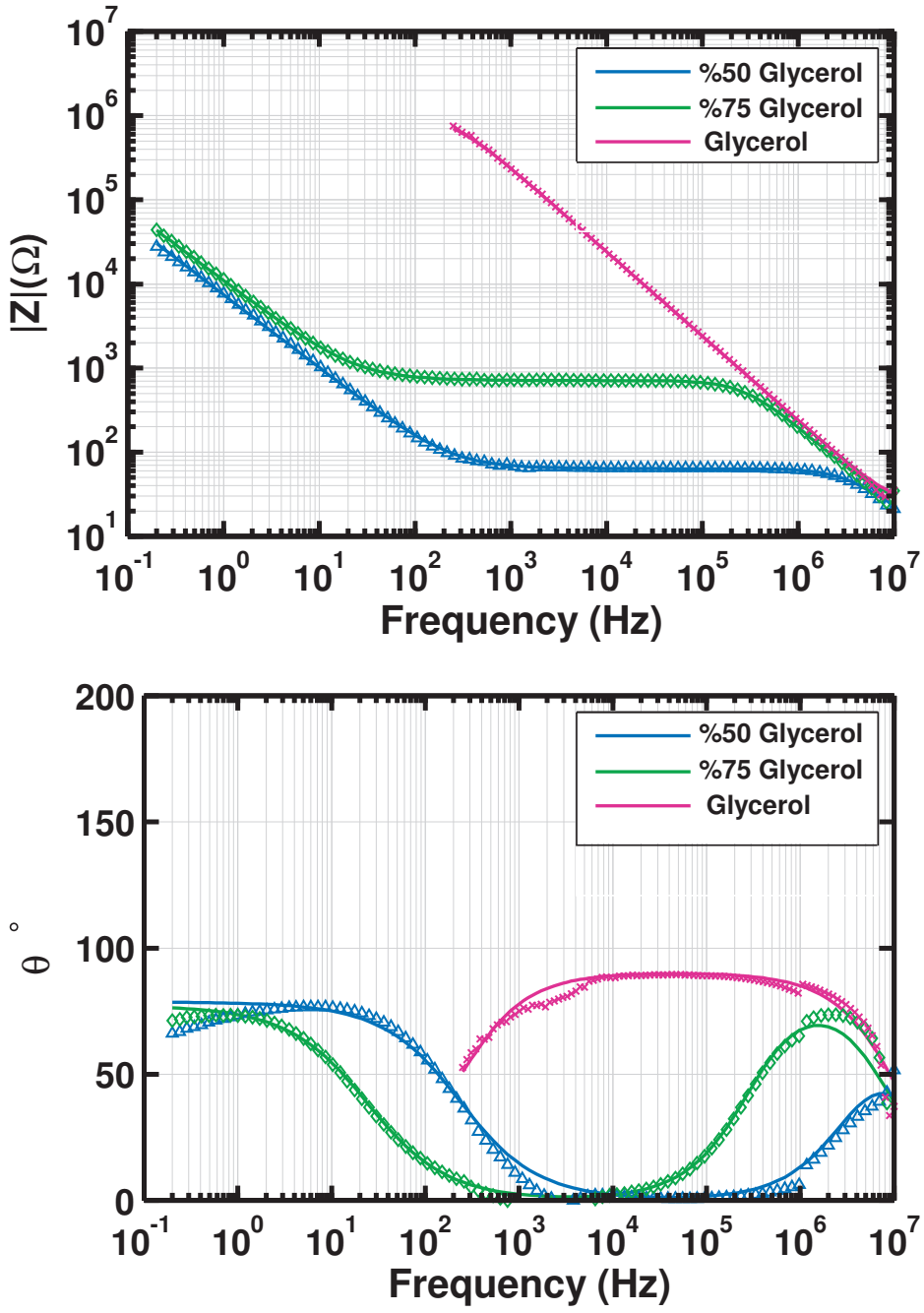

Figure 5.20: Bode plots of the EIS experiment with glycerol-salt water (KCl 10^{-2}M) mixtures for different glycerol contents. Symbols represent measurements and lines represent equivalent circuit model fit to the measurements.

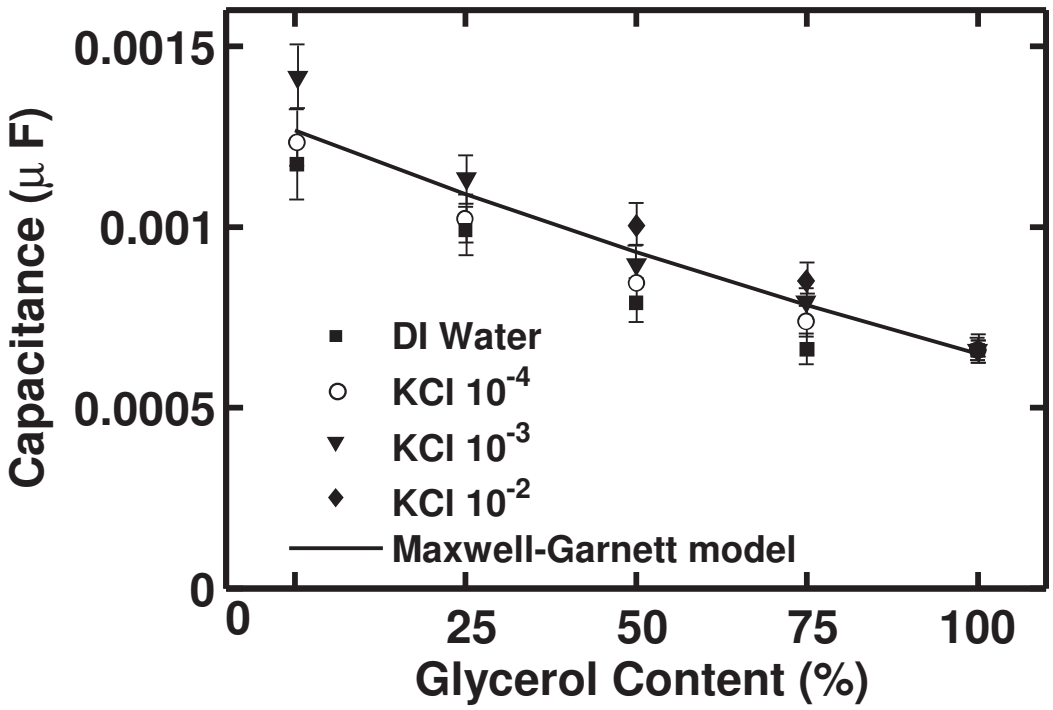

Figure 5.21: Capacitance of glycerol-water mixtures versus glycerol content for different salt concentrations. The experimental results obtained from equivalent circuit modeling are compared to the capacitance obtained based on Maxwell-Garnett model for mixture permittivity. For glycerol (ϵ_r = 40) and water (ϵ_r = 80), the Maxwell-Garnett model is very close to parallel capacitor (linear) model.

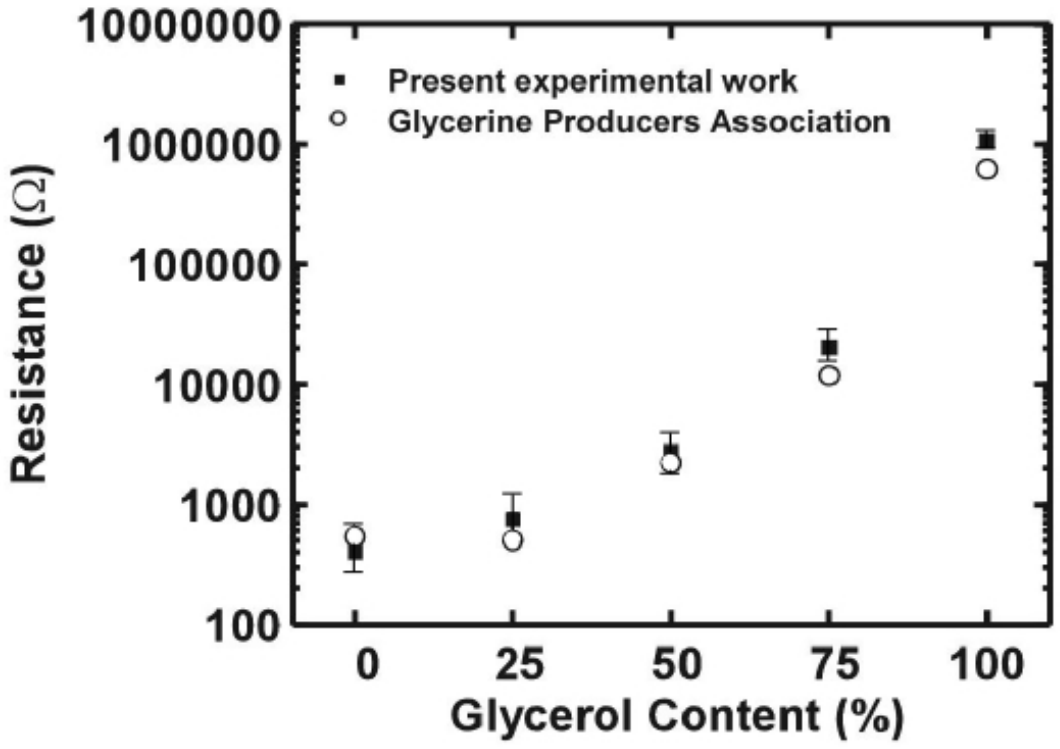

Figure 5.22: Resistance of glycerol-water mixtures versus glycerol content for different salt concentrations. The experimental results obtained from equivalent circuit modeling are compared to the resistance obtained based on the conductivity data provided by Glycerine Producers Association.

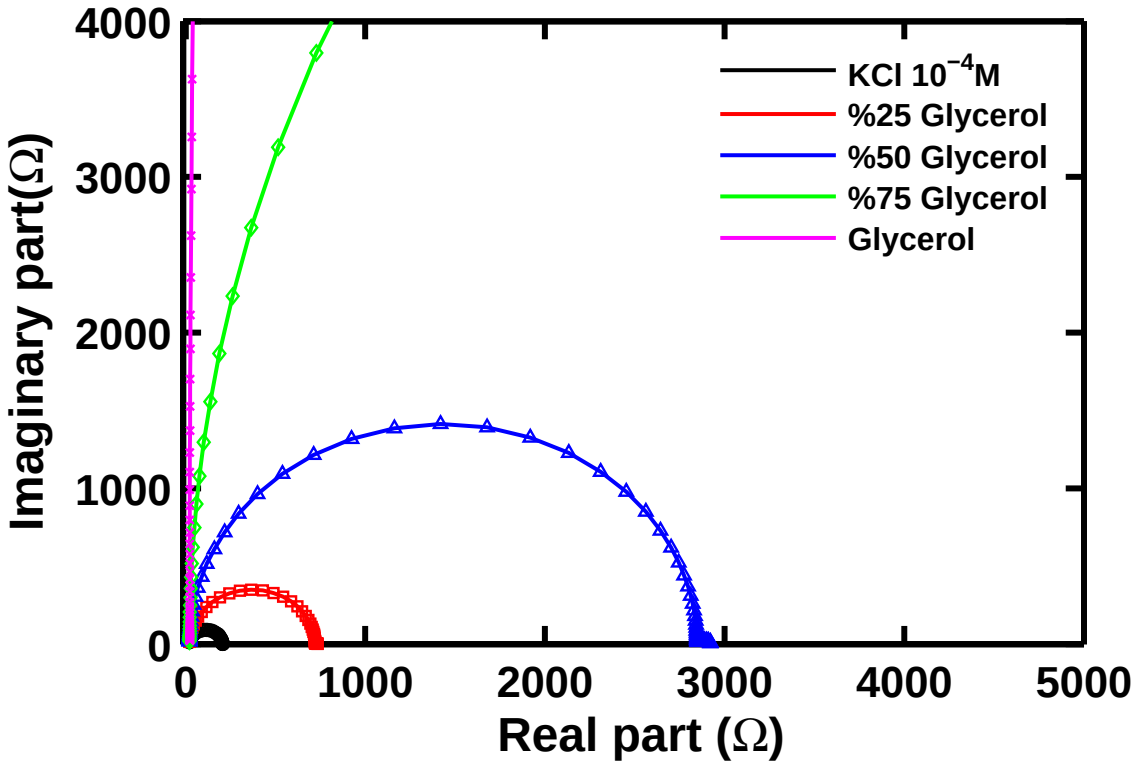

Figure 5.23: Nyquist plot of the 4-electrode EIS experiment with glycerol-salt water (KCl 10^{-4}M) mixtures for different glycerol contents. Symbols represent measurements and lines represent equivalent circuit model fit to the measurements.

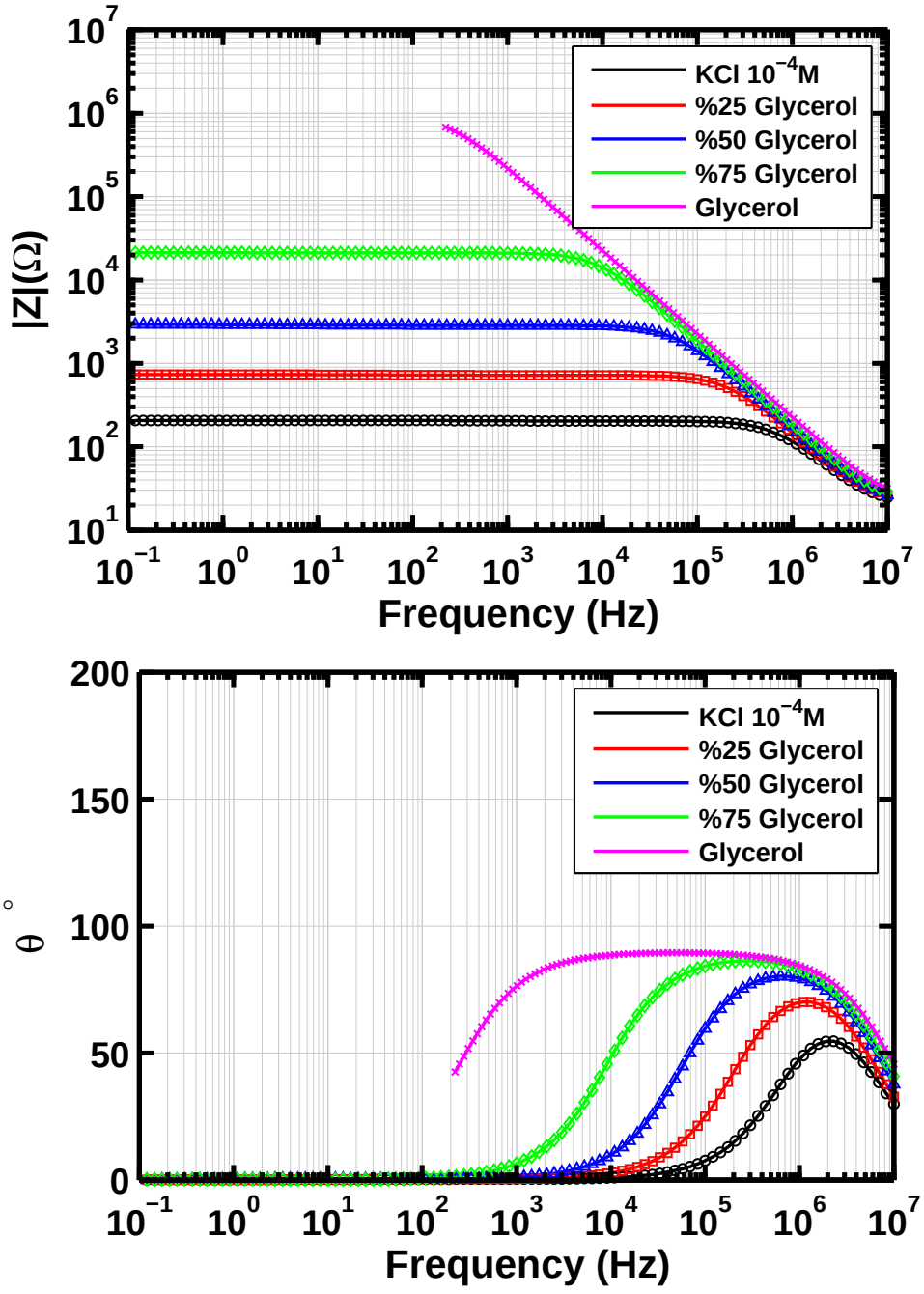

Figure 5.24: Bode plots of the 4-electrode EIS experiment with glycerol-salt water (KCl 10^{-4}M) mixtures for different glycerol contents. Symbols represent measurements and lines represent equivalent circuit model fit to the measurements.

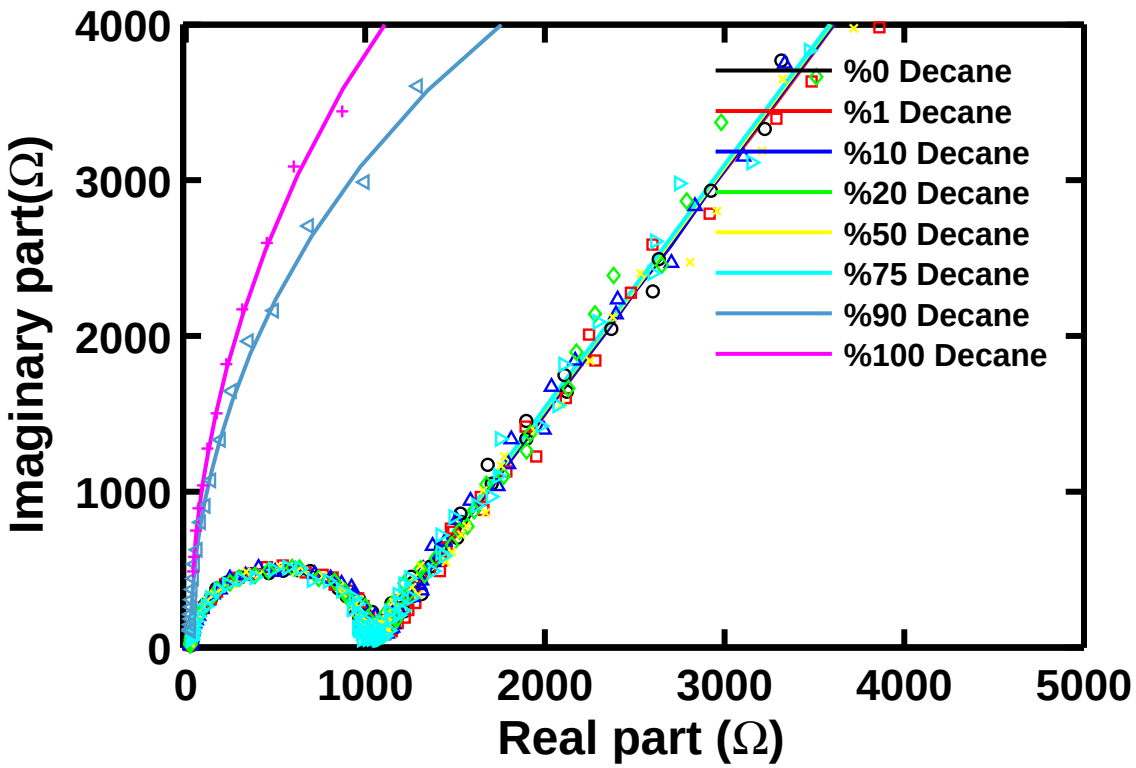

Figure 5.25: Nyquist plot of the EIS experiment with fresh decane-DI water emulsions for different oil contents. Symbols represent measurements and lines represent equivalent circuit model fit to the measurements.

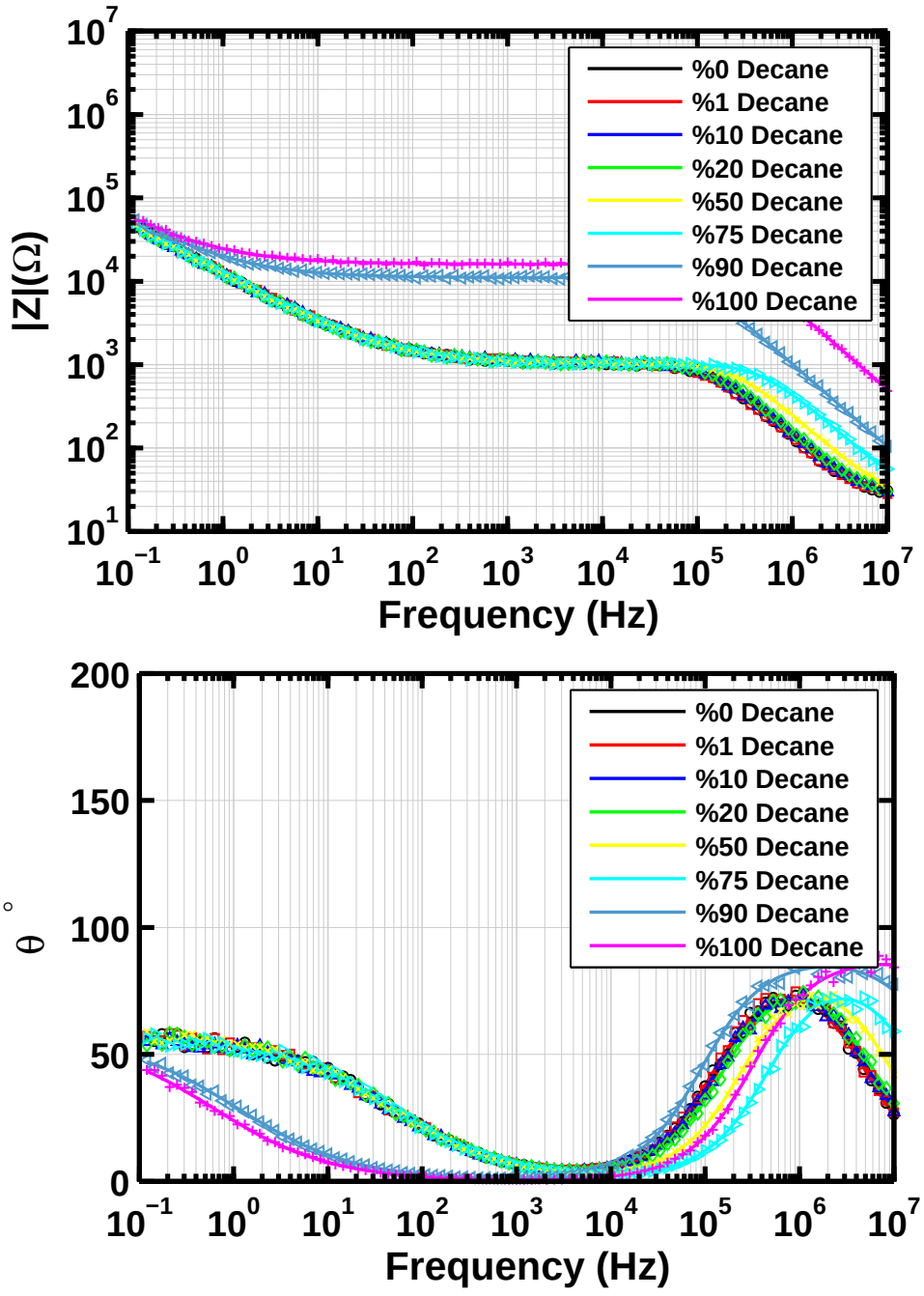

Figure 5.26: Bode plots of the EIS experiment with fresh decane-DI water emulsions for different oil contents. Symbols represent measurements and lines represent equivalent circuit model fit to the measurements.

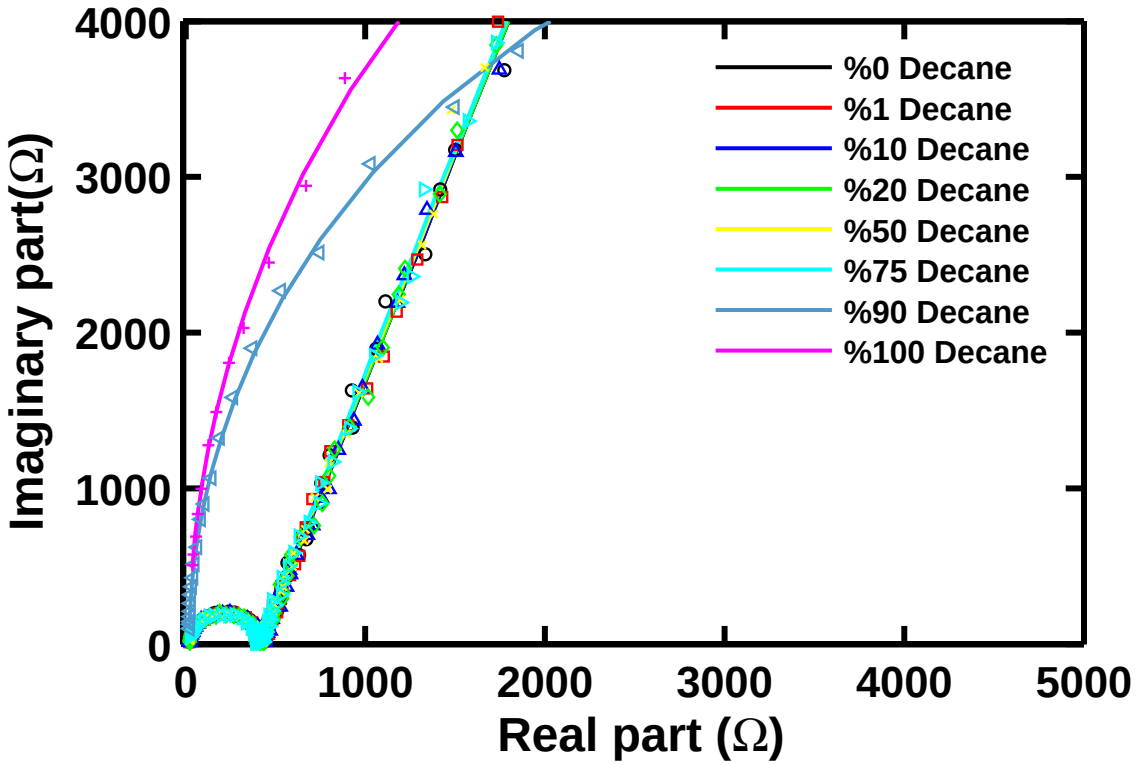

Figure 5.27: Nyquist plot of the EIS experiment with fresh decane-salt water (KCl 10^{-4}M) emulsions for different oil contents. Symbols represent measurements and lines represent equivalent circuit model fit to the measurements.

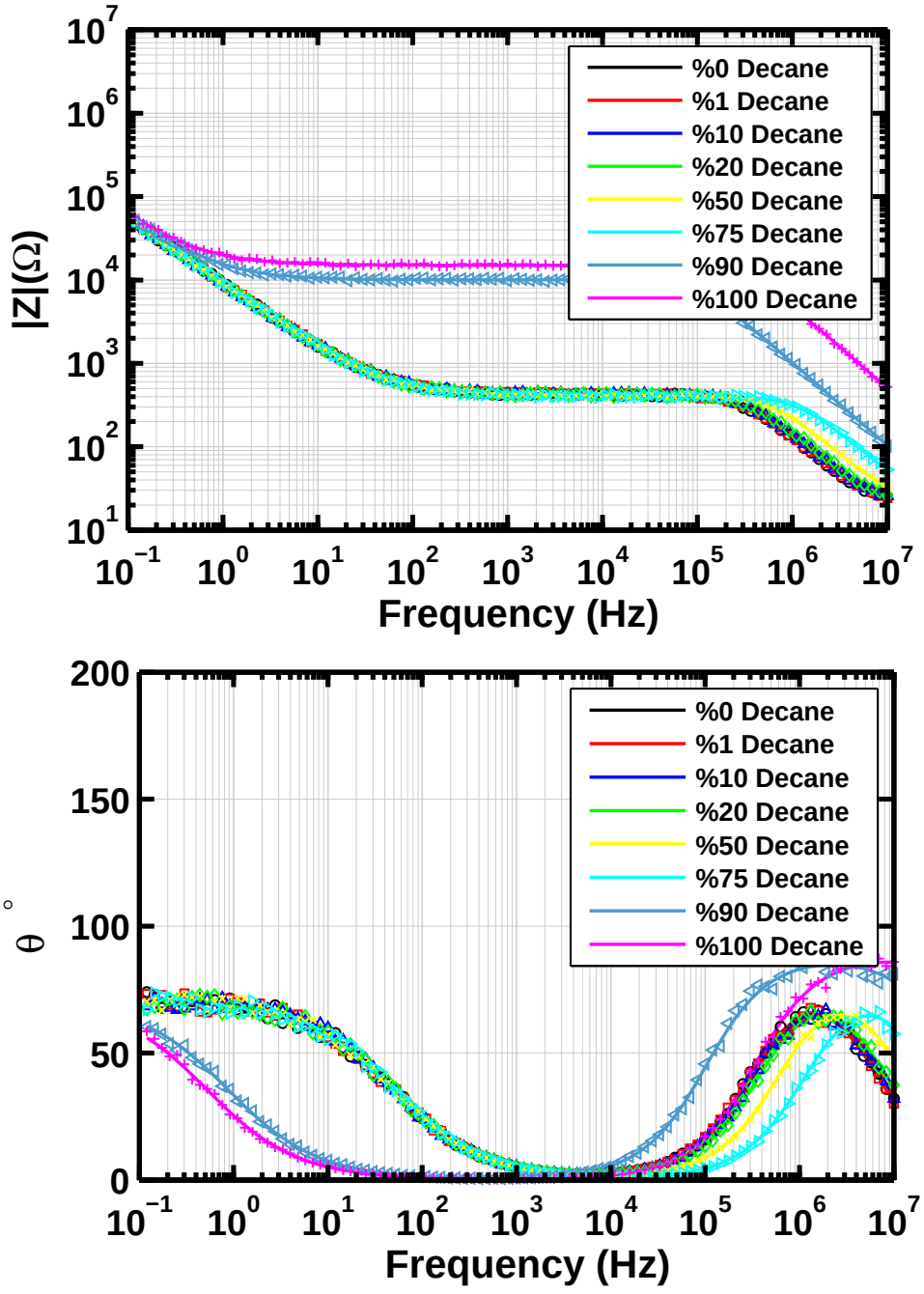

Figure 5.28: Bode plots of the EIS experiment with fresh decane-salt water (KCl 10^{-4}M) emulsions for different oil contents. Symbols represent measurements and lines represent equivalent circuit model fit to the measurements

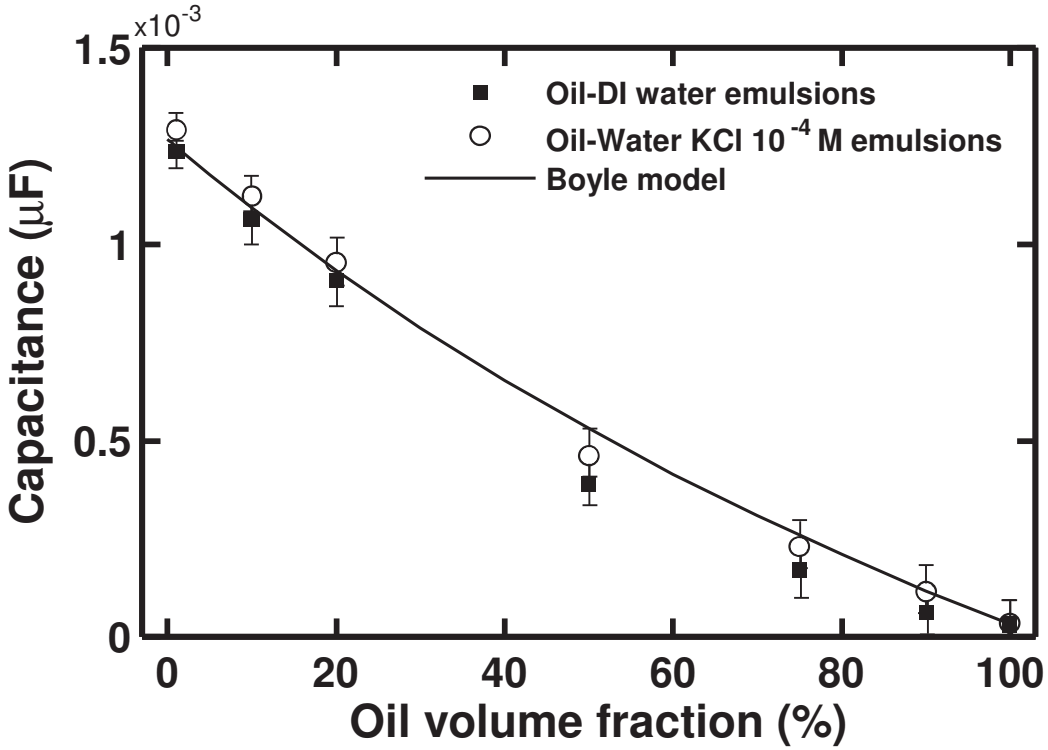

Figure 5.29: Capacitance of fresh decane-water emulsions versus oil content for different salt concentrations. The experimental results obtained from equivalent circuit modeling are compared to the capacitance obtained based on Boyle model for permittivity of complex media.

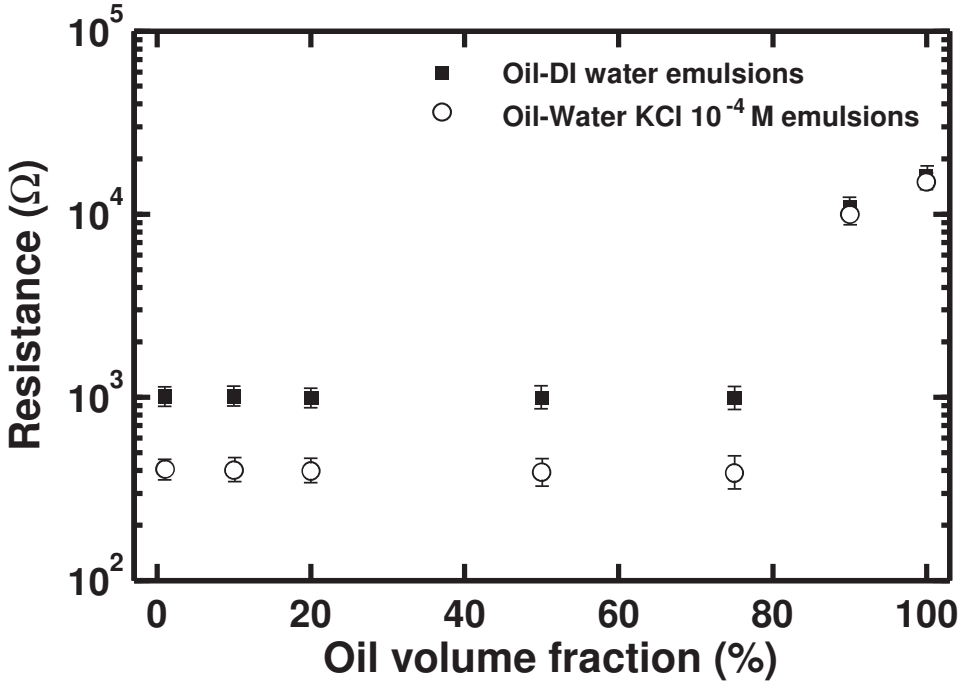

Figure 5.30: Resistance of fresh decane-water emulsions versus oil content for different salt concentrations. The measurements show very little variation in resistance until the oil content is increased to 90% where a sudden increase is observed.

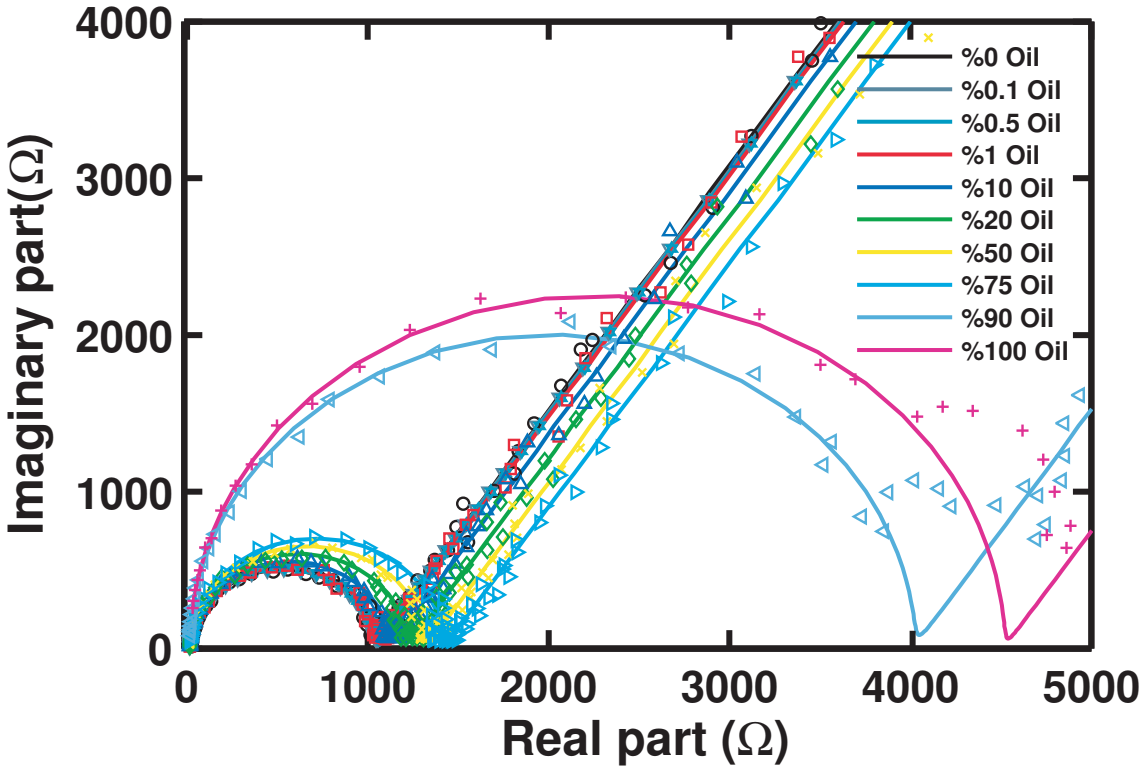

Figure 5.31: Nyquist plot of the EIS experiment with fresh castor oil-DI water emulsions for different oil contents. Symbols represent measurements and lines represent equivalent circuit model fit to the measurements.

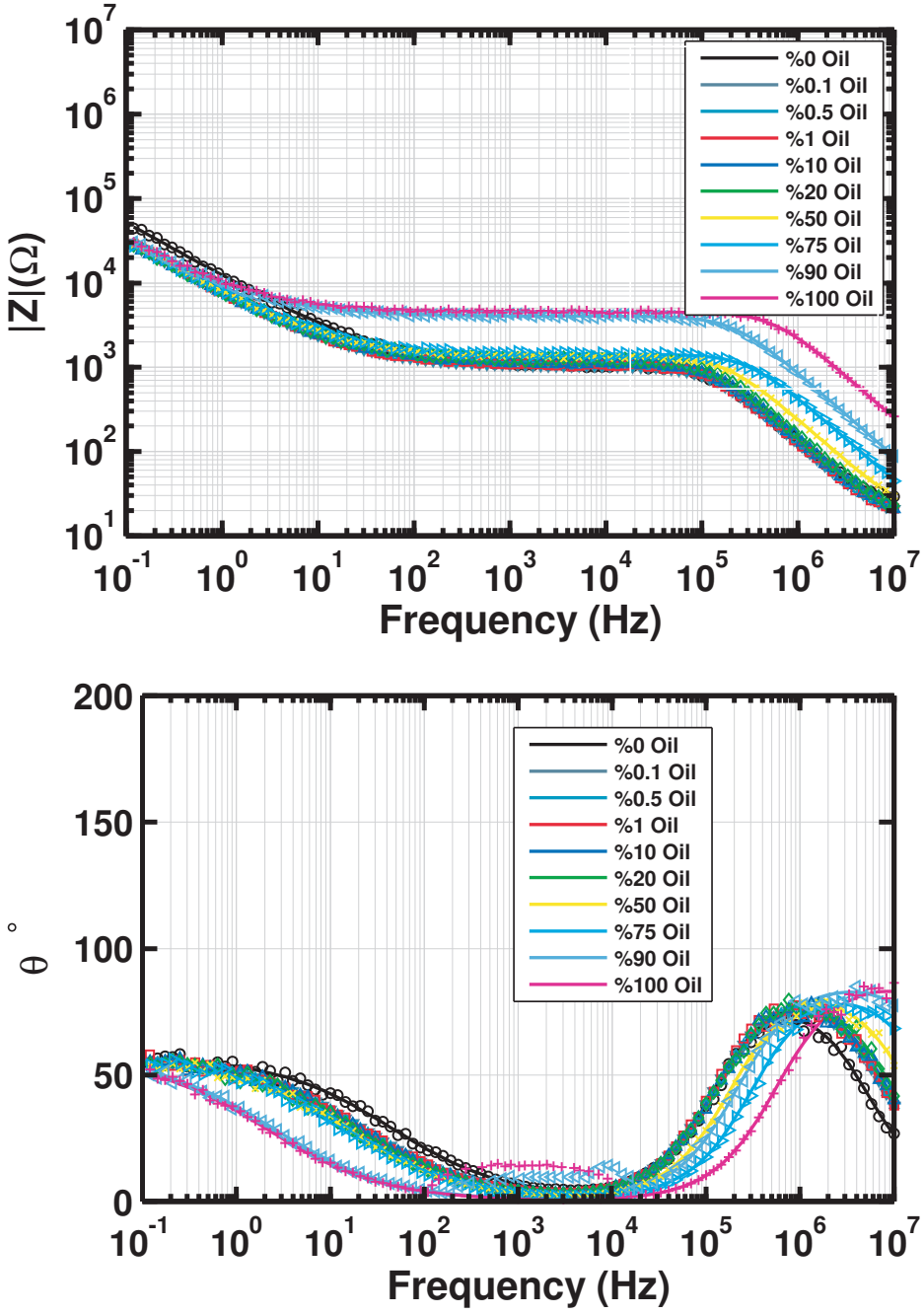

Figure 5.32: Bode plots of the EIS experiment with fresh castor oil-DI water emulsions for different oil contents. Symbols represent measurements and lines represent equivalent circuit model fit to the measurements.

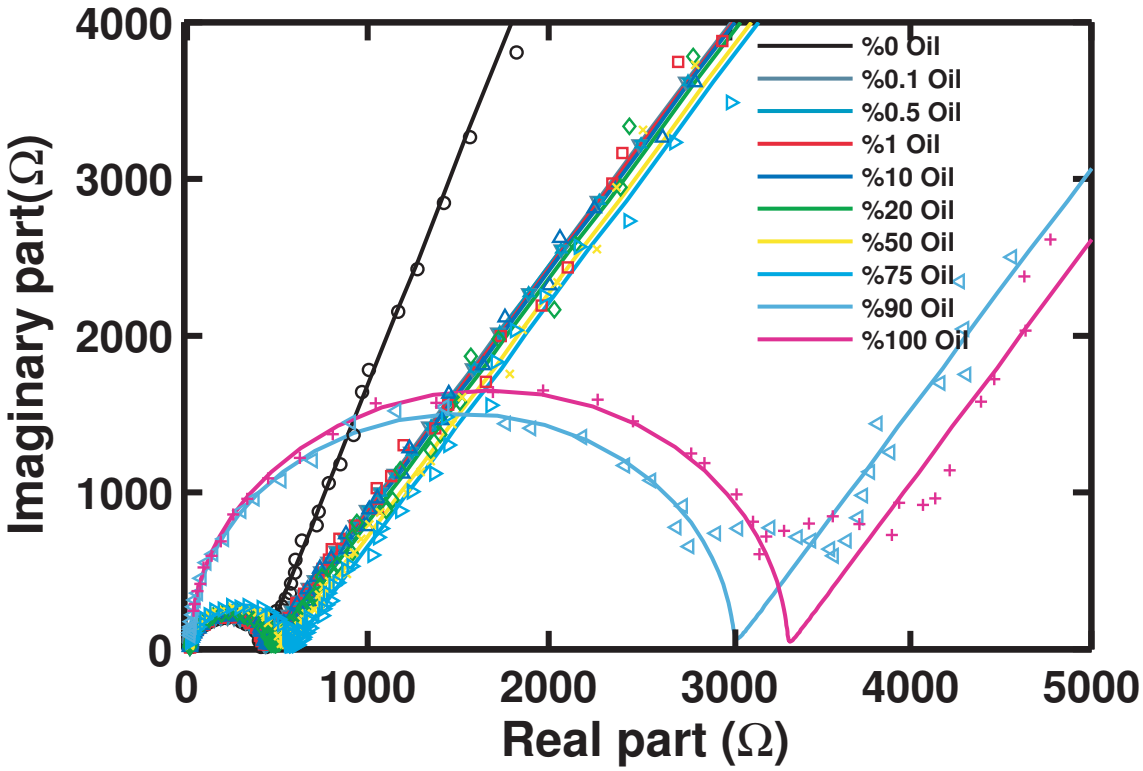

Figure 5.33: Nyquist plot of the EIS experiment with fresh castor oil-salt water (KCl 10^{-4}M) emulsions for different oil contents. Symbols represent measurements and lines represent equivalent circuit model fit to the measurements.

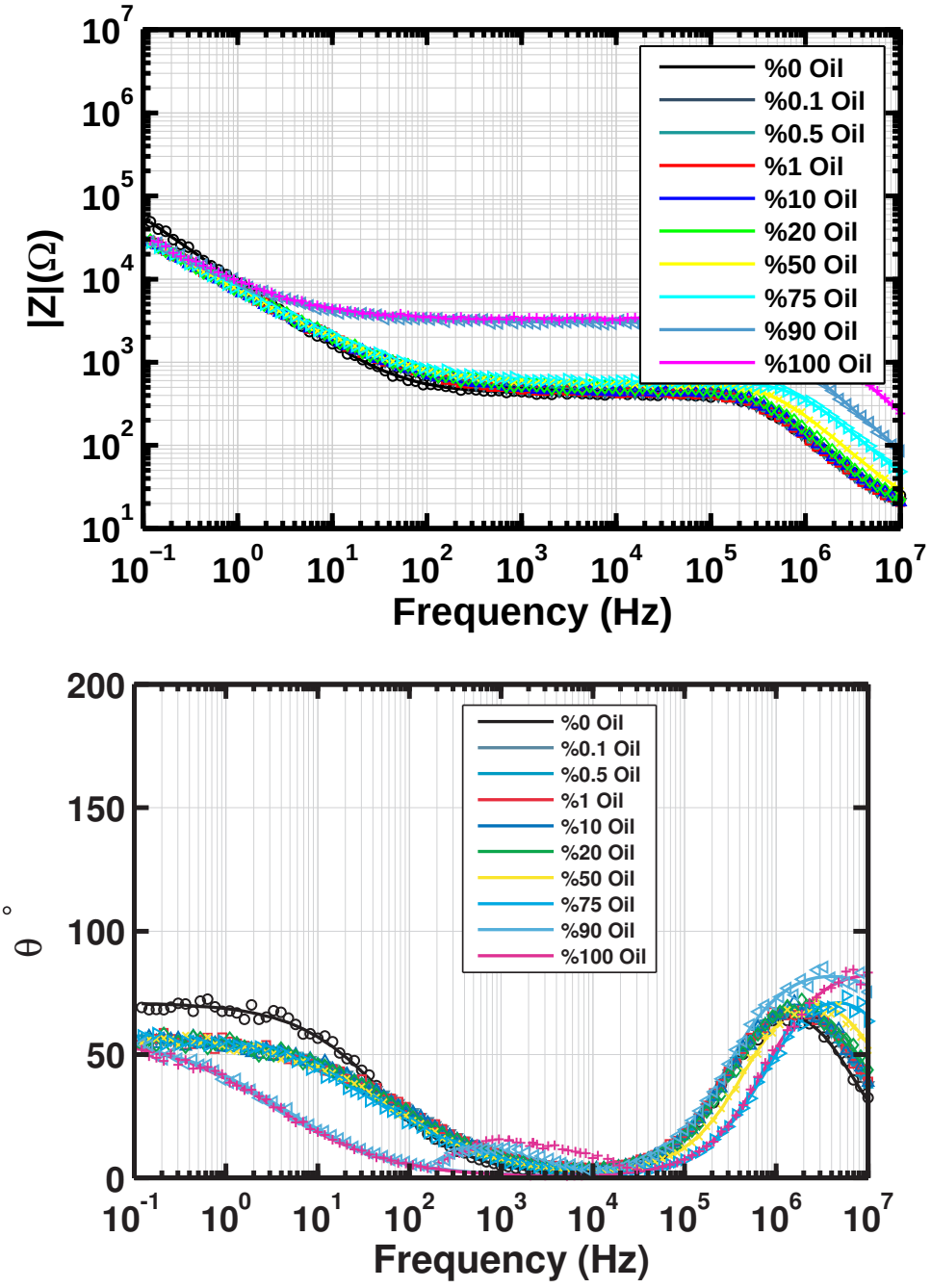

Figure 5.34: Bode plots of the EIS experiment with fresh castor oil-salt water (KCl 10^{-4}M) emulsions for different oil contents. Symbols represent measurements and lines represent equivalent circuit model fit to the measurements.

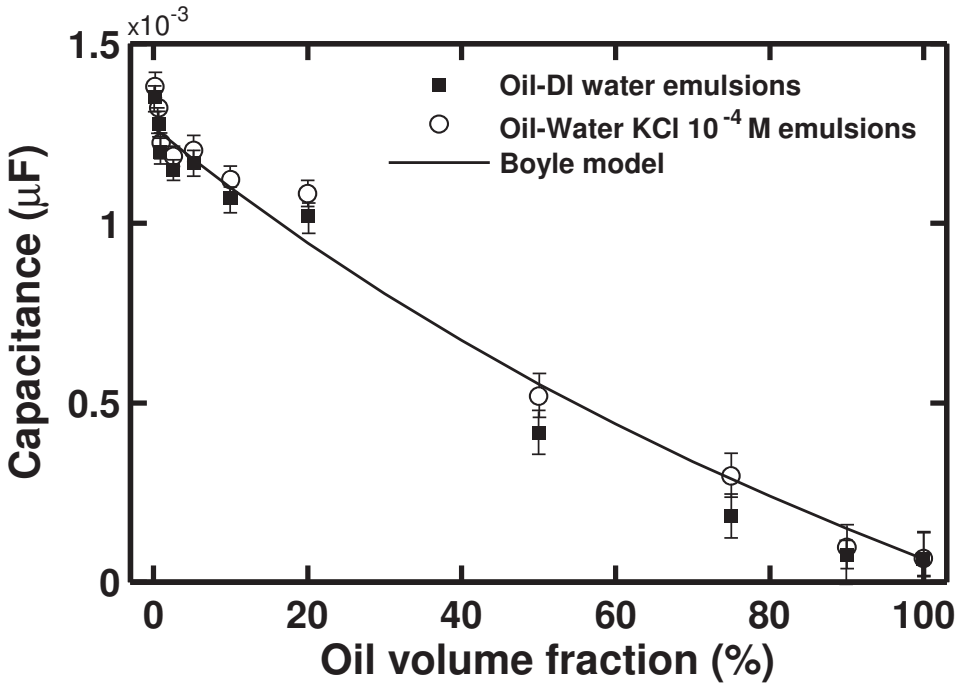

Figure 5.35: Capacitance of fresh castor oil-water emulsions versus oil content for different salt concentrations. The experimental results obtained from equivalent circuit modeling are compared to the capacitance obtained based on Boyle model for permittivity of complex media.

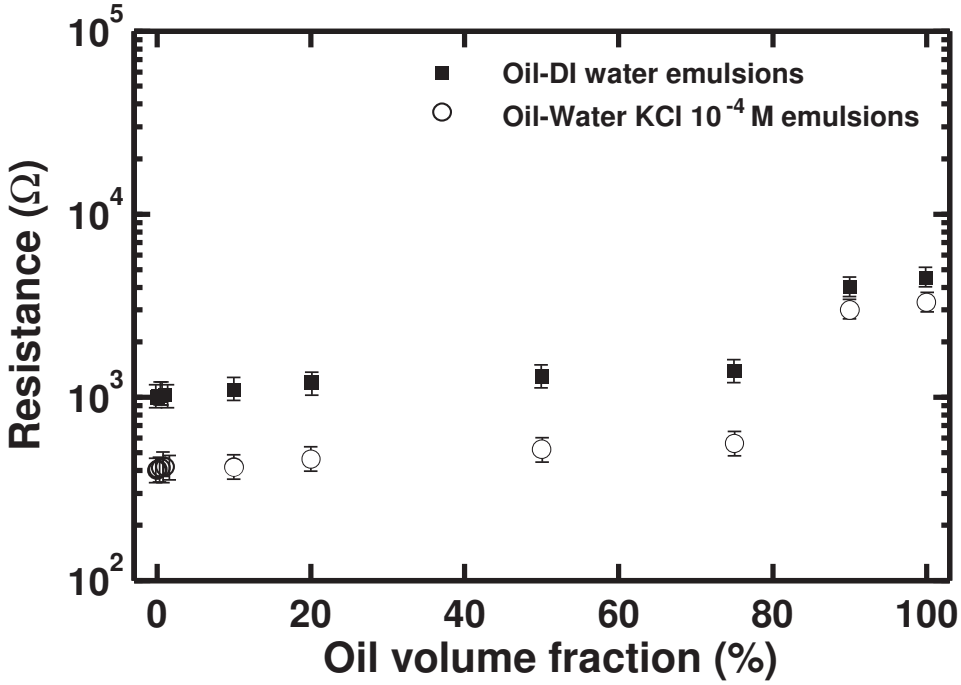

Figure 5.36: Resistance of fresh castor oil-water emulsions versus oil content for different salt concentrations. The measurements show very little variation in resistance until the oil content is increased to 90% where a sudden increase is observed.

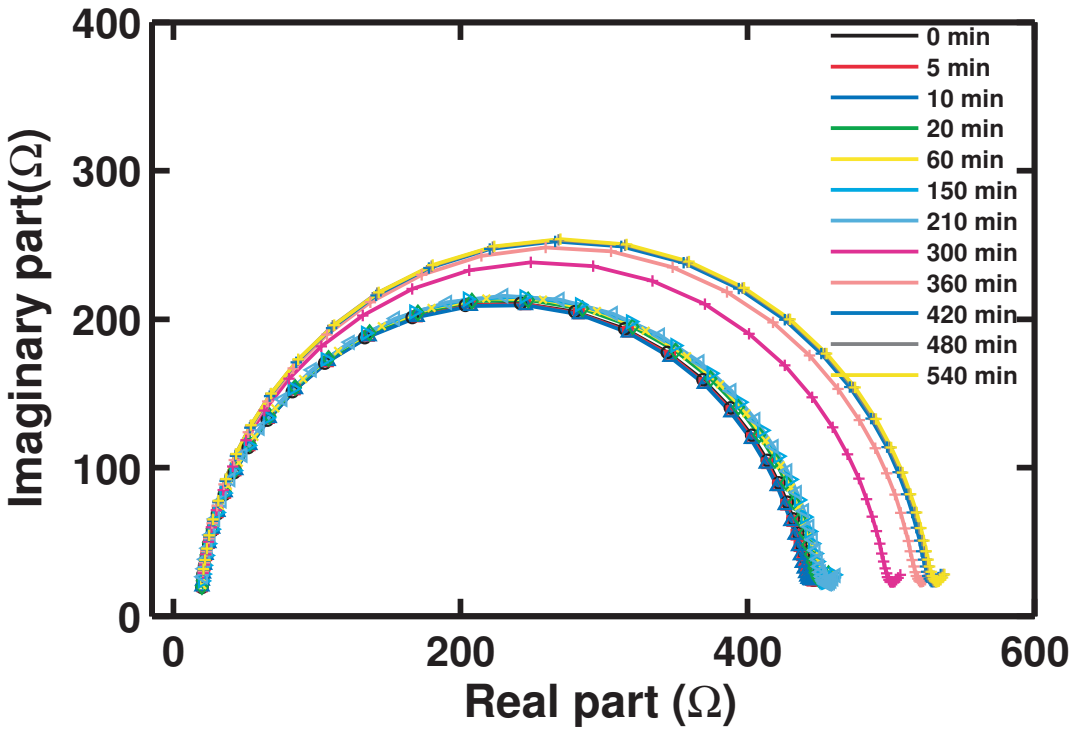

Figure 5.37: Nyquist plot of the EIS experiment with 5% decane-salt water (KCl 10^{-4}M) emulsion (homogenized with no surfactant) over time as the sample undergoes gradual phase separation. Symbols represent measurements and lines represent equivalent circuit model fit to the measurements.

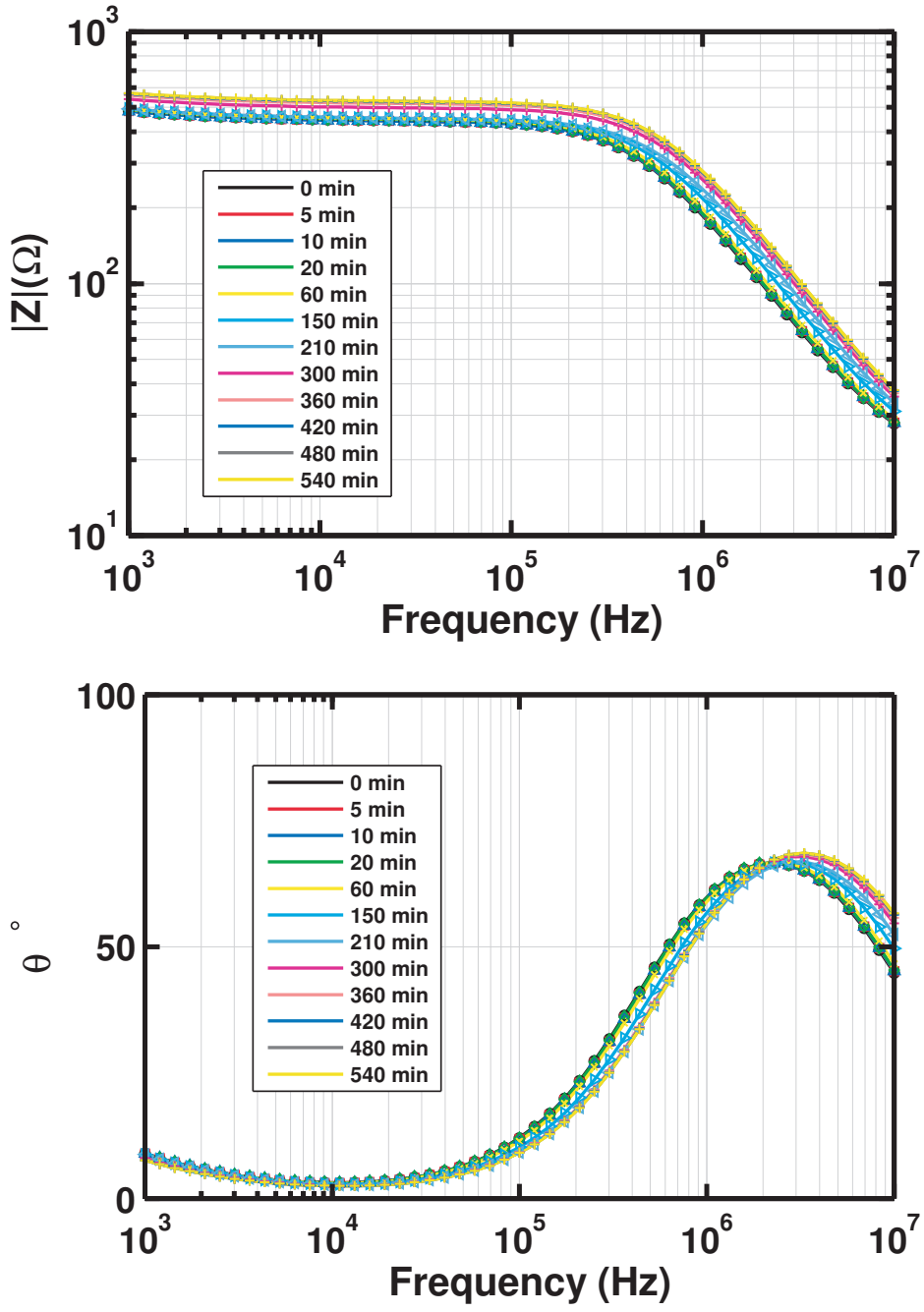

Figure 5.38: Bode plots of the EIS experiment with 5% decane-salt water (KCl 10^{-4}M) emulsion (homogenized with no surfactant) as the sample undergoes gradual phase separation. Symbols represent measurements and lines represent equivalent circuit model fit to the measurements.

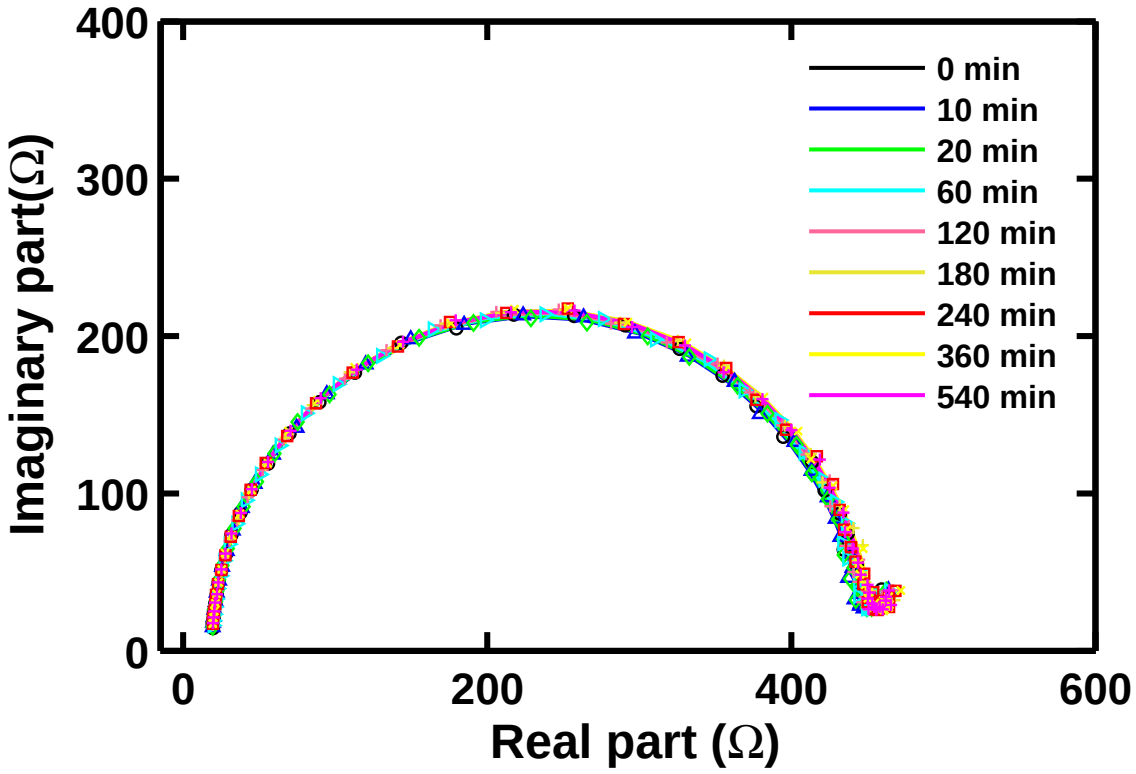

Figure 5.39: Nyquist plot of the EIS experiment with 5% decane-salt water (KCl 10^{-4}M) emulsion (homogenized with Tween80 concentration of 20CMC) over time as the sample undergoes gradual phase separation. Symbols represent measurements and lines represent equivalent circuit model fit to the measurements.

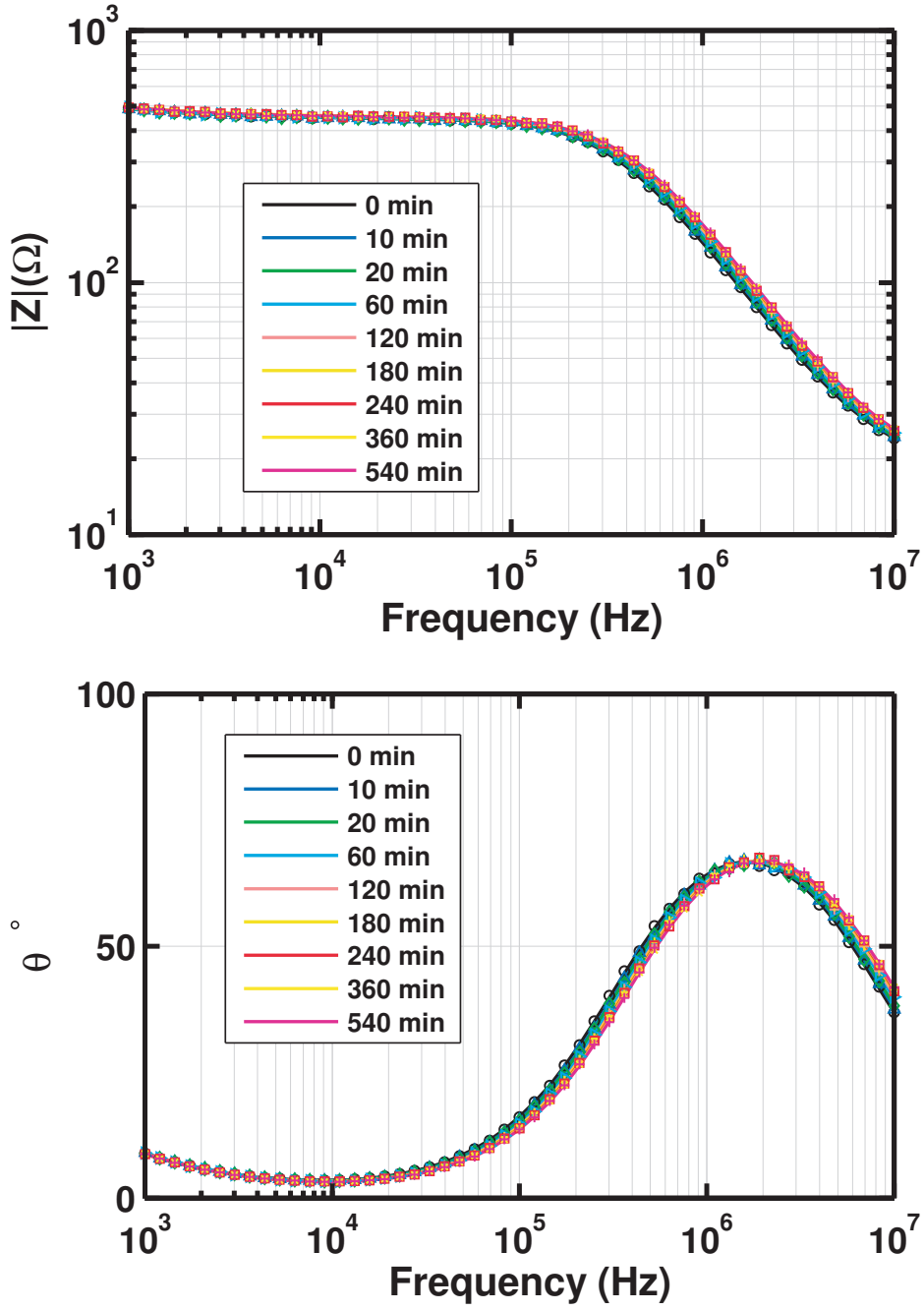

Figure 5.40: Bode plots of the EIS experiment with 5% decane-salt water (KCl 10^{-4}M) emulsion (homogenized with Tween80 concentration of 20CMC) over time as the sample undergoes gradual phase separation. Symbols represent measurements and lines represent equivalent circuit model fit to the measurements.

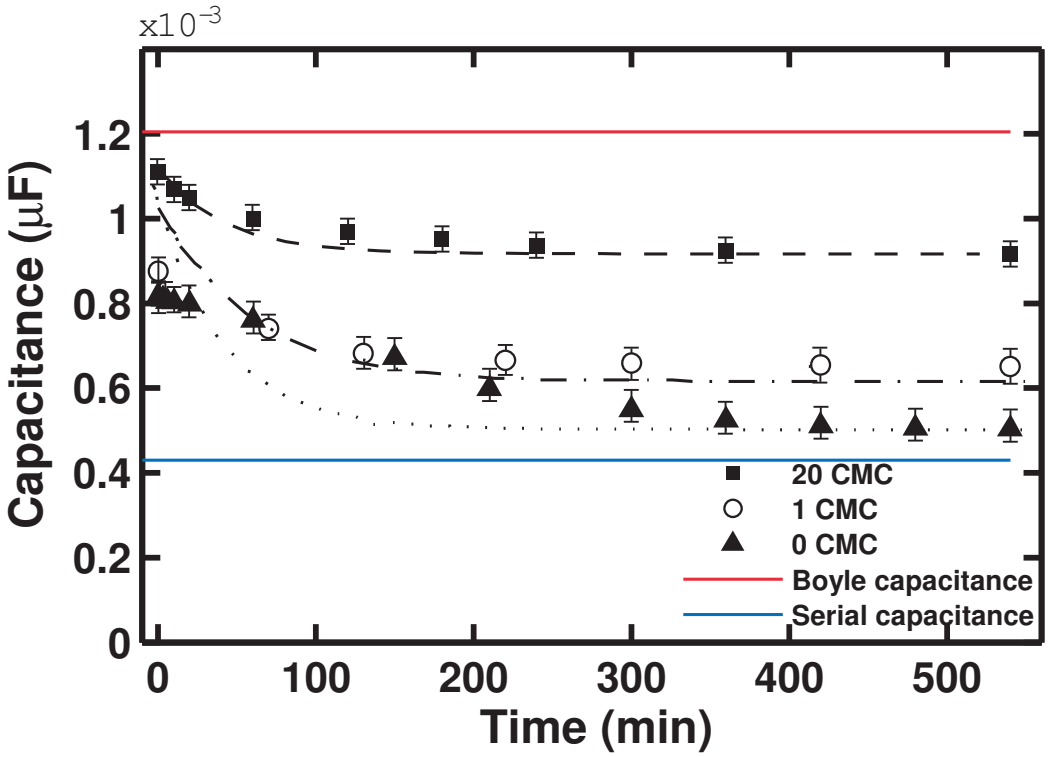

Figure 5.41: Capacitance of homogenized 5% decane-salt water (KCl 10^{-4}M) emulsions versus time for different surfactant dosages as the emulsions undergo phase separation. It is observed that the capacitance of the emulsions that are more stable (with higher surfactant dosages) decay from the well-emulsified value to a value larger than the serial capacitance while the emulsion with 0 surfactant, decays to a value very close to the serial capacitance. The dashed and dash-dot lines show the exponential decay function fitted to the systems' behavior.

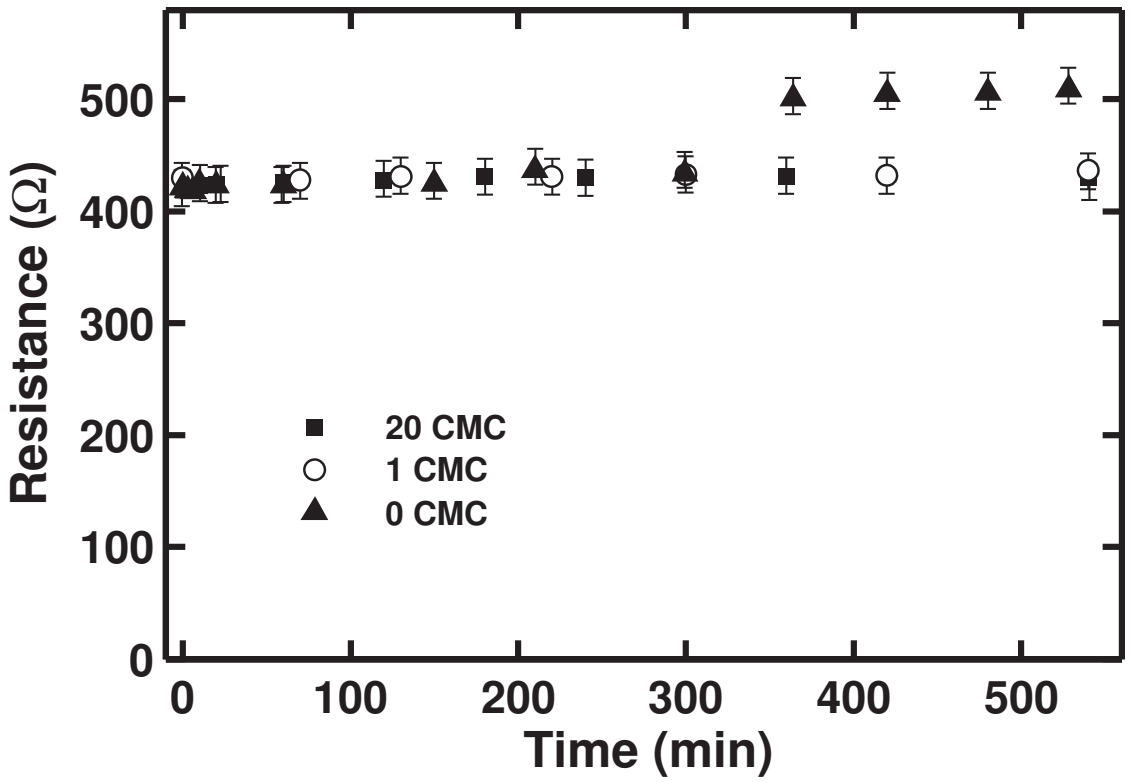

Figure 5.42: Resistance of homogenized 5% decane-salt water (KCl 10^{-4}M) emulsions versus time for different surfactant dosages as the emulsions undergo phase separation. In the emulsion with 0 surfactant an increase in the resistance is observed while the resistance of other emulsions are almost constant.

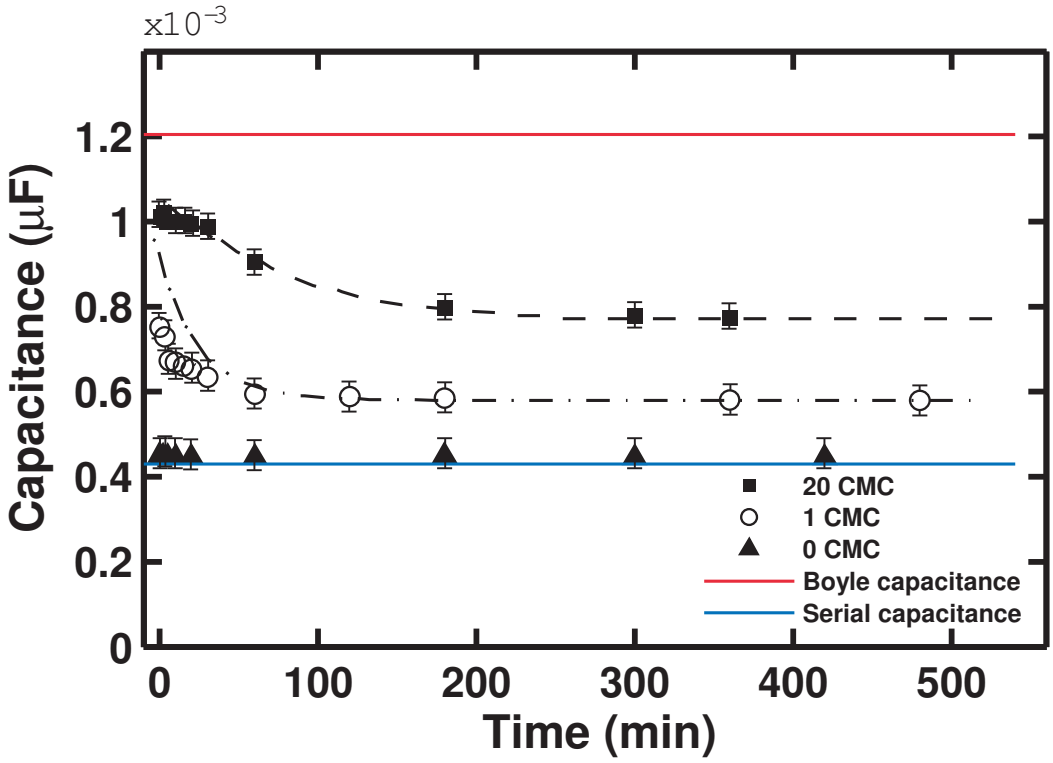

Figure 5.43: Capacitance of unhomogenized 5% decane-salt water (KCl 10^{-4}M) emulsions versus time for different surfactant dosages as the emulsions undergo phase separation. It is observed that the capacitance of the emulsions that are more stable (with higher surfactant dosages) decay from the well-emulsified value to a value larger than the serial capacitance while the emulsion with 0 surfactant, very quickly (even before the first measurement) decays to a value very close to the serial capacitance. The dashed and dash-dot lines show the exponential decay function fitted to the systems' behavior.

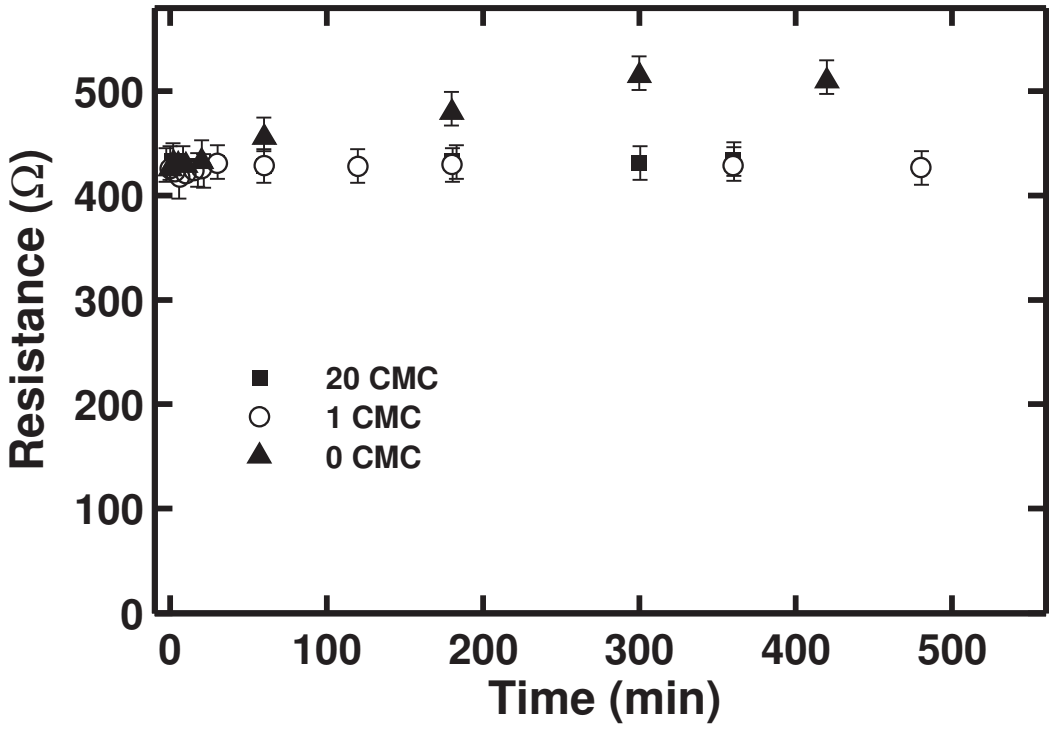

Figure 5.44: Resistance of unhomogenized 5% decane-salt water (KCl 10^{-4}M) emulsions versus time for different surfactant dosages as the emulsions undergo phase separation. In the emulsion with 0 surfactant an increase in the resistance is observed while the resistance of other emulsions are almost constant.

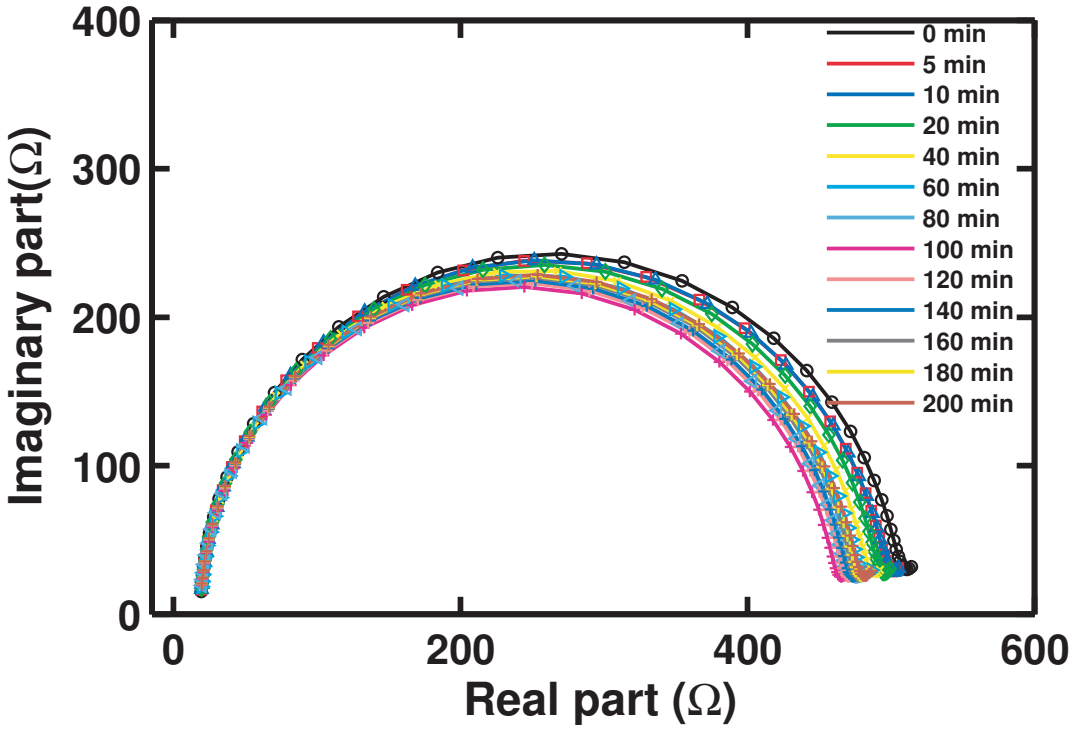

Figure 5.45: Nyquist plot of the EIS experiment with 10% castor oil-salt water (KCl 10^{-4}M) emulsion (homogenized with no surfactant) over time as the sample undergoes gradual phase separation. Symbols represent measurements and lines represent equivalent circuit model fit to the measurements.

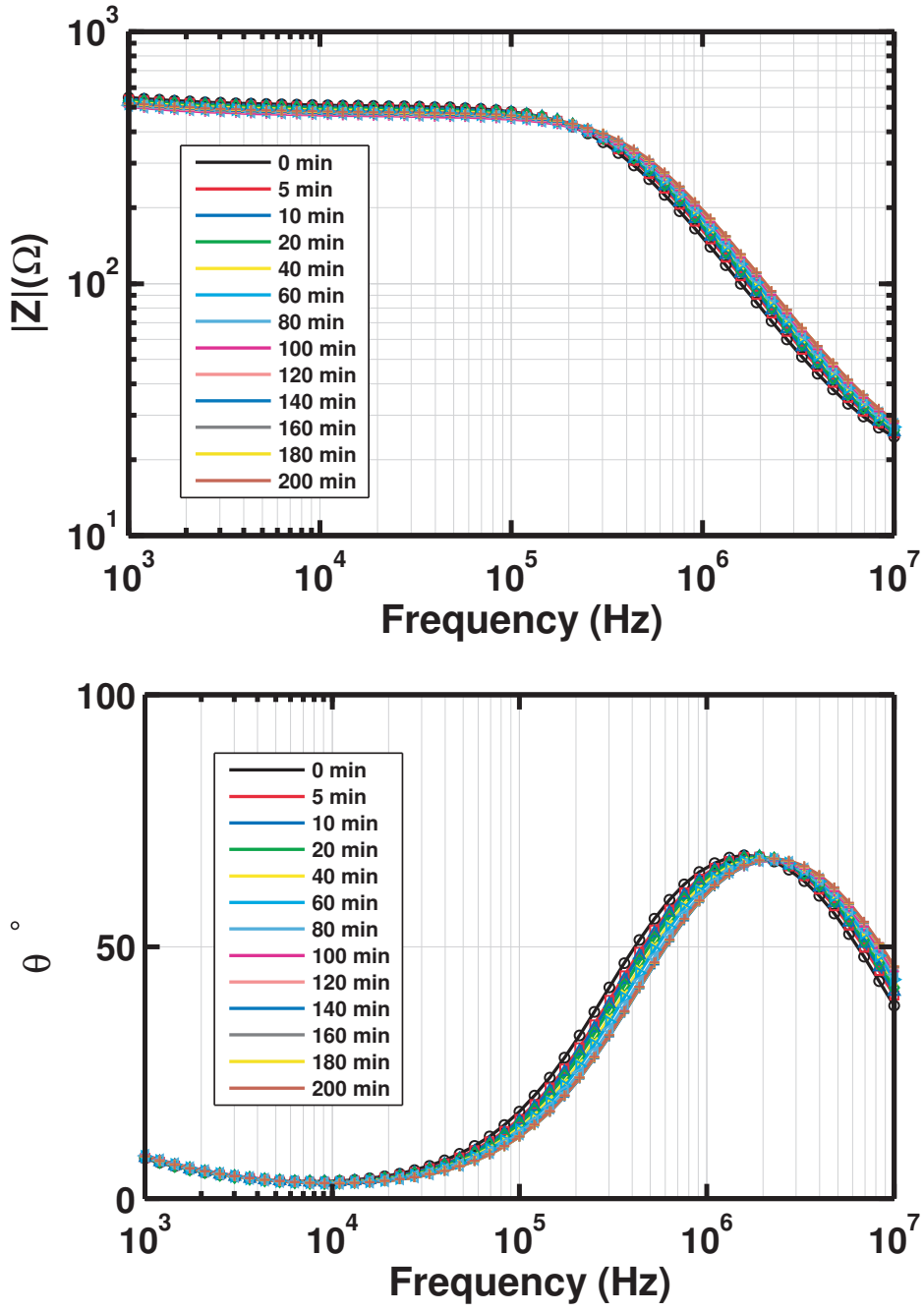

Figure 5.46: Bode plots of the EIS experiment with 10% castor oil-salt water (KCl 10^{-4}M) emulsion (homogenized with no surfactant) over time as the sample undergoes gradual phase separation. Symbols represent measurements and lines represent equivalent circuit model fit to the measurements.

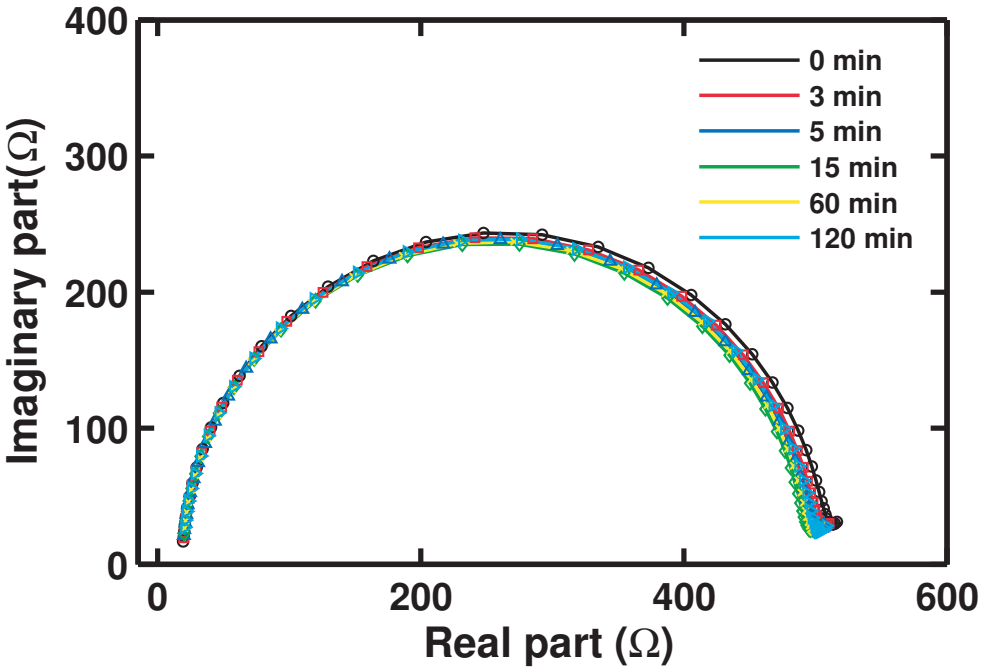

Figure 5.47: Nyquist plot of the EIS experiment with 10% castor oil-salt water (KCl 10^{-4}M) emulsion (uhomogenized, only stirred with no surfactant) over time as the sample undergoes gradual phase separation. Symbols represent measurements and lines represent equivalent circuit model fit to the measurements.

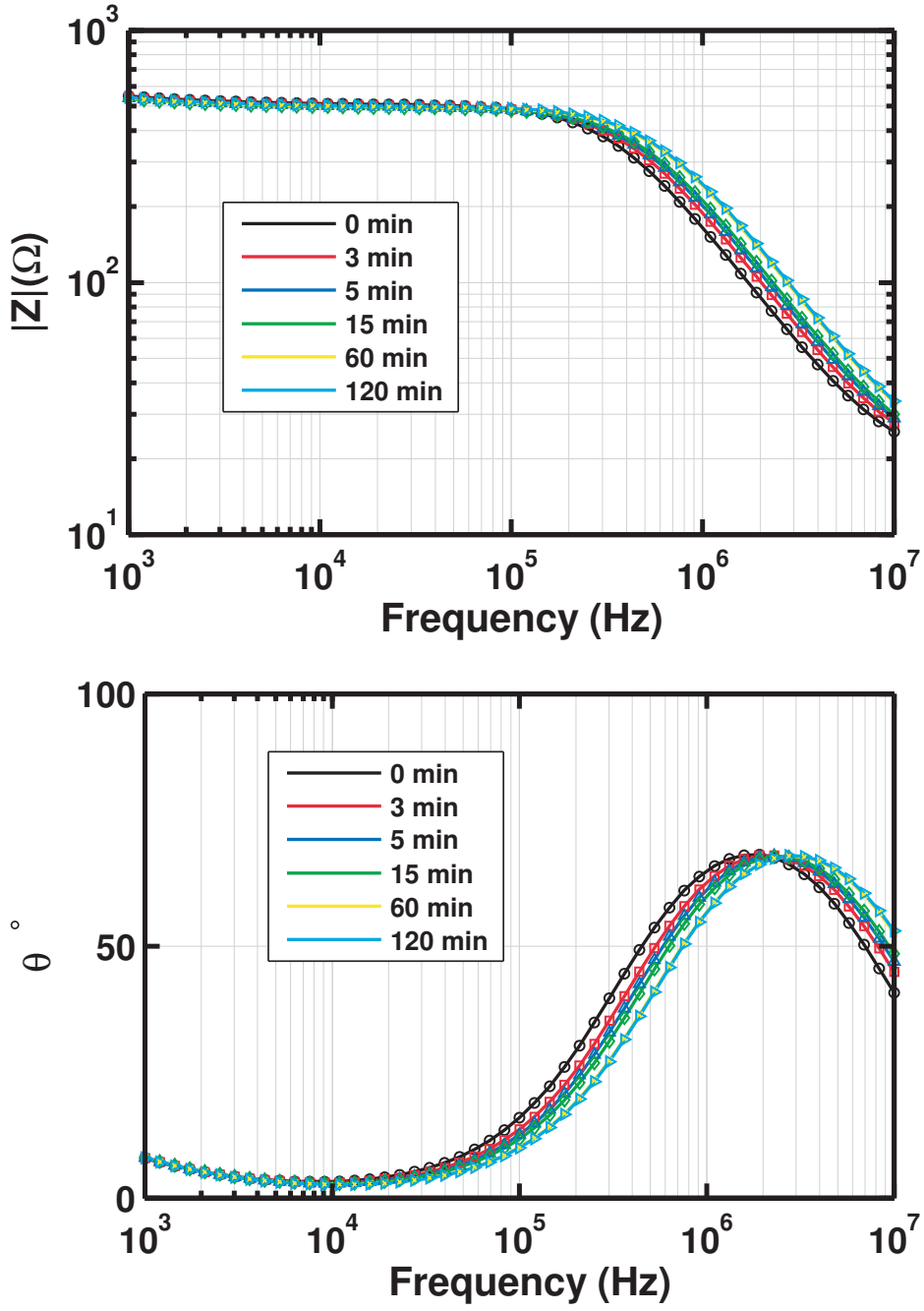

Figure 5.48: Bode plots of the EIS experiment with 10% castor oil-salt water (KCl 10^{-4}M) emulsion (uhomogenized, only stirred with no surfactant) over time as the sample undergoes gradual phase separation. Symbols represent measurements and lines represent equivalent circuit model fit to the measurements.

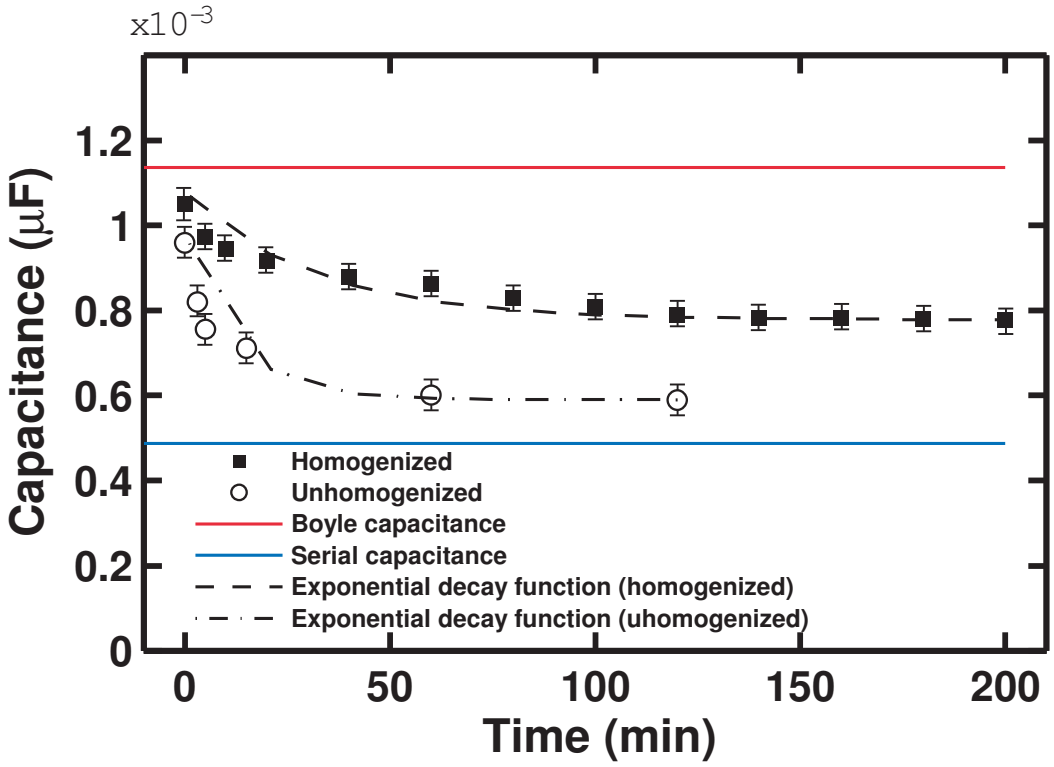

Figure 5.49: Capacitance of homogenized and unhomogenized 10% castor oil-salt water (KCl 10^{-4}M) emulsions versus time as the emulsions undergo phase separation. It is observed that both emulsions have a capacitance close to the Boyle model for homogeneous complex media when fresh, but as they undergo phase separation, the unhomogenized emulsion decays to a value closer to the serial capacitance value compared to the homogenized emulsion. The dashed and dash-dot lines show the exponential decay function fitted to the systems' behavior.

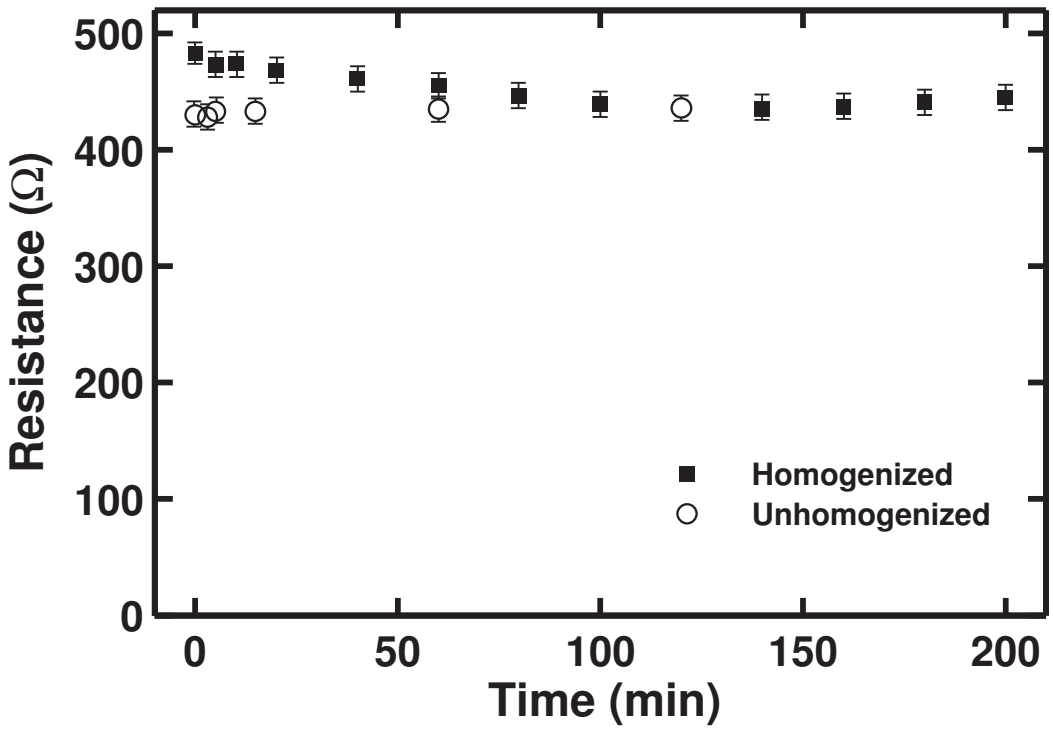

Figure 5.50: Resistance of homogenized and unhomogenized 10% castor oil-salt water (KCl 10^{-4}M) emulsions versus time as the emulsions undergo phase separation. No considerable variation in resistance was observed.

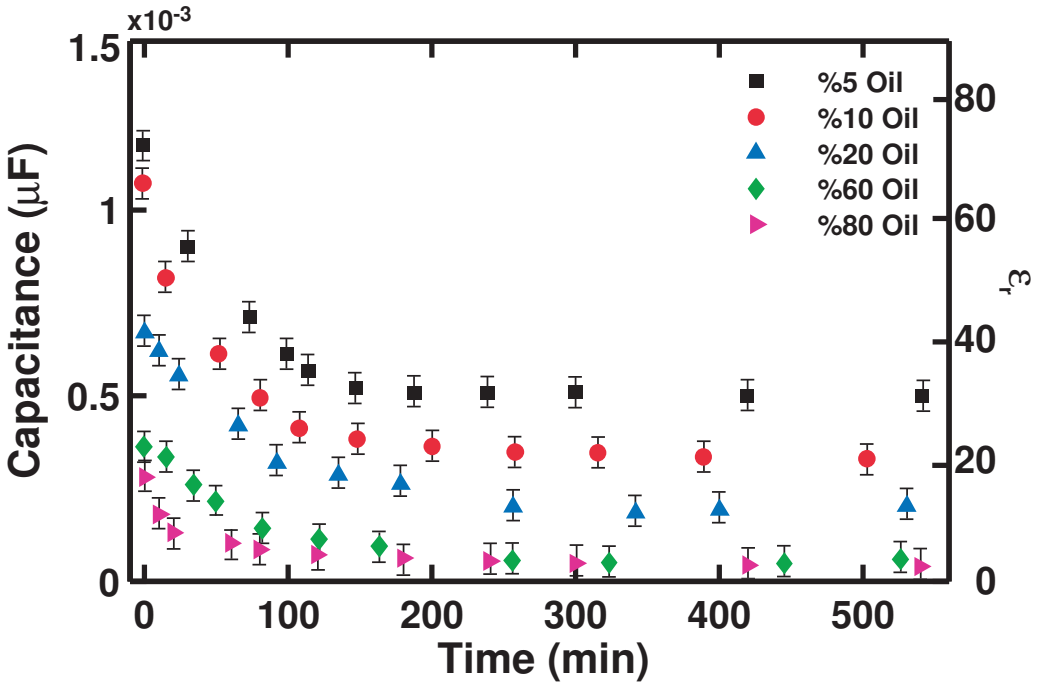

Figure 5.51: Capacitance of decane-salt water (KCl 10^{-4}M) emulsions with different oil contents versus time as the emulsions undergo phase separation. It is observed that as the oil content is increased, the initial (fresh) permittivity becomes smaller, therefore the permittivity decay caused by phase separation becomes less sensible.

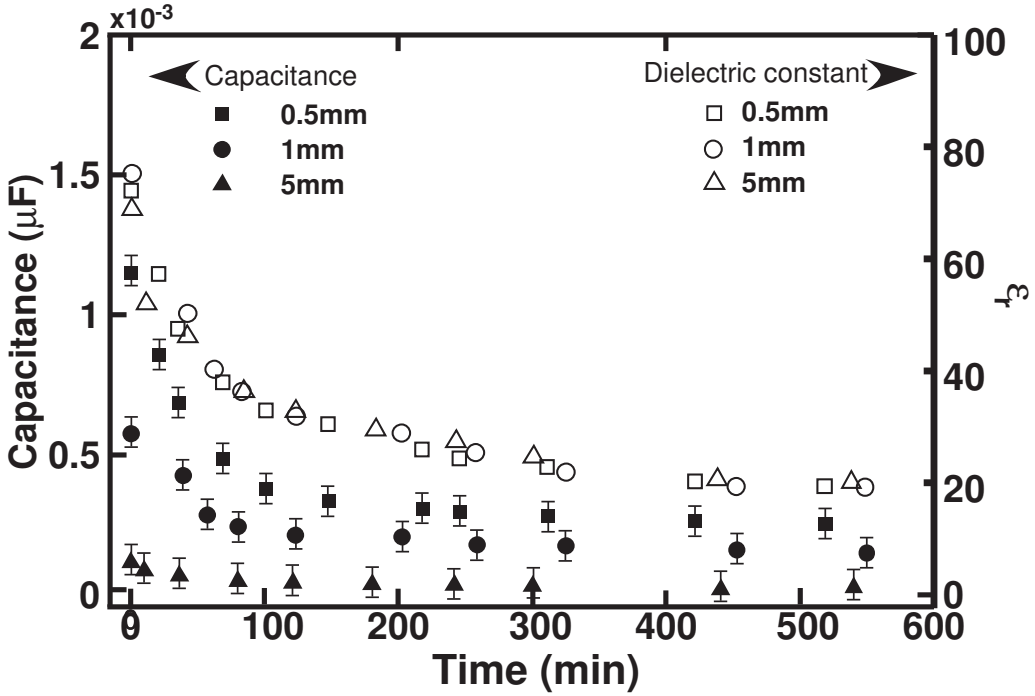

Figure 5.52: Capacitance (left) and dielectric constant (right) of 10% decane-salt water (KCl 10^{-4}M) emulsions with different sample thicknesses versus time as the emulsions undergo phase separation. It is observed that while the capacitance is affected by the sample thickness, the measured permittivity decay does not show considerable variation with thickness.

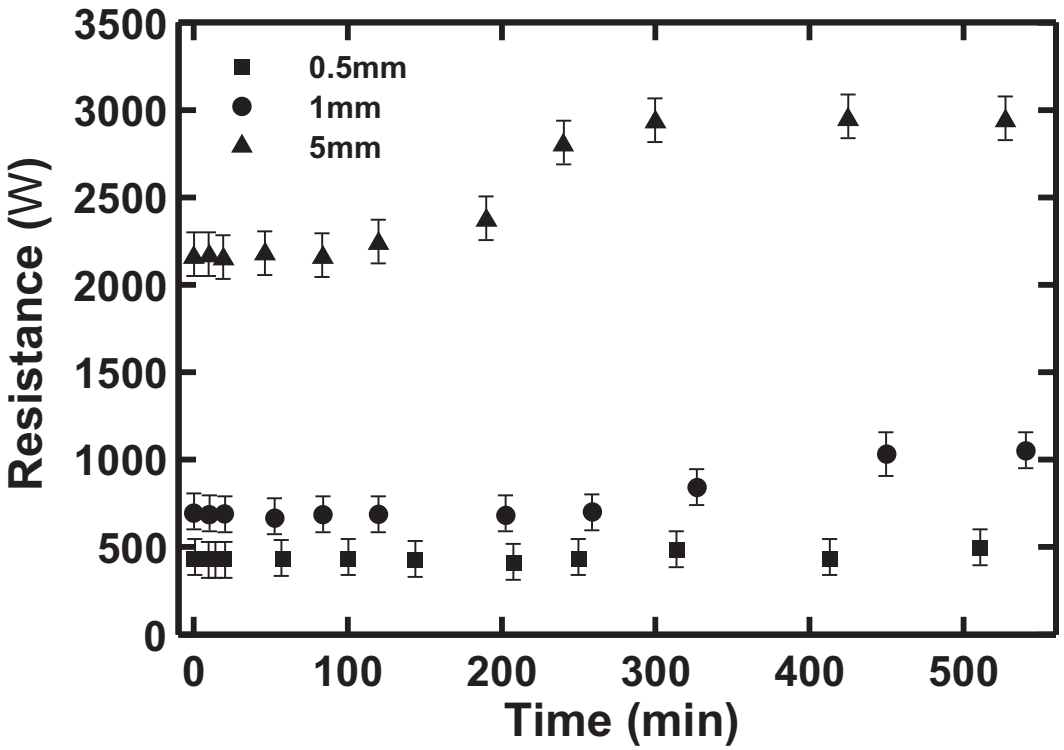

Figure 5.53: Resistance of 10% decane-salt water (KCl 10^{-4}M) emulsions with different sample thicknesses versus time as the emulsions undergo phase separation. It is observed that the increase in resistance becomes larger and more sensible. Also, the resistance increase happens earlier as the sample thickness is increased.

CHAPTER 6

CONCLUSIONS AND FUTURE WORK

6.1 CONCLUSIONS

The objectives of this thesis and the scope of the work was defined in chapter 1. As per those objectives, the main concluding remarks of this thesis are listed below.

1. Based on the results of the numerical simulation of emulsion permittivity, it was observed that if the droplet diameter of an emulsion is in the same order of magnitude as the thickness of the EIS sample liquid, the electric field is distorted to the extent that bulk properties of the emulsion (for instance volume fraction) will not be sensible. In other words, when the length scale of the test cell is in the same order of magnitude as the mean droplet size, the EIS system senses a large electric field distortion near the electrodes that can easily outweigh emulsion bulk properties. Therefore, based on the application, enough care should be given to the choice of EIS test length scale. Specifically, micron-size EIS test fixtures are fundamentally flawed for detecting bulk properties of emulsions.

2. In this work, an inexpensive, easily fabricated, yet robust and reliable, "milli-fluidic" experimental EIS test fixture was introduced. This test cell solves the problem of setup cleaning after testing industrially-relevant samples, as it can be disposed of after each test.

3. While previous theoretical models and experimental studies investigated dielectric properties of *homogeneous* distributions of dispersed elements, in this thesis, dielectric behavior of oil-water emulsions during phase separation processes (creaming/sedimentation) was investigated analytically, numerically, and experimentally.

4. It was observed that in O/W emulsions, electrical conductivity does not change considerably during phase separation unless the system becomes completely separated and is allowed to rest to the extent that no water remains in the oil-rich creamed layer. This was attributed to the fact that even small amounts of water can maintain electric current passages in the oil-rich phase. In summary, it can be concluded that conductivity is not a good measure for monitoring the degree of phase separation.

5. It was observed that permittivity is a function of the topological structure of the dispersed phase, rather than presence of electric-current passages. So capacitance-based measurement provides a good diagnostic tool for detecting phase separation. A permittivity decay was observed as the emulsion systems underwent phase separation. Therefore, phase separation processes can be detected and monitored based on measuring the permittivity. Moreover, a relation for the thickness of the separated layer in a two-phase oil-water system as a function of the measured capacitance was derived, that can be directly used in a capacitance-based process monitoring unit to assess extent of phase separation.

6. It was observed that permittivity-based phase separation detection is more effective in O/W emulsions rater than W/O ones. This is because phase separation detection is based on permittivity decay, and as the oil content is increased, the initial permittivity becomes lower, making the decay sensing more difficult.

6.2 POSSIBLE FUTURE DIRECTIONS

Based on the conclusions of this thesis and based on the literature review provided in chapter 2, possible future directions that can be pursued beyond this research are presented below.

1. As discussed in chapter 4, in this thesis, a new aspect of emulsion phase behavior was studied, namely dielectric properties during gravity-driven phase separation, with a new inexpensive disposable experimental fixture. Phase separation process can be studied using optical microscopy by looking at the sample from the side, not top or bottom. Therefore, in this work, it was experimentally difficult to see phase separation under the microscope. A simple next step would be to modify the experimental fixture to enable the experimenter to see the phase separation process under the microscope while doing EIS measurement.

2. This study provided a method for sensing phase separation in emulsions in an off-line test fixture. A possible future direction could be designing and fabricating an experimental test platform for studying dielectric behavior of oil-water emulsions under flow.

3. Multiphase liquids show a considerably different dielectric behavior when flowing. After designing the appropriate experimental test setup, an interesting research can involve studying dielectric behavior of emulsions, especially during phase separation, with flowing samples.

4. A long-term direction of this project can be integrating the frequency response apparatus on a chip, and developing a portable online monitoring system that can be installed on pipelines or any physicochemical reactor, to detect phase separation in the working two-phase fluids.

Bibliography

[1] Randy J Mikula. Emulsion characterization. In *Advances in Chemistry*, volume 231, pages 79–129–. American Chemical Society, May 1992.

[2] A.J. Bard and L.R. Faulkner. *Electrochemical Methods: Fundamentals and Applications*. Wiley, 2000.

[3] E. Barsoukov and J.R. Macdonald. *Impedance Spectroscopy: Theory, Experiment, and Applications*. Wiley, 2005.

[4] David Julian Mcclements. Critical review of techniques and methodologies for characterization of emulsion stability. *Critical Reviews in Food Science and Nutrition*, 47(7):611–649, 2007. PMID: 17943495.

[5] Koji Asami. Characterization of heterogeneous systems by dielectric spectroscopy. *Progress in Polymer Science*, 27(8):1617 – 1659, 2002.

[6] J.S. Seybold. *Introduction to RF Propagation*. Wiley, 2005.

[7] Koji Asami. Dielectric properties of microvillous cells simulated by the three-dimensional finite-element method. *Bioelectrochemistry*, 81(1):28 – 33, 2011.

[8] J. Sjoblom. *Encyclopedic Handbook of Emulsion Technology*. Taylor & Francis, 2010.

[9] F. Bordi, C. Cametti, and T. Gili. Reduction of the contribution of electrode polarization effects in the radiowave dielectric measurements of highly conductive biological cell suspensions. *Bioelectrochemistry*, 54(1):53 – 61, 2001.

[10] Farshid Karimi Mostowfi. *Electric breakdown of thin liquid films*. PhD thesis, University of Alberta (Canada), 2007.

[11] Farshid Mostowfi, Jan Czarnecki, Jacob Masliyah, and Subir Bhattacharjee. A microfluidic electrochemical detection technique for assessing stability of thin films and emulsions. *Journal of Colloid and Interface Science*, 317(2):593 – 603, 2008.

[12] Vadim F. Lvovich and Matthew F. Smiechowski. Impedance characterization of industrial lubricants. *Electrochimica Acta*, 51:1487 – 1496, 2006.

[13] Simon S. Wang, Shyam P. Maheswari, and Simon C. Tung. Ac impedance measurements of the resistance and capacitance of lubricants. *A S L E Transactions*, 30(4):436–443, 1986.

[14] M. Ono, T. Ino, M. Koyama, A. Takashima, and A. Nishiyama. Influences of nonuniformity in metal concentration in gate dielectric silicate on cmis inverters' propagation delay time. *Solid-state Electronics*, 48(12):2191–2198, December 2004.

[15] Johan Sjoblom, Tore Skodvin, Thorvald Jakobsen, and Stanislav S. Dukhin. Dielectric spectroscopy and emulsions. a theoretical and experimental approach. *Journal of Dispersion Science and Technology*, 15(4):401–421, 1994.

[16] VadimF. Lvovich and MatthewF. Smiechowski. Ac impedance investigation of conductivity of automotive lubricants using two- and four-electrode electrochemical cells. *Journal of Applied Electrochemistry*, 39(12):2439–2452, 2009.

[17] W.T. Coffey. Theory of anomalous dielectric relaxation. In SylwesterJ. Rzoska and VitalyP. Zhelezny, editors, *Nonlinear Dielectric Phenomena in Complex Liquids*, volume 157 of *NATO Science Series II: Mathematics, Physics and Chemistry*, pages 19–29. Springer Netherlands, 2005.

[18] K. S. Cole and R. H. Cole. Dispersion and absorption in dielectrics i. alternating current characteristics. *Journal of Chemical Physics*, 9(4):341–351, April 1941.

[19] K. S. Cole and R. H. Cole. Dispersion and absorption in dielectrics ii direct current characteristics. *Journal of Chemical Physics*, 10(2):98–105, February 1942.

[20] D. W. Davidson and R. H. Cole. Dielectric relaxation in glycerol, propylene glycol, and normal-propanol. *Journal of Chemical Physics*, 19(12):1484–1490, 1951.

[21] G. Williams and D. C. Watts. Non-symmetrical dielectric relaxation behaviour arising from a simple empirical decay function. *Transactions of the Faraday Society*, 66(565P):80–&, 1970.

[22] Camelia Prodan and Corina Bot. Correcting the polarization effect in very low frequency dielectric spectroscopy. *Journal of Physics D: Applied Physics*, 42(17):175505–, 2009.

[23] Rangadhar Pradhan, Analava Mitra, and Soumen Das. Characterization of electrode/electrolyte interface of ecis devices. *Electroanalysis*, 24(12):2405–2414, 2012.

[24] J.C. Maxwell. *A Treatise on Electricity and Magnetism*. Number v. 2 in A Treatise on Electricity and Magnetism. OUP Oxford, 1873.

[25] J. C. Maxwell Garnett. Colours in metal glasses and in metallic films. *Philosophical Transactions of the Royal Society of London. Series A, Containing Papers of a Mathematical or Physical Character*, 203(359-371):385–420, January 1904.

[26] KarlWilly Wagner. Erklaorung der dielektrischen nachwirkungsvorgaonge auf grund maxwellscher vorstellungen. *Arch. Elektrotechnik*, 2(9):371–387, 1914.

[27] D. A. G Bruggeman. Berechnung versciedener physikalischer konstanten von heterogenen substanzen. *Annalen der Physik*, 24:636–679, 1935.

[28] Tetsuya Hanai, Naokazu Koizumi, and Rempei Gotoh. Dielectric properties of emulsions. *Kolloid-Zeitschrift*, 167(1):41–43, 1959.

[29] M.H. Boyle. The electrical properties of heterogeneous mixtures containing an oriented spheroidal dispersed phase. *Colloid and Polymer Science*, 263(1):51–57, 1985.

[30] T. Skodvin and J. Sjoblom. Dielectric spectroscopy on w/o emulsions under influence of shear forces. *Colloid and Polymer Science*, 274(8):754–762, August 1996.

[31] R.W. Sillars. The properties of a dielectric containing semiconducting particles of various shapes. *Wireless Section, Institution of Electrical Engineers - Proceedings of the*, 12(35):139–155, 1937.

[32] Koji Asami, Tetsuya Hanai, and Naokazu Koizumi. Dielectric approach to suspensions of ellipsoidal particles covered with a shell in particular reference to biological cells. *Japanese Journal of Applied Physics*, 19(2):359–365, 1980.

[33] T. SKODVIN, J. SJOBLOM, J. O. SAETEN, O. URDAHL, and B. GESTBLOM. Water-in-crude-oil emulsions from the norwegian continental-shelf .9. a dielectric spectroscopic characterization of authentic as well as model systems. *Journal of Colloid and Interface Science*, 166(1):43–50, August 1994.

[34] Tao Sun, Shady Gawad, Catia Bernabini, Nicolas G Green, and Hywel Morgan. Broadband single cell impedance spectroscopy using maximum length sequences:

theoretical analysis and practical considerations. *Measurement Science and Technology*, 18(9):2859, 2007.

[35] Hywel Morgan, Tao Sun, David Holmes, Shady Gawad, and Nicolas G Green. Single cell dielectric spectroscopy. *Journal of Physics D: Applied Physics*, 40(1):61, 2007.

[36] Tetsuya Hanai. Theory of the dielectric dispersion due to the interfacial polarization and its application to emulsions. *Kolloid-Zeitschrift*, 171(1):23–31, 1960.

[37] T. HANAI. Dielectric properties of emulsions .3. dielectric behavior of w/o emulsions. *Kolloid-zeitschrift and Zeitschrift Fur Polymere*, 177(1):57–&, 1961.

[38] T. HANAI, T. IMAKITA, and N. KOIZUMI. Analysis of dielectric relaxations of w/o emulsions in the light of theories of interfacial polarization. *Colloid and Polymer Science*, 260(11):1029–1034, 1982.

[39] U. Genz, J.A. Helsen, and J. Mewis. Dielectric spectroscopy of reversibly flocculated dispersions during flow. *Journal of Colloid and Interface Science*, 165(1):212 – 220, 1994.

[40] Tao Sun, Catia Bernabini, and Hywel Morgan. Single-colloidal particle impedance spectroscopy: Complete equivalent circuit analysis of polyelectrolyte microcapsules. *Langmuir*, 26(6):3821–3828, 2010. PMID: 19845351.

[41] E. Tuncer, S.M. Gubanski, and B. Nettelblad. Dielectric relaxation in dielectric mixtures: Application of the finite element method and its comparison with dielectric mixture formulas. *Journal of Applied Physics*, 89:8092–8100, 2001.

[42] E. Tuncer, Y.V. Serdyuk, and S.M. Gubanski. Dielectric mixtures: electrical properties and modeling. *Dielectrics and Electrical Insulation, IEEE Transactions on*, 9(5):809–828, 2002.

[43] K. Sekine, C. Kuroda, and N. Torii. Boundary-element calculations for dielectric relaxation of water-in-oil-in-water emulsions consisting of spherical droplets with a spheroidal core. *Colloid and Polymer Science*, 280(1):71–77, January 2002.

[44] Koji Asami. Simulation of dielectric relaxation in periodic binary systems of complex geometry. *Journal of Colloid and Interface Science*, 292(1):228–235, December 2005.

[45] Yanzhen Zhang, Yonghong Liu, Xiaolong Wang, Yang Shen, Renjie Ji, and Baoping Cai. Investigation of the charging characteristics of micrometer sized droplets based on parallel plate capacitor model. *Langmuir*, 29(5):1676–1682, February 2013.

[46] C. Boned and J. Peyrelasse. Etude de la permittivite complexe d'ellipsodes disperses dans un milieu continu. analyses theorique et numerique. *Colloid and Polymer Science*, 261(7):600–612, 1983.

[47] Ian D. Chapman. Effect of the emulsifying agent on the dielectric properties of water-in-oil emulsions. *The Journal of Physical Chemistry*, 75(4):537–541, 1971.

[48] T. SKODVIN, T. JAKOBSEN, and J. SJOBLOM. Dielectric-properties of w/o emulsions under flow. *Journal of Dispersion Science and Technology*, 15(4):423–448, 1994.

[49] O. Midttun, H. Kallevik, J. Sjoblom, and O. M. Kvalheim. Multivariate screening analysis of water-in-oil emulsions in high external electric fields as studied by means of dielectric time domain spectroscopy - iii - model emulsions containing asphaltenes and resins. *Journal of Colloid and Interface Science*, 227(2):262–271, July 2000.

[50] M. Lagues and C. Sauterey. Percolation transition in water in oil microemulsions. electrical conductivity measurements. *The Journal of Physical Chemistry*, 84(26):3503–3508, 1980.

[51] Xiaoguang Zhang, Jinfeng Dong, and Gaoyong Zhang. The conductance percolation and droplets dimension of aot in alkanol systems. *Journal of Dispersion Science and Technology*, 30(5):592–596, April 2009.

[52] S. K. Mehta, R. K. Dewan, and Kiran Bala. Percolation phenomenon and the study of conductivity, viscosity, and ultrasonic velocity in microemulsions. *Phys. Rev. E*, 50(6):4759–4762, December 1994.

[53] Mauricio S. Baptista and Chieu D. Tran. Electrical conductivity, near-infrared absorption, and thermal lens spectroscopic studies of percolation of microemulsions. *The Journal of Physical Chemistry B*, 101(21):4209–4217, 1997.

[54] Charlly Mathew, Phool Kumar Patanjali, Afzal Nabi, and Amarnath Maitra. On the concept of percolative conduction in water-in-oil microemulsions. *Colloids and Surfaces*, 30(34):253 – 263, 1988.

[55] Y. Feldman, N. Kozlovich, Y. Alexandrov, R. Nigmatullin, and Y. Ryabov. Mechanism of the cooperative relaxation in microemulsions near the percolation threshold. *Physical Review E*, 54(5):5420–5427, November 1996.

[56] Harald Fordedal and Johan Sjoblom. Percolation behavior in w/o emulsions stabilized by interfacially active fractions from crude oils in high external electric fields. *Journal of Colloid and Interface Science*, 181(2):589–594, August 1996.

[57] Guoxing Gu, Wenqing Wang, and Haike Yan. Electric percolation of water-in-oil microemulsions: The application of effective medium theory to system sodium do-

decylbenzenesulfonate (ddbs)/n-pentanol/n-heptane/water. *Journal of Colloid and Interface Science*, 178(1):358 – 360, 1996.

[58] G.J. Brug, A.L.G. van den Eeden, M. Sluyters-Rehbach, and J.H. Sluyters. The analysis of electrode impedances complicated by the presence of a constant phase element. *Journal of Electroanalytical Chemistry and Interfacial Electrochemistry*, 176(12):275 – 295, 1984.

[59] U. Rammelt and G. Reinhard. On the applicability of a constant phase element (cpe) to the estimation of roughness of solid metal electrodes. *Electrochimica Acta*, 35(6):1045 – 1049, 1990.

[60] Helene Vralstad, Oyvind Spets, Cedric Lesaint, Lars Lundgaard, and Johan Sjoblom. Dielectric properties of crude oil components. *Energy Fuels*, 23(11):5596–5602, October 2009.

[61] Vicky Mei-Wen Huang, Vincent Vivier, Mark E. Orazem, Nadine Pbre, and Bernard Tribollet. The apparent constant-phase-element behavior of a disk electrode with faradaic reactions: A global and local impedance analysis. *Journal of The Electrochemical Society*, 154(2):C99–C107, 2007.

[62] Vicky Mei-Wen Huang, Vincent Vivier, Mark E. Orazem, Nadine Pbre, and Bernard Tribollet. The apparent constant-phase-element behavior of an ideally polarized blocking electrode: A global and local impedance analysis. *Journal of The Electrochemical Society*, 154(2):C81–C88, 2007.

[63] Herman P. Schwan and Clifford D. Ferris. Four electrode null techniques for impedance measurement with high resolution. *Review of Scientific Instruments*, 39(4):481–485, 1968.

[64] Zu-yao Chang, G. A M Pop, and G. C M Meijer. A comparison of two- and four-electrode techniques to characterize blood impedance for the frequency range of 100 hz to 100 mhz. *Biomedical Engineering, IEEE Transactions on*, 55(3):1247–1249, 2008.

[65] Evando S. Araujo and Helinando P. de Oliveira. Phase inversions in emulsions probed by electrical impedance spectroscopy. *Journal of Dispersion Science and Technology*, 32(11):1649–1654, 2011.

[66] D. A. B. Barbosa, C. W. A. Paschoal, H. C. Louzeiro, K. K. M. Mendonca, A. P. Maciel, F. C. Silva, and H. P. de Oliveira. Impedance spectroscopy investigation of the water-in-oil microemulsions formation. *Colloids and Surfaces B-biointerfaces*, 84(2):325–328, June 2011.

[67] Sebastian Beer, Dorota Dobler, Alexander Gross, Martin Ost, Christiane Elseberg, Ulf Maeder, Thomas Michael Schmidts, Michael Keusgen, Martin Fiebich, and Frank Runkel. In line monitoring of the preparation of water-in-oil-in-water (w/o/w) type multiple emulsions via dielectric spectroscopy. *International Journal of Pharmaceutics*, 441(12):643 – 647, 2013.

[68] N. Perini, A.R. Prado, C.M.S. Sad, E.V.R. Castro, and M.B.J.G. Freitas. Electrochemical impedance spectroscopy for in situ petroleum analysis and water-in-oil emulsion characterization. *Fuel*, 91(1):224–228, January 2012.

[69] Janet T. Tesfai, Renee N. Perry, and Erin L. Jablonski. Water-in-oil emulsion separation within a milli-fluidic device. *Journal of Colloid and Interface Science*, 354(2):895–899, February 2011.

[70] Cedric Lesaint, Oyvind Spets, Wilhelm R. Glomm, Sebastien Simon, and Johan Sjoblom. Dielectric response as a function of viscosity for two crude oils with

different conductivities. *Colloids and Surfaces A-physicochemical and Engineering Aspects*, 369(1-3):20–26, October 2010.

[71] Cedric Lesaint, Helene Vralstad, Oyvind Spets, Sebastien Simon, Andreas Hannisdal, Lars Lundgaard, Dag Lihnjell, and Johan Sjoblom. Analysis of crude oils by frequency domain spectroscopyeffect of composition and physical properties on conductivity and dielectric response. *Journal of Dispersion Science and Technology*, 32(6):PII 937917441, 2011.

[72] Helene Vralstad, Oyvind Spets, Cedric Lesaint, Lars Lundgaard, and Johan Sjoblom. Dielectric properties of crude oil components. *Energy & Fuels*, 23:5596–5602, November 2009.

[73] Qingjun Liu, Jinjiang Yu, Lidan Xiao, Johnny Cheuk On Tang, Yu Zhang, Ping Wang, and Mo Yang. Impedance studies of bio-behavior and chemosensitivity of cancer cells by micro-electrode arrays. *Biosensors and Bioelectronics*, 24(5):1305 – 1310, 2009. ¡ce:title¿Selected Papers from the Tenth World Congress on Biosensors Shangai, China, May 14-16, 2008¡/ce:title¿.

[74] Ciprian Iliescu, Daniel P. Poenar, Mihaela Carp, and Felicia C. Loe. A microfluidic device for impedance spectroscopy analysis of biological samples. *Sensors and Actuators B: Chemical*, 123(1):168 – 176, 2007.

[75] Fei Tan, Polly H.M. Leung, Zong bin Liu, Yu Zhang, Lidan Xiao, Weiwei Ye, Xin Zhang, Li Yi, and Mo Yang. A pdms microfluidic impedance immunosensor for e. coli o157:h7 and staphylococcus aureus detection via antibody-immobilized nanoporous membrane. *Sensors and Actuators B: Chemical*, 159(1):328 – 335, 2011.

[76] Xuanhong Cheng, Yi-shao Liu, Daniel Irimia, Utkan Demirci, Liju Yang, Lee Zamir, William R. Rodriguez, Mehmet Toner, and Rashid Bashir. Cell detection and

counting through cell lysate impedance spectroscopy in microfluidic devices. *Lab Chip*, 7:746–755, 2007.

[77] Tao Zhu, Zhenhua Pei, Jianyong Huang, Chunyang Xiong, Shenggen Shi, and Jing Fang. Detection of bacterial cells by impedance spectra via fluidic electrodes in a microfluidic device. *Lab Chip*, 10:1557–1560, 2010.

[78] T. Houssin, J. Follet, E. Dei Cas, and Vincent Senez. Electrochemical impedance spectroscopy for detection of parasites in drinking water. In *Sensors, 2009 IEEE*, pages 396–399, 2009.

[79] M Ebrahimi, M Johari-Ahar, H Hamzeiy, J Barar, O Mashinchian, and Y Omidi. Electrochemical impedance spectroscopic sensing of methamphetamine by a specific aptamer. *Bioimpacts*, 2(2):91–95–, 2012.

[80] R. Gomez-Sjoberg, D.T. Morisette, and R. Bashir. Impedance microbiology-on-a-chip: Microfluidic bioprocessor for rapid detection of bacterial metabolism. *Microelectromechanical Systems, Journal of*, 14(4):829–838, 2005.

[81] Rajeev Jain, Ramkishor Sharma, Rajeev Kumar Yadav, and Ratnanjali Shrivastava. Graphene based electrochemical sensor for detection and quantification of dopaminergic agonist drug pramipexole: An electrochemical impedance spectroscopy and atomic force microscopy study. *Journal of The Electrochemical Society*, 160(3):H179–H184, 2013.

[82] Rafael Masot, Miguel Alcaniz, Ana Fuentes, Franciny C. Schmidt, Jose M. Barat, Luis Gil, Diana Baigts, Ramon Martinez-Manez, and Juan Soto. Design of a low-cost non-destructive system for punctual measurements of salt levels in food products using impedance spectroscopy. *Sensors and Actuators A-physical*, 158(2):217–223, March 2010.

[83] Luigi Ragni, Eleonora Iaccheri, Chiara Cevoli, Annachiara Berardinelli, Alessandra Bendini, and Tullia Gallina Toschi. A capacitive technique to assess water content in extra virgin olive oils. *Journal of Food Engineering*, 116(1):246 – 252, 2013.

[84] C. Brosseau and A. Beroual. Computational electromagnetics and the rational design of new dielectric heterostructures. *Progress In Materials Science*, 48(5):PII S0079–6425(02)00013–0, 2003.

[85] X. H. Zhao, Y. G. Wu, Z. G. Fan, and F. Li. Three-dimensional simulations of the complex dielectric properties of random composites by finite element method. *Journal of Applied Physics*, 95(12):8110–8117, June 2004.

[86] I. Krakovsky and V. Myroshnychenko. Modeling dielectric properties of composites by finite-element method. *Journal of Applied Physics*, 92(11):6743–6748, December 2002.

[87] D. A. Robinson and S. P. Friedman. Electrical conductivity and dielectric permittivity of sphere packings: Measurements and modelling of cubic lattices, randomly packed monosize spheres and multi-size mixtures. *Physica A-statistical Mechanics and Its Applications*, 358(2-4):447–465, December 2005.

[88] J. P. Calame. Evolution of davidson-cole relaxation behavior in random conductor-insulator composites. *Journal of Applied Physics*, 94(9):5945–5957, November 2003.

[89] J. R. Macdonald, J. Schoonman, and A. P. Lehnen. The applicability and power of complex non-linear least-squares for the analysis of impedance and admittance data. *Journal of Electroanalytical Chemistry*, 131(JAN):77–95, 1982.

[90] Yoshihiro Mori, Hiroyuki Shinoda, Taiji Kitagawa, and Taku Nakano. Intra- and intermicellar triplettriplet annihilation of pyrenetetrasulfonate in an aot reverse micel-

lar solution: relation to the electric percolation transition. *The Journal of Physical Chemistry B*, 108(41):16313–16321, 2004.

[91] S. Lipgens, D. Schbel, L. Schlicht, J.-H. Spilgies, G. Ilgenfritz, J. Eastoe, and R. K. Heenan. Percolation in nonionic water-in-oilmicroemulsion systems: a small angle neutron scattering study. *Langmuir*, 14(5):1041–1049, 1998.

[92] J.H. Masliyah and S. Bhattacharjee. *Electrokinetic and Colloid Transport Phenomena*. John Wiley & Sons, 2006.

[93] R. Somaraju and J. Trumpf. Frequency, temperature and salinity variation of the permittivity of seawater. *Antennas and Propagation, IEEE Transactions on*, 54(11):3441–3448, 2006.

[94] M. A. Malicki and R. T. Walczak. Evaluating soil salinity status from bulk electrical conductivity and permittivity. *European Journal of Soil Science*, 50(3):505–514, 1999.

[95] F. H. Drake, G. W. Pierce, and M. T. Dow. Measurement of the dielectric constant and index of refraction of water and aqueous solutions of kcl at high frequencies. *Phys. Rev.*, 35(6):613–622, March 1930.

[96] J. H. Christensen, A. J. Smith, R. B. Reed, and K. L. Elmore. Dielectric properties of phosphoric acid solutions at 25 c. *Journal of Chemical & Engineering Data*, 11(1):60–63, 1966.

[97] D.R. Lide. *CRC Handbook of Chemistry and Physics: A Ready-reference Book of Chemical and Physical Data*. CRC Press, 1993.

[98] Andrzej Lasia. Electrochemical impedance spectroscopy and its applications. In B. E. Conway, J. O M. Bockris, and Ralph E. White, editors, *Modern Aspects of*

Electrochemistry, volume 32 of *Modern Aspects of Electrochemistry*, pages 143–248. Springer US, 2002. 10.1007/0-306-46916-2-2.

[99] J. Macdonald. Levm, http://www.jrossmacdonald.com/levminfo.html.

[100] Divya Padmaraj, John H. Miller Jr., Jarek Wosik, and Wanda Zagozdzon-Wosik. Reduction of electrode polarization capacitance in low-frequency impedance spectroscopy by using mesh electrodes. *Biosensors and Bioelectronics*, 29(1):13–17, November 2011.

[101] Farshid Mostowfi, Khristo Khristov, Jan Czarnecki, Jacob Masliyah, and Subir Bhattacharjee. Electric field mediated breakdown of thin liquid films separating microscopic emulsion droplets. *Applied Physics Letters*, 90(18):184102–184102–3, 2007.

[102] S. Avramov-Zamurovic and Rae Duk Lee. A high-stability capacitance sensor system and its evaluation. *Instrumentation and Measurement, IEEE Transactions on*, 58(4):955–961, 2009.

[103] M. Santo Zarnik and D. Belavic. An experimental and numerical study of the humidity effect on the stability of a capacitive ceramic pressure sensor. *RADIOENGINEERING*, 21:201–206, 2012.

[104] R.M.C. Dawson, D.C. Elliott, W.H. Elliott, and K.M. Jones. *Data for Biochemical Research*. Oxford Science Publications. Oxford University Press, USA, 1989.

[105] Andreas Tiehm. Degradation of polycyclic aromatic hydrocarbons in the presence of synthetic surfactants. *APPLIED AND ENVIRONMENTAL MICROBIOLOGY*, pages 258–263, 1994.

[106] J.S. Newman and K.E. Thomas-Alyea. *Electrochemical Systems*. Electrochemical Society series. J. Wiley, 2004.

[107] D.R. Lide. *CRC Handbook of Chemistry and Physics 2004-2005: A Ready-Reference Book of Chemical and Physical Data*. CRC Handbook of Chemistry and Physics, 85th Ed. CRC PressI Llc, 2004.

[108] R. Behrends, K. Fuchs, U. Kaatze, Y. Hayashi, and Y. Feldman. Dielectric properties of glycerol/water mixtures at temperatures between 10 and 50 [degree]c. *The Journal of Chemical Physics*, 124(14):144512, 2006.

[109] Glycerine Producers Association. *Physical Properties of Glycerine and Its Solutions*. Glycerine Producers' Association, 1963.

[110] Robert J. Moffat. Describing the uncertainties in experimental results. *Experimental Thermal and Fluid Science*, 1(1):3 – 17, 1988.

[111] R. J. Moffat. Contributions to the theory of single-sample uncertainty analysis. *Journal of Fluids Engineering*, 104(2):250–258, June 1982.

APPENDIX A

STANDARD OPERATING MANUAL (SOP) FOR CONDUCTING EIS EXPERIMENTS

A.1 SAMPLE PREPARATION

Since a major objective of this research to study the effect of phase separation on dielectric properties of emulsions, some samples were prepared in a way that they underwent phase separation within 9 hours after preparation. Then, the effect of different parameters such as surfactant dosage was studied. Homogenization, as described in section 4.7 of chapter 4, was used as a means to adjust emulsion stability. It was observed that by dissolving water-soluble surfactant (Tween80) in water and oil-soluble surfactant (Tegopren 700) in oil (only for decane with above %50 content), adding the dispersed phase dropwise while stirring at 700 rpm, and final 20-minute homogenization in 13,000 rpm resulted in the desired stability of decane-water and castor oil-water emulsions. The fresh emulsions (within first 30 minutes) did not show any observable phase separation.

A.2 SAMPLE LOADING

For liquid mixture samples, sample loading will be easier if the experimenter closes the test setup and tightens the screws, leaving about 0.5mm of the bottom electrode out. Then the sample can be injected with a syringe and the bottom electrode can be pushed inside

the test. However, for emulsions, injecting with a syringe may affect the sample in terms of droplet size distribution. Therefore, it is recommended to fix the top and bottom electrodes on the top and bottom holders of the fixture, respectively, load emulsions samples on the bottom electrode, put the top electrode (held with the top holder) on it, and then tighten the screws. Guides can be used (the holes are designed on the setup) to direct the top part right onto the sample so that the sample cannot be pushed out, and air bubbles cannot enter the test chamber.

A.3 CONNECTIONS TO THE FRA

Four the two-electrode measurements, the connections to the FRA are the same as connection for in-circuit impedance spectroscopy. Figure A.1 shows the connections based on the Soartron 1260 manual instructions. The dashed lines are the shield of the cables. Short-circuiting the outer bolts of the BNC cables together is recommended in order to provide same ground for all shields. This acts as the external node as shown in figure A.1.

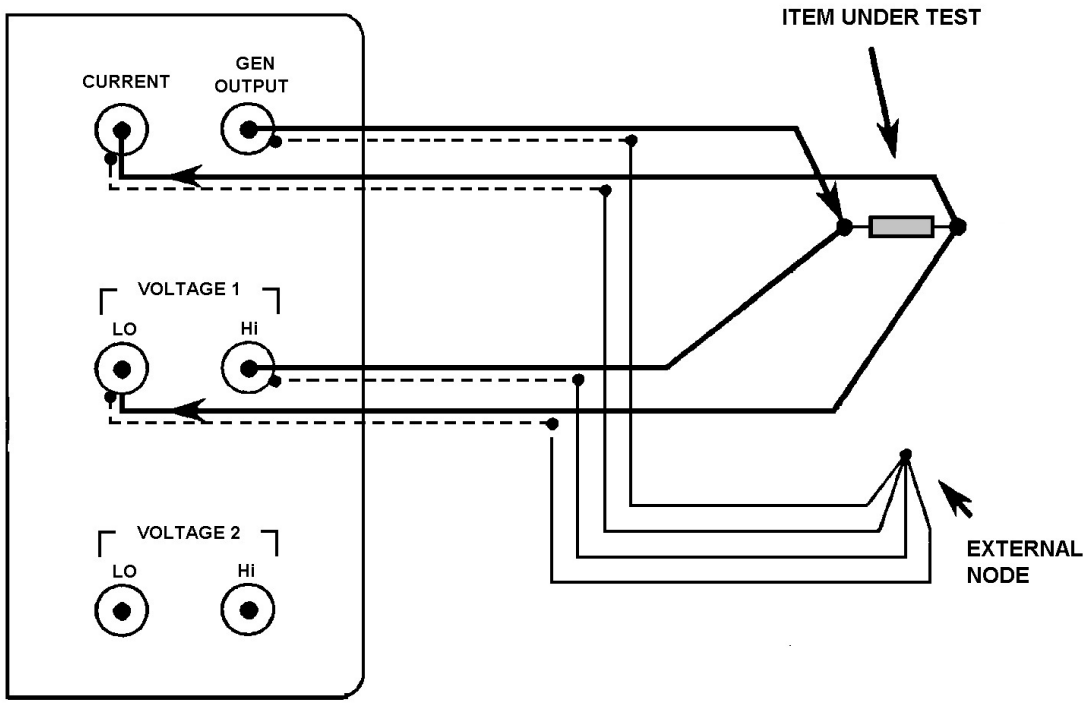

Figure A.1: Schematic diagram of electrode connections to Solartron 1260 based on the manual.

Appendix B

CUSTOM EQUIVALENT CIRCUIT MODELING CODE

The basics of equivalent circuit modeling was discussed in chapter 3 and it was mentioned that a custom program in MATLAB has been developed for fitting a known model to experimental data. Unlike the LEVM software, this code enables the user to use different minimization weights. In this model, the "fminsearch" function is used for minimization. The code, including the function defined separately and used in the main code, is provided below.

```
clear all;
close all;
clc;


R=20*1000;
C=100*10^(-6);

[re_exp im_exp omega]=imped_exp_simulation(R,C);
%returns from the simulated experiment the real and imaginary parts ...
   and the corresponding frequency
```

```
c_r=1;
c_i=1;

w(:,1)=1./(c_r*re_exp(:,1).$^2$+c_i*im_exp(:,1).^2);

[RC_opt value]=...
fminsearch(@(RC)(sum(w(:,1).*(re_exp(:,1)-Re_Model(RC,omega)).^2+...
w(:,1).*(im_exp(:,1)-Im_model(RC,omega)).^2)),[10000 0.0001])




function[re_exp,im_exp,omega]=imped_exp_simulation(R,C)


H = tf([R],[R*C 1])
% which represents R/(RCs+1) as the transfer function of simple ...
   parallel RC circuit


w={0.0001,100000};

nyquist(H,w)
[re_exp im_exp ww]=nyquist(H,w);

reexp=squeeze(re_exp);                              %"squeeze" ...
   eliminates the singleton indices
imexp=squeeze(im_exp);
omega=squeeze(ww);
```

```
figure;
bode(H,w)
[mag,ph,www]=bode(H,w);


www=squeeze(www);
mag=squeeze(mag);
ph=squeeze(ph);


semilogx(www,ph);
plot(re,im);

end
```